Diazotrophy in the Deep:
An analysis of the distribution, magnitude, geochemical controls, and biological mediators of deep-sea benthic nitrogen fixation

Thesis by

Anne Elizabeth Dekas

In Partial Fulfillment of the Requirements for the Degree

of

Doctor of Philosophy

CALIFORNIA INSTITUTE OF TECHNOLOGY

Pasadena, California

2013

(Defended October 17, 2012)

ACKNOWLEDGEMENTS

I would like to first thank my advisor, Victoria Orphan, without whom this work would not have been possible. Victoria's curiosity, scientific insight, and unfailingly positive attitude are inspiring. The opportunities and resources she provided me over the past six years were incredible, and I am extremely grateful. I am lucky to have spent my formative years as a scientist under her wing.

I would like to thank several other professors, staff, and visiting scientists who have had meaningful contributions to my work and my experience at Caltech, including the members of my thesis advisory committee (Alex Sessions, Dianne Newman, Joe Kirschvink, and Jim Howard) as well as Woody Fischer, John Eiler, Yunbin Guan, Nathan Dalleska, Jared Leadbetter, and John Grotzinger. I have benefited greatly from the classes, field trips, seminars, and conversations we have shared. I thank them for being excellent teachers and role models.

I would like to thank the past and present members of the Orphan Lab group, including Shana Goffredi, Patty Tavormina, Tsege Embaye, David Fike, Jake Bailey, Olivia Mason, Rachel Poretsky, Crystal Gammon, Ben Harrison, Abbie Green-Saxena, Jeff Marlow, Josh Steele, Roland Hatzenpichler, Jennifer Glass, Shawn McGlynn, Kat Dawson, David Case, Elizabeth Trembath-Reichert, Hiro Imachi, Grayson Chadwick, and Stephanie Connon. They have given me excellent feedback on my presentations, posters, manuscripts, proposals, protocols, and ideas. I have learned from each of them, and I am thankful to have shared the last six years with them in lab. I specifically thank Stephanie and Gray for their direct participation in the projects described in the following dissertation. Working with both of them has been a pleasure, and one of the highlights of my time at Caltech. I thank Crystal and Abbie for many important conversations, scientific and otherwise, and am deeply grateful for their help in the lab, as well as their friendships.

I thank the many people who were involved in the sample collection process required for these experiments, involving seven research cruises over the course of six years. I thank Orphan Lab members Victoria, Shana, David, Jake, Abbie, Josh, Elizabeth, Jeff, and Jen, as well as Ally Pasulka, Leah Brandt, Burt Thomas, Lisa Levin, and the entire shipboard crews and science parties of AT15-11, AT15-44, AT15-59, AT15-68, AT18-10, Western Flyer DR097-101, and Western Flyer DR204-209, for being excellent teammates during these often intense endeavors. Their late-night hard work, clear thinking, problem solving, and (sometimes whacky) energy made these experiments possible.

I would like to thank many students and postdoctoral scholars in the GPS department outside of the Orphan Lab group for their contagious enthusiasm for science, as well as their direct impact on my research. In particular, Nithya Thiagarajan, Anna Beck, and Steve Skinner, for engaging in the details of my research, as well as providing an interdisciplinary perspective (and occasionally baked goods). I also thank Renata Cummins for her invaluable contribution to the compiling of this document (specifically, the page numbers).

I would like to thank the excellent administrative staff within the GPS department, and in particular Jan Haskell, Marcia Hudson, and Dian Buchness. They have made being a student here as easy as possible, allowing me to focus my time on research.

I would like to thank my friends and family outside of Caltech for the incredible support and encouragement they have offered in my pursuit of science. My parents and sister, Nan Bredar, Bob Dekas, and Kathryn Dekas, have encouraged me at every step. From butterfly nets to pet frogs, pep-talk emails to thesis-writing-survival-kits, they have cultivated my interest in science and made me believe that my passion could be my profession. Their confidence in me and their belief in the importance of my work motivates me daily. I thank John Delacruz for his support the last six years, watching presentations, proofreading manuscripts, and listening to the daily up and downs of my lab work. He has made my research, as well as my life, infinitely better. I thank many other friends, including Jenny Fogarty, Katie Weiland, Sara Clark, and the Pocahos, whose phone calls, emails, and visits always energize me. Thank you for giving me perspective.

ABSTRACT

Biological nitrogen fixation (the conversion of N_2 to NH_3) is a critical process in the oceans, counteracting the production of N_2 gas by dissimilatory bacterial metabolisms and providing a source of bioavailable nitrogen to many nitrogen-limited ecosystems. One currently poorly studied and potentially underappreciated habitat for diazotrophic organisms is the sediments of the deep-sea. Although nitrogen fixation was once thought to be negligible in non-photosynthetically driven benthic ecosystems, the present study demonstrates the occurrence and expression of a diversity of *nifH* genes (those necessary for nitrogen fixation), as well as a widespread ability to fix nitrogen at high rates in these locations. The following research explores the distribution, magnitude, geochemical controls, and biological mediators of nitrogen fixation at several deep-sea sediment habitats, including active methane seeps (Mound 12, Costa Rica; Eel River Basin, CA, USA; Hydrate Ridge, OR, USA; and Monterey Canyon, CA, USA), whale-fall sites (Monterey Canyon, CA), and background deep-sea sediment (off-site Mound 12 Costa Rica, off-site Hydrate Ridge, OR, USA; and Monterey Canyon, CA, USA). The first of the five chapters describes the FISH-NanoSIMS method, which we optimized for the analysis of closely associated microbial symbionts in marine sediments. The second describes an investigation of methane seep sediment from the Eel River Basin, where we recovered *nifH* sequences from extracted DNA, and used FISH-NanoSIMS to identify methanotrophic archaea (ANME-2) as diazotrophs, when associated with functional sulfate-reducing bacterial symbionts. The third and fourth chapters focus on the distribution and diversity of active diazotrophs (respectively) in methane seep sediment from Mound 12, Costa Rica, using a combination of ^{15}N-labeling experiments, FISH-NanoSIMS, and RNA and DNA analysis. The fifth chapter expands the scope of the investigation by targeting diverse samples from methane seep, whale-fall, and background sediment collected along the Eastern Pacific Margin, and comparing the rates of nitrogen fixation observed to geochemical measurements collected in parallel. Together, these analyses represent the most extensive investigation of deep-sea nitrogen fixation to date, and work towards understanding the contribution of benthic nitrogen fixation to global marine nitrogen cycling.

TABLE OF CONTENTS

LIST OF ILLUSTRATIONS AND TABLES

Chapter Number-Figure Number (SI indicates Supplemental Information)

Introduction

Microbial metabolisms collectively shape the chemistry of our planet. Nitrogen fixation, the biological conversion of N_2 gas into NH_3 for growth, is one such metabolism, and is the main source of biologically accessible nitrogen to the biosphere. Biological nitrogen fixation both closes the nitrogen cycle by counteracting the N_2 production of other microbial metabolisms (e.g., denitrification and anammox) and controls the rate of growth in ecosystems limited by the availability of nitrogen, thus dictating the rate at which many environmentally relevant molecules, such as CO_2, flow through the biosphere.

Nitrogen limitation occurs despite the great abundance of nitrogen present as N_2 in the Earth's atmosphere because the stability of the N_2 triple bond prevents most organisms from assimilating nitrogen gas directly. Most organisms, including all plants and animals, require "bioavailable" nitrogen, typically including organic material or NH_4^+/NH_3, NO_3^{2-}, or NO_2^-. The ultimate source of all bioavailable nitrogen in natural environments (those without the input of anthropogenic nitrogen) is both abiotic and biotic: lightening induces the oxidation of N_2 to NO in the atmosphere, which can oxidize further to HNO_3 (which is water soluble and therefore transported by rain), and the enzyme nitrogenase mediates biological nitrogen fixation in a small sub-set of bacteria and archaea, directly introducing NH_3 to the biosphere (*1*).

Currently, biological nitrogen fixation is a more significant input of fixed nitrogen to the planet than lightening, however atmospheric reactions are hypothesized to have been a more significant input on the early Earth, when lightening may have been more frequent (*2*). Although biological nitrogen fixation may have evolved in response to a

decrease in lightening-induced bioavailable nitrogen during the Archaean, and a subsequent "nitrogen crisis" (*2*), it has also been hypothesized that bioavailable nitrogen was plentiful when it evolved. This raises the possibility that the original primary function of nitrogenase may have been unrelated to nitrogen assimilation. Rather, it may have evolved to reduce other small, triply-bonded molecules, such as cyanide, potentially as a detoxification mechanism (*3–5*). Substrate promiscuity continues to be a characteristic of modern nitrogenase (*4*), consistent with what is demonstrated in Chapter 1 of this work.

The microorganisms capable nitrogen fixation, known as diazotrophs (derived from the French root "azote" meaning "nitrogen" and the Greek root "troph" meaning "eater of" (*6*)) have been researched for over 100 years. The usage of leguminous plants (later shown to host diazotrophic symbionts) to increase the fertility of agricultural soils dates back to pre-Roman times, but the observation of cells growing on N_2 as the sole nitrogen source, and the recognition that diazotrophs were widespread, did not occur until the late 1800s and early 1900s (*7, 8*). Since then the knowledge of their ecological significance has grown continually, as they have been well characterized in agricultural soils, fresh water lakes, several animal and plant symbioses, and the upper marine water column (*9–12*, *and references therein*). Although some of the first reports of marine diazotrophy investigated marine sediments (*8, and references therein*), for many years the study of marine nitrogen fixation focused nearly exclusively on diazotrophs in the upper water column, and particularly *Trichodesmium* (*13*). Although a few species of photosynthetic cyanobacteria do fix the majority of nitrogen in the oceans, recent work has underscored the potential importance of other marine diazotrophs, such as a diversity

of unicellular cyanobacteria, heterotrophic bacteria, diatom symbionts, and benthic microorganisms (*reviewed in 9, 14, 15*).

In particular, until about six years ago, very little was known about nitrogen fixation in deep-sea sediments (defined here as > 100 m water depth). In 1978 Hartwig and Stanley measured rates of N_2 fixation via the acetylene reduction assay in abyssal plain sediments off the coast of Scotland, from 150 to 4,800 meters water depth (*16*). They found minimal rates of nitrogenase activity, up to 1.3 x 10^{-3} nmol C_2H_4 g^{-1} h^{-1} (and none at 4,800 m), and concluded: "Nitrogen fixation does not appear to be a major source of organic nitrogen to the deep-sea benthos". Their results were consistent with the commonly accepted paradigm at the time that nitrogen fixation would be unlikely in marine sediments due to the assumed presence of sufficiently high preferable nitrogen sources, and follow-up studies were not pursued. The acetylene reduction assay has since been recognized to inhibit many environmentally relevant microbes, and particular those living in anaerobic sediments (*11, 12*), raising the possibility that nitrogen fixation was overlooked in the Hartwig and Stanley study due to the methods employed.

Our understanding of the diversity of diazotrophs in general, and in the deep-sea in particular, began to change with the development of molecular tools in microbiology, and particularly with the use of *nifH* as a molecular marker for diazotrophy (*17, 18*). The ability to fix nitrogen is conferred by the *nif* genes, a suite of up to 20 genes encoding the enzyme nitrogenase as well as its (typically tightly controlled) regulation. Nitrogenase consists of two component proteins, the MoFe protein (also known as dinitrogenase), a tetramer encoded by *nifD* and *nifK,* and the Fe protein (also known as dinitrogenase reductase), a dimer encoded by *nifH* (*19, 20*). *nifH* has become the most widely used

genetic marker for the potential for nitrogen fixation, with the public database for *nifH* containing more sequences than nearly any other functional (non-ribosomal) gene.

Twenty-five years after the Hartwig and Stanley experiments, in 2003, a wide diversity of *nifH* sequences were recovered from a deep-sea hydrothermal vent (*21*), and three years later, a deep-sea methanogen capable of nitrogen fixation was isolated from the same site (*22*). A similar breadth of *nifH* sequences were later detected at two additional sites of deep-sea methane seepage (*23, 24*). At one of these, a methane seep off shore Japan, *nifH* transcripts in addition to *nifH* DNA sequences were detected (*24*). The possibility of nitrogen fixation in deep-sea sediments, and particularly the possibility of localized nitrogen limitation at hydrothermal vents and methane seeps, seemed increasingly likely.

However, evidence of *nifH* sequences falls short of indicating diazotrophy. Many *nifH* sequences in the environment are either not functional or used for functions other than nitrogen fixation [i.e., *nifH* group IV and V (*25*)]. Additionally, because nitrogen fixation is an ATP-intensive process, organisms capable of fixing nitrogen only actually do it when ambient bioavailable nitrogen concentrations fall below what is necessary for growth. The detection of *nifH* sequences, and even transcripts, therefore do not guarantee active diazotrophy. More direct measurements of nitrogen fixation, such as the bulk experiments pursued by Hartwig and Stanley in 1978, and the $^{15}N_2$ pure culture experiment by Mehta et al. in 2006, were necessary to investigate whether or not the diversity of *nifH* sequences detected on the seafloor reflected a diverse and widespread community of active deep-sea diazotrophs.

At the same time, investigations of nitrogen fixation in near-shore benthic environments were beginning to show evidence suggesting that benthic diazotrophy may contribute bioavailable nitrogen to the water column (*26*). This was significant because a growing body of literature suggested that the marine nitrogen cycle inventory was not in balance, and specifically that rates of N_2 production exceeded that of N_2 consumption (e.g., *27*, *28*). The possibility of ocean sediments as a source of bioavailable nitrogen to the marine biosphere and nitrogen cycle was an intriguing possibility. Covering over two-thirds of the planet, if deep-sea sediments hosted even low rates of diazotrophic activity, the impact on the nitrogen cycle could be profound.

Meanwhile, in 2008, the study of the anaerobic oxidation of methane (AOM) in marine sediments started to collide with that of the nitrogen cycle when the first metagenomic data for the microbial consortia mediating AOM (consisting of anaerobic methane-oxidizing archaea, ANME, and tightly associated sulfate-reducing bacterial symbionts, SRB) was obtained, and included *nif* homologues (*29*). In 2001 it had been confirmed that sulfate-dependent anaerobic oxidation of methane was indeed biologically mediated, and that the responsible microorganisms existed as tightly associated symbionts (*30, 31*). These microbial consortia were found to consume approximately 80% of the methane naturally seeping upwards from marine sediment, preventing it from reaching the water column (*32*) and subsequently the atmosphere, where it would have a greenhouse warming effect. These organisms therefore played an important role in global climate as well as their local ecosystem, supplying both carbon and electrons (e.g., hydrogen sulfide) to support the abundant and productive micro- and macrofauna at methane seeps (*33*).

The investigation of the ANME-SRB is challenging, because their slow growth rate (*34*) and unknown mechanism for coupling methane oxidation to sulfate reduction (*35*) has hindered their isolation. A. Pernthaler and V. Orphan therefore developed Magneto-FISH, a method by which specific ANME-SRB aggregates could be selectively removed from the sediment, resulting in an enrichment of ANME-SRB aggregates compared to the bulk sediment community (*29*). Subsequent 454 metagenomic analysis of the enriched fraction was pursued, and nearly 29 Mb of sequence, including a nearly complete *nif* operon, was recovered. For this study, I generated archaeal and bacterial clone libraries from the bulk sediment to determine that Magneto-FISH enriched the ANME-2 archaea from 26 to 92% of the archaeal community, and their known SRB partners from 25 to 42% of the bacterial community (*Table 1 in 29*). Also for this study, I pursued the possibility of nitrogen fixation in the ANME-SRB with $^{15}N_2$ incubations of bulk sediment collected from a methane seep within the Eel River Basin (depth ~500 m), and detected ^{15}N uptake within the ANME-SRB consortia via Secondary Ion Mass Spectrometry (CAMECA 1270 housed at UCLA) (*Figure 4 in 36*).

Although $^{15}N_2$-uptake in the consortia suggested that either the ANME or the SRB were diazotrophic, further work was necessary both to eliminate the possibility of ^{15}N recycling within the sediment and to determine which of these partners were mediating the diazotrophic activity. Nitrogen fixation in the ANME archaea would extend the known lower limit of respiratory energy capable of fueling nitrogen fixation, expand the demonstrated diazotrophic ability in the Archaea outside of the guild of the methanogens, and put the ANME at the base of both the carbon and nitrogen food-chain at methane

seeps. Nitrogen fixation in either partner already challenged the traditional paradigm that nitrogen fixation would not occur in marine sediments, and opened up the possibility of nitrogen limitation and even a diversity of active diazotrophs at methane seeps.

The pursuit of previously overlooked nitrogen sources in the marine system and the ongoing attempt to better understand the ANME-SRB symbiosis therefore converged. The following work was pursued in an attempt to elucidate both the role of diazotrophy within the ANME-SRB symbiosis and their local ecosystem, as well as the role of deep-sea diazotrophy in the marine nitrogen cycle. In the following dissertation, four aspects of deep-sea benthic diazotrophy are investigated: (1) the biological mediators of N_2 fixation, via single-cell, NanoSIMS analysis of community members as well as transcript analysis of diazotrophic sediments (Chapters 1 and 4), (2) the extent of nitrogen limitation on the seafloor, via direct measurements of bioavailable nitrogen in areas of increased productivity and background sediments (Chapters 3 and 5), (3) the magnitude and distribution of the ability to fix nitrogen, measured by observing $^{15}N_2$ uptake in spatially discreet sediments from four geographically distinct regions of the deep-sea (Chapter 3 and 5), and (4) the geochemical controls on deep-sea nitrogen fixation, via comparison of $^{15}N_2$ uptake rates to geochemical conditions (Chapter 3 and 5). This represents the most extensive body of work characterizing deep-sea diazotroph to date, and hopefully will serve as a spring board for future analyses of deep-sea nutrient limitation and nitrogen cycling.

WORKS CITED

1. D. J. Jacob, *Introduction to atmospheric chemistry*. (Princeton University Press, Princeton, N.J., 1999), pp. xii, 266 p.
2. R. Navarro-Gonzalez, C. P. McKay, D. N. Mvondo, A possible nitrogen crisis for Archaean life due to reduced nitrogen fixation by lightning. *Nature* **412**, 61 (2001).
3. W. S. Silver, J. R. Postgate, Evolution of Asymbiotic Nitrogen-Fixation. *Journal of Theoretical Biology* **40**, 1 (1973).
4. I. Berman-Frank, P. Lundgren, P. Falkowski, Nitrogen fixation and photosynthetic oxygen evolution in cyanobacteria. *Res Microbiol* **154**, 157 (2003).
5. R. Fani, R. Gallo, P. Lio, Molecular evolution of nitrogen fixation: The evolutionary history of the nifD, nifK, nifE, and nifN genes. *Journal of Molecular Evolution* **51**, 1 (2000).
6. J. Corredor, An Etymology of Nitrogen and Other Related Words. *Biogeochemistry* **46**, 5 (1999).
7. M. W. Beijerinck, The root-nodule bacteria. *Botanische Zeitung* **46**, 725 (1888).
8. S. A. Waksman, M. Hotchkiss, C. L. Carey, Marine bacteria and their role in the cycle of life in the sea: II. Bacteria concerned in the cycle of nitrogen in the sea. *The Biological Bulletin* **65**, 137 (1933).
9. J. A. Sohm, E. A. Webb, D. G. Capone, Emerging patterns of marine nitrogen fixation. *Nat Rev Microbiol* **9**, 499 (2011).
10. R. W. Howarth, R. Marino, J. Lane, Nitrogen fixation in freshwater, estuarine, and marine ecosystems. 1. Rates and importance. *Limnology and Oceanography* **33**, 669 (1988).
11. D. G. Capone, in *Nitrogen Cycling in Coastal Marine Environments,* T. H. Blackburn, J. Sorensen, Eds. (John Wiley & Sons, New York, 1988), p. 85.
12. Karl et al., Dinitrogen Fixation in the world's oceans. *Biogeochemistry* **57/58**, 47 (2002).
13. D. G. Capone, J. P. Zehr, H. W. Paerl, B. Bergman, E. J. Carpenter, Trichodesmium, a Globally Significant Marine Cyanobacterium *Science (New York, N.Y* **276**, 1221 (1997).
14. J. P. Zehr, Nitrogen fixation by marine cyanobacteria. *Trends Microbiol* **19**, 162 (2011).
15. E. J. Carpenter, D. G. Capone, in *Nitrogen in the Marine Environment,* D. G. Capone, D. Bronk, M. Mulholland, E. J. Carpenter, Eds. (Elsevier, Academic Press, San Diego, 2008), pp. 141-198.
16. E. O. Hartwig, S. O. Stanley, Nitrogen Fixation in Atlantic deep-sea and Coastal sediments. *Deep-Sea Research* **25**, 411 (1978).
17. J. P. Zehr, B. B. Ward, Nitrogen cycling in the ocean: new perspectives on processes and paradigms. *Applied and Environmental Microbiology* **68**, 1015 (2002).
18. J. P. Zehr, B. D. Jenkins, S. M. Short, G. F. Steward, Nitrogenase gene diversity and microbial community structure: a cross-system comparison. *Environmental Microbiology* **5**, 539 (2003).

19. J. B. Howard, D. C. Rees, Structural basis of biological nitrogen fixation. *Chem Rev* **96**, 2965 (1996).
20. J. P. W. Young, in *Genomes and Genomics of Nitrogen-fixing Organisms,* R. Palacios, W. E. Newton, Eds. (Springer, The Netherlands, 2005), pp. 221-241.
21. M. P. Mehta, D. A. Butterfield, J. A. Baross, Phylogenetic diversity of nitrogenase (nifH) genes in deep-sea and hydrothermal vent environments of the Juan de Fuca Ridge. *Applied and Environmental Microbiology* **69**, 960 (2003).
22. M. P. Mehta, J. A. Baross, Nitrogen fixation at 92 degrees C by a hydrothermal vent archaeon. *Science (New York, N.Y* **314**, 1783 (2006).
23. H. Dang, X. Luan, J. Zhao, J. Li, Diverse and novel nifH and nifH-like gene sequences in the deep-sea methane seep sediments of the Okhotsk Sea. *Applied and Environmental Microbiology* **75**, 2238 (2009).
24. J. Miyazaki et al., Molecular characterization of potential nitrogen fixation by anaerobic methane-oxidizing archaea in the methane seep sediments at the number 8 Kumano Knoll in the Kumano Basin, offshore of Japan. *Applied and Environmental Microbiology* **75**, 7153 (2009).
25. J. Raymond, J. L. Siefert, C. R. Staples, R. E. Blankenship, The natural history of nitrogen fixation. *Molecular Biology and Evolution* **21**, 541 (2004).
26. R. W. Fulweiler, S. W. Nixon, B. A. Buckley, S. L. Granger, Reversal of the net dinitrogen gas flux in coastal marine sediments. *Nature* **448**, 180 (2007).
27. L. A. Codispoti, An oceanic fixed nitrogen sink exceeding 400 Tg Na-1 vs the concept of homeostasis in the fixed-nitrogen inventory. *Biogeosciences* **4**, 233 (2007).
28. C. Mahaffey, A. F. Michaels, D. G. Capone, The conundrum of marine N2 fixation. *Am J Sci* **305**, 546 (2005).
29. A. Pernthaler et al., Diverse syntrophic partnerships from deep-sea methane vents revealed by direct cell capture and metagenomics. *Proceedings of the National Academy of Sciences of the United States of America* **105**, 7052 (2008).
30. V. J. Orphan, C. H. House, K. U. Hinrichs, K. D. McKeegan, E. F. DeLong, Methane-consuming archaea revealed by directly coupled isotopic and phylogenetic analysis. *Science (New York, N.Y* **293**, 484 (2001).
31. A. Boetius et al., A marine microbial consortium apparently mediating anaerobic oxidation of methane. *Nature* **407**, 623 (2000).
32. W. S. Reeburgh, Oceanic methane biogeochemistry. *Chem Rev* **107**, 486 (2007).
33. L. A. Levin, Ecology of cold seep sediments: Interactions of fauna with flow, chemistry and microbes. *Oceanogr Mar Biol* **43**, 1 (2005).
34. V. J. Orphan, K. A. Turk, A. M. Green, C. H. House, Patterns of ^{15}N assimilation and growth of methanotrophic ANME-2 archaea and sulfate-reducing bacteria within structured syntrophic consortia revealed by FISH-SIMS. *Environmental Microbiology* (2009).
35. K. Nauhaus, A. Boetius, M. Kruger, F. Widdel, In vitro demonstration of anaerobic oxidation of methane coupled to sulphate reduction in sediment from a marine gas hydrate area. *Environmental Microbiology* **4**, 296 (2002).
36. A. Pernthaler et al., Diverse syntrophic partnerships from deep-sea methane vents revealed by direct cell capture and metagenomics. *Proceedings of the National Academy of Sciences* **105**, 7052 (2008).

C h a p t e r 1

Identification of Diazotrophic Microorganisms in Marine Sediment Via Fluorescence *In Situ* Hybridization Coupled to Nanoscale Secondary Ion Mass Spectrometry (FISH-NanoSIMS)

Anne E. Dekas[1] and Victoria J. Orphan[1]

[1]Division of Geological and Planetary Sciences,
California Institute of Technology Pasadena, CA 91125

Originally published in Methods in Enzymology,
Volume 486, Chapter 12, © 2011, Elsevier, Inc.

CHAPTER TWELVE

Identification of Diazotrophic Microorganisms in Marine Sediment via Fluorescence *In Situ* Hybridization Coupled to Nanoscale Secondary Ion Mass Spectrometry (FISH-NanoSIMS)

Anne E. Dekas *and* Victoria J. Orphan

Contents

Division of Geological and Planetary Sciences, California Institute of Technology, Pasadena, California, USA

Methods in Enzymology, Volume 486
ISSN 0076-6879, DOI: 10.1016/S0076-6879(11)86012-X

Abstract

Growing appreciation for the biogeochemical significance of uncultured microorganisms is changing the focus of environmental microbiology. Techniques designed to investigate microbial metabolism *in situ* are increasingly popular, from mRNA-targeted fluorescence *in situ* hybridization (FISH) to the "-omics" revolution, including metagenomics, transcriptomics, and proteomics. Recently, the coupling of FISH with nanometer-scale secondary ion mass spectrometry (NanoSIMS) has taken this movement in a new direction, allowing single-cell metabolic analysis of uncultured microbial phylogenic groups. The main advantage of FISH-NanoSIMS over previous noncultivation-based techniques to probe metabolism is its ability to directly link 16S rRNA phylogenetic identity to metabolic function. In the following chapter, we describe the procedures necessary to identify nitrogen-fixing microbes within marine sediment via FISH-NanoSIMS, using our work on nitrogen fixation by uncultured deep-sea methane-consuming archaea as a case study.

1. Introduction

1.1. Background

Nitrogen is required in numerous biomolecules including amino and nucleic acids and is therefore an essential element for life. Although nitrogen is extremely abundant on the surface of the earth, most organisms are unable to assimilate the majority of this nitrogen, gaseous N_2, due to the stability of its triple bond. Nitrogen limitation in natural biological communities is therefore common, and the abundance of bioavailable nitrogen sources (such as nitrate and ammonia) can regulate overall productivity and chemical exchange. Importantly, a small subset of phylogenetically diverse prokaryotes known as diazotrophs are able to convert N_2 into NH_3, using a well-conserved enzyme called nitrogenase and a large input of ATP. Biological nitrogen fixation, or simply nitrogen fixation, essentially unlocks the reservoir of nitrogen in the atmosphere and provides a source of bioavailable nitrogen for the rest of the food chain. This conversion is additionally important in the context of global nitrogen cycling, because it compensates for the production of N_2 by energy-generating microbial processes (e.g., denitrification and anammox).

From the onset of marine nitrogen fixation research over 100 years ago, a variety of habitats have been recognized to host diazotrophs, including both the water column and sediments (Capone, 1988; Herbert, 1999; Howarth *et al.*, 1988; Waksman *et al.*, 1933). However, most marine nitrogen fixation research and global rate modeling have focused on *Trichodesmium*, a pelagic cyanobacteria, due to its abundance and important role in biogeochemical cycling (Capone *et al.*, 1997). In the past decade this focus has broadened, as an increasing number of studies have highlighted the great

and occasionally unexpected phylogenetic and geographic diversity of marine diazotrophs (Capone, 2001; Karl *et al.*, 2002; Mahaffey *et al.*, 2005). Specifically, the development and wide-scale application of culture-independent techniques, including DNA and complementary DNA (cDNA) clone libraries (Mehta *et al.*, 2003; Miyazaki *et al.*, 2009), net N_2 flux measurements (Fulweiler *et al.*, 2007), quantitative PCR (QPCR) (Moisander *et al.*, 2010), quantitative reverse transcriptase PCR (Q-RT-PCR) (Foster *et al.*, 2009; Short and Zehr, 2007; Veit *et al.*, 2006), and single-cell level ^{15}N-tracer studies (Dekas *et al.*, 2009; Finzi-Hart *et al.*, 2009; Lechene *et al.*, 2007; Popa *et al.*, 2007), have revealed a previously unrecognized breadth of diazotrophs both within the cyanobacteria and throughout the prokaryotic domains.

These findings show that nitrogen fixation is more widespread than previously appreciated and suggest that some marine habitats may have been overlooked as net sources of bioavailable nitrogen. This possibility is significant in the context of the global marine nitrogen cycle, which for many years has been reported to have incongruous sources and sinks of fixed nitrogen (Codispoti, 1995, 2007; Codispoti and Christensen, 1985; Codispoti *et al.*, 2001; Ganeshram *et al.*, 1995; Gruber and Sarmiento, 1997; Mahaffey *et al.*, 2005; McElroy, 1983). The recent developments in our understanding of diazotroph diversity support an artifact explanation for the incongruence: the perceived imbalance in the nitrogen cycle may be a result of an underestimation of marine nitrogen fixation rather than a real and significant departure from steady state (Brandes and Devol, 2002; Brandes *et al.*, 2007; Codispoti, 2007; Fulweiler, 2009; Gruber and Sarmiento, 1997; Mahaffey *et al.*, 2005). The further study of nitrogen fixation, both on an organismal and global scale, is therefore extremely timely.

1.2. Methods to investigate nitrogen fixation: Why FISH-NanoSIMS?

While informative and relatively easy to employ, a limitation of most molecular techniques and standard geochemical analyses is their inability to link specific phylogenetically identified microorganisms in environmental samples with their metabolic processes. Bulk analyses, such as the acetylene reduction assay, ^{15}N tracer experiments (measured with an elemental analyzer-isotope ratio mass spectrometer, EA-IRMS), and N_2 flux experiments (measured with the N_2/Ar technique; Fulweiler *et al.*, 2007), can demonstrate active nitrogen fixation, along with quantitative rate data, but cannot identify the specific phylogenetic groups of microorganisms responsible for the conversion. And, although the acetylene reduction assay is typically credited with higher sensitivity than bulk $^{15}N_2$ tracer studies, it is subject to several sources of error (described in Karl *et al.*, 2002), in addition to causing inhibition of some environmentally relevant

microbes, including methanogens and anaerobic methanotrophs (Dekas *et al.*, 2009; Oremland and Taylor, 1975; Sprott *et al.*, 1982).

Targeted molecular approaches similarly have drawbacks. DNA investigations of relevant metabolic genes and the *nifH* genes, in particular (Mehta *et al.*, 2003), can be considered an investigation of the metabolic potential of the community, but not the activity. Investigations of transcripts, and in particular, quantitative reverse transcriptase PCR (Q-RT-PCR) studies of *nifH* (Foster *et al.*, 2009; Short and Zehr, 2007; Veit *et al.*, 2006), are generally considered robust and even quantitative indicators of active nitrogen fixation (Short and Zehr, 2005). However, posttranscription and posttranslational regulation are known to occur, and activity may deviate from what the transcript level suggests (Kessler and Leigh, 1999; Liang *et al.*, 1991; Zhang *et al.*, 1993). Additionally, neither a cDNA clone library nor Q-RT-PCR targeting particular *nif* genes can reliably reveal the microbial source of the gene in terms of its 16S rRNA identity due to incongruence between *nif* and 16S phylogenies attributed to lateral gene transfer (Kechris *et al.*, 2006).

An extremely promising approach to simultaneously measuring diazotrophic activity and phylogenetic identity is stable isotope probing with $^{15}N_2$ ($^{15}N_2$-DNA-SIP) (Buckley *et al.*, 2007a). Although DNA-SIP with ^{13}C-labeled compounds is relatively common (Dumont and Murrell, 2005), the additional complications related to density separation of labeled and unlabeled DNA from ^{15}N-labeling experiments, which confer a smaller mass difference than ^{13}C-labeling experiments, have only been resolved recently (Buckley *et al.*, 2007b). Although this method is superior to bulk ^{15}N incorporation experiments in that it can indicate which organisms incorporate ^{15}N, it is limited by grouping organisms into density fractions, equivalent to ranges in ^{15}N-incorporation, instead of directly measuring a $\delta^{15}N$ value for each member of the community. In fact, CHIP-SIP, a method where the labeled nucleic acids are hybridized to biopolymer microarrays and then analyzed individually via nanoscale secondary ion mass spectrometry (NanoSIMS) has been employed to overcome the limitations of traditional DNA-SIP density fractions (CHIP-SIP; Pett-Ridge *et al.*, 2010). However, if spatial information is also desired, including chemical interactions between symbionts or variation in activity within clustered cells, whole cell visualization and analysis (e.g. FISH-NanoSIMS) rather than investigation of extracted nucleic acids must be pursued.

1.3. A case study: Coupling function and phylogeny in a diazotrophic deep-sea symbiotic archaea using FISH-NanoSIMS

In recent work, we demonstrated the ability of methane-oxidizing archaea (ANME-2c) to fix nitrogen when physically connected to a metabolically active sulfate-reducing bacterial symbiont (Dekas *et al.*, 2009). These

microorganisms are found in methane-rich marine sediment, such as methane seeps along continental margins, and have not yet been obtained in pure culture. It was hypothesized that at least one of these archaeal–bacterial symbionts was diazotrophic after the genes encoding nitrogenase, the *nif* genes, were detected in a metagenomic study of these microorganisms (Pernthaler *et al.*, 2008). To test this hypothesis, bulk methane seep sediment was anaerobically incubated with methane and ^{15}N-labeled nitrogen sources over a period of 6 months at 8 °C, a temperature approximating *in situ* conditions. Using fluorescence *in situ* hybridization (FISH) to phylogenetically identify individual microbial cells within the incubated sediment, and NanoSIMS to measure the isotopic composition of the positively hybridized microorganisms, we were able to track ^{15}N from $^{15}N_2$ into the ANME-2c biomass. This demonstrated their ability to fix nitrogen. A less enriched $^{15}N/^{14}N$ ratio was also observed in the bacterial symbiont (affiliated with the deltaproteobacterial sulfate-reducing *Desulfosarcina/Desulfococcus* lineage; Orphan *et al.*, 2001a), which in combination with molecular data collected in parallel suggested a passage of ^{15}N-labeled fixed nitrogen from the archaea to the bacteria. The FISH-NanoSIMS approach builds upon previous techniques by coupling phylogenetic identity to metabolic function at single-cell resolution. It can effectively test the hypotheses set forth by traditional bulk or molecular methods.

The following section describes the method we employed to identify the ANME-2c archaea as diazotrophs without requiring pure cultures or even sediment-free enrichments. The nanometer resolution of the NanoSIMS is particularly well suited to study small, closely associated symbiotic microorganisms and has been used in other studies to demonstrate metabolic capabilities of microorganisms as well, including nitrogen fixation in cocultures, free-living planktonic microorganisms, and symbiotic metazoans (Finzi-Hart *et al.*, 2009; Halm *et al.*, 2009; Lechene *et al.*, 2006, 2007; Ploug *et al.*, 2010; Popa *et al.*, 2007) (see Boxer *et al.*, 2009; Herrmann *et al.*, 2007b; Orphan and House, 2009 for reviews). With minor modifications (noted where possible), these procedures could be applied to a wide range of biogeochemical studies where the metabolic capability of specific microorganisms can be directly assessed on a single cell level.

2. Methods

2.1. ^{15}N-labeling sediment incubations

Methane seep sediment samples are combined with anoxic media approximately 1:1 by volume within an anaerobic chamber or under a stream of argon. Recommended media are seawater filtered through a 0.2-μm filter, preferably collected at the sampling site, or sterilized artificial seawater

modified to enrich for organisms of interest, and/or eliminate alternative nitrogen sources (such as the media described in Widdel *et al.*, 2006). Once combined, the sediment slurry is homogenized. The mixture is then equally aliquoted via volumetric pipette into sterilized serum bottles, leaving at least half of the bottle volume empty for the addition of a gas headspace. (Wheaton Science Products, Millville, NJ, #223748). Bottles are capped with butyl stoppers (Geo-Microbial Technologies, Inc., Ochelata, OK, #1313) and metal crimp seals (Wheaton, #224178-01). Using an entrance needle, which is connected to the gas tank and inserted first, and an exit needle, which is open to the air, the headspace within the bottle is flushed with methane, or the headspace gas of choice (needles: Becton Dickinson, Frankling Lakes, NJ, #305167). Previous incubation studies have shown that the rate of growth of ANME-2/*Desulfosarcina* aggregates increases with increasing methane partial pressure (Nauhaus *et al.*, 2002). By setting the methane tank regulator to the desired pressure, removing the exit needle from the incubation bottle, and only removing the entrance needle once the ripples on the surface of the sediment slurry within the bottle cease, this defined higher pressure can be achieved. A pressure of 2 bar can be safely maintained in 125 ml serum bottles and is what we routinely use for our enrichment studies. Appropriate safety precautions should be taken when over-pressurizing glass incubation bottles, as bottles can explode.

$^{15}N_2$ is commercially available (Sigma-Aldrich Isotec, #364584; Cambridge Isotopes Laboratories, NLM-363) and can be transferred several ways into the serum bottles. It is advisable to consult with a technical representative to determine which regulator would be appropriate for the particular cylinder selected. We recommend connecting a septum-fitted syringe attachment (Supelco, Bellefonte, PA, #609010) to the $^{15}N_2$ bottle (or attached regulator) and using a gas tight syringe (Becton Dickinson, #309602; Hamilton Company, GASTIGHT 1000 Series, Reno NV) to remove and transfer quantitative amounts of $^{15}N_2$. The syringe and needle should be flushed first with methane or other gas to remove air. The $^{15}N_2$ drawn from the bottle can then be added directly to the incubation bottles. Capone and Montoya (2001) report that a 0.5-ml bubble of $^{15}N_2$ in a liquid-filled 250-ml bottle is sufficient to yield bulk enrichment values of 12–13 atm% in liquid cultures, and we have observed similar enrichment values in single cells after adding 3 ml $^{15}N_2$ to the methane headspace of our 125-ml sediment incubations (approximately 1:4 liquid:headspace ratio). Adding undiluted ^{15}N-labeled dinitrogen did not have an effect on sulfate reduction in our incubations, measured by sulfide production, compared to unlabeled N_2. However, diluting $^{15}N_2$ in unlabeled N_2 may be desirable in order to provide environmentally relevant N_2 concentrations at lower cost. In this case, the isotopic composition of the dinitrogen gas mix should be determined before the experiment begins if quantitative bulk rate data are also desired. Bulk rates of nitrogen fixation can be determined following the

equations in Capone and Montoya (2001) and Montoya *et al.* (1996). Bottles should be stored inverted to minimize gas exchange across the stopper and at the *in situ* temperature. In our study of deep sea sediments the *in situ* temperature was ~8 °C.

2.2. Subsampling and preservation

Subsamples from the stoppered serum bottles can be collected outside of an anaerobic chamber using an Ar-flushed disposable needle and syringe. Opening each bottle completely at each time point is not recommended because it will require replenishing the headspace and $^{15}N_2$ gas. Care should be taken to control the plunger on the syringe when removing sediment slurry from over-pressured bottles.

Sediment subsamples for FISH-NanoSIMS analysis should be fixed with freshly prepared, 0.2 μm filtered paraformaldehyde (Electron Microscopy Sciences, Hatfield, PA, #15713) that has been diluted to 4% in 1× phosphate buffered saline (PBS). Formaldehyde, glutaraldehyde, and ethanol are alternate fixatives and can be used depending on the microbial target and sample. Subsampled sediment should be immediately dispensed into eppendorf tubes containing an equal volume of fixative, to a final paraformaldehyde concentration of 2%. Fixed samples should be incubated at room temperature for 1 h or alternatively, overnight at 4 °C. After incubation, samples are then briefly centrifuged to remove traces of fixative, the supernatant removed and disposed of as hazardous waste, and the sediment pellets resuspended and washed twice, once with PBS and once with a 1:1 mixture of PBS and ethanol. The final sediment pellets are brought up in 1 ml 100% ethanol and can be stored at −80 °C for several years (some cell loss and degradation may be observed over this time, making timely analysis of the samples preferred). Similar protocols for sediment preparation for FISH can be found in the references cited below.

2.3. Selecting and preparing microprobe slides for sample deposition

NanoSIMS sample cartridges are designed to hold round samples of 1 in., 0.5 in., or 10 mm in diameter. Samples must be conductive for analysis, making round silicon wafers (Ted Pella, Inc.) a good choice for pure cultures, when specific cells do not need to be identified as targets prior to NanoSIMS analysis. However, for analysis of seep sediment microorganisms, samples must be mapped with both epifluorescence (to recognize hybridized cells) and transmitted light (to facilitate relocating the target within the NanoSIMS via a CCD camera) prior to NanoSIMS analysis (see Section 2.6). To allow mapping with transmitted light, the sample surface must be clear. Optically clear and conductive materials are therefore

ideal for this purpose, including indium tin oxide (ITO), which can be purchased commercially and cut to size on site, or, if proper equipment is available, sputtered directly onto precut round glass microprobe slides (Lakeside Brand, Monee IL, #458; Pokaipisit *et al.*, 2007). Alternatively, cells can be mapped directly on round glass microprobe slides and then gold sputtered (30 nm) just prior to NanoSIMS analysis. Depending on the isotopes analyzed (e.g., natural abundance $\delta^{13}C$), glass microprobe slides should be precleaned and combusted to remove any organic residue and handled with gloves throughout the sample preparation. The microprobe slide of the desired material should be completely cleaned and dry before adding the sample. Using a diamond scribe, the surface can be etched with reference marks. These score marks are important to the mapping process and greatly facilitate the relocation of sample target with the NanoSIMS. We recommend that these score marks be unique and nonsymmetric and toward the center of the slide. Deep cuts that traverse the entire surface could impact conductivity and should be avoided. The deposition of regular metal grids with letter and number identifiers can also be added to the sample surface to aid in sample relocation.

2.4. Concentrating cells using density gradients and deposition onto microprobe slides

In order to streamline the FISH-NanoSIMS analysis, separating cells from sediment using a density gradient prior to deposition on the sample round is recommended. Prior separation can be particularly helpful for the detection and measurement of low abundance community members and minority morphologies and associations. Although many types of density gradients exist and may be useful for some samples, we routinely use Percoll (Sigma-Aldrich, #P4937) gradients for the concentration of ANME/SRB aggregates (>3 μm). For the separation of single cells and small cell aggregates, including the ANME-1, sucrose and Nycodenz are recommended alternatives to Percoll.

The protocol for establishing Percoll gradients has been previously described in Orphan *et al.* (2002). Briefly, Percoll and PBS are mixed 1:1 (final volume approximately 10 ml) and centrifuged at 17,000 rpm for 30 min at 4 °C. Meanwhile, fixed sediment slurry is diluted in PBS and sonicated 3 × 10 s on ice. The exact dilution ratio of slurry to PBS will depend on density of material in the sample, but a 1:20 dilution is standard. One milliliter of the sonicated, diluted sediment slurry is floated onto the top of the Percoll gradient by slowly pipet dispensing the sample down the tilted edge of the tube. The gradient is then centrifuged at 4400 rpm for 15 min at 4 °C in a swinging bucket centrifuge. For sucrose gradients: 1 volume sonicated, diluted sampled is added to 2.5 volumes 1.95 *M* sucrose,

then centrifuged at 1000 rcf for 20 min (Sigma-Aldrich, #S0389). For Nycodenz gradients: 1 volume sonicated, diluted sample is added to 3 volumes 70% by weight Nycodenz in sterile PBS and centrifuged at 12,000 rpm for 15 min (Sigma-Aldrich, #37890).

The entire fluid of the Percoll density gradient (excluding the sediment pellet) is transferred to a clean glass filter tower containing a 3-μm white polycarbonate filter (Millipore, #TSTP02500) backed with a glass microfiber filter (Millipore, GF/F, #1825-025). Percoll is difficult to filter through a pore size less than 2 μm, but water soluble Nycodenz or sucrose gradients can be used with 0.2 μm filters for single-cell investigations, as stated earlier. A low vacuum should be used to draw down the fluid, and the filter washed with several rinses of sterile PBS. Once the filter is nearly dry, it should be removed immediately from the filter tower and inverted onto the cleaned and marked microprobe slide containing a drop of deionized sterile water added to the region of the slide where the sample will be deposited. In some cases, placing the slide on a frozen block during filter inversion can increase the percentage of cells successfully transferred from the filter to the slide. The filter can be sectioned with a razor blade before inverting onto the glass round to allow the creation of several microprobe slides from a single filter (e.g., intended for different FISH probes or treatments) and to leave space for the addition of other samples and standards on the microprobe. The filter should be allowed to dry on the glass round until almost dry, but still stuck to the glass, and then gently peeled off. Depending on the sample, most material will transfer and stick to the glass.

Flow cytometry, and in particular, fluorescence-activated cell sorting (FACS), is another method to concentrate microbial cells from environmental samples before SIMS analysis. Although no published studies have combined these methods to date, FACS has been successfully coupled with bulk isotopic analysis of $\delta^{13}C$ of sorted cells (Eek *et al.*, 2007) and our lab has had success imaging ^{13}C enrichment in individual FACS sorted methanotrophic microorganisms from lake sediment using the NanoSIMS 50L (M. Kalyuzhnaya, M. Lidstrom, and V. Orphan, in preparation). However, FACS is not compatible with all samples, and sediment samples, in particular, can be problematic. Therefore, as long as mapping of hybridized target cells is performed and the desired cells are generally abundant in the sample, density gradient separation is a fast and effective method to concentrate cells from marine sediment for NanoSIMS analysis.

2.5. FISH on microprobe slide-deposited cells

There are currently several methods of FISH coupled to NanoSIMS analysis, including monolabeled FISH (Dekas *et al.*, 2009), catalyzed reporter deposition FISH (CARD-FISH) (Fike *et al.*, 2008), and FISH or CARD-FISH with halogenated probes (i.e., El-FISH, HISH-SIMS, SIMSISH) (Behrens

et al., 2008; Halm *et al.*, 2009; Li *et al.*, 2008; Musat *et al.*, 2008). In El-FISH, SIMSISH, and HISH-SIMS, a halogen (i.e., ^{19}F, ^{81}Br, ^{127}I) that is typically rare in biomass but readily detectable via NanoSIMS is attached to a particular phylogenetic group of microorganisms during a modified protocol of either monolabeled or CARD-FISH. The NanoSIMS measurement can therefore be conducted without prior mapping (Musat *et al.*, 2008) and can indicate phylogenetic identity (via detection of the halogen) and isotopic composition of the biomass simultaneously. Although a promising direction for the future, the results of this technique can be difficult to interpret in complex environmental samples, such as sediments, due to high background signal relative to the often low (~1–30 counts/pixel) signal of the added element. For this chapter, we therefore focus on standard monolabeled FISH and CARD-FISH, and how to link the phylogenetic information they provide with NanoSIMS results.

CARD-FISH allows the deposition of many fluorophores for each hybridized gene target, thereby amplifying the fluorescent signal many times over that achieved with mono label FISH. CARD-FISH is therefore particularly helpful in cells with a low number of ribosomes and samples with high autofluorescence background, such as microbial mats (Fike *et al.*, 2008). Although CARD-FISH can be successfully employed in deep-sea sediments, it is not usually necessary for the detection of AOM aggregates. AOM aggregates have a distinctive morphology and a bright mono label FISH signal due to the many ribosomes present in a single aggregate of cells. It should be noted that CARD-FISH does introduce more exogenous C and N into the cell and can therefore have an effect on sensitive isotopic analyses. The reader is referred to the following references for details on the reactions: mono-FISH (Pernthaler *et al.*, 2001) and CARD-FISH (Pernthaler and Pernthaler, 2007; Pernthaler *et al.*, 2002). The procedure for FISH hybridization on a microprobe slide is the same as that on a traditional microscope slide or filter. The cells do not typically wash off during the hybridization. Oligonucleotide probe sequences for ANME and SRB can be found in Boetius *et al.* (2000) and can be custom ordered from Sigma-Aldrich. Especially for samples that require Z-stack image collection in epifluorescence light, Alexa Fluors [rather than cyanine (Cy3 or Cy5) or fluorescein isothiocyanate (FITC)] are recommended.

In some cases, such as samples with distinct cell morphology or defined cultures, general phylogenic identifications can be inferred without FISH. Even for well-defined samples, however, some type of imaging is recommended to accompany the NanoSIMS image. For example, TEM sectioning and imaging prior to NanoSIMS analysis (Finzi-Hart *et al.*, 2009; Lechene *et al.*, 2007) or collecting scanning electron images within the NanoSIMS in parallel to the analysis (Popa *et al.*, 2007) can provide sufficient context to allow identification without FISH for some well-defined samples. Complex environmental samples, or studies targeting

morphologically standard cells, will almost always require FISH to identify the community present.

2.6. Mapping sample targets

Mapping sample targets is perhaps the most critical and time-consuming portion of this method. The goal of mapping is to identify good target cells for NanoSIMS analysis using epifluorescence microscopy and to create a map of the sample, indicating selected targets, in transmitted light at a range of magnifications (Fig. 12.1). Stitched panel images of transmitted light micrographs collected at low magnification (10× or 20× objective) will resemble the view of the sample produced by the CCD camera once the sample is loaded into the NanoSIMS. Depending on how the sample is loaded, however, the CCD image may be rotated relative to the map.

2.6.1. Selecting cells for analysis

The round microprobe slide with the hybridized cells is placed on top of a standard microscope slide and the edges fixed to the slide using standard lab tape (seen in Fig. 12.2). Securing the microprobe slide with tape is not only important for imaging using an inverted microscope, but also stabilizes the microprobe slide to prevent changes in orientation throughout the mapping procedure. If high magnification oil microscope objectives will be used, a drop of glycerol-based, water-soluble DAPI mounting medium is added to the hybridized sample, and a square coverslip placed on top, seated between the edges of the tape. To make DAPI mounting medium, combine 10 ml

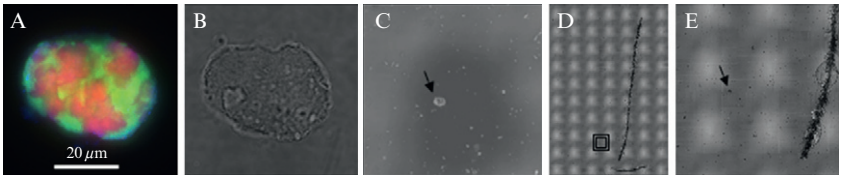

Figure 12.1 Targets for NanoSIMS analysis are identified at high magnification with epifluorescence light microscopy (A, an aggregate of cells hybridized with ANME-2 (red) and *Desulforsarcina/Desulfococcus* (green) targeted oligonucleotide probes) and then photographed in transmitted light at high (B) and lower (C) magnifications. A series of low magnification images are collected over the entire area of interest, and stitched together to create a sample map (D, double line box indicates the approximate size and location of panel C on the stitched image). The target is then located on the stitched image based on its position relative to reference-etched marks (the line visible in D and E) and distinctive neighboring particles (E). Black arrows point to the target identified in A and B. The etch marks will be visible in the NanoSIMS CCD camera, allowing the relocation of the identified target without epifluorescence microscopy.

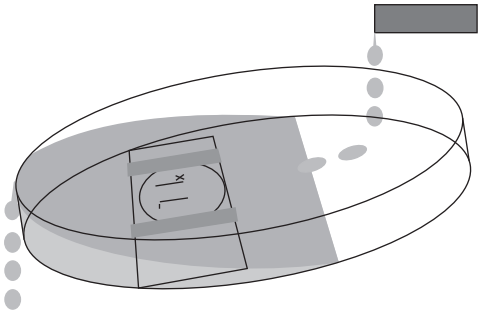

Figure 12.2 The round microprobe slide with etched reference marks is taped to a traditional rectangular microscope slide. After mapping with oil at high resolution, the cover slip can be slid off the side, and the DAPI mounting medium can be slowly rinsed with water indirectly in a tilted Petri dish.

citifluor mountant media (Ted Pella, #19470) with 1 ml 0.2 μm filtered PBS and 50 μl of 1 mg/ml DAPI (Sigma, #D8417). The sample should be stored in the dark for at least 15 min to allow the DAPI to fully permeate the cells prior to imaging with epifluorescence. If high resolution, high magnification epifluorescence images are not required, dry objectives can be used exclusively (Orphan *et al.*, 2001b). Dry objectives have the advantage of not requiring the addition of mounting medium to the slide, eliminating the possibility of losing targets during the washing procedure or of incomplete removal of exogenous material.

We use an Applied Precision DeltaVision RT microscope equipped with the Softworx software package. In particular, the automated stage and ability to store and relocate X,Y locations as well as collect and stitch low magnification panel images in Softworx make the system ideal for sample mapping. However, it is possible to map samples with any microscope with a mounted camera (see our recommendations at the end of this section). If using a system like ours, the first step is to locate the etched reference lines on the microprobe slide (see previous section). Once these markings are located and the X,Y positions stored, the sample can be investigated for positively hybridized cells.

Preferred NanoSIMS targets are clean of contaminating materials such as undesired neighboring cells and sediment particles, but close to (~20–100 μm distance) reference marks or other distinctive particles. Proximity to reference marks allows for easier recognition with the NanoSIMS CCD camera. One advantage of NanoSIMS analysis is that cells do not have to be completely separated from other particles, since the measurement will not be averaged over the entire analysis space. During analysis with conventional ion microprobes, such as the CAMECA 1270 ims, with a 10–15 μm spot size for the primary beam, complete separation of the target cell is

necessary to get an accurate measurement. The small beam diameter of the NanoSIMS and ion-imaging capabilities enables the selection of "regions of interest" from a complex field of view during postacquisition data analysis. Still, minimizing the material within the analysis frame simplifies identifying the target cell (see Fig. 12.1; a well-separated target). Good targets should be photographed at high magnification (we use a 60× oil objective for aggregates of cells, but a 100× objective may be preferred for single cells) (Fig. 12.1A), including acquisition of a z-stack (for 3D reconstruction), and their X,Y location should be saved. All targets should also be imaged in transmitted or reflected light at high magnification (Fig. 12.1B). At least five times the number of targets desired for analysis should be mapped due to sample loss in washing and difficulty refinding targets with the NanoSIMS.

2.6.2. Creating the map

Once all targets are identified, photographed in both epifluorescence and transmitted light, and their locations recorded, the microscope slide can be removed from the microscope and the taped-on microprobe slide gently cleaned of the DAPI mounting medium. Cleaning is accomplished by sliding the coverslip off, placing the attached slides in a slightly tilted Petri dish, and adding a slow stream of DI water to the raised end of the tilted dish (Fig. 12.2). The mounting medium will float in the water and wash out over the lower side of the dish with the water flow. Complete removal of the DAPI mounting medium requires about 5 min in the flowing water bath. Placing the slide directly in the stream of water or washing too rigorously could lead to sample loss or the detachment of cells and material from the slide. The microprobe slide (still taped to the microscope slide) is then dipped in ethanol (100%), air dried in the dark, and returned to the microscope in exactly the same position that it was previously.

All targets should then be revisited using a lower magnification, dry objective (e.g., 40× and/or 20× and 10×) and reimaged using transmitted or reflected light. These transmitted light micrographs more closely approximate the morphology of the target visible with the NanoSIMS CCD, assisting with confirmation of the target during analysis. Small adjustments in position may be necessary to ensure that the targets are in view when their stored X,Y positions are revisited with the software package. Finally, a 10× stitched image is created of the sample area containing both the reference marks and the sample targets (Fig. 12.1D). This can also be collected and stitched manually using image processing software such as Adobe Photoshop. It is useful to set the resolution of the stitched image such that individual features are still visible when zooming in on regions of interest. An image of the location of the saved targets and reference points as well as X,Y coordinates should also be saved. Then, starting with the highest magnification image, a target can be found by eye in the series of

transmitted light images based on its morphology and orientation with respect to other nearby particles. Once located at high magnification, cell targets should be identified in the lower magnification photomicrographs and finally on the stitched image (Fig. 12.1E). Annotation of target locations on the map (consisting of the low magnification stitched image of the reference marks and targets) can be assembled in either Adobe Photoshop or Illustrator, or other image visualization software.

If using a system without point relocation capabilities, dry objectives are recommended. Each time a target is identified, the entire set of images (60×, 40×, and 10× magnifications) should be taken before moving to the next target. Additionally, a series of overlapping low magnification (10×) images should be collected and manually aligned to create a single image between the nearest reference mark and the target. The entire process—the series of images at different magnifications and the overlapping path of images to the nearest reference mark—is repeated for each additional target.

2.7. Sectioning samples prior to analysis

Sectioning cells prior to NanoSIMS analysis is optional but can improve measurements. Perfectly flat samples are generally recommended for SIMS analysis to reduce artifacts due to variable sample topology (Orphan and House, 2009). Additionally, although the destructive nature of the NanoSIMS primary ion beam allows for analysis with depth, in some cases, higher resolution of internal cellular components can be achieved with prior sectioning. Focused ion beam (FIB) sectioning uses a narrow primary beam (such as Ga^+) to sputter away layers of material, exposing a flat and fresh interior surface (Fig. 12.3). This sputtering approach differs from that of the NanoSIMS because the beam can be applied parallel to the sample surface instead of normal to it. During perpendicular sputtering, the variable sputtering efficiency in a heterogeneous material such as a cell, or cell in sediment can result in uneven material removal and slightly irregular surface. With parallel sputtering, the beam can fully remove any material over a particular sample height (Fig. 12.3B). The FIB can be used to section samples in two ways: the first is by parallel sputtering, and the second is by creating a vertical thin section by removing the material on either side of the vertical section and then laying the section on its side (Weber *et al.*, 2009). It is also possible to embed cells or tissue in epoxy resin and create thin sections using an ultramicrotome or other device (Herrmann *et al.*, 2007a; Lechene *et al.*, 2007; Slaveykova *et al.*, 2009); however, in complex samples (i.e., natural sediments), locating the target cells of interest in the resin block is challenging and requires production and screening of many thin sections. For stable isotope tracer experiments not requiring high intracellular spatial resolution, for instance, when magnitude of incorporation is desired (i.e., evidence of nitrogen fixation), or gross trends in

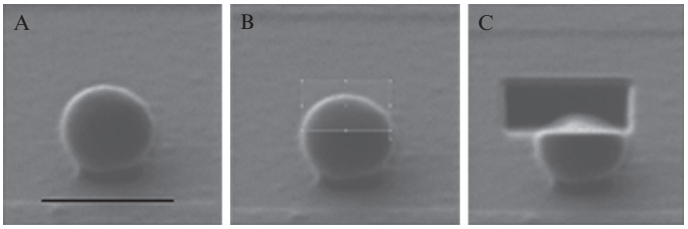

Figure 12.3 Cells can be sectioned prior to NanoSIMS analysis with a focused ion beam (FIB). Scale bar in A represents 1 μm. A bacterial spore is imaged via scanning electron microscopy (SEM) at a 60° angle from the surface (A). The area to be removed is identified (B), and a focused Ga^+ beam sputters away the material (C).

intracellular concentrations are sufficient, whole cell analysis with no prior sectioning is recommended (Ghosal *et al.*, 2008).

2.8. NanoSIMS analysis

NanoSIMS instruments use a high-energy focused primary ion beam, typically Cs^+ or O^-, with a diameter ranging from 50 to 150 nm to bombard, embed within, and sputter secondary ions from the sample surface. These charged secondary ions are focused through a series of lenses, separated via differences in momentum due to mass and charge, and counted using electron multipliers or faraday cups. For the latest generation CAMECA NanoSIMS 50L instrument, up to seven ions can be simultaneously collected from the same sample volume. By rastoring the small primary ion beam across an area of the sample, an ion image is created, displaying the number of ions collected for each pixel of the image. As NanoSIMS analysis is a destructive process, repeated rastor cycles over the same area provide analysis with increasing depth into the sample. These individual images can be merged together to increase the number of ions per pixel, or alternatively, single layers can be compared to create a three-dimensional ion representation of the target (Fig. 4 in Finzi-Hart *et al.*, 2009 and Fig. 3 in Dekas *et al.*, 2009). The depth resolution of the NanoSIMS using a Cs^+ primary beam has been measured to be 14.3 nm, which is greater than the lateral resolution (Ghosal *et al.*, 2008). This feature can be particularly useful when examining closely associated microorganisms in consortia, such as the ANME–SRB aggregates.

While interest and acquisition of NanoSIMS instruments is increasing at universities worldwide, there are currently only 27 instruments in operation at the time of this printing. However, many of the instruments at universities are available to visitors and the managers can be contacted with inquiries for use. Full-time support staff typically oversees the daily operation of the NanoSIMS instruments and may be available to assist with

instrument operation and set up. We will not describe the setup, tuning, or use of the NanoSIMS here, but we refer the reader to the CAMECA website to learn more: www.cameca.com/instruments-for-research/NanoSIMS.aspx.

2.8.1. Sample preparation

The NanoSIMS operates under ultrahigh vacuum and biological samples that are not completely dehydrated or which are prepared with an inappropriate type of embedding resin can lead to analysis delays due to sample off gassing. Dehydration steps using ethanol, such as those which are routine after FISH, can assist with drying prior to SIMS analysis. If the microprobe slide is not conductive, or if the sample occupies a large area of the slide (such as a millimeter-scale microbial mat thin section; Fike *et al.*, 2008), the sample must be sputter coated with a conductive metal (e.g., 30 nm gold) prior to analysis by SIMS, similar to standard preparations for SEM analysis. NanoSIMS facilities typically have sputter coaters on site for this purpose.

2.8.2. Sample analysis

Optimizing ion counts for single microbial cells can be a challenge because cells are small targets and contain elements with low sputtering efficiencies. For instance, the lack of useful secondary ion formation by the element nitrogen (mass 14, 15) has led to the routine analysis of the molecular cyanide ion (CN^-, mass 25, 26) as a proxy for nitrogen (McMahon *et al.*, 2006; Peteranderl and Lechene, 2004). Additionally, some studies have collected the molecular C_2^- mass rather than C^- to increase the carbon ions collected (Orphan *et al.*, 2001b, 2002). Furthermore, organic material, and particularly single cells, can sputter away quickly depending on the intensity of the primary beam. It is therefore recommended that tuning take place on a nearby nontarget cell rather than the cell of interest. The primary ion beam can also be adjusted to a lower intensity, more narrow focus, and shorter dwell time to allow the collection of the most highly resolved datasets in both the planar and Z dimensions. Analysis acquisition can be performed in two main modes: image acquisition and numerical isotope acquisition.

2.8.3. Standards

Element abundance and isotopic measurements acquired with the NanoSIMS may be precise but not accurate. The inaccuracy can be due to several instrumental factors (Slodzian, 2004) as well as the matrix effects in the sample itself (Herrmann *et al.*, 2007b). It is therefore necessary to measure standards not only of known elemental abundance and isotopic composition, but the standard should be composed of material as similar in physical

structure and elemental composition as the sample itself. Information on selecting appropriate standards can be found in Davission *et al.* (2008), Herrmann *et al.* (2007b), and Orphan and House (2009). We routinely use two standards. The first is a polished piece of graphite of known C isotopic composition. The second is a pure culture of cells (either *Escherichia coli* or *Clostridia* spores) prepared before each NanoSIMS session by dotting PBS or water-washed cells onto a clean area on the same microprobe slide as the sample. An aliquot of the same culture is then measured via elemental analysis isotope ratio mass spectrometry (EA-IRMS) for bulk elemental and isotope information. The variation within these pure cultures is typically within 10‰ in both $\delta^{13}C$ and $\delta^{15}N$ (Orphan and House, 2009). Greater than 10 cells in the pure cultures are measured with the same analysis parameters as the sample during each standard run, which is repeated before and after analysis sessions. These standard measurements enable the user to correct for matrix effects and instrumental mass fractionation during the analysis (Orphan and House, 2009). Precision on NanoSIMS measurements is usually controlled by counting statistics, which is described in Fitzsimons *et al.* (2000).

2.9. Interpreting NanoSIMS results

Several software programs are available to assist in analyzing NanoSIMS data, such as the program L'IMAGE PV-WAVE (written by Larry Nittler) and a free downloadable add-on to ImageJ (http://rsbweb.nih.gov/ij/, add-on OpenMIMS). Matlab scripts can also be created to analyze the raw output data directly, depending on the scientific question(s) and data processing required. Examples of strategies of data processing, including extracting data from individual regions of interest, and investigating isotopic composition with depth into the sample, can be found in the articles referenced in this chapter (for example, Dekas *et al.*, 2009, Finzi-Hart *et al.*, 2007, Lechene *et al.*, 2007).

Correlating FISH and NanoSIMS images is critical for this method, as it provides the link between 16S identity and metabolic activity. For a well-mapped sample, this process only requires looking at the two corresponding images and adjusting for slight rotations. For roughly symmetrical targets, such as spherical ANME–SRB aggregates, it is often helpful to correlate the images of nearby asymmetrical targets analyzed on the same microprobe round first, to ensure that the correct rotations are applied.

Direct coregistration of FISH and NanoSIMS images can be challenging for some samples due to image aberrations and sample topography. A technique to aid in image correlation that is currently under development is the use of functionalized quantum dots (QD) for intracellular rRNA or protein detection. QD are nanometer-sized fluorescent particles with a

heavy metal core, such as Se and Cd. Selenium (mass 78.9) is a moderate negative secondary ion producer and in theory can be used for ion imaging and spatial localization of QD-bound intracellular biomolecules or cell surface constituents in microbial cells. QD or gold particles, commonly applied in immunofluorescence staining, may also be used as cell-associated reference markers to assist in coregistering paired FISH and secondary ion images and identification of possible aberrations or shifts in the ion image during acquisition.

As mentioned previously, it is frequently recommended that flat and polished samples (e.g., thin sections or TEM preparations) be used for SIMS analysis for optimal spatial resolution and to minimize potential artifacts from uneven sample topology. While the benefit of prepolishing has been studied to some extent in geological materials and biological tissues, a comprehensive investigation of the specific effects of topography and uneven sputtering for microbial cell aggregates and heterogeneous environmental samples is still lacking. It is an important consideration when attempting to directly correlate a series of images of the same target generated with a NanoSIMS and generated with a microscope, or construct and compare 3-D representations. The NanoSIMS will generate secondary ions from the entire exposed surface of a target, which would be a curved, hemispherical plane in the case of a cell or aggregate of cells. Theoretically, the topology of the sample surface is then propagated throughout a depth analysis, yielding successive curved layers, and shrinking the lateral size of the target as the edges sputter to completion. (Although the edges may be subject to a lesser sputter rate than the center, due to the decreased angle of incidence of the primary beam, they will likely still sputter to completion before the center of the target because of the difference in thickness.) The resulting series of 2-D NanoSIMS images with depth may actually represent a series of more complex 3-D planes of analysis (Fig. 12.4, right). The NanoSIMS output with depth may therefore not be perfectly consistent with a paired Z-stack of images collected with a confocal microscope, or generated with deconvolution software, where each image represents a planar field of depth (Fig. 12.4).

We observed experimental support for this concept while analyzing seven roughly ellipsoidal aggregates with curved, dome-like surfaces. Although the diameters of these aggregates clearly increased with depth in the individual deconvolved Z-stack images collected by epifluorescence microscopy, the diameters of the of aggregates only decreased with increasing cycle number in the NanoSIMS image acquisition (Fig. 12.4). Further work is required to better understand the influence of geometry on the sputtering of biological targets, but for analyses requiring more than broad trends with depth, we encourage researchers to consider potential distortions.

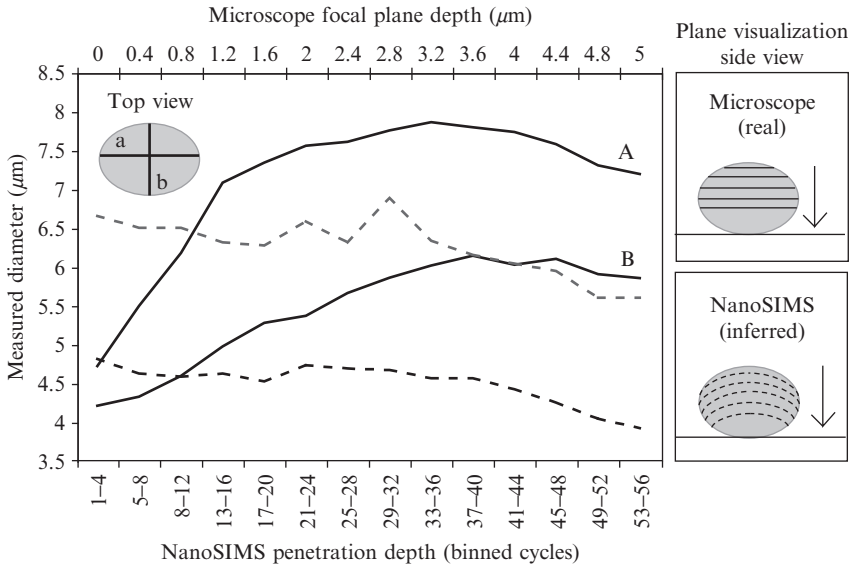

Figure 12.4 **The geometry of the plane of NanoSIMS analysis depends on sample surface topology. Diameters of a single cellular aggregate measured on images collected with depth, created by deconvolved epifluorescence microscopy (solid line) and NanoSIMS (dashed line), show different trends. Diameters were collected in two directions perpendicular to each other for each type of analysis (A and B). A proposed explanation is that although the microscope images with depth represent parallel planes through the target, the NanoSIMS images may represent curved, peel-like layers as the curved surface topology is propagated throughout the sample.**

2.10. Complementary additional analyses

Several analyses can be performed in addition to FISH and NanoSIMS imaging to support and enhance the data collected. The sample height can be measured with atomic force microscopy (AFM) or a profilometer before and after the SIMS analysis to quantify the depth of sample measured. The depth penetrated by the primary ion beam depends on instrument parameters and tuning as well as the nature of the sample material (as previously mentioned), making the sputter rate variable. The depth therefore must be determined on individual targets by measuring sample height before and after analysis if an exact value is desired. Additionally, sample visualization with either AFM or scanning electron microscopy (SEM) postanalysis can confirm the geometry of the rastor region. Although theoretically a rastor region is always a perfect square, nonoptimized instrument setup can result in a skewing of this region. The sputtered area can be visualized using these methods and any rastor area aberrations can be observed.

2.11. Measuring metal cofactors as indicators of nitrogenase

Traditional nitrogenase consists of an Fe protein as well as an MoFe protein; however, alternative nitrogenases do not require Mo and instead use V or additional Fe (Eady, 1996). Theoretically, these metals can be measured via NanoSIMS analysis in individual cells and used to provide independent information on the type of nitrogenase produced by specific microorganisms, and/or locate sites of active nitrogen fixation (e.g., Mo enrichment in heterocysts of cyanobacteria; Pett-Ridge *et al.*, 2006). However, these analyses are challenging due to the low abundance of the metals of interest and possibility of background contamination. Additionally, the greatest ionization potential for most biologically relevant trace metals is typically as a positively charged secondary ion, which is created using a negative primary ion beam O^-, rather than Cs^+. Therefore, there is a trade-off between obtaining the maximal secondary ion yield from trace metals (using O^-) and the simultaneous analysis of other biologically important ions such as carbon, nitrogen and sulfur (by Cs^+).

In a pilot study performed on *Azotobacter*, a diazotroph with the genetic make-up to generate traditional nif, vnf, and anf forms of nitrogenase, we analyzed cells grown in different metal concentrations under nitrogen fixing conditions using a O^- primary ion beam with the CAMECA NanoSIMS 50L (James Howard, A. Dekas, and V. Orphan, unpublished data). The data collected in spot analysis mode indicated that the intracellular concentration of the three metals varied in three *Azotobacter* cultures, suggesting that the diazotrophic cells were synthesizing different forms of nitrogenase in each. While these controlled pure culture studies lack the complications of single-cell analysis in environmental samples, these and previously collected data (Pett-Ridge *et al.*, 2006; Slaveykova *et al.*, 2009) suggest that the NanoSIMS holds promise for quantifying the variation and spatial distribution of trace metals relevant to nitrogen fixation within and between microorganisms.

3. Concluding Remarks

FISH-NanoSIMS is a powerful tool in the investigation of metabolic activity in environmental microorganisms. The technique is particularly useful in single-cell observations of nitrogen fixation via ^{15}N incorporation from $^{15}N_2$ and has elucidated processes involved in nitrogen-based symbioses as well as identified new and unexpected diazotrophs. The strength of FISH-NanoSIMS is largely in its ability to bridge the gap between geochemical and molecular biological studies, linking cells of a particular species or group with a specific metabolism. However, the additional information accessible with this method, including patterns of substrate

sharing between cells, variations in metabolic rates between members of the same community, and temporal and physical separation of particular intracellular activities, can also greatly improve our understanding of microbial ecosystems. With the installation of NanoSIMS at a growing number of institutes worldwide, we anticipate that the application of this technology to environmental microbiology will continue and expand for years to come.

ACKNOWLEDGMENTS

We thank Christopher House, Yunbin Guan, John Eiler, Kendra Turk, Annelie Pernthaler, Sameer Walavalkar, Kevin McKeegan, Raj Singh, and Mark Ellisman for helping to develop and optimize the method. We thank James Howard, Sameer Walavalkar, and Eric Matson for sample and data contributions to this chapter. We also thank two anonymous reviewers for helpful suggestions. This research was supported by grants from the Department of Energy (Career award, #DE-SC0003940) and Gordon and Betty Moore Foundation (to VJO) and the National Science Foundation (graduate fellowship to AED).

REFERENCES

Behrens, S., Losekann, T., Pett-Ridge, J., Weber, P. K., Ng, W.-O., Stevenson, B. S., Hutcheon, I. D., Relman, D. A., and Spormann, A. M. (2008). Linking microbial phylogeny to metabolic activity at the single-cell level by using enhanced element labeling-catalyzed reporter deposition fluorescence in situ hybridization (EL-FISH) and NanoSIMS. *Appl. Environ. Microbiol.* **74,** 3143–3150.

Boetius, A., Ravenschlag, K., Schubert, C. J., Rickert, D., Widdel, F., Gieseke, A., Amann, R., Jorgensen, B. B., Witte, U., and Pfannkuche, O. (2000). A marine microbial consortium apparently mediating anaerobic oxidation of methane. *Nature* **407,** 623–626.

Boxer, S. G., Kraft, M. L., and Weber, P. K. (2009). Advances in imaging secondary ion mass spectrometry for biological samples. *Annu. Rev. Biophys.* **38,** 53–74.

Brandes, J. A., and Devol, A. H. (2002). A global marine-fixed nitrogen isotopic budget: Implications for Holocene nitrogen cycling. *Global Biogeochem. Cycles* **16,** 1120–1134.

Brandes, J. A., Devol, A. H., and Deutsch, C. (2007). New developments in the marine nitrogen cycle. *Chem. Rev.* **107,** 577–589.

Buckley, D. H., Huangyutitham, V., Hsu, S. F., and Nelson, T. A. (2007a). Stable isotope probing with 15N2 reveals novel noncultivated diazotrophs in soil. *Appl. Environ. Microbiol.* **73,** 3196–3204.

Buckley, D. H., Huangyutitham, V., Hsu, S. F., and Nelson, T. A. (2007b). Stable isotope probing with 15N achieved by disentangling the effects of genome G+C content and isotope enrichment on DNA density. *Appl. Environ. Microbiol.* **73,** 3189–3195.

Capone, D. G., and Montoya, J. (2001). Nitrogen fixation and denitrification. *Methods Microbiol.* **30,** 501–513.

Capone, D. G. (1988). Benthic nitrogen fixation. *In* "Nitrogen Cycling in Coastal Marine Environments," (T. H. Blackburn and J. Sorensen, eds.), pp. 85–123. John Wiley & Sons, New York.

Capone, D. G. (2001). Marine nitrogen fixation: What's the fuss? *Curr. Opin. Microbiol.* **4,** 341–348.

Capone, D. G., Zehr, J. P., Paerl, H. W., Bergman, B., and Carpenter, E. J. (1997). Trichodesmium, a globally significant marine cyanobacterium. *Science* **276,** 1221–1229.

Codispoti, L. A. (1995). Is the ocean losing nitrate? *Nature* **376,** 724.
Codispoti, L. A. (2007). An oceanic fixed nitrogen sink exceeding 400 Tg Na-1 vs the concept of homeostasis in the fixed-nitrogen inventory. *Biogeosciences* **4,** 233–253.
Codispoti, L. A., Brandes, J. A., Christensen, J. P., Devol, A. H., Naqvi, S. W. A., Paerl, H. W., and Yoshinari, T. (2001). The oceanic fixed nitrogen and nitrous oxide budgets: Moving targets as we enter the anthropocene? *Sci. Mar.* **65,** 85–105.
Codispoti, L. A., and Christensen, J. P. (1985). Nitrification, denitrification, and nitrous oxide cycling in the eastern tropical South Pacific ocean. *Mar. Chem.* **16,** 277–300.
Davission, M. L., Weber, P. K., Pett-Ridge, J., and Singer, S. (2008). Development of standards for NanoSIMS analyses of biological materials. pp. 1–39. L.L.N. Laboratory, Livermore, CA. DOI: 10.2172/945782.
Dekas, A. E., Poretsky, R. S., and Orphan, V. J. (2009). Deep-sea archaea fix and share nitrogen in methane-consuming microbial consortia. *Science* **326,** 422–426.
Dumont, M. G., and Murrell, J. C. (2005). Stable isotope probing—Linking microbial identity to function. *Nat. Rev. Microbiol.* **3,** 499–504.
Eady, R. R. (1996). Structureminus signfunction relationships of alternative nitrogenases. *Chem. Rev.* **96,** 3013–3030.
Eek, K. M., Sessions, A. L., and Lies, D. P. (2007). Carbon-isotopic analysis of microbial cells sorted by flow cytometry. *Geobiology* **5,** 85–95.
Fike, D. A., Gammon, C. L., Ziebis, W., and Orphan, V. J. (2008). Micron-scale mapping of sulfur cycling across the oxycline of a cyanobacterial mat: A paired NanoSIMS and CARD-FISH approach. *ISME J.* **2,** 749–759.
Finzi-Hart, J. A., Pett-Ridge, J., Weber, P. K., Popa, R., Fallon, S. J., Gunderson, T., Hutcheon, I. D., Nealson, K. H., and Capone, D. G. (2009). Fixation and fate of C and N in the cyanobacterium Trichodesmium using nanometer-scale secondary ion mass spectrometry. *Proc. Natl. Acad. Sci. USA* **106,** 6345–6350.
Fitzsimons, I. C. W., Harte, B., and Clark, R. M. (2000). SIMS stable isotope measurement: Counting statistics and analytical precision. *Mineralog. Mag.* **64,** 59–83.
Foster, R. A., Subramaniam, A., and Zehr, J. P. (2009). Distribution and activity of diazotrophs in the Eastern Equatorial Atlantic. *Environ. Microbiol.* **11,** 741–750.
Fulweiler, R. W. (2009). Microbiology. Fantastic fixers. *Science* **326,** 377–378.
Fulweiler, R. W., Nixon, S. W., Buckley, B. A., and Granger, S. L. (2007). Reversal of the net dinitrogen gas flux in coastal marine sediments. *Nature* **448,** 180–182.
Ganeshram, R. S., Pedersen, T. F., Calvert, S. E., and Murray, J. W. (1995). Large changes in oceanic nutrient inventories from glacial to interglacial periods. *Nature* **376,** 755–758.
Ghosal, S., Fallon, S. J., Leighton, T. J., Wheeler, K. E., Kristo, M. J., Hutcheon, I. D., and Weber, P. K. (2008). Imaging and 3D elemental characterization of intact bacterial spores by high-resolution secondary ion mass spectrometry. *Anal. Chem.* **80,** 5986–5992.
Gruber, N., and Sarmiento, J. L. (1997). Global patterns of marine nitrogen fixation and denitrification. *Glob. Biogeochem. Cycles* **11,** 235–266.
Halm, H., Musat, N., Lam, P., Langlois, R., Musat, F., Peduzzi, S., Lavik, G., Schubert, C. J., Sinha, B., LaRoche, J., and Kuypers, M. M. (2009). Co-occurrence of denitrification and nitrogen fixation in a meromictic lake, Lake Cadagno (Switzerland). *Environ. Microbiol.* **11,** 1945–1958.
Herbert, R. A. (1999). Nitrogen cycling in coastal marine ecosystems. *FEMS Microbiol. Rev.* **23,** 563–590.
Herrmann, A. M., Clode, P. L., Fletcher, I. R., Nunan, N., Stockdale, E. A., O'Donnell, A. G., and Murphy, D. V. (2007a). A novel method for the study of the biophysical interface in soils using nano-scale secondary ion mass spectrometry. *Rapid Commun. Mass Spectrom.* **21,** 29–34.

Herrmann, A. M., Ritz, K., Nunan, N., Clode, P. L., Pett-Ridge, J., Kilburn, M. R., Murphy, D. V., O'Donnell, A. G., and Stockdale, E. A. (2007b). Nano-scale secondary ion mass spectrometry—A new analytical tool in biogeochemistry and soil ecology: A review article. *Soil Biol. Biochem.* **39,** 1835–1850.

Howarth, R. W., Marino, R., and Lane, J. (1988). Nitrogen fixation in freshwater, estuarine, and marine ecosystems. 1. Rates and importance. *Limnol. Oceanogr.* **33,** 669–687.

Karl, D., Michaels, A., Bergman, B., Capone, D., Carpenter, E., Letelier, R., Lipschultz, F., Paerl, H., Sigman, D., and Stal, L. (2002). Dinitrogen Fixation in the world's oceans. *Biogeochemistry* **57/58,** 47–98.

Kechris, K. J., Lin, J. C., Bickel, P. J., and Glazer, A. N. (2006). Quantitative exploration of the occurrence of lateral gene transfer by using nitrogen fixation genes as a case study. *Proc. Natl. Acad. Sci. USA* **103,** 9584–9589.

Kessler, P. S., and Leigh, J. A. (1999). Genetics of nitrogen regulation in *Methanococcus maripaludis*. *Genetics* **152,** 1343–1351.

Lechene, C., Hillion, F., McMahon, G., Benson, D., Kleinfeld, A. M., Kampf, J. P., Distel, D., Luyten, Y., Bonventre, J., Hentschel, D., Park, K. M., Ito, S., *et al.* (2006). High-resolution quantitative imaging of mammalian and bacterial cells using stable isotope mass spectrometry. *J. Biol.* **5,** 20.

Lechene, C. P., Luyten, Y., McMahon, G., and Distel, D. L. (2007). Quantitative imaging of nitrogen fixation by individual bacteria within animal cells. *Science* **317,** 1563–1566.

Li, T., Wu, T. D., Mazeas, L., Toffin, L., Guerquin-Kern, J. L., Leblon, G., and Bouchez, T. (2008). Simultaneous analysis of microbial identity and function using NanoSIMS. *Environ. Microbiol.* **10,** 580–588.

Liang, J. H., Nielsen, G. M., Lies, D. P., Burris, R. H., Roberts, G. P., and Ludden, P. W. (1991). Mutations in the draT and draG genes of Rhodospirillum rubrum result in loss of regulation of nitrogenase by reversible ADP-ribosylation. *J. Bacteriol.* **173,** 6903–6909.

Mahaffey, C., Michaels, A. F., and Capone, D. G. (2005). The conundrum of marine N2 fixation. *Am. J. Sci.* **305,** 546–595.

McElroy, M. B. (1983). Marine biological controls on atmospheric CO_2 and climate. *Nature* **302,** 328–329.

McMahon, G., Saint-Cyr, H. F., Lechene, C., and Unkefer, C. J. (2006). CN- secondary ions form by recombination as demonstrated using multi-isotope mass spectrometry of 13C- and 15N-labeled polyglycine. *J. Am. Soc. Mass Spectrom.* **17,** 1181–1187.

Mehta, M. P., Butterfield, D. A., and Baross, J. A. (2003). Phylogenetic diversity of nitrogenase (nifH) genes in deep-sea and hydrothermal vent environments of the Juan de Fuca Ridge. *Appl. Environ. Microbiol.* **69,** 960–970.

Miyazaki, J., Higa, R., Toki, T., Ashi, J., Tsunogai, U., Nunoura, T., Imachi, H., and Takai, K. (2009). Molecular characterization of potential nitrogen fixation by anaerobic methane-oxidizing archaea in the methane seep sediments at the number 8 Kumano Knoll in the Kumano Basin, offshore of Japan. *Appl. Environ. Microbiol.* **75,** 7153–7162.

Moisander, P. H., Beinart, R. A., Hewson, I., White, A. E., Johnson, K. S., Carlson, C. A., Montoya, J. P., and Zehr, J. P. (2010). Unicellular cyanobacterial distributions broaden the oceanic N2 fixation domain. *Science* **327,** 1512–1514.

Montoya, J. P., Voss, M., Kahler, P., and Capone, D. G. (1996). A Simple, high-precision, high-sensitivity tracer assay for N(inf2) fixation. *Appl. Environ. Microbiol.* **62,** 986–993.

Musat, N., Halm, H., Winterholler, B. R., Hoppe, P., Peduzzi, S., Hillion, F., Horreard, F., Amann, R., Jørgensen, B. B., and Kuypers, M. M. M. (2008). A single-cell view on the ecophysiology of anaerobic phototrophic bacteria. *Proc. Natl. Acad. Sci. USA* **105,** 17861–17866.

Nauhaus, K., Boetius, A., Kruger, M., and Widdel, F. (2002). In vitro demonstration of anaerobic oxidation of methane coupled to sulphate reduction in sediment from a marine gas hydrate area. *Environ. Microbiol.* **4,** 296–305.

Oremland, R. S., and Taylor, B. F. (1975). Inhibition of methanogenesis in marine sediments by acetylene and ethylene: validity of the acetylene reduction assay for anaerobic microcosms. *Appl. Microbiol.* **30,** 707–709.

Orphan, V. J., Hinrichs, K. U., Ussler, W., 3rd, Paull, C. K., Taylor, L. T., Sylva, S. P., Hayes, J. M., and Delong, E. F. (2001a). Comparative analysis of methane-oxidizing archaea and sulfate-reducing bacteria in anoxic marine sediments. *Appl. Environ. Microbiol.* **67,** 1922–1934.

Orphan, V. J., and House, C. H. (2009). Geobiological investigations using secondary ion mass spectrometry: Microanalysis of extant and paleo-microbial processes. *Geobiology* **7,** 360–372.

Orphan, V. J., House, C. H., Hinrichs, K. U., McKeegan, K. D., and DeLong, E. F. (2001b). Methane-consuming archaea revealed by directly coupled isotopic and phylogenetic analysis. *Science* **293,** 484–487.

Orphan, V. J., House, C. H., Hinrichs, K. U., McKeegan, K. D., and DeLong, E. F. (2002). Multiple archaeal groups mediate methane oxidation in anoxic cold seep sediments. *Proc. Natl. Acad. Sci. USA* **99,** 7663–7668.

Pernthaler, A., Dekas, A. E., Brown, C. T., Geoffredi, S. K., Embaye, T., and Orphan, V. J. (2008). Diverse syntrophic partnerships from deep-sea methane vents revealed by direct cell capture and metagenomics. *Proc. Natl. Acad. Sci. USA* **105,** 7052–7057.

Pernthaler, A., and Pernthaler, J. (2007). Fluorescence in situ hybridization for the identification of environmental microbes. *Methods Mol. Biol.* **353,** 153–164.

Pernthaler, A., Pernthaler, J., and Amann, R. (2002). Fluorescence in situ hybridization and catalyzed reporter deposition for the identification of marine bacteria. *Appl. Environ. Microbiol.* **68,** 3094–3101.

Pernthaler, J., Glöckner, F.-O., Schönhuber, W., and Amann, R. (2001). Fluorescence in situ hybridization (FISH) with rRNA-targeted oligonucleotide probes. *Methods Microbiol.* **30,** 207–226.

Peteranderl, R., and Lechene, C. (2004). Measure of carbon and nitrogen stable isotope ratios in cultured cells. *Am. Soc. Mass Spectrom.* **15,** 478–485.

Pett-Ridge, J., Mayali, X., DeSantis, T., Karaoz, U., Andersen, G., Mabery, S., Hoeprich, P., Weber, P., and Brodie, E. (2010). CHIP-SIP: Linking Microbial Identity to Function in Marine and Terrestrial Systems. ISME-13 Stewards of a Changing Planet, Seattle, WA, Abstract CT11.001.

Pett-Ridge, J., Weber, P. K., Finzi, J., Hutcheon, I. D., and Capone, D. G. (2006). NanoSIMS Analyses of Mo Indicate Nitrogenase Activity and Help Solve a N and C Fixation Puzzle in a Marine Cyanobacterium. American Geophysical Union Annual Meeting, Abstract #B23D-1111. San Francisco, CA.

Ploug, H., Musat, N., Adam, B., Moraru, C. L., Lavik, G., Vagner, T., Bergman, B., and Kuypers, M. M. (2010). Carbon and nitrogen fluxes associated with the cyanobacterium *Aphanizomenon* sp. in the Baltic Sea. *ISME J.* **4,** 1215–1223.

Pokaipisit, A., Horprathum, M., and Limsuwan, P. (2007). Effect of films thickness on the properties of ITO thin films prepared by electron beam evaporation. *Kasetsart J.* **41,** 255–261.

Popa, R., Weber, P. K., Pett-Ridge, J., Finzi, J. A., Fallon, S. J., Hutcheon, I. D., Nealson, K. H., and Capone, D. G. (2007). Carbon and nitrogen fixation and metabolite exchange in and between individual cells of *Anabaena oscillarioides*. *ISME J.* **1,** 354–360.

Short, S. M., and Zehr, J. P. (2005). Quantitative analysis of nifH genes and transcripts from aquatic environments. *Methods Enzymol.* **397,** 380–394.

Short, S. M., and Zehr, J. P. (2007). Nitrogenase gene expression in the Chesapeake Bay Estuary. *Environ. Microbiol.* **9,** 1591–1596.

Slaveykova, V. I., Guignard, C., Eybe, T., Migeon, H. N., and Hoffmann, L. (2009). Dynamic NanoSIMS ion imaging of unicellular freshwater algae exposed to copper. *Anal. Bioanal. Chem.* **393,** 583–589.

Slodzian, G. (2004). Challenges in localized high precision isotope analysis by SIMS. *Appl. Surf. Sci.* **231–232,** 3–12.

Sprott, G. D., Jarrell, K. F., Shaw, K. M., and Knowles, R. (1982). Acetylene as an inhibitor of methanogenic bacteria. *J. Gen. Microbiol.* **128,** 2453–2462.

Veit, K., Ehlers, C., Ehrenreich, A., Salmon, K., Hovey, R., Gunsalus, R. P., Deppenmeier, U., and Schmitz, R. A. (2006). Global transcriptional analysis of Methanosarcina mazei strain Go1 under different nitrogen availabilities. *Mol. Genet. Genomics* **276,** 41–55.

Waksman, S. A., Hotchkiss, M., and Carey, C. L. (1933). Marine bacteria and their role in the cycle of life in the sea: II. Bacteria concerned in the cycle of nitrogen in the sea. *Biol. Bull.* **65,** 137–167.

Weber, P. K., Graham, G. A., Teslich, N. E., Chan, W. M., Ghostal, S., Leighton, T. J., and Wheeler, K. E. (2009). NanoSIMS imaging of Bacillus spores sectioned by focused ion beam. *J. Microsc.* **238,** 189–199.

Widdel, F., Boetius, A., and Rabus, R. (2006). Anaerobic biodegradation of hydrocarbons including methane. *Prokaryotes* **2,** 1028–1049.

Zhang, Y., Burris, R. H., Ludden, P. W., and Roberts, G. P. (1993). Posttranslational regulation of nitrogenase activity by anaerobiosis and ammonium in *Azospirillum brasilense*. *J. Bacteriol.* **175,** 6781–6788.

C h a p t e r 2

Deep-Sea Archaea Fix and Share Nitrogen in Methane-Consuming Microbial Consortia

Anne E. Dekas[1], Rachel S. Poretsky[1], and Victoria J. Orphan[1]

[1]Division of Geological and Planetary Sciences,
California Institute of Technology Pasadena, CA 91125

Originally published in Science*, Volume 326, pages 422–426 (2009)*

ABSTRACT

Nitrogen-fixing microorganisms regulate productivity in diverse ecosystems; however, the identities of diazotrophs are unknown in many oceanic environments. Using single-cell resolution NanoSIMS images of ^{15}N incorporation, we show that deep-sea anaerobic methane-oxidizing archaea fix N_2, as well as structurally similar CN^-, and share the products with sulfate-reducing bacterial symbionts. These archaeal/bacterial consortia are already recognized as the major sink of methane in benthic ecosystems, and we now identify them as a source of bioavailable nitrogen as well. The archaea maintain their methane-oxidation rates while fixing N_2 but reduce growth, likely in compensation for the energetic burden of diazotrophy. This finding extends the demonstrated lower limits of respiratory energy capable of fueling N_2 fixation and reveals a link between the global carbon, nitrogen, and sulfur cycles.

REPORT

Nitrogen-fixing (diazotrophic) bacteria and archaea convert dinitrogen (N_2) into ammonia (NH_3) for assimilation. Biological N_2 fixation counteracts the remineralization of nitrogen by microbial processes such as denitrification and anaerobic ammonium oxidation (anammox), and provides bioavailable nitrogen to the majority of the biosphere that cannot directly assimilate N_2. Many photosynthetic cyanobacteria fix N_2 in ocean surface waters, and have been the primary focus of studies on marine diazotrophy. Recently, a discrepancy between the calculated rates of oceanic denitrification and N_2 fixation has suggested that other less well studied or currently unknown diazotrophic

microorganisms may exist and fix significant amounts of N_2 (*1–5*). Indeed, recent discoveries of new phylogenetically and physiologically diverse diazotrophs, including hyperthermophilic methanogens from hydrothermal vents (*6*), have shown that N_2 fixation can occur in extreme environments and localized habitats of enhanced productivity in the deep sea (*5, 7, 8*).

Here we show that syntrophic aggregates of archaea (ANME-2) and bacteria (*Desulfosarcina/Desulfococcus, DSS*) mediating sulfate-dependent anaerobic oxidation of methane (AOM) in deep-sea sediments are capable of N_2 fixation. The ANME-2/DSS consortia have been studied in recent years both because of their potentially critical role in marine carbon cycling and their enigmatic obligate syntrophy (*9, 10*). These consortia are most abundant in areas of high methane, such as cold seeps, but are present throughout continental margin sediments (*9 and references therein*). They currently represent the main filter for oceanic methane release to the atmosphere, consuming up to 80% of naturally released methane in marine sediment (*9*); however the specific mechanism(s) coupling the ANME-2 and DSS remains unclear. Recent metagenomic sequencing of the ANME-2/DSS consortia identified the presence of nitrogenase genes required for N_2 fixation (*nif*) (*11*). This result, along with preliminary nitrogen isotope data, suggests that microbes within the consortia are able to fix nitrogen (*11*). We used submicron-scale ion imaging by nanometer secondary ion mass spectrometry (nanoSIMS) coupled to fluorescence *in situ* hybridization (FISH) to specifically identify the ANME-2 species as diazotrophs while detailing and quantifying patterns of N assimilation within the individual members of these metabolically interdependent consortia.

Sediment samples from an active methane seep in the Eel River Basin, California, USA, were collected and anaerobically incubated with methane and one of several ^{15}N-labeled nitrogen sources (*12*). Nitrogen fixation, as demonstrated by assimilation of ^{15}N from $^{15}N_2$ in co-aggregated ANME-2 and DSS cells, occurred in all AOM consortia measured after 6 months of incubation with methane (*12*) (Fig. 1A, 1B; Fig. 2). ^{15}N enrichment within the consortia was as high as 10.5 ^{15}N atom %, 26 times the highest value observed in unlabeled ANME-2/DSS consortia (ranging from 0.35 to 0.4 ^{15}N atom %). Inhibition of either methane oxidation (incubations lacking methane) or sulfate reduction (incubations treated with the inhibitor sodium molybdate, Na_2MoO_4), prevented ^{15}N incorporation (Fig. 2), implying that N_2 fixation requires a functioning symbiosis between the methane-oxidizing ANME-2 and sulfate-reducing DSS partners. Other microbial cells from the $^{15}N_2$ incubation were not enriched in ^{15}N (max. 0.38 ^{15}N atom %; n=10), suggesting that $^{15}N_2$ incorporation was specific to the ANME-2/DSS consortia over the incubation period and not due to non-specific cycling of reduced ^{15}N after fixation by an unrelated group of organisms. ^{15}N was also incorporated from ^{15}N-labeled cyanide ($C^{15}N^-$), a toxic molecule structurally similar to N_2 and known to be detoxified and assimilated by some, but not all, diazotrophs (e.g., *13*) (Fig. 1D and Fig. 2). The potentially broad substrate recognition by this nitrogenase is believed to be a relict ability from when the protein first evolved, when it may have primarily catalyzed reactions other than N_2 fixation (e.g., cyanide detoxification; (*12, 14–16*).

N_2 fixation appears to be primarily mediated by ANME-2, based on the distribution of ^{15}N within the consortia. In aggregates of shelled morphology (an inner sphere of archaeal cells surrounded by an outer layer of bacterial cells, approximately 500

Figure. 1. Incorporation and distribution of ^{15}N in representative methanotrophic ANME-2/DSS consortia from sediments incubated with methane and different ^{15}N-labeled nitrogen sources, as indicated. Left panels (A-E): Fluorescence *in situ* hybridization using probes targeting ANME-2 (Eel_932) in red and *Desulfobacteraceae* (DSS_658), in green. Right panels (I-V): ion micrographs of $^{12}C^{15}N/^{12}C^{14}N$ ratios of the same microbial consortia imaged by FISH in panels A-E, demonstrating the location of ^{15}N incorporation. Note that the scale range varies between ion micrographs, with the minimum consistently set to natural abundance $^{15}N/^{14}N$.

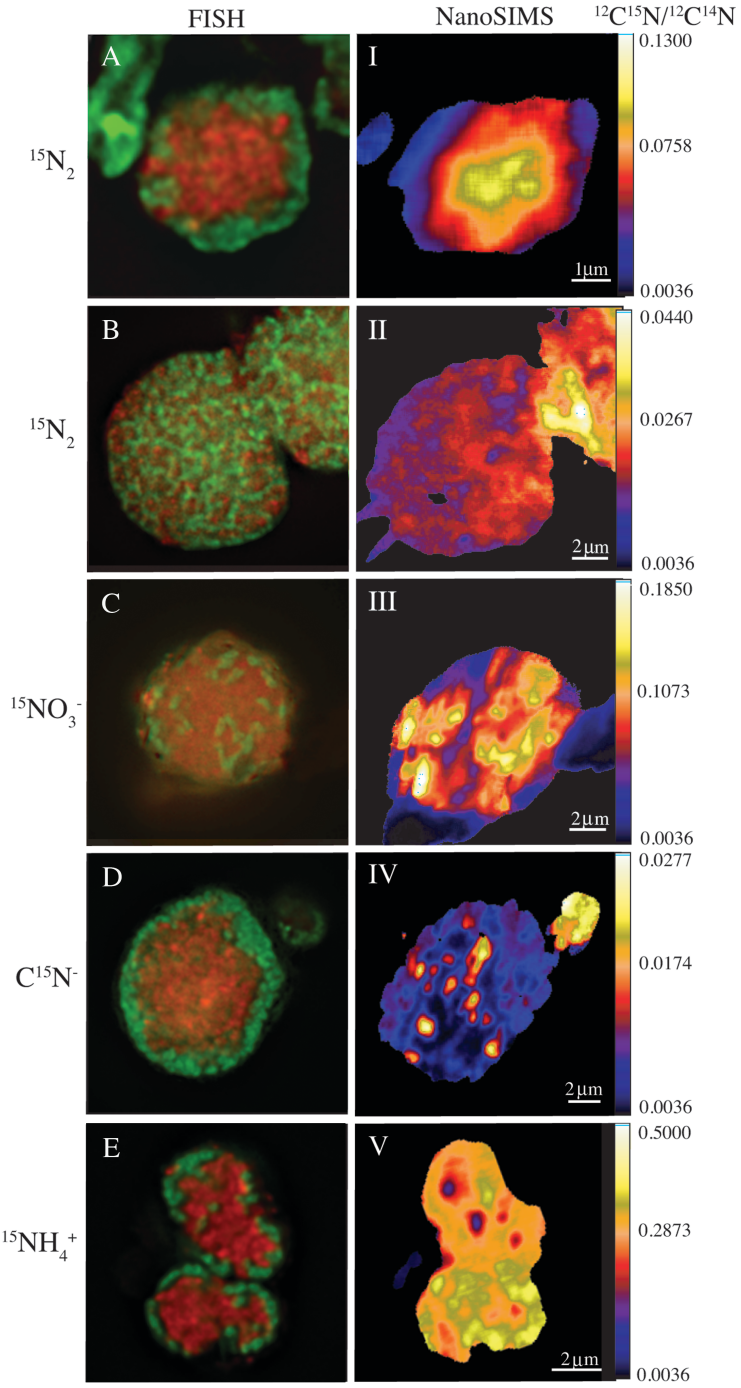

Figure. 2. Effect of nitrogen source on rates of cellular growth and respiration. (A) ^{15}N incorporation in ANME-2/DSS consortia from bulk sediment incubated with each of the indicated nitrogen sources and/or inhibitors. Each data point represents the ^{15}N (atom %) value of the most ^{15}N-enriched ion image of a single aggregate. Symbol size and shape indicates time aggregate was incubated: (•) one month, (o) three months, (O) 4 months, (O) 6 months. Dashed line represents natural abundance $^{15}N/^{14}N$. NM indicates not measured. Inset: Change in abundance of aggregates (aggs) over time in the N_2 (dashed line) and NH_4^+ (solid line) incubations determined by DAPI staining. Error bars represent 1 SD from the mean. (B) Sulfide production (mM) in the different ^{15}N sediment incubations. Each data point (square symbol) represents the value for a single incubation bottle at the time sampled, following the same symbol size and color trend noted in (A). Note no inhibition by BES (12).

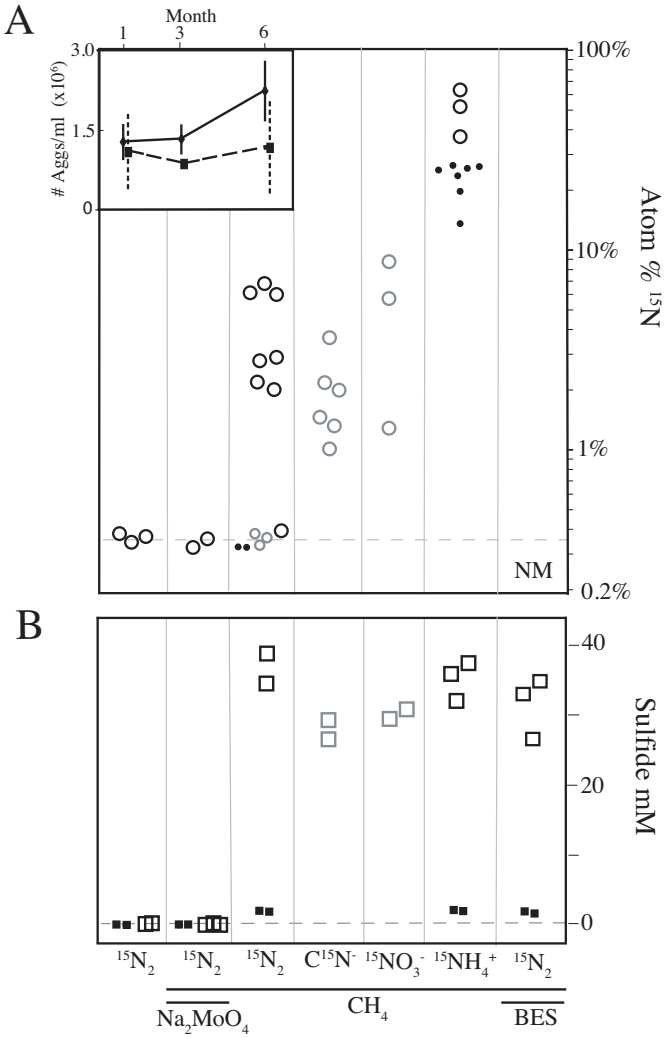

cells total, n=5), the ^{15}N label was concentrated in the center of the aggregate, where the ANME-2 biomass was concentrated (Fig. 1A; Fig. 3). Additionally, ANME-2/DSS aggregates showed ^{15}N enrichment co-localized with light $\delta^{13}C$ biomass, a signal diagnostic of methanotrophic ANME-2 species (*11, 17*) (n=6; Fig. S1). This differs from the variable pattern of ^{15}N incorporation observed in the majority of aggregates from incubations amended with ^{15}N-labeled ammonium ($^{15}NH_4^+$) and nitrate ($^{15}NO_3^-$), and indicates that the elevated enrichment from $^{15}N_2$ within the ANME-2 archaea is attributable to diazotrophic activity, not simply a varying rate of protein synthesis between cells (Fig. 1).

Serial FISH and SIMS images collected through individual aggregates reveal the three-dimensional distribution of ^{15}N enrichment from $^{15}N_2$ within AOM consortia (Fig. 3). The difference in ^{15}N atom % between the group of cells on the aggregate exterior (DSS-dominated) and group in the interior (ANME-dominated) became greater with increasing penetration into the core of the aggregate, corresponding to an increasingly pure population of ANME in the interior (Fig. 3). Although the aggregate exterior averaged 31% less ^{15}N enrichment than the interior, all of the DSS cells on the periphery of the aggregate were enriched in ^{15}N relative to natural abundance [average ^{15}N atom % = 3.47 exterior; (n=313 regions of interest (ROI's)), 5.01% interior; (n=297 ROI's), Fig. 3] suggesting a passage of reduced nitrogen from the ANME cells in the interior to the DSS-dominated exterior. The reduced ^{15}N enrichment in the DSS cells relative to the ANME cells is consistent with the trend observed in ^{15}N labeling studies of other symbioses in which reduced N is shared between a diazotrophic and a non-diazotrophic partner (*18, 19*). Transfer of reduced N species between symbionts is common, often in

Figure. 3. Serial FISH and $^{12}C^{15}N/^{12}C^{14}N$ ion images in a representative shelled ANME-2/DSS aggregate showing the distribution of ^{15}N incorporation from $^{15}N_2$ with depth (Left panels). In the FISH series, red indicates archaeal cells and green indicates bacteria. Comparison of ^{15}N incorporation on the inside of the aggregate (dominated by archaea) and the outside (dominated by bacteria) is shown on the right. Each gray data point represents the $^{15}N/^{14}N$ of a hand-drawn region of interest (ROI), approximating the size of a cell (1 µm) (*12*). Box and whisker plots indicate 75%, median, and 25% values for all ROI's drawn in either the inside (ANME-2, red) or outside (DSS, green) at a particular depth in the aggregate. Inset shows an example of ROI's designated for interior and exterior portions of the cell aggregate from a single depth. All ion micrograph values are scaled from .0036 to 0.11.

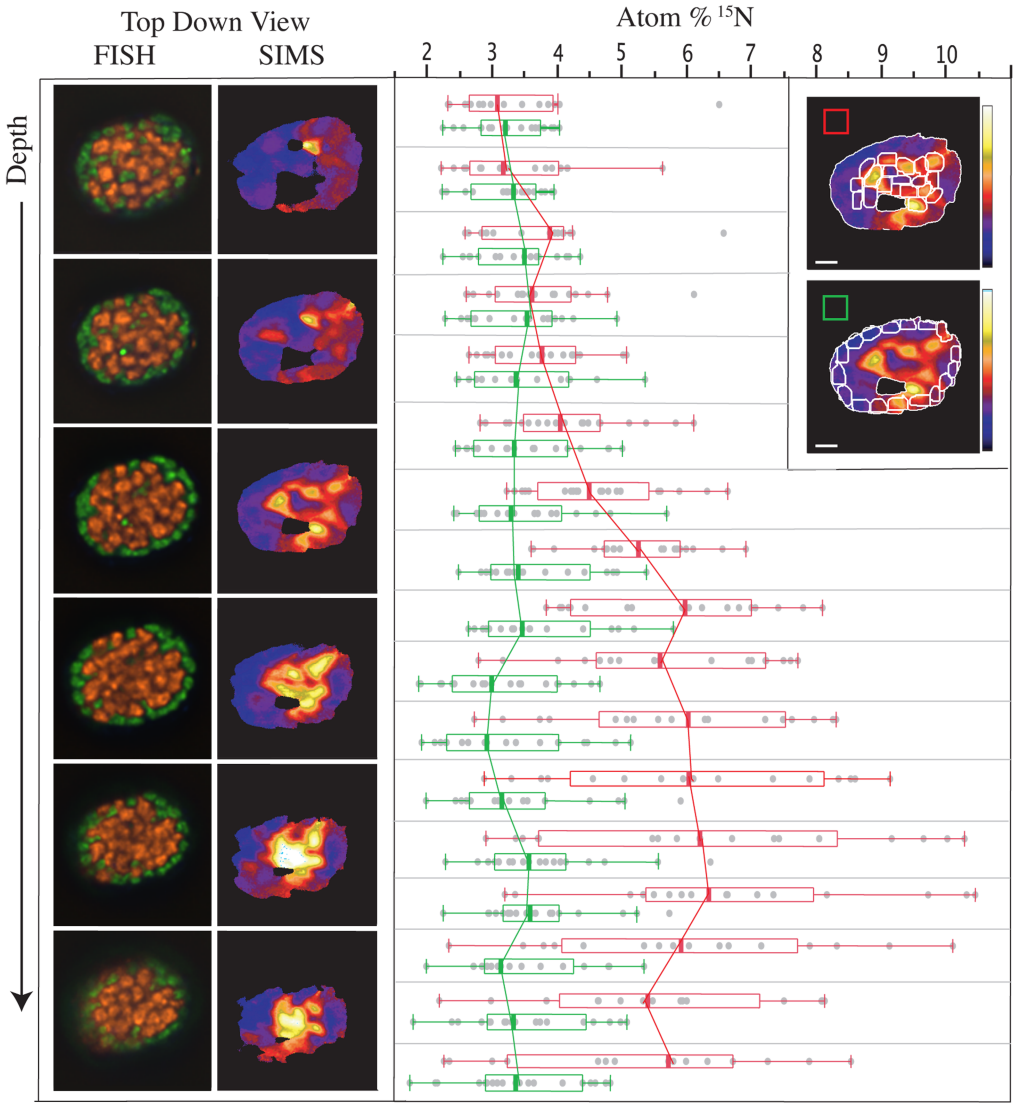

exchange for energy-rich metabolites or structural protection (*20*). It is possible that inherent variations in metabolism and growth between the two partners may also lead to an offset in ^{15}N enrichment (*21*), and the possibility of concurrent fixation by both syntrophic partners at differing rates cannot be excluded at this time. However, in the context of molecular data acquired in parallel, this scenario appears less likely.

The analysis of *nif* sequences recovered from the $^{15}N_2$ sediment incubation was consistent with previous reports of a methane seep-specific *nif*H clade (Fig. S2). The diverse *nif*H genes recovered clustered primarily within a divergent clade of sequences reported from geographically distant deep-sea methane seeps and whole-cell enrichments of ANME-2/DSS consortia from the Eel River Basin (*11, 22*) (Fig. S2). The existence of this *nif*H clade highlights the strong similarities between putative diazotrophs at geographically distant methane seeps, however its divergence from known diazotrophs has made previous attempts to assign the clade to either the Bacteria or Archaea speculative (*22*). We therefore collected and analyzed partial *nif* operons from the incubations and found that they contained the typical gene order (*nif*H*, nif*I1*, nif*I2*, nif*D*, and nif*K) of the 'C-type' operon in methanogenic archaea and some non-proteobacterial anaerobic diazotrophs (*23*) (Fig. S3). Additionally, the *nif*D phylotypes within these operons grouped within a well-supported clade containing sequences retrieved from other methane seep sediment samples, methanogenic archaea (*Methanococcus*, 49% similarity), and non-proteobacterial nitrogen-fixing lineages rarely found at methane seeps but which have been hypothesized to have undergone lateral gene transfer with archaea (e.g., *Clostridia, Roseiflexus* spp.) (*23, 24*) (Fig. 4). In the context of seep microorganisms, these data are most consistent with an archaeal origin for these operons.

Figure. 4. Unrooted neighbor-joining tree of translated *nifD* sequences following global alignment. Bootstrap values from 85-100% (•) and from 70-85% (o) are indicated at the nodes. The scale bar represents changes per amino acid position. The sequences obtained in this study are shown in bold. Alternative nitrogenases are those that use V-Fe and Fe-Fe cofactors (*vnf*D and *anf*D, respectively). Roman numerals represent nitrogenase clusters as originally defined in (*30*).

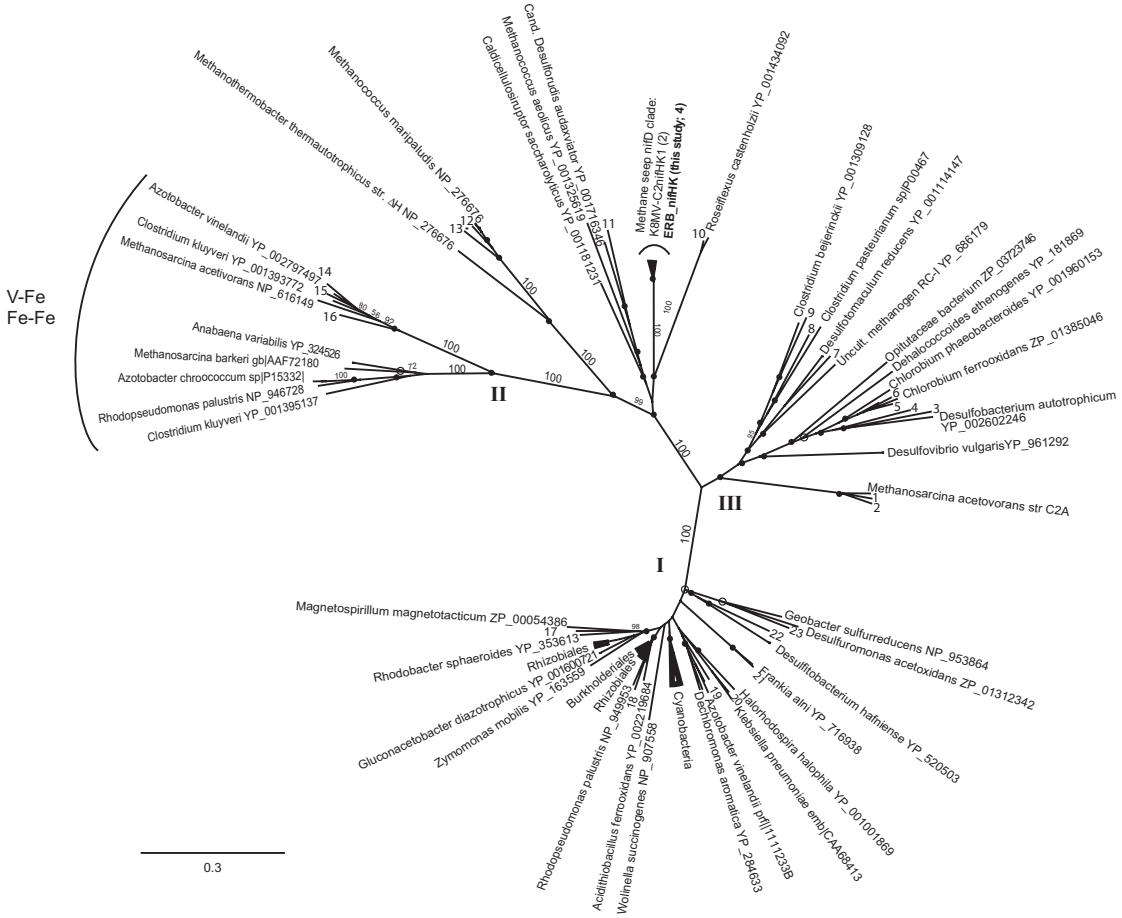

The *nif*H fragments of the partial operons cluster within the putatively seep-specific *nif*H clade, suggesting that this clade is archaeal, and supporting our designation of the ANME-2 archaea as the primary diazotrophic microorganism in the consortia.

N_2 fixation in ANME-2/DSS consortia is intriguing from an energetic standpoint; its cost is one of the highest for any anabolic process, requiring an investment of up to 16 ATP (equivalent to ~ 800 kJ) for each N_2 molecule reduced (*8*). Moreover, AOM coupled to sulfate-reduction is thought to be one of the least energetically productive metabolisms known (*10*). At methane seeps, coupled methane-oxidation and sulfate-reduction reactions yield a total of approximately 40 kJ/mol CH_4 (*10*) that must be shared between the two syntrophic partners. Although other energy-limited diazotrophic microorganisms exist (e.g., methanogens) none to our knowledge generate less energy per mole substrate than the ANME-2. One possibility is that in unusual environments, such as the deep sea, structural or mechanistic differences in the N_2 fixation machinery may alter the energetic burden. The low sequence similarity of the recovered *nif* genes to those previously described suggest some deviation from characterized N_2-fixing systems (Fig. 4, S2, S3).

Slowed growth is a common response to the energetic burden of N_2 fixation in active diazotrophs, including methanogenic archaea (*25*). Accordingly, using ^{15}N incorporation as a proxy for growth, the ANME-2/DSS consortia in this study actively fixing nitrogen grew approximately 20 times slower on average than aggregates grown in parallel with ammonium (Fig. 2). Although ANME-2/DSS growth rates are significantly affected by the available nitrogen source, the rate of AOM by the consortia [estimated by methane-dependent sulfide production (*12*)] was similar during growth on either N_2 or NH_4 (Fig. 2B). Therefore, regardless of the exact amount of energy required to fix N_2 in

these organisms, the consortia appear to compensate for the energetic burden of N_2 fixation by slowing growth while maintaining similar rates of respiration.

The maintenance of *nif* genes by the ANME-2, and their consortial ability to fix nitrogen in the laboratory, implies that they do so in marine environments. Diazotrophy within deep-sea methane seeps has not been detected directly, but N_2 fixation has been suggested at these locales, based on low $\delta^{15}N$ values of seep sediment and fauna (*26, 27*). Why N_2 fixation would occur in anoxic marine sediments, often replete with ammonium, warrants further consideration. One explanation is that the methane seep environment differs from typical anoxic sediment in that the main source of carbon (CH_4) is unaccompanied by nitrogen, poising its consumers for nitrogen limitation, similar to photoautotrophs (*8*) and aerobic methanotrophs (*28*). Indeed, measurements of pore water ammonium from the Eel River Basin methane seeps were highly variable, ranging from 101 μM to 16 μM over a 6 cm sediment depth profile; these concentrations would not completely inhibit N_2 fixation in cultured diazotrophic methanogens (e.g., *Methanococcus maripaludis*) (*29*). Even in ammonium-replete sediments, localized zones of nitrogen limitation may occur (e.g., within densely packed microbial consortia). Although the loss of nitrate and ammonium from methane seep sediments by catabolic bacterial processes (e.g., denitrification or anammox) has not yet been determined, these sinks for fixed nitrogen may also promote enhanced diazotrophy by the *in situ* microbial assemblage (*3*). Additionally, the current discrepancy in the oceanic fixed N budget underscores the possibility of new sources of fixed nitrogen in non-traditional and potentially unexpected habitats (*1–3, 7*). The extent to which the ANME-2/DSS consortia contribute to the putatively missing fraction of global fixed N inputs is unknown, but

their input is likely not the only missing term in the equation. N_2 fixation in the ANME-2, combined with the diversity of *nif*H genes recovered from marine sediments here and previously (*5, 11, 22*), suggests our inventory of marine diazotrophs is incomplete, and that we are only beginning to understand the extent and significance of benthic marine N_2 fixation.

WORKS CITED AND NOTES

1. L. A. Codispoti, *Biogeosciences* **4**, 233 (2007).
2. C. Mahaffey, A. F. Michaels, D. G. Capone, *Am J Sci* **305**, 546 (2005).
3. C. Deutsch, J. L. Sarmiento, D. M. Sigman, N. Gruber, J. P. Dunne, *Nature* **445**, 163 (2007).
4. R. W. Fulweiler, S. W. Nixon, B. A. Buckley, S. L. Granger, *Nature* **448**, 180 (2007).
5. J. P. Zehr, B. D. Jenkins, S. M. Short, G. F. Steward, *Environ Microbiol* **5**, 539 (2003).
6. M. P. Mehta, J. A. Baross, *Science* **314**, 1783 (2006).
7. M. C. Horner-Devine, A. C. Martiny, *Science* **320**, 757 (2008).
8. Karl *et al.*, *Biogeochemistry* **57/58**, 47 (2002).
9. W. S. Reeburgh, *Chemical Reviews* **107**, 486 (2007).
10. M. Strous, M. S. M. Jetten, *Annual Review of Microbiology* **58**, 99 (2004).
11. A. Pernthaler *et al.*, *Proc Natl Acad Sci U S A* **105**, 7052 (2008).
12. *Information on materials and methods is available on Science Online and in the following supplementary material*.
13. J. K. Liu, C. H. Liu, C. S. Lin, *Proc Natl Sci Counc Repub China B* **21**, 37 (1997).
14. W. S. Silver, J. R. Postgate, *Journal of Theoretical Biology* **40**, 1 (1973).
15. J. Raymond, *Reviews in Mineralogy and Geochemistry* **59**, 211 (2005).
16. I. Berman-Frank, P. Lundgren, P. Falkowski, *Research in Microbiology* **154**, 157 (2003).
17. V. J. Orphan, C. H. House, K. U. Hinrichs, K. D. McKeegan, E. F. DeLong, *Science* **293**, 484 (2001).
18. C. P. Lechene, Y. Luyten, G. McMahon, D. L. Distel, *Science* **317**, 1563 (2007).
19. S. Behrens *et al.*, *Appl. Environ. Microbiol.* **74**, 3143 (2008).
20. M. K. Udvardi, D. A. Day, *Annual Review of Plant Physiology and Plant Molecular Biology* **48**, 493 (1997).
21. V. J. Orphan, K. A. Turk, A. M. Green, C. H. House, *Environmental Microbiology* **11**, 1777 (2009).
22. H. Dang, X. Luan, J. Zhao, J. Li, *Appl Environ Microbiol* **75**, 2238 (2009).

23. J. P. W. Young, in *Genomes and Genomics of Nitrogen-fixing Organisms,* R. Palacios, W. E. Newton, Eds. (Springer, The Netherlands, 2005), pp. 221-241.
24. J. A. Leigh, *Curr. Issues Mol. Biol.* **2**, 125 (2000).
25. P. A. Murray, S. H. Zinder, *Nature* **312**, 284 (1984).
26. S. B. Joye *et al.*, *Chemical Geology* **205**, 219 (2004).
27. J. Brooks *et al.*, *Science* **238**, 1138 (1987).
28. D. H. Buckley, V. Huangyutitham, S. F. Hsu, T. A. Nelson, *Soil Biology and Biochemistry* **40**, 1272 (2007).
29. P. S. Kessler, C. Daniel, J. A. Leigh, *Journal of Bacteriology* **183**, 882 (2001).
30. Y.-T. Chien, A. Auerbuch, A. D. Brabban, S. H. Zinder, *J. Bact.* **182**, 3247 (2000).
31. We thank C. House, A. Schmitt, K. McKeegan, Y. Guan, J. Eiler and L. Remusat for assistance with the ion microprobe data collection. We also thank S. Joye, M. Boyles, M. Walton, J. Howard, N. Dalleska, O. Mason, A. Green, P. Tavormina, S. Goffredi, C. Gammon and the shipboard party and crew of the R/V Atlantis and DSSV Alvin for support in the field and laboratory. We are grateful to J. Howard, W. Fischer, J. Amend, C. Anderson, D. Fike, D. Sigman, J. Howard, W. Fischer, V. Rich, J. Bailey, D. Newman, J. Grotzinger, T. Hoehler, J. Delacruz and three anonymous reviewers for helpful suggestions regarding this manuscript. Funding was provided from the NSF (MCB-0348492), the Gordon and Betty Moore Foundation and an NSF Graduate Research Fellowship (AED). The Caltech Center for Microanalysis and nanoSIMS 50L is funded by the Gordon and Betty Moore Foundation and the UCLA ion microprobe is partially supported by the NSF Instrumentation and Facilities Program.

SUPPORTING ONLINE INFORMATION

Deep-sea archaea fix and share nitrogen in methane-consuming microbial consortia

Anne E. Dekas, Rachel S. Poretsky, and Victoria J. Orphan

This file contains Supplementary Materials and Methods (Page 2), Results and Discussion (Page 9), and Figures and Tables (Page 15). These sections provide additional information regarding the ^{15}N substrate incubation experiments and characteristics of the putative ANME nitrogenase operon. Figure S1 displays the results from the FISH-SIMS analysis of natural abundance $\delta^{13}C$ and $^{15}N_2$ assimilation in individual ANME-2/DSS consortia using the CAMECA 1270 ims ion microprobe instrument (housed at the University of California, Los Angeles). Figure S2 shows the diversity of *nifH* genes recovered from the $^{15}N_2$ sediment incubation experiments. Figure S3 displays the partial nitrogenase operon structure and conserved amino acid residues of the *nifD* gene, which encodes for the alpha subunit of the dinitrogenase. Table S1 summarizes the ^{15}N sediment incubation experiments and Tables S2 and S3 provide information regarding taxa used in the phylogenetic analysis of *nifH* and *nifD*. Table S4 reports the inhibition of AOM and sulfate reduction in the presence of acetylene.

Supplementary Materials and Methods

Sediment collection and preparation. Seafloor methane seeps within the Eel River Basin (ERB) off the coast of Eureka, California were sampled at depths ranging from 500-520 meters. The region supports localized areas of active methane venting, sulfide-oxidizing bacterial mats, and *Calyptogena pacifica* clam beds, as previously described (*S1*). Sediment push-cores (PC) were collected from two different sediment habitat types located along the ERB Southern ridge (40° 47.1919'N; 124 °35.7057'W; 520 m) in October 2006 using the D.S.R.V. *Alvin.* PC-14 was collected through a microbial mat and PC-11 was taken within a clam bed. Sediments used in incubation experiments were extruded from the push core liner, transferred into whirlpak bags under a stream of argon, and sealed in mylar bags. Sediments were then stored 4°C until processing in the laboratory.

^{15}N Incubation. The top 15 cm of PC-14 were homogenized and supplemented 1:1 with artificial marine media containing 40 mM sulfate (modified from (*S2*) by eliminating reduced N species). PC-11 (0-12 cm) was similarly homogenized and supplemented with 0.2 μm filtered seawater collected above the ERB seep (~ 500 m). Both core samples were stored in the dark in 1 liter anaerobic bottles at 4°C with an overpressure of methane (2 atm) for one month prior to isotope labeling experiments. The sediment slurries were subsequently prepared in an anaerobic chamber and sub-sampled into serum bottles that were sealed with butyl rubber stoppers and amended with various nitrogen substrates and inhibitors. Sediment incubation conditions are detailed in Table 1, with replicates for each treatment done in duplicate or triplicate. 2-bromoethanesulfonic acid (BES, 5 mM

and 20 mM) was added as an inhibitor of anaerobic methane oxidation/methanogenesis, and sodium molybdate (Na_2MoO_4, 25 mM) as an inhibitor of sulfate reduction (*S3*). Sediment slurries were periodically sampled through the butyl rubber stopper with a sterile 3 cc disposable syringe and fixed with formaldehyde and/or analyzed for sulfide concentration (see below). PC-14 sediment slurries were sampled initially (T=0) and then after one, three, and six months and PC-11 sediment slurries were sampled initially and at four months. Long incubation times were required in order to allow at least one doubling time, which has been estimated to range between 3-6 months for ANME-2/DSS consortia (*S4-7*).

Sulfide Production. Incubations were sampled initially, and then after one and either six (PC-14) or four (PC-11) months to measure dissolved sulfide via the Cline Assay (*S8*). Briefly, $FeCl_3$ (in 6N HCl) and N,N-dimethyl-p-phenylenediamine dihydrochloride (in 6N HCl) were added to incubation subsamples 20-200 µl removed via syringe. The product of the reaction, methylene blue, was measured spectrophotometrically at 670 nm and calibrated to sulfide concentration with a sodium sulfide standard.

Fluorescence In Situ Hybridization (FISH). Sediment slurry was removed via syringe and immediately fixed in PBS buffered 2% formaldehyde for 1 hour at room temperature, washed with 1X phosphate buffered saline (PBS) twice, and stored at -20ºC in 50:50 PBS:ethanol. Microbial aggregates were concentrated using a Percoll (Sigma) gradient and adhered to a 1" diameter round microprobe slide (Lakeside city, IL) as described in (*S9*). Fluorescence *in situ* hybridization was carried out as described previously (*S9*)

using both group-specific (EelMS932 and DSS658) and Domain-level probes (Arch915 and EUB338) (*S10, 11*). The location of positively hybridized cell targets were mapped on the 1" glass rounds using both epifluorescence and transmitted light microscopy as described in (*S6*), using a DeltaVision RT (Applied Precision, Inc., WA). Images were collected through the z-plane and deconvolved and processed using softWoRx® Suite software (Applied Precision, Inc.).

Secondary Ion Mass Spectrometry (SIMS). Prior to SIMS analysis, mapped rounds were sputter coated with gold (30 nm) and analyzed either with a CAMECA 1270 IMS (CAMECA, Gennevilliers Cedex, France), housed at the University of California Los Angeles, or a CAMECA NanoSIMS 50L, housed in the Division of Geological and Planetary Sciences at the California Institute of Technology. With both instruments, samples were pre-sputtered using the primary ion beam for 3-15 minutes to locally remove the gold coat.

On the CAMECA 1270 IMS, a primary Cs^+ beam (~0.5 to ~2.5 nA) with a diameter of ~10 μm was used to generate negative secondary ions from a phylogenetically identified microbial aggregate. Mono-collection mode was used as previously described (*S6*), with an on-axis electron multiplier detector cycling through the following masses: $^{12}C_2^-$, $^{13}C^{12}C^-$, $^{12}C^{14}N^-$, $^{12}C^{15}N^-$. The $^{12}CN^-$ mass was collected to measure the $^{15}N/^{14}N$ of the sample (*S12-14*). Analyses of each target lasted approximately 1 hour, with the end of the analyses determined by a drop in C and N ion counts, indicating the near complete sputtering of the target.

Measurements were collected in both Image and Isotope mode on the CAMECA NanoSIMS 50L, with a resolving power of ~5,000. Four secondary ions were simultaneously collected: $^{12}C^-$, $^{13}C^-$, $^{12}C^{14}N^-$, and $^{12}C^{15}N^-$. In Image mode, an ~2.5 pA primary Cs^+ beam with a nominal spot size of ~100-200 nm was used. The beam rastered over square regions of sides 5 to 20 μm, depending on the size of the target, at 256 x 256 pixel resolution. A complete square raster or "frame," representing a layer of the target, was completed every 10 to 20 minutes, with several to 150 frames collected per target. Complete analysis of large targets (aggregates of diameter >15 μm) lasted up to 48 hours, but analysis of smaller targets (aggregates with diameter ~5 μm) were completed in approximately 12 hours. Measurements in Isotope mode were collected with an ~30-40 pA primary Cs^+ beam, over square regions of the same size but typically with a reduced resolution of 128 x128 pixels, a per frame acquisition time of 30 seconds, and a total acquisition time of one to three hours. Although not yielding an image, Isotope mode measurements allowed more rapid screening of samples. Both Image and Isotope modes were used to measure *E. coli* cell standards as described in (*S6*).

NanoSIMS images were processed with L'image (developed by L. Nittler, Carnegie Institution of Washington, Washington D.C.). Each series of frames was corrected for drift and detector dead time. When analyzing trends in the series of frames with depth, every 3-5 frames were binned into a single image (Fig. 2 and 3). Discrete regions of Interest (ROI's), approximately 1 μm in diameter, were hand-drawn on the ion images guided by the corresponding 3D FISH data and isotope ratios were subsequently calculated for the particular regions.

nifH Phylogeny. DNA was extracted from PC-14 sediment incubated with $^{15}N_2$ and CH_4 after 6 months using a modified protocol of the Ultraclean soil DNA Isolation Kit (MoBio Laboratories, CA) according to (*S15*). The *nifH* gene was amplified using *nifH* specific PCR primers designed by (*S16*)in a PCR reaction with PuReTaq Ready-To-Go PCR beads (GE Healthcare) with the following conditions: 2 min 94°C, and 35 cycles of 30 s 94°C, 30 s 55°C, 30 s 72°C with a final extension of 72°C for 10 min. Amplicons from PCR reactions using diluted (1:10) and undiluted DNA template were pooled (n=2) and cloned using the TOPO4 cloning kit (Invitrogen, CA). Plasmids were extracted with the Qiaprep Spin Miniprep Kit (Qiagen). Seventy-one clones were sequenced with a CEQ 8800 Genetic Analysis System (Beckman Coulter, CA). Sequences were globally aligned with Geneious Pro 4.6.2 using the ClustalW algorithm. Neighbor-joining trees were constructed using the Geneious Pro 4.6.2 Tree-Builder (Jukes-Cantor distance model and 100 bootstrap replicates). *nif*H sequences have been deposited in GenBank with accession numbers GQ452697 to GQ452775.

Nif Operon Structure and nifD Phylogeny. DNA was extracted from a PC-14 sediment incubation with N_2 and CH_4 using a Ultraclean Soil DNA Isolation Kit (Mobio Laboratories, CA). Primers targeting *nifH* to *nifK* (nifHfw:GGHAARGGHGGHATHG GNAARTC, nifK1rv: RCAKCCYTGKGANCCGTG; Miyazaki, J.; NCBI GenBank entry AB362197) were used in a touchdown PCR of the following program: 94°C 2 min, 2 x (94°C 1 min, 70°C 1 min, 72°C 3 min), 2 x (94°C 1 min, 69°C 1 min, 72°C 3 min), 2 x (94°C 1 min, 68°C 1 min, 72°C 3 min), 2 x (94°C 1 min, 67°C 1 min, 72°C 3 min), 2 x (94°C 1 min, 66°C 1 min, 72°C 3 min), 2 x (94°C 1 min, 64°C 1 min, 72°C 3 min), 2 x

(94°C 1 min, 62°C 1 min, 72°C 3 min), 30 x (94°C 1 min, 61°C 1 min, 72°C 3 min) with PuReTaq Ready-To-Go PCR beads (GE Healthcare). The 3KB amplicon was excised from an agarose gel, purified using an Ultrafree-DA filter (Millipore) and ligated with a TOPO4 vector cloning kit (Invitrogen). Four complete sequences representing unique clones in the library were obtained (Laragen, Inc., CA). Primer walking was necessary to sequence the whole fragment, typically using 2 internal primer sets for each sequence. The *nifD* portion of the sequence was identified and sequences were globally aligned with Geneious Pro 4.6.2 using the ClustalW algorithm. Neighbor-joining trees for the *nifD* subunits were constructed using the Geneious Pro 4.6.2 Tree-Builder (Jukes-Cantor distance model and 100 bootstrap replicates). A tree with the same topology was obtained using Bayesian analysis (Mr. Bayes) (not shown). Sequences were deposited in GenBank with accession numbers GQ477542 to GQ477545.

Aggregate abundance. Aliquots of fixed sediment (see above) from the N_2 and NH_4 incubations were diluted with PBS and filtered onto 0.2 um Isopore GTBP Membrane Filters (Millipore). Filters were treated with 4',6-diamidino-2-phenylindole (DAPI) at least 30 minutes before examination. Both single cells and cell aggregates morphologically resembling ANME-2/DSS aggregates were counted using UV epifluorescence. For each time point in the dinitrogen and ammonium incubations, 3-4 replicate filters were analyzed, with 40 frames counted per filter (representing approximately 400-900 cells per filter).

Ammonia measurements. Pore water was collected from ERB sediments using a pore water squeezer as previously described (*S1*). Pore water aliquots for ammonia analysis were filtered (0.2 μm) and measured using the colorimetric phenol hypochlorite method (*S17*) in the laboratory of Dr. S. Joye, University of Georgia.

Acetylene incubations with $^{15}N_2$

Sediment from PC-14 was also used to measure nitrogen fixation via the Acetylene Reduction Assay (*S18, 19*). Sediment was mixed 1:1 with artificial seawater in an anaerobic chamber, as described above, and 7 ml of the slurry was aliquoted into 20 ml serum bottles sealed with a butyl rubber stopper (n=15). Headspace in the treatment bottles contained methane (2 atm) and 0 to 10% acetylene (lowest % acetylene added was 0.2%). Bottles were incubated at 10ºC and measured weekly for one month. Ethylene and acetylene were analyzed by gas chromatography (GC) on a polystyrene-divinylbenzene based column (HP PLOT-Q 30m x 0.320mm ID x 20 micron) with flame ionization detection (FID). A Hewlett-Packard 5890 Series II GC with a split-splitless injector (2 mm ID liner) was operated in the split mode. The split flow was 20 mL/min. Ultra-high purity helium was used for carrier gas, and the column was operated at a constant flow rate of 2.2 mL/min (37 cm/sec average linear velocity). The headspace of each was sampled (50 μl) with a gastight syringe and injected manually. Oven temperature was isothermal at 50 ºC. The injector was maintained at 125 ºC and the detector at 250 ºC. Methane, ethylene, and acetylene were baseline resolved under these conditions. Positive controls using a diazotrophic culture of *Azotobacter vinelandii* demonstrated active

conversion of acetylene to ethylene by this method. Sulfide concentrations in the acetylene incubation experiments were measured using the Cline Assay (see above) at the 3.5, 8, and 10-week time points.

Supplementary Results and Discussion

Nitrogen assimilation from cyanide (CN^-)

ANME-2/DSS consortia in sediment incubations containing 1 mM ^{15}N-cyanide ($Na^{13}C^{15}N$) incorporated the ^{15}N at comparable levels to those observed in the ^{15}N-dinitrogen incubation (Fig. 2). Cyanide is structurally similar to dinitrogen and reduction of this triple bonded compound has been shown to be catalyzed by purified nitrogenases *in vitro* . In only a handful of studies, however, has cyanide been demonstrated as a nitrogen source for diazotrophic microorganisms using nitrogenase (e.g. *S20, 21*). Nitrogenase is believed to have evolved early, prior to the divergence of Bacteria and Archaea, and the projected levels of cyanide and reduced nitrogen on Earth during that time has led to speculation that the function of 'primitive' nitrogenases was primarily to detoxify cyanide, rather than catalyzing dinitrogen fixation (*S22-26*). While methanogens have demonstrated sensitivity to cyanide via inhibition of carbon monoxide dehydrogenase (CODH) (*S27, 28*), the methanotrophic ANME-2/DSS consortia appeared to be unaffected by this toxic compound, exhibiting active ^{15}N assimilation and equivalent rates of sulfate reduction (Fig. 2). The ANME nitrogenase may be directly mediating this detoxification. Alternatively, more variability of ^{15}N incorporation in the cyanide incubations, including ^{15}N hotspots within both the archaea and bacterial AOM partners, underscores the possibility of alternative mechanisms for cyanide catabolism/

detoxification either through a different nitrogenase, or through another enzymatic pathway entirely (Fig.1C). Regardless of the mechanism, this result demonstrates the tolerance of the ANME-2/DSS consortia to this common toxin, and could imply that this methane-fueled symbiosis was well suited to survive during an early, cyanide-rich atmosphere (*S26*).

Inhibition by acetylene

Although the ANME-2/DSS consortia were able to respire and grow in the presence of up to 1 mM cyanide, they were inhibited by acetylene. Acetylene is similar to cyanide and dinitrogen in its structure, and its reduction to ethylene is commonly used as an indirect measure of nitrogenase activity in both cell extracts and intact cells (*S18*). However, in bulk sediment incubations amended with methane (overpressurized to 2 atm) and acetylene (0.2 to 7.9%), neither nitrogen fixation (measured by production of ethylene) nor AOM activity (measured via sulfide production) was observed (n=12; Table S4). The lack of AOM activity with acetylene concentrations as low as 0.2%, compared to the active sulfide production (4-fold increase during the incubation period) measured in replicate bottles lacking acetylene, suggests that one or both members of the ANME-2/DSS consortia were inhibited by this compound. Methanogenic archaea are often inhibited by acetylene (*S29, 30*), and considering the great similarity between their metabolic machinery (*S31*) suggests that the ANME-2 archaea in particular may have been adversely affected.

Lack of inhibition by 2-bromoethanesulfonic acid (BES)

BES did not inhibit methane oxidation at either 5 mM (PC 11 and PC 14 sediment) or 20 mM (PC 11; PC 14 not tested). BES is a structural analogue of coenzyme M and an inhibitor of the traditional methanogenic pathway (*S3*). The anaerobic oxidation of methane is hypothesized to occur in the ANME cells via "reverse methanogenesis," (*S31*), suggesting that inhibitors of methanogenesis should inhibit anaerobic methanotrophy as well. Indeed, several studies have documented the complete or partial (>50%) inhibition of AOM by BES in marine sediments, using a range of concentrations (e.g. 1 mM (*S32*), 60 mM (*S33*)). However, there is a growing body of evidence that BES does not always inhibit AOM (no inhibition at 5 mM (*S34*)or 20 mM (*S35*)), in addition to the results in the present study. It is possible that 20 mM is insufficient to inhibit AOM, and in fact, the authors of (*S33*) emphasize the need to add excess BES in sediment slurry incubations in order or overcome sorption and sequestering of BES. However, the unpredictable response to BES at a range of concentrations (i.e. complete inhibition of AOM at 1mM and no effect at 5 mM and 20 mM) suggests that other factors besides adsorption may influence sensitivity of AOM consortia to this inhibitor in different environments.

Variation in ^{15}N incorporation within the ANME-2 and DSS

The nanoSIMS images of individual aggregates revealed large heterogeneity in labeled nitrogen assimilation between individuals within each population (ANME-2 and DSS) for each nitrogen source studied (Fig. 1, Fig. 3). For instance, in the representative consortia in Fig. 3, ^{15}N enrichment within the interior (ANME-2) ranged from 2.2 to 10.4 atom %. This likely reflects cell specific variation in growth, and is consistent with previous

SIMS-based reports of single species isotopic heterogeneity in isotope-labeling experiments (*S36, 37*). Despite the predicted energetic benefit from close spatial proximity between the syntrophic partners, there was not a visually apparent trend in the ANME $^{15}N_2$ incorporation related to distance between the ANME and DSS cells within the aggregate.

Aggregate replication and division

The ^{15}N experiments also yielded insight into syntrophic aggregate replication and division. How the dual species ANME-2/DSS consortia form associations and replicate within the methane seep environment is unknown, although it has been proposed, based on visual observations from fluorescence *in situ* hybridization experiments, that aggregates replicate by budding (*S38*). Our FISH-nanoSIMS results provided evidence in support of this hypothesis. We repeatedly observed well-structured ANME-2/DSS aggregates attached to other aggregates in this study, with high levels of ^{15}N incorporation at the bridge point between the aggregates and within the presumably newly formed aggregate 'bud' (e.g. Fig. 1B, 1D and 1E). This implies that ANME-2/DSS aggregates maintain close spatial contact between syntrophic partners and may coordinate division from intact consortia, rather than by requiring the establishment of new associations from single cells.

Nitrogenase phylogeny and operon structure

Recovered *nifD* sequences from the $^{15}N_2$ incubation experiments were distinct from well-characterized Mo-Fe nitrogenases (Fig. 4), but contained key histidine and cysteine

residues, Hisα-442 and Cysα-75, involved in metal cofactor binding in *Azotobacter vinelandii* (*S39*). Major differences occurred in the flanking regions of these residues, indicating possible differences in the metal composition of the cofactor used (Fig. S3). The Hisα-442 region in particular has characteristics of both typical Mo-Fe cofactor binding sites and alternative V-Fe binding sites, as well as binding sites found in members of the *Methanococcus*. It has been speculated that these differences in the primary structure of the metal cofactor binding site are important adaptations to an anaerobic lifestyle, as most of the organisms with the canonical *A. vinelandii*-like Mo-Fe nitrogenase are not strict anaerobes (*S40*). The metal binding site of the putative ANME *nifD* sequences are consistent with anaerobic diazotrophs and appear to be suggestive of a possible combination of bacterial Mo-Fe nitrogenases and methanogenic V-Fe nitrogenase.

The *nifH* sequences obtained in this study were diverse and suggest that a range of microorganisms in Eel River Basin sediments may possess nitrogenase. Representative sequences were identified from several of the major nitrogenase gene clusters (II-IV; Fig. S2, Table S3). Cluster II is typically represented by methanogens and bacterial *anfH* nitrogenases, Cluster III contains a variety of anaerobic bacteria, including sulfate-reducers and methanogens, and Cluster IV includes divergent *nifH*-like genes from archaea (*S41*). The largest number of recovered *nifH* sequences clustered with sequences that appear to be unique to methane seep habitats (recovered from multiple sites in the Eel River Basin as well as from the Nankai Trough and hydrate-bearing sediments from the Sea of Okhotsk), but for which no taxonomic information can be obtained due to the lack of cultured representatives from these environments and the divergence from

sequences of known phylogeny. The involvement of other microorganisms in nitrogen fixation within the methane seep environment and factors influencing the environmental regulation of this process will require further study.

Figure S1. Relationship between ^{15}N incorporation from $^{15}N_2$ and $\delta^{13}C$ in single ANME-2/DSS consortia measured by FISH-SIMS using a CAMECA 1270 IMS instrument. Each data point represents the average ^{15}N atom % and $\delta^{13}C$ of a single cycle during the analysis of the cell target. All data points collected from a particular aggregate are represented by the same symbol, and represent depth related trends in ^{13}C and ^{15}N associated with a single aggregate. Consortia with a distinct shell morphology are represented by filled black data points (n=2), shelled aggregates associated with sediment particles are distinguished by open or filled linear symbols (n=3), and a single mixed aggregate is represented by gray triangles (n=1). It is expected that the sediment-associated ANME-2/DSS aggregates would show a smaller range of variation in $\delta^{13}C$ due to the simultaneous collection of sediment-derived carbon with roughly natural abundance $\delta^{13}C$.

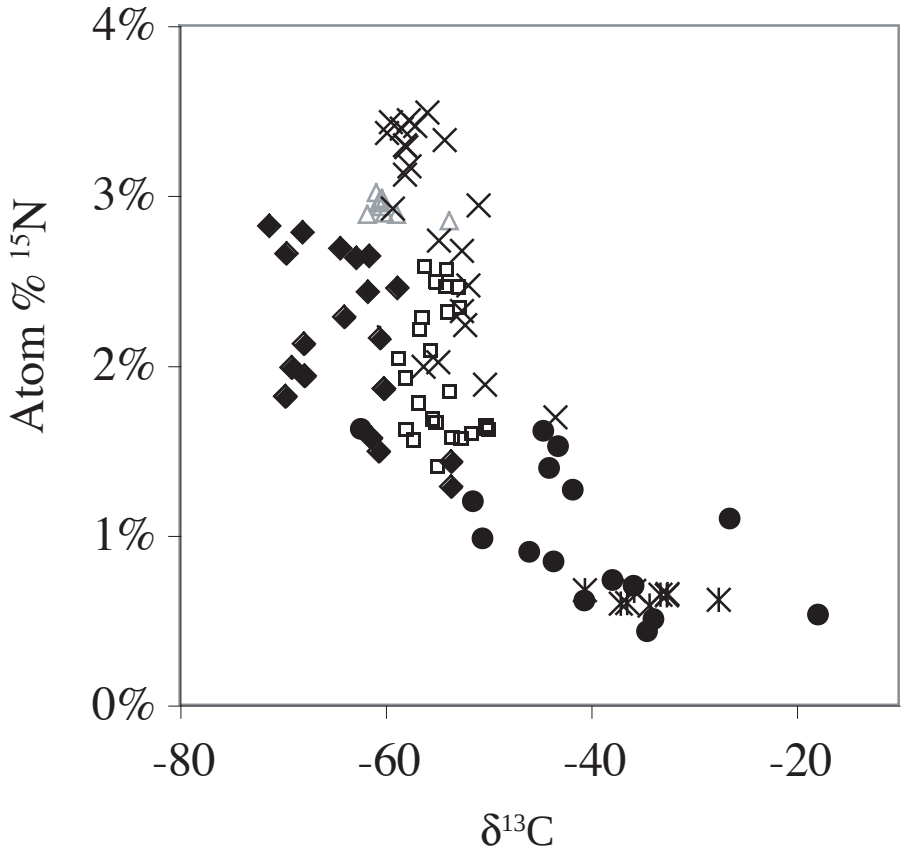

Figure S2. Unrooted neighbor-joining tree of translated *nif*H sequences constructed using the Geneious Pro 4.6.2 Tree-Builder (Jukes-Cantor distance model and 100 bootstrap replicates) following global alignment with Geneious Pro 4.6.2 using the ClustalW algorithm. Bootstrap values >50% are indicated. The scale bar represents changes per amino acid position. The sequences obtained in this study are shown in red. Roman numerals refer to previously described *nif*H clusters (*S41*). Additional environmental sequences, including others from the Eel River Basin methane seeps are from (*S16, 42*).

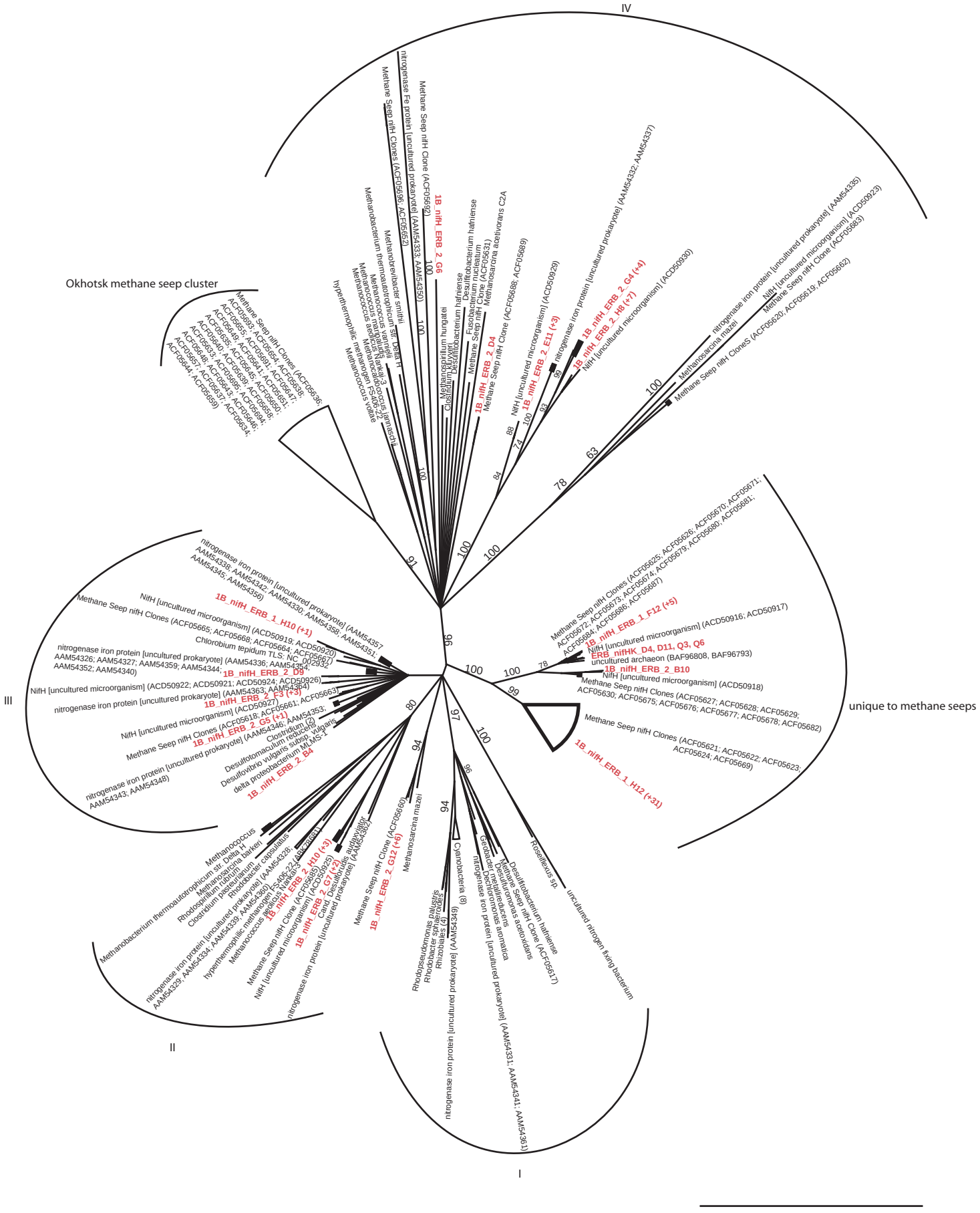
IV
Okhotsk methane seep cluster
Methane Seep nifH Clones (ACF05636; ACF05637; ACF05638; ACF05639; ACF05640; ACF05641; ACF05642; ACF05643; ACF05644; ACF05645; ACF05646; ACF05647; ACF05648; ACF05649; ACF05650; ACF05651; ACF05652; ACF05653; ACF05654; ACF05655; ACF05656; ACF05657; ACF05658; ACF05659)
nitrogenase Fe protein [uncultured prokaryote] (AAM54333; AAM54350)
Methane Seep nifH Clones (ACF05660; ACF05662)
Methane Seep nifH Clone (ACF05692)
1B_nifH_ERB_2_G6
Methanobacterium thermoautotrophicum str. Delta H
Methanococcus maripaludis
Methanococcus aeolicus Nankai-3
Methanococcus vannielii
Methanococcus voltae
Methanococcus jannaschii
hyperthermophilic methanogen FS406-22
Methanobrevibacter smithii
Methanosphaera stadtmanae
Clostridium thermocellum
Desulfitobacterium hafniense
Fusobacterium nucleatum
Methane Seep nifH Clone (ACF05631)
Methanosarcina acetivorans C2A
1B_nifH_ERB_2_D4
Methane Seep nifH Clone (ACF05688; ACF05689)
NifH [uncultured microorganism] (ACD50929)
1B_nifH_ERB_2_E11 (+3)
nitrogenase iron protein [uncultured prokaryote] (AAM54332; AAM54337)
1B_nifH_ERB_2_G4 (+4)
1B_nifH_ERB_2_H8 (+7)
NifH [uncultured microorganism] (ACD50930)
nitrogenase iron protein [uncultured prokaryote] (AAM54335)
NifH [uncultured microorganism] (ACD50923)
Methanosarcina mazei
Methane Seep nifH Clone (ACF05683)
Methane Seep nifH CloneS (ACF05619; ACF05620; ACF05662)
unique to methane seeps
Methane Seep nifH Clones (ACF05625; ACF05626; ACF05670; ACF05671; ACF05672; ACF05673; ACF05674; ACF05679; ACF05680; ACF05681; ACF05684; ACF05685; ACF05686; ACF05687)
1B_nifH_ERB_1_F12 (+5)
NifH [uncultured microorganism] (ACD50916; ACD50917)
1B_nifHK_D4, D11, Q3, Q6
ERB_nifHK_D4, D11, Q3, Q6
uncultured archaeon (BAF96808, BAF96793)
1B_nifH_ERB_2_B10
NifH [uncultured microorganism] (ACD50918)
Methane Seep nifH Clones (ACF05627; ACF05628; ACF05629; ACF05630; ACF05675; ACF05676; ACF05677; ACF05678; ACF05682)
Methane Seep nifH Clones (ACF05621; ACF05622; ACF05623; ACF05624; ACF05669)
1B_nifH_ERB_1_H12 (+31)
III
nitrogenase iron protein [uncultured prokaryote] (AAM54357; AAM54338; AAM54342; AAM54330; AAM54358; AAM54351; AAM54345; AAM54356)
Methane Seep nifH Clones (ACF05665; ACF05668; ACF05664; ACF05667)
NifH [uncultured microorganism] (ACD50919; ACD50920)
1B_nifH_ERB_1_H10 (+1)
Chlorobium tepidum TLS, NC_002932
nitrogenase iron protein [uncultured prokaryote] (AAM54336; AAM54364; AAM54326; AAM54327; AAM54359; AAM54344; AAM54352; AAM54340)
1B_nifH_ERB_2_D9
NifH [uncultured microorganism] (ACD50922; ACD50921; ACD50924; ACD50926)
nitrogenase iron protein [uncultured prokaryote] (AAM54363; AAM54364)
1B_nifH_ERB_2_F3 (+3)
NifH [uncultured microorganism] (ACD50927)
Methane Seep nifH Clones (ACF05618; ACF05661; ACF05663; AAM54353; AAM54346; AAM54362)
1B_nifH_ERB_2_G5 (+1)
Clostridium tepidum (2)
Desulfotomaculum reducens
Desulfovibrio vulgaris subsp. vulgaris
delta proteobacterium MLMS-1
nitrogenase iron protein [uncultured prokaryote] (AAM54348; AAM54343)
1B_nifH_ERB_2_B4
II
Methanobacterium thermoautotrophicum str. Delta H
Methanosphaera barkeri
Rhodospirillum rubrum
Clostridium pasteurianum
Rhodobacter capsulatus
nitrogenase iron protein [uncultured prokaryote] (AAM54360; AAM54334; AAM54339; AAM54329; AAM54328; AAM54337)
hyperthermophilic methanogen FS406-22
Methanococcus maripaludis Nankai-3
1B_nifH_ERB_2_H10 (+3)
Methane Seep nifH Clone (ACF05685)
1B_nifH_ERB_2_G10 (+2)
NifH [uncultured microorganism] (ACD50925)
Cand. Desulforudis audaxviator
nitrogenase iron protein [uncultured prokaryote] (AAM54362)
Methane Seep nifH Clone (ACF05660)
1B_nifH_ERB_2_G12 (+6)
Methanosarcina mazei
I
Rhodopseudomonas palustris
Rhodobacter sphaeroides
Rhizobiales (4)
Cyanobacteria (8)
nitrogenase iron protein [uncultured prokaryote] (AAM54349)
Geobacter metallireducens
Desulfuromonas acetoxidans
Desulfuromonas aromatica
nitrogenase iron protein [uncultured prokaryote] (AAM54331; AAM54341; AAM54361)
Desulfitobacterium hafniense
Methane Seep nifH Clone (ACF05617)
Roseiflexus sp.
uncultured nitrogen fixing bacterium
0.2

Figure S3. Panel A: Comparison of partial nitrogenase operon structure for putative ANME-2-affiliated nitrogenase and other taxa harboring the gene order *nifH, nifI1, nifI2, nifD* and *nifK*). Numbers indicate base pairs between coding regions. Breaks in *nifK* indicate end of partial sequences. Panel B: Amino acid sequences flanking the conserved Hisα-442 residue of the nifD, nitrogenase α subunit. Key residues at this known metal cofactor binding site in *Azotobacter vinelandii* (*S39*) indicate possible differences in the metal composition of the cofactor used. Typical conserved flanking regions of the Hisα-442 of the α subunit of Mo-Fe, V-Fe, and Fe-Fe nitrogenase proteins are shown. It has been speculated that these differences in the primary structure of the metal cofactor binding site are important adaptations to an anaerobic lifestyle, as most of the organisms with the canonical *A. vinelandii*-like Mo-Fe nitrogenase are not strict anaerobes (*S40*).

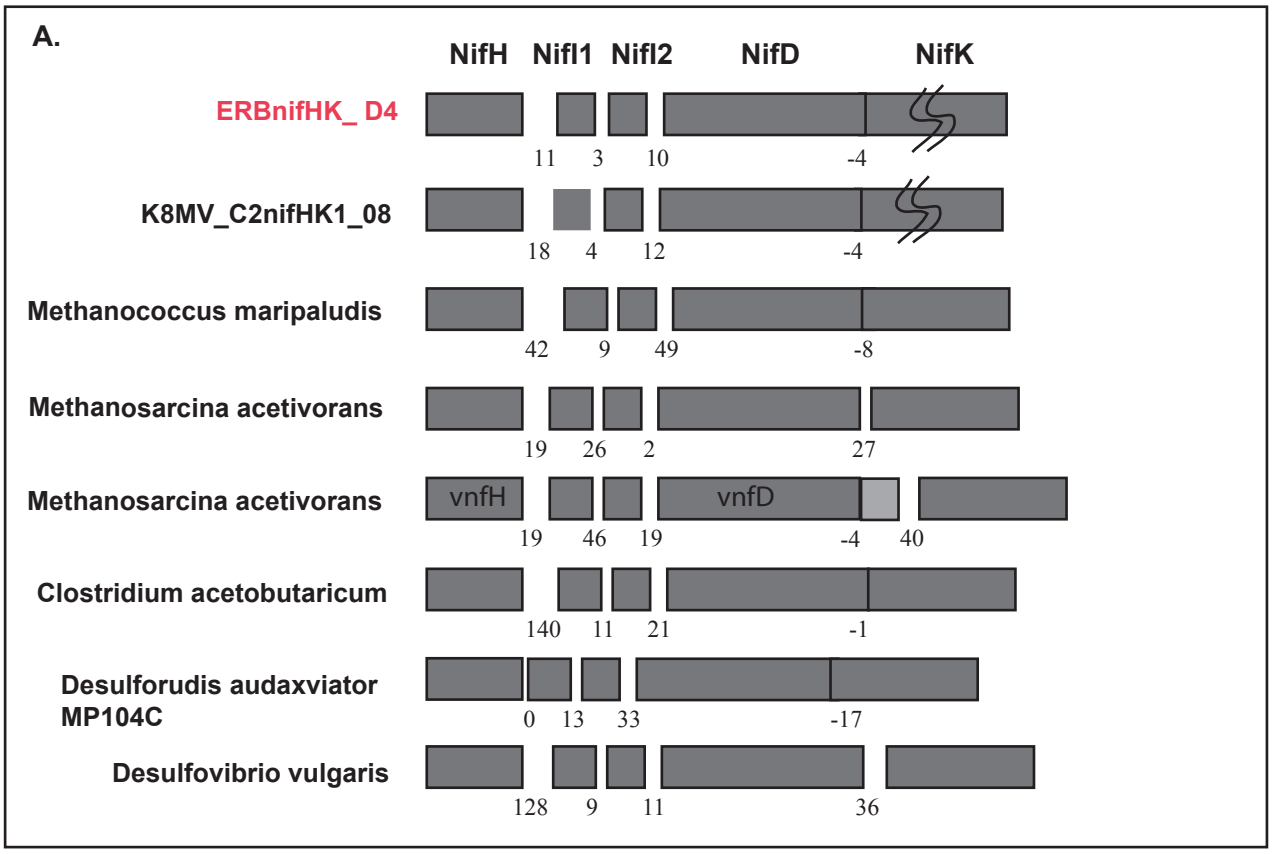

B.

Residues Flanking nifD metal binding sites (Cisα275 and Hisα442)

	Cisα275	Hisα442
Desulfobacterium autotrophicum HRM2	LNAVMCHRSINY	MKQLHSYDS
delta proteobacterium MLMS-1	LNAVMCHRSINY	MKQLHSYDS
Desulfovibrio vulgaris subsp.	LNLVMCHRSINY	CKQLHNYDY
Desulfatibacillum alkenivorans AK-01	LNCIMCHRSINY	LKQLHSYDY
Desulfotomaculum reducens MI-1 1	LNLVQCHRSINY	AKQLHSYDY
Clostridium butyricum 5521	LNVIQCHRSINY	SRQLHSYDY
Uncultured methanogenic archaeon RC-I	LNLVQCHRSINY	SRQLHSYDY
Methanosarcina barkeri	LSILVCHRSINY	SRQIHSYDY
Methanosarcina mazei	LSILLCHRSINY	SRQIHSYDY
Candidatus Desulforudis audaxviator_2	LNILHCYRSMNY	TLNSHSYEK
Methanococcus aeolicus Nankai-3	LNLIHCYRSMNY	TVNSHSYEE
ERB_nifHK_Q3	LVLIHCYRSMNY	FVNGHSYER
ERB_nifHK_Q6	LNLVHCYRSMNY	FVNGHSYER
ERB_nifHK_D11	LNLIHCYRSMNY	FVNGHSYER
ERB_nifHK_D4	LNVIHCYRSMNY	FVNGHSYER
K8MV-C2nifHK1_08	LNLIHCYRSMNY	FVNGHSYER
K8MV-C2nifHK1_40	LNVVHCQRSATY	FVNGHSYER
Roseiflexus sp. RS-1	LNVVHCQRSAEY	FVNGHTYDT
Methanococcus maripaludis strain S2	LNVMHCQRSTPY	SVMIHSYEN
Methanothermobacter thermautotrophicus str. Delta H	LNVMHCQRSTPY	CVLIHSYEN
Bradyrhizobium japonicum USDA 110	LNVMHCQRSTPY	FRQMHSWDY
Sinorhizobium meliloti 1021	LNVMHCQRSTPY	FRQMHSWDY
Nostoc sp. PCC 7120	LNVMHCQRSTPY	FRQMHSWDY
Azotobacter vinelandii	LNVMHCQRSTLY	FRQMHSWDY
Frankia sp. CcI3	LNIVHCQRSATY	FRQMHSWDY
Desulfuromonas acetoxidans DSM 684	LSLVRCQRSATY	FRQMHSWDY
Geobacter sulfurreducens PCA	LSLVRCQRSATY	FRQMHSWDY
Anabaena variabilis ATCC 29413 vnfD	LNVTNCARSAGY	YVNGHGYHN
Azotobacter vinelandii DJ vnfD	LNVVNCARSSGY	YVNGHGYHN
Azotobacter chroococcum (strain mcd 1) vnfD	LNVVNCARSSGY	YVNGHGYHN
Methanosarcina acetivorans str. C2A anfD	LNVLECARSAEY	YLNIHGYHN
Methanosarcina barkeri vnfD	LNVVNCARSAGY	YINGHAYHN
Rhodobacter capsulatus anfD	LNVLECARSAEY	YLNAHAYHN
Rhodopseudomonas palustris CGA009 anfD	LNVLECARSAEY	YLNAHAYHN
Clostridium kluyveri DSM 555 anfD	LNVLECARSAEY	YLNAHAYHN
Azotobacter vinelandii DJ anfD	LNVLECARSAEY	YLNAHAYHN

Table S1. Incubation conditions.

Push Core*	Status	Medium†	Vol‡ (ml)	$^{15}N_2$ § (%)	N_2 § (%)	CH_4 § (%)	Amendment	H_2S production¶
14	Live	A	35	5.2	0	94.8	--	+
14	Live	A	35	5.2	0	94.8	$^{15}NH_3$ (2 mM)	+
14	Live	A	35	5.2	0	94.8	BES‖ (5 mM)	+
14	Live	A	35	5.2	0	94.8	Na_2MoO_4 (25 mM)	-
14	Live	A	35	5.2	95.5	--	--	-
14	Killed	A	35	5.2	0	94.8	--	-
11	Live	FSW	15	--	--	100	$Na^{15}NO_3$ (2mM)	+
11	Live	FSW	15	--	--	100	$K^{13}C^{15}N$ (1mM)	+
11	Live	FSW	15	--	--	100	BES (5 mM)	+
11	Live	FSW	15	--	--	100	BES (20 mM)	+
11	Live	FSW	15	--	--	100	--	+
11	Live	FSW	15	--	100	--	--	-
11	Killed	FSW	15	--	--	100	--	-

*PC 14 assays were performed in triplicate in 140 ml serum bottles. PC 11 assays were performed in duplicate in 60 ml bottles.
†A = Artificial seawater, as described in text. FSW = Eel River Basin 0.2 μm filtered seawater collected near methane seep (500 m).
‡Volume of sediment slurry.
§The headspace in all treatments was at an overpressure of 2 atm.
‖2-bromoethanesulfonic acid.
¶ "+" indicates 25-40 mM (note artificial seawater contained 40 mM sulfate), "-" indicates H_2S levels ≤ killed control"

Table S2. NifD sequences used in phylogenetic analysis. "Bp" indicates length of sequence in base pairs. "Ref #" indicates the number the sequence is represented by in Figure 4.

Name	Accession Number	Description	Bp	Ref #
Methanothermobacter thermautotrophicus str. Delta H	NP_276676.1|	nitrogenase NifD subunit [Methanothermobacter thermautotrophicus str. Delta H]	469	1
Methanosarcina barkeri	sp|P55170|NIFD_METBA	Methanosarcina barkeri nitrogenase molybdenum-iron protein alpha chain	532	2
delta proteobacterium MLMS-1	ZP_01287659.1|	MldDRAFT_1221 Nitrogenase molybdenum-iron protein alpha chain:Nitrogenase component I, alpha chain [delta proteobacterium MLMS-1, unfinished sequence: NZ_AAQF01000015]	539	3
Desulfatibacillum alkenivorans AK-01	YP_002430685.1|	DalkDRAFT_0718 nitrogenase molybdenum-iron protein alpha chain [Desulfatibacillum alkenivorans AK-01, unfinished sequence: NZ_ABII01000029]	554	4
Pelodictyon luteolum DSM 273	YP_375431.1|	Plut_1531 Nitrogenase molybdenum-iron protein alpha chain [Pelodictyon luteolum DSM 273: NC_007512]	539	5
Chlorobium tepidum TLS	NP_662420.1|	nifD nitrogenase molybdenum-iron protein, alpha subunit [Chlorobium tepidum TLS: NC_002932]	536	6
Dethiobacter alkaliphilus AHT 1	ZP_03735355.1|	nitrogenase molybdenum-iron protein alpha chain [Dethiobacter alkaliphilus AHT 1]	538	7
Clostridium acetobutylicum ATCC 824	NP_346897.1|	nifD Nitrogenase molybdenum-iron protein, alpha chain (nitrogenase component I) gene nifD [Clostridium acetobutylicum ATCC 824: NC_003030]	522	8
Clostridium butyricum 5521	ZP_02948849.1|	nifD nitrogenase molybdenum-iron protein alpha chain [Clostridium butyricum 5521, unfinished sequence: NZ_ABDT01000049]	521	9
Roseiflexus sp. RS-1	YP_001275556.1|	nitrogenase component I, alpha chain [Roseiflexus sp. RS-1]	466	10
Moorella thermoacetica ATCC 39073	YP_429424.1|	nitrogenase component I, alpha chain [Moorella thermoacetica ATCC 39073] gi|83589415|ref|YP_429424.1|	486	11
Methanococcus maripaludis strain S2	NP_987976.1|	nifD Oxidoreductase, nitrogenase component 1 [Methanococcus maripaludis strain S2: BX950229]	484	12
Methanococcus vannielii SB	YP_001322588.1|	Mevan_0062 nitrogenase alpha chain [Methanococcus vannielii SB: NC_009634]	475	13
Chloroherpeton thalassium ATCC 35110	YP_001996735.1|	Ctha_1831 nitrogenase alpha chain [Chloroherpeton thalassium ATCC 35110: NC_011026]	467	14
Rhodopseudomonas palustris CGA009	NP_946728.1|	nitrogenase vanadium-iron protein alpha chain gi|39934452|ref|NP_946728.1|	472	15
Rhodobacter capsulatus	emb|CAA49625.1|	alternative nitrogenase [Rhodobacter capsulatus]	526	16
Rhodospirillum rubrum ATCC 11170	YP_426099.1|	Rru_A1011 Nitrogenase molybdenum-iron protein alpha chain [Rhodospirillum rubrum ATCC 11170: NC_007643]	484	17

Methylacidiphilum infernorum V4	YP_001940526.1|	nifD Nitrogenase molybdenum-cofactor protein, alpha chain [Methylacidiphilum infernorum V4: NC_010794]	489	18
Magnetococcus sp. MC-1	YP_865118.1|	Mmc1_1201 nitrogenase molybdenum-iron protein alpha chain [Magnetococcus sp. MC-1: NC_008576]	479	19
Erwinia carotovora subsp. atroseptica	YP_051046.1|	nifD nitrogenase molybdenum-iron protein alpha chain [Erwinia carotovora subsp. atroseptica SCRI1043: NC_004547]	482	20
Frankia sp. CcI3	YP_483562.1|	Francci3_4487 nitrogenase molybdenum-iron protein alpha chain [Frankia sp. CcI3: NC_007777]	486	21
Heliobacterium modesticaldum Ice1	YP_001679707.1|	nifD dinitrogenase molybdenum-iron protein alpha subunit nifd [Heliobacterium modesticaldum Ice1: NC_010337]	485	22
Pelobacter carbinolicus DSM 2380	YP_357509.1|	Pcar_2099 nitrogenase molybdenum-iron protein, alpha chain [Pelobacter carbinolicus DSM 2380: NC_007498]	486	23
Acidithiobacillus ferrooxidans	YP_002219684.1|	Lferr_1239 nitrogenase molybdenum-iron protein alpha chain [Acidithiobacillus ferrooxidans ATCC 53993: NC_011206]	491	
Anabaena variabilis ATCC 29413	YP_324526.1|	nitrogenase vanadium-iron protein, alpha chain gi|75910230|ref|YP_324526.1|	587	
Azoarcus sp. BH72	YP_932043.1|	nifD nitrogenase molybdenum-iron protein alpha chain [Azoarcus sp. BH72: NC_008702]	486	
Azorhizobium caulinodans ORS 571	YP_001523956.1|	nifD nitrogenase molybdenum-iron protein alpha chain [Azorhizobium caulinodans ORS 571: NC_009937]	490	
Azotobacter chroococcum (strain mcd 1)	sp|P15332|VNFD_AZOCH	RecName: Full=Nitrogenase vanadium-iron protein alpha chain gi|138885|sp|P15332.2|VNFD_AZOCH	473	
Azotobacter vinelandii	prf||1111233B	Azotobacter vinelandii nitrogenase MoFe protein alpha gi|224698|prf||1111233B	492	
Azotobacter vinelandii DJ	YP_002797497.1|	vanadium nitrogenase, alpha subunit, vnfD gi|226942424|ref|YP_002797497.1|	474	
Bradyrhizobium japonicum USDA 110	NP_768383.1|	nifD nitrogenase molybdenum-iron protein alpha chain [Bradyrhizobium japonicum USDA 110: NC_004463]	490	
Bradyrhizobium sp. ORS278	YP_001207333.1|	nifD nitrogenase molybdenum-iron protein alpha chain, nifD [Bradyrhizobium sp. ORS278: NC_009445]	490	
Burkholderia xenovorans	YP_553848.1|	nifD Nitrogenase, molybdenum-iron protein alpha chain(NifD) [Burkholderia xenovorans LB400 chromosome 2: NC_007952]	485	
Caldicellulosiruptor saccharolyticus DSM 8903	YP_001181231.1|	nitrogenase component I, alpha chain [Caldicellulosiruptor saccharolyticus DSM 8903]	461	
Candidatus Desulforudis audaxviator_2	YP_001716346.1|	Daud_0146 nitrogenase component I, alpha chain [Candidatus Desulforudis audaxviator MP104C: NC_010424]	481	
Chlorobium chlorochromatii CaD3	YP_379551.1|	Cag_1247 Nitrogenase molybdenum-iron protein alpha chain [Chlorobium chlorochromatii CaD3: NC_007514]	537	

Chlorobium ferrooxidans DSM 13031	ZP_01385046.1|	CferDRAFT_1910 nitrogenase molybdenum-iron protein alpha chain:Nitrogenase component I, alpha chain [Chlorobium ferrooxidans DSM 13031, unfinished sequence: NZ_AASE01000001]	537
Chlorobium phaeobacteroides BS1	YP_001960153.1|	Cphamn1_1754 nitrogenase molybdenum-iron protein alpha chain [Chlorobium phaeobacteroides BS1: NC_010831]	533
Clostridium beijerinckii NCIMB 8052	YP_001309128.1|	Cbei_2002 nitrogenase molybdenum-iron protein alpha chain [Clostridium beijerinckii NCIMB 8052: NC_009617]	520
Clostridium kluyveri DSM 555	YP_001395137.1|	VnfD gi|153954372|ref|YP_001395137.1|	462
Clostridium kluyveri DSM 556	YP_001393772	AnfD [Clostridium kluyveri DSM 555]	516
Clostridium pasteurianum	sp|P00467|NIFD_CLOPA	nitrogenase molybdenum-iron protein alpha-subunit [Clostridium pasteurianum] gi|47827220|gb|AAA83531.2|	534
Crocosphaera watsonii WH 8501	ZP_00516387.1|	CwatDRAFT_3819 Nitrogenase molybdenum-iron protein alpha chain:Nitrogenase component I, alpha chain [Crocosphaera watsonii WH 8501, unfinished sequence: NZ_AADV02000024]	478
Cupriavidus taiwanensis	YP_001796235.1|	nifD NifD nitrogenase molybdenum-iron protein alpha chain (Nitrogenase component I) (Dinitrogenase) [Cupriavidus taiwanensis plasmid pRALTA: NC_010529]	488
Cyanothece sp. ATCC 51142	YP_001801977.1|	nifD nitrogenase molybdenum-iron protein alpha chain [Cyanothece sp. ATCC 51142 chromosome circular: NC_010546]	480
Cyanothece sp. ATCC 51142 2	ZP_01727766.1|	CY0110_22417 Nitrogenase molybdenum-iron protein alpha chain [Cyanothece sp. CCY0110, unfinished sequence: NZ_AAXW01000004]	480
Dechloromonas aromatica	YP_284633.1|	Daro_1414 Nitrogenase molybdenum-iron protein alpha chain:Nitrogenase component I, alpha chain [Dechloromonas aromatica RCB: NC_007298]	489
Dehalococcoides ethenogenes	YP_181869.1|	nifD nitrogenase molybdenum-iron protein alpha chain [Dehalococcoides ethenogenes 195: NC_002936]	533
Desulfitobacterium hafniense DCB-2 1	YP_520503.1|	Dhaf_0410 nitrogenase molybdenum-iron protein alpha chain [Desulfitobacterium hafniense DCB-2, unfinished sequence: NZ_AAAW04000004]	477
Desulfitobacterium hafniense DCB-2 2	YP_520503.1|	Dhaf_0410 nitrogenase molybdenum-iron protein alpha chain [Desulfitobacterium hafniense DCB-2, unfinished sequence: NZ_AAAW04000004]	477
Desulfitobacterium hafniense Y51	YP_520503.1|	DSY4270 nitrogenase iron-molybdenum protein alpha chain [Desulfitobacterium hafniense Y51: NC_007907]	493
Desulfobacterium autotrophicum HRM2	YP_002602246.1|	NifD2 [Desulfobacterium autotrophicum HRM2]	554
Desulfotomaculum reducens MI-1 1	YP_001114147.1|	Dred_2818 nitrogenase molybdenum-iron protein alpha chain [Desulfotomaculum reducens MI-1: NC_009253]	539

Desulfovibrio vulgaris subsp.	YP_009052.1|	nifD nitrogenase molybdenum-iron protein alpha chain [Desulfovibrio vulgaris subsp. vulgaris str. Hildenborough megaplasmid: NC_005863]	536
Desulfovibrio vulgaris subsp. vulgaris	YP_961292.1|	Dvul_3093 nitrogenase molybdenum-iron protein alpha chain [Desulfovibrio vulgaris subsp. vulgaris DP4 plasmid pDVUL01: NC_008741]	542
Desulfuromonas acetoxidans DSM 684	ZP_01312342.1|	Dace_2254 nitrogenase molybdenum-iron protein alpha chain [Desulfuromonas acetoxidans DSM 684, unfinished sequence: NZ_AAEW02000007]	480
ERB_nifHK_D11	**this study**		**456**
ERB_nifHK_D4	**this study**		**459**
ERB_nifHK_Q3	**this study**		**456**
ERB_nifHK_Q6	**this study**		**455**
Frankia alni ACN14a	YP_716938.1|	nifD Nitrogenase molybdenum-iron protein alpha chain (Nitrogenase component I) (Dinitrogenase) [Frankia alni ACN14a: NC_008278]	486
Geobacter sulfurreducens PCA	NP_953864.1|	nifD nitrogenase molybdenum-iron protein, alpha chain [Geobacter sulfurreducens PCA: NC_002939]	479
Gluconacetobacter diazotrophicus	YP_001600721.1|	nifD FeMo protein of nitrogenase alpha subunit	497
Gluconacetobacter diazotrophicus PAl 5	YP_001600721.1|	GdiaDRAFT_0505 nitrogenase molybdenum-iron protein alpha chain [Gluconacetobacter diazotrophicus PAl 5, unfinished sequence: NZ_ABPH01000001]	497
Halorhodospira halophila SL1	YP_001001869.1|	Hhal_0273 nitrogenase molybdenum-iron protein alpha chain [Halorhodospira halophila SL1: NC_008789]	488
Herbaspirillum seropedicae	sp|P77874|NIFD_HERSE	nitrogenase Mo-Fe protein alpha chain [Herbaspirillum seropedicae]	484
K8MV-C2nifHK1_08	dbj|BAF96796.1|	dinitrogenase alpha subunit [K8MV-C2nifHK1_08]	456
K8MV-C2nifHK1_40	dbj|BAF96811.1|	dinitrogenase alpha subunit [K8MV-C2nifHK1_40]	456
Klebsiella pneumoniae	emb|CAA68413.1|	nitrogenase alpha-subunit [Klebsiella pneumoniae]	483
Leptothrix cholodnii SP-6	YP_001790464.1|	Lcho_1431 nitrogenase molybdenum-iron protein alpha chain [Leptothrix cholodnii SP-6: NC_010524]	485
Magnetospirillum magnetotacticum MS-1	ZP_00054386.1|	COG2710: Nitrogenase molybdenum-iron protein, alpha and beta chains [Magnetospirillum magnetotacticum MS-1]	485
Mesorhizobium loti MAFF303099	NP_106490.1|	mlr5906 nitrogenase molybdenum-iron protein alpha chain, nifD [Mesorhizobium loti MAFF303099: NC_002678]	498
Methanococcus aeolicus Nankai-3	YP_001325619.1|	nitrogenase component I, alpha chain [Methanococcus aeolicus Nankai-3]	474
Methanococcus maripaludis C5	YP_001097187.1|	MmarC5_0661 nitrogenase alpha chain [Methanococcus maripaludis C5: NC_009135]	476
Methanococcus maripaludis C6	YP_001549843.1|	MmarC6_1800 nitrogenase alpha chain [Methanococcus maripaludis C6: NC_009975]	477
Methanococcus maripaludis C7_1	YP_001329322.1|	nitrogenase alpha chain [Methanococcus maripaludis C7]	476

Methanosarcina acetivorans str. C2A	NP_618769.1|	nifD nitrogenase, subunit alpha [Methanosarcina acetivorans str. C2A: AE010299]	527
Methanosarcina acetivorans str. C2A	NP_616149.1|	nitrogenase, subunit D [Methanosarcina acetivorans C2A]	520
Methanosarcina barkeri	gb|AAF72180.1|AF254784_1	putative vanadium dinitrogenase alpha subunit gi|8099626|gb|AAF72180.1|AF254784_1	465
Methanosarcina mazei	NP_632746.1|	NifD [Methanosarcina mazei]	532
Methylococcus capsulatus str. Bath	YP_112765.1|	nifD nitrogenase molybdenum-iron protein alpha chain [Methylococcus capsulatus str. Bath: NC_002977]	484
Nodularia spumigena CCY9414	ZP_01628430.1|	N9414_15055 Nitrogenase molybdenum-iron protein alpha chain [Nodularia spumigena CCY9414, unfinished sequence: NZ_AAVW01000003]	480
Nostoc sp. PCC 7120	NP_485484.1|	nifD nitrogenase molybdenum-iron protein alpha chain [Nostoc sp. PCC 7120: NC_003272]	494
Opitutaceae bacterium TAV2	ZP_03723746.1|	ObacDRAFT_0896 nitrogenase molybdenum-iron protein alpha chain [Opitutaceae bacterium TAV2, unfinished sequence: NZ_ABEA01000244]	563
Pseudomonas stutzeri A1501	YP_001171864.1|	nifD MoFe protein, alpha subunit [Pseudomonas stutzeri A1501: NC_009434]	487
Rhizobium etli CFN 42	NP_659737.1|	nitrogenase, iron-molybdenum alpha chain protein [Rhizobium etli CFN 42]	496
Rhizobium etli CIAT 652	ZP_03512900.1|	nifD3 nitrogenase protein, iron-molybdenum alpha chain NifD [Rhizobium etli CIAT 652 plasmid pB: NC_010996]	497
Rhizobium leguminosarum bv. viciae 3841	YP_770439.1|	nifD nitrogenase molybdenum-iron protein alpha chain [Rhizobium leguminosarum bv. viciae 3841 plasmid pRL10: NC_008381]	492
Rhodobacter sphaeroides 2.4.1	YP_353613.1|	nifD Nitrogenase iron-molybdenum protein, alpha chain [Rhodobacter sphaeroides 2.4.1 chromosome 1: NC_007493]	491
Rhodopseudomonas palustris CGA009	NP_949953.1|	nifD nitrogenase molybdenum-iron protein alpha chain, nifD [Rhodopseudomonas palustris CGA009: NC_005296]	487
Roseiflexus castenholzii DSM 13941	YP_001434092.1|	nitrogenase component I, alpha chain [Roseiflexus castenholzii DSM 13941]	476
Sinorhizobium meliloti 1021	NP_435696.1|	nifD NifD nitrogenase Fe-Mo alpha chain [Sinorhizobium meliloti 1021 plasmid pSymA: NC_003037]	493
Synechococcus sp. JA-3-3Ab	YP_475237.1|	nifD nitrogenase molybdenum-iron protein alpha chain [Synechococcus sp. JA-3-3Ab: NC_007775]	487
Uncultured methanogenic archaeon RC-I	YP_686179.1|	nifD nitrogenase molybdenum-iron protein, subunit alpha (dinitrogenase) [Uncultured methanogenic archaeon RC-I: NC_009464]	534
Wolinella succinogenes DSM 1740	NP_907558.1|	NIFD NIFD [Wolinella succinogenes DSM 1740: NC_005090]	484
Xanthobacter autotrophicus Py2	YP_001415005.1|	Xaut_0089 nitrogenase molybdenum-iron protein alpha chain [Xanthobacter autotrophicus Py2: NC_009720]	490
Zymomonas mobilis subsp. mobilis ZM4	YP_163559.1|	nifD nitrogenase FeMo alpha subunit [Zymomonas mobilis subsp. mobilis ZM4: NC_006526]	489

Table S3. NifH sequences used in phylogenetic analysis. "Bp" indicates length of sequence in base pairs.

Name	Bp	Accession Number	nifH Group
Anabaena variabilis ATCC 29413 Ava_4247: NC_007413	128	gi|75910445|ref|YP_324741.1|	cluster I
Azotobacter vinelandii AvOP, NZ_AAAU03000003	129	_NZ_AAAU03000003	cluster I
Bradyrhizobium sp. BTAi1: NC_009485	128	gi|148257143|ref|YP_001241728.1|	cluster I
Crocosphaera watsonii WH 8501, unfinished sequence: NZ_AADV02000024	128	_unfinished_sequence:_NZ_AADV02000024	cluster I
Cyanothece sp. ATCC 51142 chromosome circular: NC_010546	127	gi|172035475|ref|YP_001801976.1|	cluster I
Dechloromonas aromatica RCB: NC_007298	129	gi|71907047|ref|YP_284634.1|	cluster I
Desulfitobacterium hafniense DCB-2 Dhaf_0411, unfinished sequence: NZ_AAAW04000004	129	_unfinished_sequence:_NZ_AAAW04000004	cluster I
Desulfuromonas acetoxidans DSM 684, unfinished sequence: NZ_AAEW02000007	129	_unfinished_sequence:_NZ_AAEW02000007	cluster I
Frankia sp. CcI3: NC_007777	128	gi|86743163|ref|YP_483563.1|	cluster I
Geobacter metallireducens GS-15: NC_007517	129	gi|78221882|ref|YP_383629.1|	cluster I
Heliobacterium modesticaldum Ice1: NC_010337	129	gi|167629207|ref|YP_001679706.1|	cluster I
Lyngbya sp. PCC 8106, unfinished sequence: NZ_AAVU01000012	128	_unfinished_sequence:_NZ_AAVU01000012	cluster I
Mesorhizobium loti MAFF303099: NC_002678	128	gi|20804123|emb|CAD31326.1|	cluster I
Nostoc punctiforme PCC 73102 Npun_F5903: NC_010628 1	128	gi|186685943|ref|YP_001869139.1|	cluster I
Oscillochloris trichoides	128	gi|71905239|gb|AAZ52660.1|	cluster I
Pelobacter carbinolicus DSM 2380: NC_007498	129	gi|77919693|ref|YP_357508.1|	cluster I
Pseudomonas stutzeri A1501: NC_009434	129	gi|146281710|ref|YP_001171863.1|	cluster I
Rhizobium etli CIAT 652 plasmid pB: NC_010996	128	gi|21492662|ref|NP_659736.1|	cluster I
Rhodobacter sphaeroides ATCC 17025: NC_009428	128	gi|146277293|ref|YP_001167452.1|	cluster I
Rhodopseudomonas palustris CGA009 nifH4: NC_005296	128	gi|115526522|ref|YP_783433.1|	cluster I
Roseiflexus castenholzii DSM 13941: NC_009767	128	gi|148655353|ref|YP_001275558.1|	cluster I
Roseiflexus sp. RS-1: NC_009523	128	gi|148655353|ref|YP_001275558.1|	cluster I
Sinorhizobium meliloti 1021 plasmid pSymA: NC_003037	128	gi|16262902|ref|NP_435695.1|	cluster I
Synechococcus sp. JA-2-3B'a(2-13): NC_007776	128	gi|86606475|ref|YP_475238.1|	cluster I
Trichodesmium erythraeum IMS101: NC_008312	129	gi|113477556|ref|YP_723617.1|	cluster I
uncultured nitrogen fixing bacterium	128	gi|159145977|gb|ABW90511.1|	cluster I
uncultured prokaryote (Dang, 2009)	129	gi|192764146|gb|ACF05617.1|	cluster I
uncultured prokaryote (Mehta, 2003)	127	gi|21586711|gb|AAM54331.1|	cluster I
uncultured prokaryote (Mehta, 2003)	127	gi|21586731|gb|AAM54341.1|	cluster I
uncultured prokaryote (Mehta, 2003)	126	gi|21586747|gb|AAM54349.1|	cluster I
uncultured prokaryote (Mehta, 2003)	127	gi|21586771|gb|AAM54361.1|	cluster I

1B_nifH_ERB_1_G7 - translation	**129**	**this study**	**cluster II**
1B_nifH_ERB_1_H9 - translation	**129**	**this study**	**cluster II**
1B_nifH_ERB_2_C12 - translation	**127**	**this study**	**cluster II**
1B_nifH_ERB_2_E3 - translation	**122**	**this study**	**cluster II**
1B_nifH_ERB_2_G7 - translation	**129**	**this study**	**cluster II**
1B_nifH_ERB_2_H10 - translation	**129**	**this study**	**cluster II**
1B_nifH_ERB_2_H3 - translation	**108**	**this study**	**cluster II**
Candidatus Desulforudis audaxviator MP104C: NC_010424	129	gi|169830361|ref|YP_001716343.1|	cluster II
Clostridium pasteurianum	129	gi|128214|sp|P09553.1|NIFH3_CLOPA	cluster II
Methanobacterium thermoautotrophicum str. Delta H MTH1560: AE000666	129	gi|20138869|sp|O27602.2|NIFH1_METTH	cluster II
Methanococcus aeolicus Nankai-3 Maeo_1434: NC_009635	129	gi|150401856|ref|YP_001325622.1|	cluster II
Methanococcus maripaludis strain S2: BX950229	129	gi|134045698|ref|YP_001097184.1|	cluster II
Methanococcus vannielii SB Mevan_0065: NC_009634	129	gi|150398824|ref|YP_001322591.1|	cluster II
Methanosarcina barkeri	129	gi|1709268|sp|P54799.1|NIFH1_METBA	cluster II
Rhodobacter capsulatus	129	gi|730149|sp|Q07942.1|NIFH2_RHOCA	cluster II
Rhodospirillum rubrum ATCC 11170 Rru_A1395: NC_007643	129	gi|83592731|ref|YP_426483.1|	cluster II
1B_nifH_ERB_2_C7 - translation	**129**	**this study**	**cluster II**
1B_nifH_ERB_2_D1 - translation	**129**	**this study**	**cluster II**
1B_nifH_ERB_2_E12 - translation	**129**	**this study**	**cluster II**
1B_nifH_ERB_2_F11 - translation	**129**	**this study**	**cluster II**
1B_nifH_ERB_2_F4 - translation	**129**	**this study**	**cluster II**
1B_nifH_ERB_2_G12 - translation	**129**	**this study**	**cluster II**
1B_nifH_ERB_2_H11 - translation	**129**	**this study**	**cluster II**
Methanosarcina mazei strain Goe1 MM0719: AE008384	128	gi|21226821|ref|NP_632743.1|	cluster II
uncultured prokaryote (Dang, 2009)	129	gi|192764232|gb|ACF05660.1|	cluster II
Bead capture (Pernthaler, 2008)	129	gi|188485521|gb|ACD50925.1|	cluster II
hyperthermophilic methanogen FS406-22	129	gi|118197434|gb|ABK78681.1|	cluster II
uncultured prokaryote (Dang, 2009)	129	gi|192764282|gb|ACF05685.1|	cluster II
uncultured prokaryote (Mehta, 2003)	127	gi|21586705|gb|AAM54328.1|	cluster II
uncultured prokaryote (Mehta, 2003)	127	gi|21586707|gb|AAM54329.1|	cluster II
uncultured prokaryote (Mehta, 2003)	127	gi|21586717|gb|AAM54334.1|	cluster II
uncultured prokaryote (Mehta, 2003)	129	gi|21586727|gb|AAM54339.1|	cluster II
uncultured prokaryote (Mehta, 2003)	129	gi|21586769|gb|AAM54360.1|	cluster II
uncultured prokaryote (Mehta, 2003)	127	gi|21586773|gb|AAM54362.1|	cluster II
1B_nifH_ERB_1_H10 - translation	**127**	**this study**	**Cluster III**
1B_nifH_ERB_2_B4 - translation	**128**	**this study**	**Cluster III**
1B_nifH_ERB_2_D9 - translation	**129**	**this study**	**Cluster III**
1B_nifH_ERB_2_E1 - translation	**125**	**this study**	**Cluster III**
1B_nifH_ERB_2_E2 - translation	**129**	**this study**	**Cluster III**
1B_nifH_ERB_2_F3 - translation	**129**	**this study**	**Cluster III**
1B_nifH_ERB_2_G5 - translation	**137**	**this study**	**Cluster III**
1B_nifH_ERB_2_H2 - translation	**129**	**this study**	**Cluster III**
1B_nifH_ERB_2_H9 - translation	**129**	**this study**	**Cluster III**
Chlorobium tepidum TLS: NC_002932	129	gi|21674352|ref|NP_662417.1|	Cluster III
Chloroherpeton thalassium ATCC 35110: NC_011026	129	gi|193214747|ref|YP_001995946.1|	Cluster III
Clostridium beijerinckii	127	gi|150016871|ref|YP_001309125.1|	Cluster III

Clostridium kluyveri DSM 555 nifH1: NC_009706	127	gi|219854280|ref|YP_002471402.1|	Cluster III
delta proteobacterium MLMS-1, unfinished sequence: NZ_AAQF01000015	129	_unfinished_sequence:_NZ_AAQF01000015	Cluster III
Desulfonema limicola	93	gi|4529862|gb|AAD21800.1|	Cluster III
Desulfotomaculum reducens MI-1: NC_009253	127	gi|134300654|ref|YP_001114150.1|	Cluster III
Desulfovibrio gigas	129	gi|20138934|sp|P71156.1|NIFH_DESGI	Cluster III
Desulfovibrio vulgaris subsp. vulgaris DP4 plasmid pDVUL01: NC_008741	130	gi|46562231|ref|YP_009055.1|	Cluster III
Syntrophobacter fumaroxidans MPOB: NC_008554	129	gi|116748461|ref|YP_845148.1|	Cluster III
Bead capture (Pernthaler, 2008)	129	gi|188485509|gb|ACD50919.1|	Cluster III
Bead capture (Pernthaler, 2008)	129	gi|188485511|gb|ACD50920.1|	Cluster III
Bead capture (Pernthaler, 2008)	129	gi|188485513|gb|ACD50921.1|	Cluster III
Bead capture (Pernthaler, 2008)	129	gi|188485515|gb|ACD50922.1|	Cluster III
Bead capture (Pernthaler, 2008)	129	gi|188485519|gb|ACD50924.1|	Cluster III
Bead capture (Pernthaler, 2008)	129	gi|188485523|gb|ACD50926.1|	Cluster III
Bead capture (Pernthaler, 2008)	129	gi|188485525|gb|ACD50927.1|	Cluster III
uncultured prokaryote (Dang, 2009)	128	gi|192764148|gb|ACF05618.1|	Cluster III
uncultured prokaryote (Dang, 2009)	129	gi|192764234|gb|ACF05661.1|	Cluster III
uncultured prokaryote (Dang, 2009)	129	gi|192764238|gb|ACF05663.1|	Cluster III
uncultured prokaryote (Dang, 2009)	129	gi|192764240|gb|ACF05664.1|	Cluster III
uncultured prokaryote (Dang, 2009)	129	gi|192764242|gb|ACF05665.1|	Cluster III
uncultured prokaryote (Dang, 2009)	129	gi|192764246|gb|ACF05667.1|	Cluster III
uncultured prokaryote (Dang, 2009)	129	gi|192764248|gb|ACF05668.1|	Cluster III
uncultured prokaryote (Mehta, 2003)	124	gi|21586701|gb|AAM54326.1|	Cluster III
uncultured prokaryote (Mehta, 2003)	127	gi|21586703|gb|AAM54327.1|	Cluster III
uncultured prokaryote (Mehta, 2003)	127	gi|21586709|gb|AAM54330.1|	Cluster III
uncultured prokaryote (Mehta, 2003)	129	gi|21586721|gb|AAM54336.1|	Cluster III
uncultured prokaryote (Mehta, 2003)	127	gi|21586725|gb|AAM54338.1|	Cluster III
uncultured prokaryote (Mehta, 2003)	127	gi|21586729|gb|AAM54340.1|	Cluster III
uncultured prokaryote (Mehta, 2003)	129	gi|21586733|gb|AAM54342.1|	Cluster III
uncultured prokaryote (Mehta, 2003)	127	gi|21586735|gb|AAM54343.1|	Cluster III
uncultured prokaryote (Mehta, 2003)	127	gi|21586737|gb|AAM54344.1|	Cluster III
uncultured prokaryote (Mehta, 2003)	127	gi|21586739|gb|AAM54345.1|	Cluster III
uncultured prokaryote (Mehta, 2003)	127	gi|21586741|gb|AAM54346.1|	Cluster III
uncultured prokaryote (Mehta, 2003)	127	gi|21586745|gb|AAM54348.1|	Cluster III
uncultured prokaryote (Mehta, 2003)	129	gi|21586751|gb|AAM54351.1|	Cluster III
uncultured prokaryote (Mehta, 2003)	129	gi|21586753|gb|AAM54352.1|	Cluster III
uncultured prokaryote (Mehta, 2003)	127	gi|21586755|gb|AAM54353.1|	Cluster III
uncultured prokaryote (Mehta, 2003)	127	gi|21586757|gb|AAM54354.1|	Cluster III
uncultured prokaryote (Mehta, 2003)	129	gi|21586761|gb|AAM54356.1|	Cluster III
uncultured prokaryote (Mehta, 2003)	127	gi|21586763|gb|AAM54357.1|	Cluster III
uncultured prokaryote (Mehta, 2003)	127	gi|21586765|gb|AAM54358.1|	Cluster III
uncultured prokaryote (Mehta, 2003)	127	gi|21586767|gb|AAM54359.1|	Cluster III
uncultured prokaryote (Mehta, 2003)	127	gi|21586775|gb|AAM54363.1|	Cluster III
uncultured prokaryote (Mehta, 2003)	127	gi|21586777|gb|AAM54364.1|	Cluster III
1B_nifH_ERB_1_G1 - translation	**140**	**this study**	**Cluster IV**
1B_nifH_ERB_1_G5 - translation	**140**	**this study**	**Cluster IV**
1B_nifH_ERB_1_H8 - translation	**140**	**this study**	**Cluster IV**
1B_nifH_ERB_2_A9 - translation	**140**	**this study**	**Cluster IV**
1B_nifH_ERB_2_B9 - translation	**140**	**this study**	**Cluster IV**
1B_nifH_ERB_2_C5 - translation	**140**	**this study**	**Cluster IV**

1B_nifH_ERB_2_D4 - translation	**139**	**this study**	**Cluster IV**
1B_nifH_ERB_2_D7 - translation	**140**	**this study**	**Cluster IV**
1B_nifH_ERB_2_E10 - translation	**134**	**this study**	**Cluster IV**
1B_nifH_ERB_2_E11 - translation	**138**	**this study**	**Cluster IV**
1B_nifH_ERB_2_E4 - translation	**140**	**this study**	**Cluster IV**
1B_nifH_ERB_2_E5 - translation	**134**	**this study**	**Cluster IV**
1B_nifH_ERB_2_E7 - translation	**139**	**this study**	**Cluster IV**
1B_nifH_ERB_2_G4 - translation	**140**	**this study**	**Cluster IV**
1B_nifH_ERB_2_G6 - translation	**139**	**this study**	**Cluster IV**
1B_nifH_ERB_2_G9 - translation	**140**	**this study**	**Cluster IV**
1B_nifH_ERB_2_H5 - translation	**140**	**this study**	**Cluster IV**
1B_nifH_ERB_2_H8 - translation	**140**	**this study**	**Cluster IV**
Clostridium kluyveri DSM 555 nifH3: NC_009706	127	gi|153955079|ref|YP_001395844.1|	Cluster IV
Desulfitobacterium hafniense DCB-2 Dhaf_4502, unfinished sequence: NZ_AAAW04000002	128	_unfinished_sequence:_NZ_AAAW04000002	Cluster IV
Desulfitobacterium hafniense Y51 DSY0362 : NC_007907	125	gi|89893108|ref|YP_516595.1|	Cluster IV
Fusobacterium nucleatum subsp. nucleatum ATCC 25586: NC_003454	125	gi|19703648|ref|NP_603210.1|	Cluster IV
hyperthermophilic methanogen FS406-22	128	gi|118197440|gb|ABK78685.1|	Cluster IV
Methanobacterium thermoautotrophicum str. Delta H MTH643: AE000666	124	gi|15678670|ref|NP_275785.1|	Cluster IV
Methanobrevibacter smithii ATCC 35061: NC_009515	125	gi|222444802|ref|ZP_03607317.1|	Cluster IV
Methanocaldococcus jannaschii DSM 2661: NC_000909	128	gi|15669069|ref|NP_247874.1|	Cluster IV
Methanococcus aeolicus Nankai-3 Maeo_0506: NC_009635	140	gi|150400938|ref|YP_001324704.1|	Cluster IV
Methanococcus maripaludis C7: NC_009637	140	gi|150403070|ref|YP_001330364.1|	Cluster IV
Methanococcus vannielii SB Mevan_1152: NC_009634	140	gi|150399896|ref|YP_001323663.1|	Cluster IV
Methanococcus voltae	128	gi|128268|sp|P06119.1|NIFH_METVO	Cluster IV
Methanosarcina acetivorans C2A	134	gi|20090488|ref|NP_616563.1|	Cluster IV
Methanosarcina mazei strain Goe1: AE008384	127	gi|21226616|ref|NP_632538.1|	Cluster IV
Methanospirillum hungatei JF-1	126	gi|88602086|ref|YP_502264.1|	Cluster IV
Bead capture (Pernthaler, 2008)	126	gi|188485517|gb|ACD50923.1|	Cluster IV
Bead capture (Pernthaler, 2008)	140	gi|188485529|gb|ACD50929.1|	Cluster IV
Bead capture (Pernthaler, 2008)	140	gi|188485531|gb|ACD50930.1|	Cluster IV
uncultured prokaryote (Dang, 2009)	126	gi|192764150|gb|ACF05619.1|	Cluster IV
uncultured prokaryote (Dang, 2009)	125	gi|192764152|gb|ACF05620.1|	Cluster IV
uncultured prokaryote (Dang, 2009)	129	gi|192764174|gb|ACF05631.1|	Cluster IV
uncultured prokaryote (Dang, 2009)	129	gi|192764216|gb|ACF05652.1|	Cluster IV
uncultured prokaryote (Dang, 2009)	126	gi|192764236|gb|ACF05662.1|	Cluster IV
uncultured prokaryote (Dang, 2009)	126	gi|192764278|gb|ACF05683.1|	Cluster IV
uncultured prokaryote (Dang, 2009)	139	gi|192764288|gb|ACF05688.1|	Cluster IV
uncultured prokaryote (Dang, 2009)	139	gi|192764290|gb|ACF05689.1|	Cluster IV
uncultured prokaryote (Dang, 2009)	129	gi|192764296|gb|ACF05692.1|	Cluster IV
uncultured prokaryote (Dang, 2009)	129	gi|192764304|gb|ACF05696.1|	Cluster IV
uncultured prokaryote (Mehta, 2003)	140	gi|21586713|gb|AAM54332.1|	Cluster IV
uncultured prokaryote (Mehta, 2003)	134	gi|21586715|gb|AAM54333.1|	Cluster IV
uncultured prokaryote (Mehta, 2003)	124	gi|21586719|gb|AAM54335.1|	Cluster IV

uncultured prokaryote (Mehta, 2003)	138	gi|21586723|gb|AAM54337.1|	Cluster IV
uncultured prokaryote (Mehta, 2003)	134	gi|21586749|gb|AAM54350.1|	Cluster IV
uncultured prokaryote (Dang, 2009)	136	gi|192764178|gb|ACF05633.1|	Okhotsk (V)
uncultured prokaryote (Dang, 2009)	136	gi|192764180|gb|ACF05634.1|	Okhotsk (V)
uncultured prokaryote (Dang, 2009)	136	gi|192764182|gb|ACF05635.1|	Okhotsk (V)
uncultured prokaryote (Dang, 2009)	136	gi|192764184|gb|ACF05636.1|	Okhotsk (V)
uncultured prokaryote (Dang, 2009)	137	gi|192764186|gb|ACF05637.1|	Okhotsk (V)
uncultured prokaryote (Dang, 2009)	136	gi|192764188|gb|ACF05638.1|	Okhotsk (V)
uncultured prokaryote (Dang, 2009)	136	gi|192764190|gb|ACF05639.1|	Okhotsk (V)
uncultured prokaryote (Dang, 2009)	136	gi|192764192|gb|ACF05640.1|	Okhotsk (V)
uncultured prokaryote (Dang, 2009)	136	gi|192764194|gb|ACF05641.1|	Okhotsk (V)
uncultured prokaryote (Dang, 2009)	136	gi|192764198|gb|ACF05643.1|	Okhotsk (V)
uncultured prokaryote (Dang, 2009)	137	gi|192764200|gb|ACF05644.1|	Okhotsk (V)
uncultured prokaryote (Dang, 2009)	137	gi|192764202|gb|ACF05645.1|	Okhotsk (V)
uncultured prokaryote (Dang, 2009)	137	gi|192764204|gb|ACF05646.1|	Okhotsk (V)
uncultured prokaryote (Dang, 2009)	137	gi|192764206|gb|ACF05647.1|	Okhotsk (V)
uncultured prokaryote (Dang, 2009)	137	gi|192764208|gb|ACF05648.1|	Okhotsk (V)
uncultured prokaryote (Dang, 2009)	137	gi|192764210|gb|ACF05649.1|	Okhotsk (V)
uncultured prokaryote (Dang, 2009)	137	gi|192764212|gb|ACF05650.1|	Okhotsk (V)
uncultured prokaryote (Dang, 2009)	137	gi|192764214|gb|ACF05651.1|	Okhotsk (V)
uncultured prokaryote (Dang, 2009)	137	gi|192764220|gb|ACF05654.1|	Okhotsk (V)
uncultured prokaryote (Dang, 2009)	137	gi|192764222|gb|ACF05655.1|	Okhotsk (V)
uncultured prokaryote (Dang, 2009)	137	gi|192764226|gb|ACF05657.1|	Okhotsk (V)
uncultured prokaryote (Dang, 2009)	137	gi|192764228|gb|ACF05658.1|	Okhotsk (V)
uncultured prokaryote (Dang, 2009)	137	gi|192764230|gb|ACF05659.1|	Okhotsk (V)
uncultured prokaryote (Dang, 2009)	136	gi|192764294|gb|ACF05691.1|	Okhotsk (V)
uncultured prokaryote (Dang, 2009)	129	gi|192764298|gb|ACF05693.1|	Okhotsk (V)
uncultured prokaryote (Dang, 2009)	136	gi|192764300|gb|ACF05694.1|	Okhotsk (V)
uncultured prokaryote (Dang, 2009)	136	gi|192764302|gb|ACF05695.1|	Okhotsk (V)
1B_nifH_ERB_1_G11 - translation	**126**	**this study**	**Seep**
1B_nifH_ERB_1_G3 - translation	**128**	**this study**	**Seep**
1B_nifH_ERB_1_G6 - translation	**128**	**this study**	**Seep**
1B_nifH_ERB_1_H11 - translation	**128**	**this study**	**Seep**
1B_nifH_ERB_1_H12 - translation	**128**	**this study**	**Seep**
1B_nifH_ERB_1_H3 - translation	**128**	**this study**	**Seep**
1B_nifH_ERB_1_H5 - translation	**128**	**this study**	**Seep**
1B_nifH_ERB_1_H6 - translation	**128**	**this study**	**Seep**
1B_nifH_ERB_1_H7 - translation	**128**	**this study**	**Seep**
1B_nifH_ERB_2_A10 - translation	**128**	**this study**	**Seep**
1B_nifH_ERB_2_A11 - translation	**107**	**this study**	**Seep**
1B_nifH_ERB_2_A6 - translation	**128**	**this study**	**Seep**
1B_nifH_ERB_2_B10 - translation	**128**	**this study**	**Seep**
1B_nifH_ERB_2_B11 - translation	**124**	**this study**	**Seep**
1B_nifH_ERB_2_B5 - translation	**128**	**this study**	**Seep**
1B_nifH_ERB_2_B6 - translation	**128**	**this study**	**Seep**
1B_nifH_ERB_2_B8 - translation	**128**	**this study**	**Seep**
1B_nifH_ERB_2_C11 - translation	**128**	**this study**	**Seep**
1B_nifH_ERB_2_C4 - translation	**128**	**this study**	**Seep**
1B_nifH_ERB_2_D11 - translation	**125**	**this study**	**Seep**
1B_nifH_ERB_2_D12 - translation	**128**	**this study**	**Seep**
1B_nifH_ERB_2_D3 - translation	**128**	**this study**	**Seep**
1B_nifH_ERB_2_D8 - translation	**128**	**this study**	**Seep**
1B_nifH_ERB_2_E6 - translation	**128**	**this study**	**Seep**
1B_nifH_ERB_2_E8 - translation	**128**	**this study**	**Seep**

1B_nifH_ERB_2_F10 - translation	**128**	**this study**	**Seep**
1B_nifH_ERB_2_F12 - translation	**128**	**this study**	**Seep**
1B_nifH_ERB_2_F5 - translation	**128**	**this study**	**Seep**
1B_nifH_ERB_2_F6 - translation	**128**	**this study**	**Seep**
1B_nifH_ERB_2_F7 - translation	**128**	**this study**	**Seep**
1B_nifH_ERB_2_F9 - translation	**128**	**this study**	**Seep**
1B_nifH_ERB_2_G10 - translation	**128**	**this study**	**Seep**
1B_nifH_ERB_2_G11 - translation	**128**	**this study**	**Seep**
1B_nifH_ERB_2_G2 - translation	**128**	**this study**	**Seep**
1B_nifH_ERB_2_G3 - translation	**128**	**this study**	**Seep**
1B_nifH_ERB_2_H1 - translation	**128**	**this study**	**Seep**
1B_nifH_ERB_2_H6 - translation	**128**	**this study**	**Seep**
1B_nifH_ERB_2_H7 - translation	**128**	**this study**	**Seep**
BAF96793 uncultured archaeon	120	gi|164454498|dbj|BAF96793.1|	Seep
BAF96808 uncultured archaeon	120	gi|164454516|dbj|BAF96808.1|	Seep
Bead capture (Pernthaler, 2008)	128	gi|188485503|gb|ACD50916.1|	Seep
Bead capture (Pernthaler, 2008)	127	gi|188485505|gb|ACD50917.1|	Seep
Bead capture (Pernthaler, 2008)	128	gi|188485507|gb|ACD50918.1|	Seep
uncultured prokaryote (Dang, 2009)	128	gi|192764154|gb|ACF05621.1|	Seep
uncultured prokaryote (Dang, 2009)	128	gi|192764156|gb|ACF05622.1|	Seep
uncultured prokaryote (Dang, 2009)	128	gi|192764158|gb|ACF05623.1|	Seep
uncultured prokaryote (Dang, 2009)	128	gi|192764160|gb|ACF05624.1|	Seep
uncultured prokaryote (Dang, 2009)	128	gi|192764162|gb|ACF05625.1|	Seep
uncultured prokaryote (Dang, 2009)	128	gi|192764164|gb|ACF05626.1|	Seep
uncultured prokaryote (Dang, 2009)	128	gi|192764166|gb|ACF05627.1|	Seep
uncultured prokaryote (Dang, 2009)	128	gi|192764168|gb|ACF05628.1|	Seep
uncultured prokaryote (Dang, 2009)	128	gi|192764170|gb|ACF05629.1|	Seep
uncultured prokaryote (Dang, 2009)	128	gi|192764172|gb|ACF05630.1|	Seep
uncultured prokaryote (Dang, 2009)	126	gi|192764250|gb|ACF05669.1|	Seep
uncultured prokaryote (Dang, 2009)	128	gi|192764252|gb|ACF05670.1|	Seep
uncultured prokaryote (Dang, 2009)	128	gi|192764254|gb|ACF05671.1|	Seep
uncultured prokaryote (Dang, 2009)	128	gi|192764256|gb|ACF05672.1|	Seep
uncultured prokaryote (Dang, 2009)	128	gi|192764258|gb|ACF05673.1|	Seep
uncultured prokaryote (Dang, 2009)	128	gi|192764260|gb|ACF05674.1|	Seep
uncultured prokaryote (Dang, 2009)	128	gi|192764262|gb|ACF05675.1|	Seep
uncultured prokaryote (Dang, 2009)	128	gi|192764264|gb|ACF05676.1|	Seep
uncultured prokaryote (Dang, 2009)	128	gi|192764266|gb|ACF05677.1|	Seep
uncultured prokaryote (Dang, 2009)	128	gi|192764268|gb|ACF05678.1|	Seep
uncultured prokaryote (Dang, 2009)	126	gi|192764270|gb|ACF05679.1|	Seep
uncultured prokaryote (Dang, 2009)	128	gi|192764272|gb|ACF05680.1|	Seep
uncultured prokaryote (Dang, 2009)	125	gi|192764274|gb|ACF05681.1|	Seep
uncultured prokaryote (Dang, 2009)	128	gi|192764276|gb|ACF05682.1|	Seep
uncultured prokaryote (Dang, 2009)	128	gi|192764280|gb|ACF05684.1|	Seep
uncultured prokaryote (Dang, 2009)	127	gi|192764284|gb|ACF05686.1|	Seep
uncultured prokaryote (Dang, 2009)	128	gi|192764286|gb|ACF05687.1|	Seep
ERB_nifHK_D11	**128**	**this study**	**Seep**
ERB_nifHK_D4	**120**	**this study**	**Seep**
ERB_nifHK_Q3	**128**	**this study**	**Seep**
ERB_nifHK_Q6	**128**	**this study**	**Seep**

Table S4. Acetylene inhibition of sulfide production. Sulfide was measured after 10 weeks incubation of PC 14 sediment with methane. Headspace was flushed and refilled at 8 weeks. Percent acetylene in the headspace is the initial value and was measured by gas chromatography, concentration of sulfide was measured by the Cline Assay.

Acetylene (%)	Sulfide (uM)
0.0	2256
0.0	2450
0.0	4372
0.2	334
0.4	324
0.4	180
0.5	234
0.7	186
0.7	170
1.2	115
1.3	189
1.5	363
4.6	145
4.9	70
7.9	79

References

S1. V. J. Orphan *et al.*, *Chemical Geology*, 265 (2004).
S2. F. Widdel, A. Boetius, R. Rabus, *Prokaryotes* **2**, 1028 (2006).
S3. R. S. Oremland, D. G. Capone, *Advances in Microbial Ecology* **10**, 285 (1988).
S4. P. R. Girguis, A. E. Cozen, E. F. DeLong, *Appl Environ Microbiol* **71**, 3725 (2005).
S5. K. Nauhaus, M. Albrecht, M. Elvert, A. Boetius, F. Widdel, *Environmental Microbiology* **9**, 187 (2007).
S6. V. J. Orphan, K. A. Turk, A. M. Green, C. H. House, *Environmental Microbiology* **11**, 1777 (2009).
S7. M. Krueger, H. Wolters, M. Gehre, S. B. Joye, H. H. Richnow, *Fems Microbiology Ecology* **63**, 401 (2008).
S8. J. Cline, *Limnology and Oceanography* **14**, 454 (1969).
S9. V. J. Orphan, C. H. House, K. U. Hinrichs, K. D. McKeegan, E. F. DeLong, *Proc Natl Acad Sci U S A* **99**, 7663 (2002).
S10. A. Boetius *et al.*, *Nature* **407**, 623 (2000).
S11. R. I. Amann, W. Ludwig, K. H. Schleifer, *Microbiological Reviews* **59**, 143 (1995).
S12. J. B. Cliff, D. J. Gaspar, P. J. Bottomley, D. D. Myrold, *Appl Environ Microbiol* **68**, 4067 (2002).
S13. C. Lechene *et al.*, *J Biol* **5**, 20 (2006).
S14. R. Peteranderl, C. Lechene, *American Society for Mass Spectrometry* **15**, 478 (2004).
S15. V. J. Orphan *et al.*, *Geobiology* **6**, 376 (2008).
S16. M. P. Mehta, D. A. Butterfield, J. A. Baross, *Appl Environ Microbiol* **69**, 960 (2003).
S17. L. Solaranzo, *Limnology and Oceanography* **14**, 799 (1969).
S18. W. D. P. Stewart, G. P. Fitzgerald, R. H. Burris, *Proceedings of the National Academy of Sciences USA* **58**, 2071 (1967).
S19. D. Capone, J. Montoya, in *Methods in Microbiology*. (Academic Press Ltd, 2001), vol. 30 pp. 501-513.
S20. H. Stam, A. H. Stouthamer, H. W. Vanverseveld, *Archives of Microbiology* **143**, 196 (1985).
S21. J. K. Liu, C. H. Liu, C. S. Lin, *Proc Natl Sci Counc Repub China B* **21**, 37 (1997).
S22. W. S. Silver, J. R. Postgate, *Journal of Theoretical Biology* **40**, 1 (1973).
S23. Karl *et al.*, *Biogeochemistry* **57/58**, 47 (2002).
S24. R. Fani, R. Gallo, P. Lio, *Journal of Molecular Evolution* **51**, 1 (2000).
S25. J. Raymond, *Reviews in Mineralogy and Geochemistry* **59**, 211 (2005).
S26. I. Berman-Frank, P. Lundgren, P. Falkowski, *Research in Microbiology* **154**, 157 (2003).
S27. C. J. Pickett *et al.*, *Chemistry-a European Journal* **10**, 4770 (2004).
S28. J. Raymond, J. L. Siefert, C. R. Staples, R. E. Blankenship, *Mol Biol Evol* **21**, 541 (2004).
S29. R. S. Oremland, B. F. Taylor, *Appl Microbiol* **30**, 707 (1975).

S30. G. D. Sprott, K. F. Jarrell, K. M. Shaw, R. Knowles, *Journal of General Microbiology*, 2453 (1982).
S31. S. J. Hallam *et al.*, *Science* **305**, 1457 (2004).
S32. K. Nauhaus, T. Treude, A. Boetius, M. Kruger, *Environmental Microbiology* **7**, 98 (2005).
S33. T. Hoehler, M. Alperin, D. Albert, C. Martens, *Global Biogeochemical Cycles* **8**, 451 (1994).
S34. B. Orcutt, V. Samarkin, A. Boetius, S. Joye, *Environmental Microbiology* **10**, 1108 (2008).
S35. D. Alperin, W. S. Reeburgh, *Appl Environ Microbiol*, 940 (1985).
S36. N. Musat *et al.*, *Proceedings of the National Academy of Sciences* **105**, 17861 (2008).
S37. C. P. Lechene, Y. Luyten, G. McMahon, D. L. Distel, *Science* **317**, 1563 (2007).
S38. K. Nauhaus, A. Boetius, M. Kruger, F. Widdel, *Environ Microbiol* **4**, 296 (2002).
S39. R. R. Eady, *Chemical Reviews* **96**, 3013 (1996).
S40. K. J. Kechris, J. C. Lin, P. J. Bickel, A. N. Glazer, *Proceedings of the National Academy of Sciences of the United States of America* **103**, 9584 (2006).
S41. J. P. Zehr, B. D. Jenkins, S. M. Short, G. F. Steward, *Environ Microbiol* **5**, 539 (2003).
S42. H. Dang, X. Luan, J. Zhao, J. Li, *Appl Environ Microbiol* **75**, 2238 (2009).

C h a p t e r 3

Investigating Nitrogen Fixation at a Deep-Sea Methane Seep: Spatial Distribution of Diazotrophy and Significance of the ANME Archaea

Anne E. Dekas*, Grayson L. Chadwick*, Stephanie A. Connon*, Marshall W. Bowles[+†], Samantha B. Joye[+], and Victoria J. Orphan*

*California Institute of Technology, Pasadena, CA 91106
[+]University of Georgia, Athens, GA 30609
[†]Present affiliation: MARUM, Center for Marine Environmental Sciences, University of Bremen, Bremen, Germany

SUMMARY

Nitrogen fixation was investigated in six sediment push cores collected within, around and outside of Mound 12, an active mud volcano off the west coast of Costa Rica (~ 1000 m water depth), to determine the spatial distribution of diazotrophy and its biological and chemical controls. Despite the recovery of diverse *nifH* sequences in this and previous studies, two lines of evidence suggest that methanotrophic archaea (ANME), together with sulfate-reducing bacterial symbionts (SRB), are the dominant diazotrophs in seep sediment. First, nitrogen fixation was methane dependent. Second, nitrogen fixation rates reached a maximum with depth in a narrow sediment horizon corresponding to a peak in the abundance of aggregates of the diazotrophic ANME and associated SRB. ANME-2 nitrogen fixation was confirmed in Costa Rican seep sediment by Fluorescence *in situ* Hybridization coupled to Nanoscale Secondary Ion Mass Spectrometry (FISH-NanoSIMS) of $^{15}N_2$-incubated ANME-SRB aggregates, consistent with a previous report from an Eel River Basin methane seep. In addition to nitrogen fixation in ANME-2 archaea associated with *Desulfosarcina/Desulfococcus* (DSS), here we observed ANME-2 diazotrophy while in association with members of the *Desulfobulbaceae* (DSB) as well. N_2 fixation rates per unit volume biomass were independent of ANME-SRB aggregate size, morphology or identity of the associated SRB. Our results indicate that the distribution of methane seep diazotrophy is likely dictated by steep chemical gradients affecting the abundance and activity of the ANME-2 archaea.

INTRODUCTION

Nitrogen is a limiting nutrient in many ecosystems worldwide, making microorganisms capable of converting gaseous nitrogen into a bioavailable form (i.e., diazotrophs) critical for global productivity and growth. In the last six years, several

reports have suggested that diazotrophs are present and active in deep-sea marine environments (*1*–*5*), a habitat only cursorily investigated for nitrogen fixation previously (*6*), but potentially geochemically significant due to its expansive coverage of the surface of the Earth. Investigating the extent of nitrogen fixation in these cold and dark sediments may be an important component of understanding the marine nitrogen cycle (the balance of which is currently under debate, see (*7*–*9*)), as well as nutrient limitation and the flow of carbon and nitrogen through the anaerobic microbial communities mediating globally relevant metabolisms within these sediments.

The anaerobic oxidation of methane (AOM) is one such climactically critical metabolism occurring in deep-sea sediments. Consuming the majority of methane naturally released at cold methane seeps, the microorganisms mediating AOM minimize the quantity of methane reaching the water column, and therefore the atmosphere, where it would have a global warming effect (*10*). Methane seep ecosystems are complex; methanotrophic archaea (ANME) consume methane while in tight associations with sulfate-reducing bacterial symbionts (SRB), passing a yet unidentified intermediate to couple methane oxidation to sulfate reduction (*11*). Together, the ANME and associated SRB can comprise up to 94% of the total cells in methane seep sediment (*12*). Sulfide is produced by the reduction of sulfate and utilized by a diverse community of autotrophic sulfide-oxidizing microbes, which can form visible mats on the surface of sulfidic sediments (e.g., *Beggiatoa* species) (*13*), and support the growth of symbiotic metazoans (*14*). The methane metabolism of the ANME-SRB therefore provides an accessible source of carbon and electrons to the local ecosystem and results in highly elevated levels of biological productivity compared to the background seafloor (*14*). Recently, the

ANME-2 were shown to fix nitrogen in seep sediments from the Eel River Basin, raising questions about their role in nitrogen cycling within seep sediments, as well as the need for nitrogen fixation in methane seeps in general (*5*).

Little is known about nitrogen limitation at methane seeps, and if it might reduce ecosystem productivity or the rate of methane consumption. Although methane, sulfate, and bicarbonate are abundant, providing a virtually endless supply of carbon and energy, other essential nutrients are not enriched in these locales, and therefore may become depleted. A similar scenario is observed in the upper water column, where carbon and energy are plentiful from bicarbonate and light, but life can be limited by the availability of iron, phosphorus or nitrogen (*15–17*, *and references therein*). It might be expected that metabolic processes designed to overcome nutrient limitation, including scavenging, storing, and re-using (e.g., *18*) limiting elements might be observed at methane seeps, as they are in the upper water column. Nitrogen fixation may therefore be an important process at methane seeps to supplement the limited pool of bioavailable nitrogen, however the extent to which is occurs is currently unknown.

Benthic nitrogen fixation has been shown to be an important source of nitrogen in several shallow (defined here as < 50 meters water depth) marine environments (*19–21*), but evidence for deep-sea benthic diazotrophy is still sparse. With the exception of two studies identifying deep-sea diazotrophs (*1, 5*), and one investigation of deep-sea nitrogen fixation rates (*6*), most evidence for diazotrophy on the deep ocean floor consists of the detection of *nif* genes or transcripts, the genes necessary for nitrogen fixation (*2–4*). The *nifH* genes detected in these studies suggest the presence of a diverse community of deep-sea diazotrophs, but whether or not many of these genes are expressed, or even

functional, is currently unknown. The extent of nitrogen fixation occurring on the seafloor therefore remains an open question. The geochemical controls on deep-sea diazotrophy is also an area ripe for exploration, as evidence from shallow marine sediments suggest that a more complex set of environmental parameters regulate nitrogen fixation in sediments than the concentration of bioavailable nitrogen alone (*19, 21, 22*). Methane seeps may provide a valuable early vantage point in the pursuit of understanding deep-sea diazotrophy, because steep chemical gradients and closely clustered diverse habitats offer a range of geochemical conditions within which the activity of anaerobic piezotolerant diazotrophs can be examined.

In the current work, we investigate diazotrophy at Mound 12, a methane-seeping mud volcano on the convergent continental margin offshore Costa Rica at 1,000 meters water depth, to better understand seep nitrogen fixation and the diazotrophic role of ANME-2 in the seep ecosystem. Nitrogen fixation and potential protein synthesis (as a proxy for growth) were measured in sediments collected across Mound 12, representing a range of chemical regimes, in bottle incubations with $^{15}N_2$ and $^{15}NH_4^+$, respectively, by bulk Elemental Analysis Isotope Ratio Mass Spectrometer (EA-IRMS) analysis. To investigate the biological controls, we coupled our meter-scale geochemical investigations with nanometer-scale analyses of nitrogen fixation using Fluorescence *in situ* Hybridization coupled to Nanoscale Secondary Ion Mass Spectrometry (FISH-NanoSIMS), as well as microscopic cell enumeration and molecular investigations of *nifH* genes. These analyses represent the most extensive characterization of deep-sea nitrogen fixation to date, and report the first rates of deep-sea nitrogen fixation since the late 1970s (*6*).

RESULTS and DISCUSSION

Ammonium, nitrate, and nitrite concentrations in sediment pore water

Nitrogen fixation is an ATP-intensive process, and is therefore typically repressed in the presence of ammonium (*23*). Concentrations of bioavailable nitrogen (NH_4^+, NO_3^-, NO_2^-) were therefore measured in 12 sediment push cores collected in and around Mound 12, a marine mud volcano along the Costa Rica margin, to assess whether or not nitrogen fixation may be inhibited by other sources of nitrogen in Costa Rican seep sediment (Figure 1; core sampling locations in SI Table 1 and SI Figure 1). Although ammonium concentrations varied from not detectable (< 0.5 μM) to 2.5 mM, most values were less than 250 μM (Figure 1, M and N), and suggested that nitrogen fixation is likely in these sediments, given that similar values of ammonium were observed in diazotrophic sediment samples previously (*21, 24*) (see SI Discussion A).

Bulk sediment nitrogen fixation rates in mesocosm experiments

Nitrogen fixation was therefore investigated in 6 additional push cores from Mound 12 (core pore water geochemistry and sampling locations in SI Table 1 and SI Figure 1), and was detected via ^{15}N-uptake from $^{15}N_2$ in all of the cores collected within areas of active methane seepage (cores A1, A2, and A3), as well as in two of the three cores collected outside of areas of methane seepage (cores O1 and O2), when incubated in the presence of methane (Table 1, Figure 2). Cores A1 and A2 contained sediments which fixed 24.2 and 26.6 nmol N_2 g_{dw}^{-1} in 275 days, respectively, while core A3 fixed

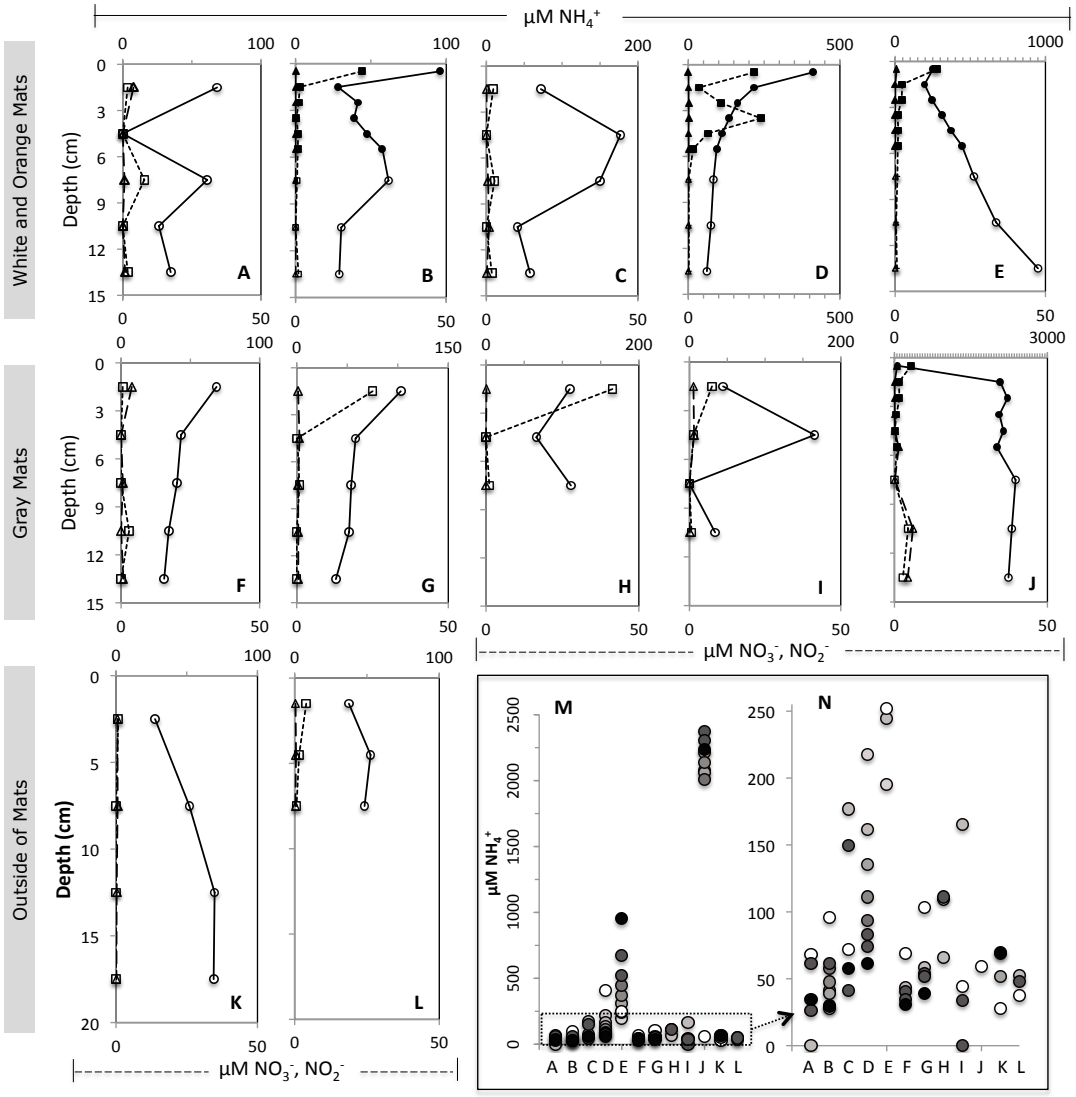

Figure 1. Bioavailable nitrogen species with depth in porewater squeezed from pushcores collected in and around areas of active methane seepage. A-L: Ammonium (NH4+) in solid lines with circles (top axis), nitrate (NO3-) in short dashed lines with squares (bottom axis), nitrite (NO2-) in long dashed lines with triangles (bottom axis). Open symbols indicate values representative of 3 cm sediment sections, closed symbols indicate values of 1 cm sections. In K, open symbols indicate 5 cm horizons. M: Ammonium concentrations by core, A-L. N: Close-up of dashed box area in M. For N and M, darker symbols indicate deeper samples. Depth in cm below seafloor.

up to just 1.8 nmol of N_2 g_{dw}^{-1} during the same period. The disparity between the diazotrophy observed between the 3–6 cm interval of A2 and A3, which were collected less than 1 meter apart (SI Figure 1c), demonstrates the great lateral variability of nitrogen fixation on Mound 12 (See SI Discussion B). Nitrogen fixation was generally lower in cores collected outside of active methane seepage than those collected within, with 3.2 and 2.9 nmol of N_2 g_{dw}^{-1} fixed by O1 and O2 during the 275-day incubation, respectively, and no diazotrophy detected in O3. In both A1 and A2, diazotrophy occurred before the first sampling point (no detectable lag time), suggesting that diazotrophy in these cores *in situ* was likely (Figure 2, A and B).

The maximum rates for A1 and A2 was observed between the 63 and 139 day time points, when they reached 9.6 and 7.1 x 10^{-3} nmol N_2 g_{dw}^{-1} hr^{-1}, respectively, (Table 1, calculated using the equations in Montoya et al., 1996 (*25*)). For comparison, this is equivalent to about 0.2 nmol N_2 cm^{-3} day^{-1}, given that each 1 ml of incubation slurry contained 0.3 g_{dw} sediment, and the slurry consisted of a 1:2 sediment to filtered sea water ratio by volume. These rates are comparable to those observed in several coastal marine sediments (see Table 3 in (*26*), and (*21*)). Additionally, the rates of nitrogen fixation within cores A1 and A2 are approximately 1.5 orders of magnitude greater than the only previously published rates of deep-sea nitrogen fixation, which were measured via the acetylene reduction assay in undisturbed sediments collected off the Scottish Coast at 2,800 m water depth (up to 4.3 x 10^{-4} nmol N_2 g_{dw}^{-1} hr^{-1}) (*6*)). This demonstrates that although it is highly variable, at least some deep-sea sediments, such as within these methane-rich cores, mediate significantly more nitrogen fixation than was previously appreciated.

Table 1. Mesocosm experimental set-up and results. Incubations with N_2 are on the left, with NH_4^+ on the right. Sulfide concentrations were measured at four time points over the course of the experiment and the production observed is summarized as follows: -, none detected; +, 1-10 mM; ++, 10-20 mM, +++, >20 mM. Concentrations of NH_4^+ are reported for the time point (40 weeks) only. Depth is measured in cm below seafloor (cmbsf).

	$^{15}N_2$ Amended							$^{15}NH_4^+$ Ammended							
	Depth (cmbsf)	Headspace	Sulfide Production	$[NH_4^+]_{final}$ μM	$\delta^{15}N$ ‰ Day 5	$\delta^{15}N$ ‰ Day 275	nmol N_2 fixed g_{dw}^{-1}	Depth (cmbsf)	Headspace	Sulfide Production	$\delta^{15}N$ ‰ Day 5	$\delta^{15}N$ ‰ Day 275	nmol NH_4 fixed g_{dw}^{-1}	% NH_4 Fixation CH_4 Dependent	% N for growth obtained from N_2
Active: A1	0-3	CH_4	+	40.9	7.3	7.6	*								
	3-6	CH_4	+++	bdl	7.3	10.2	1.2	3-6	CH_4	+++	224	2083	1926		0.12
	3-6	Ar	-	50.7	7.0	8.7	0.7								
	6-9	CH_4	++	0.4	8.9	71.4	24.2								
	9-12	CH_4	++	0.1	7.1	9.2	0.7								
	12-15	CH_4	++	2.5	7.2	7.7	*								
Active: A2	3-6	CH_4	+++	14.4	7.0	71.0	26.6	3-6	CH_4	+++	140	1886	1792	80	2.97
	3-6	Ar	-	91.1	6.7	7.4	*	3-6	Ar	-	107	436	353		
	9-12	CH_4	+++	24.0	7.0	11.6	2.0	6-9	CH_4	+++	137	1437	1355	78	0.29
	9-12	Ar	-	68.7	6.7	7.3	*	6-9	Ar	-	305	612	292		
Active: A3	3-6	CH_4	+++	60.4	6.8	8.4	*	3-6	CH_4	+++	134	2562	2224	83	
	3-6	Ar	-	52.1	6.8	7.2	*	3-6	Ar	-	118	478	386		
	9-12	CH_4	+++	1.9	6.9	10.7	1.8	6-9	CH_4	+++	107	2207	1991	83	0.18
	9-12	Ar	-	45.7	6.7	8.1	*	6-9	Ar	-	131	469	338		
Outside: O1	3-6	CH_4	+	26.4	7.2	6.7	*	3-6	CH_4	+	367	2072	776	41	
	3-6	Ar	-	56.3	6.4	10.4	0.8	3-6	Ar	-	334	1285	456		0.34
	9-12	CH_4	+		7.1	21.1	3.2	6-9	CH_4	+	229	3488	1678	84	0.39
	9-12	Ar	-	20.8	6.7	7.8	*	6-9	Ar	-	241	656	266		
Outside: O2	3-6	CH_4	-		7.6	7.7	*	3-6	CH_4	-	167	1667	1378	76	
	3-6	Ar	-		7.0			3-6	Ar	-	132	455	335		
	9-12	CH_4	+		6.6	14.6	2.9	6-9	CH_4	+	188	1560	986	83	0.59
	9-12	Ar	-		6.7	7.5	*	6-9	Ar	-	220	484	172		
O3	0-10	CH_4	-		6.8	7.5	*	0-10	CH_4	-	111	417	343		
	10-25	CH_4	-		6.9	7.0	*	10-25	CH_4	-	101	401	291		

* = Duplicate measurements varied by an average of 1.4 ‰, so changes in $\delta^{15}N$ < 1.4 permil were considered below the detection limit.

bdl = below detection limit

Methane dependency of Mound 12 N_2 fixation and implications for ANME diazotrophy

There is a striking contrast in the amount of nitrogen fixed between sediments incubated with methane and paired methane-free sediments (sampled from the same depth of the same core; n=8 pairs). In the absence of methane, sediments demonstrated no detectable diazotrophy, with the exception of low levels in the 3–6 cm depth interval of each of cores A1 and O1 (0.7 and 0.8 nmol N_2 fixed g_{dw}^{-1}, respectively, over 275 days) (Table 1, Figure 2). This suggests that the quantitatively significant community of diazotrophs is either methanotrophic or dependent on the activity of methanotrophs, and implicates the ANME, and/or associated SRB. The ANME-2 are currently the only identified diazotrophs at deep-sea methane seeps, and have been shown to demonstrate methane-dependent nitrogen fixation in incubations of seep sediment from the Eel River Basin (*5*).

Methane-dependent sulfide production, a proxy for sulfate-coupled anaerobic oxidation of methane (AOM) in seep sediment (*27, 28*), was observed in all incubations from active cores exhibiting nitrogen fixation, demonstrating the co-occurrence of AOM and diazotrophy (Table 1). However, not all incubations showing methane-dependent sulfide production demonstrated detectable nitrogen fixation (e.g., A3 3–6 cm), suggesting that the ANME-2-SRB do not constitutively fix nitrogen, which is consistent with all other known diazotrophic microorganisms. A combination of geochemical controls, and particularly the availability of bioavailable nitrogen sources, likely dictate the timing and magnitude of nitrogen fixation.

It was particularly unexpected that nitrogen fixation in cores collected outside of areas of active methane seepage would be methane dependent, considering the potential

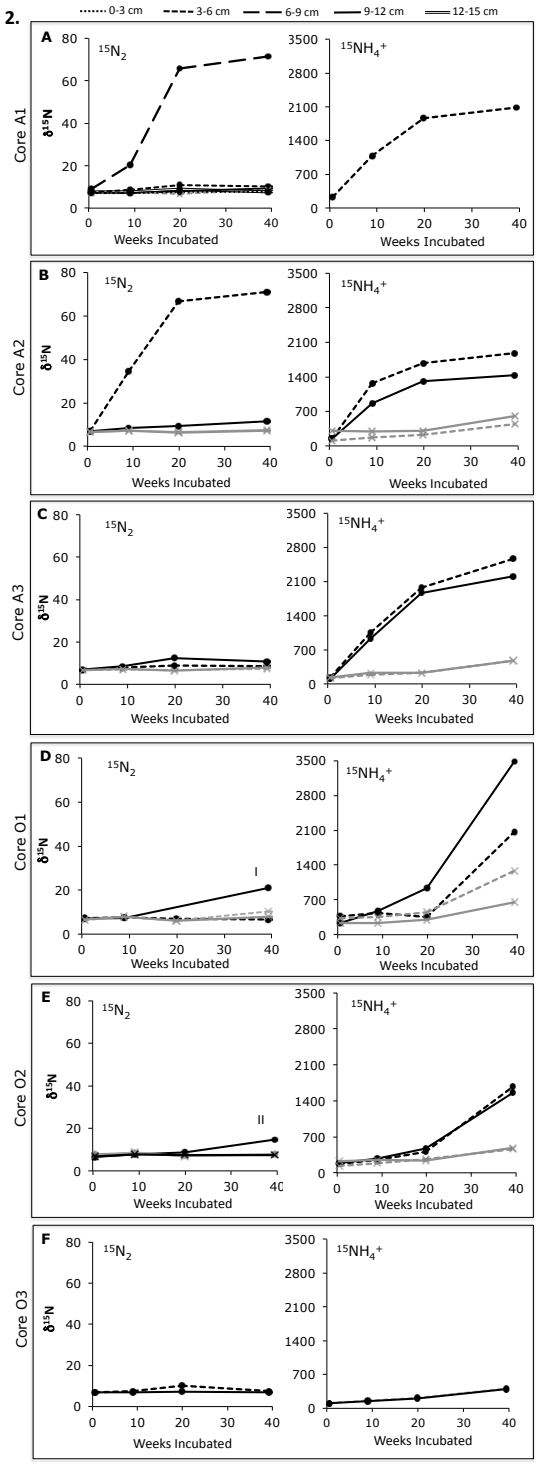

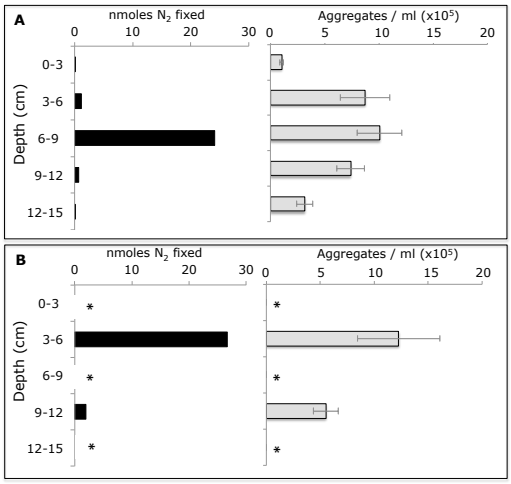

Figure 2. (Left) ^{15}N uptake from N_2 (left) and NH_4 (right) with time in bottle incubations containing sediment from 6 pushcores. Five depth intervals were incubated from core A1 (see top for legend) while only two were incubated for each of the other cores. Black lines indicate incubations amended with methane, gray lines indicate incubations amended with no methane. Core O3 did not have paired no-methane incubations, and the only interval with a paired methane incubation in core A1 is 3-6 cm with $^{15}N_2$. For cores A2, A3, O1 and O2, the two no-methane lines are both plotted, but often only one is visible due to their nearly identical trend.

Figure 3. (Above) Total nitrogen fixed during 39 week bottle incubation plotted with original depth of incubated sediment (left) and ANME-SRB aggregate abundance counted in the same incubations at the beginning of the experiment (right). Error bars indicate one standard deviation in each direction of aggregate counts on 3-5 replicate filters. Asterisks indicate depths for which no sediment was incubated.

occurrence of a variety of benthic diazotrophs, including free-living (i.e., non-ANME-associated) sulfate-reducing bacteria. Several species of SRB exhibit nitrogen fixation in pure culture (*29*), and sulfate-reducing bacteria are implicated in benthic diazotrophy in shallow marine sediments both by *nifH* sequences and patterns in activity (*21, 30, 31*). Additionally, *nifH* sequences similar to those of SRB have been detected in deep-sea sediments (*3–5, 32*). However, diazotrophy was not observed without methane, indicating that canonical SRB, growing independently of methane, are not fixing nitrogen at detectable rates in the sediments investigated from Mound 12. Interestingly, sulfide production was not observed in the absence of methane, suggesting activity of sulfate-reducing bacteria was low overall in these incubations (Table 1).

Ammonium uptake in microcosm experiments and the methane dependency of growth

All of the sediments tested demonstrated ^{15}N uptake from $^{15}NH_4^+$, in both the presence and absence of methane, indicating that all incubations contain growing anaerobic communities, and that the growth of some community members is not methane dependent (Table 1, Figure 2). ^{15}N uptake from $^{15}NH_4^+$ indicates protein synthesis, and therefore growth, and has been used as a proxy for potential growth in methane seep sediment previously (*33, 34*). The highest rate of NH_4^+ incorporation was observed in A2 3–6 cm, incubated with methane, between 4 and 63 days, at 7.75 nmol NH_4^+ fixed g_{dw}^{-1} hr^{-1} (1.1 x 10^3 nmol NH_4 g_{dw}^{-1} total in 275 days).

Ammonium incorporation in the absence of methane demonstrates the presence of a methane independent community. However, in the active cores, the majority of growth was methane dependent, with 78–83% of ^{15}N uptake from $^{15}NH_4^+$ dependent on methane

(A2 and A3; A1 was not tested) (Table 1). This is consistent with reports that ANME-SRB aggregates can comprise the majority of cells within seep sediment (*12, 35*). As expected, cores collected outside of areas of active methane seepage showed less stimulation with methane, with 41–84% of growth dependent on its presence (O1 and O2; O3 was not tested) (Table 1). The outside cores do, therefore, appear to host organisms capable of taking advantage of methane if/when it becomes available, despite low levels of methane *in situ,* and despite a lag time before growth with methane commences. This could be a due to a relic methanotrophic community remaining after previous exposure to methane seepage (see SI Discussion C). The stimulation of an AOM community in background sediment is consistent with the findings of Girguis et al., 2003 (*36*).

Contribution of nitrogen fixation to the total community nitrogen requirements

In A2 3–6 cm, the nitrogen derived from nitrogen fixation represented about 3% of the total nitrogen used for growth, determined by comparing the total N uptake from N_2 to that from NH_4^+ (Table 1). This may be an underestimate if the addition of NH_4^+ spurred growth above *in situ* levels. However, a low percentage of total nitrogen derived from diazotrophy at Mound 12 is consistent with the initial $\delta^{15}N$ values of the incubated sediment, which around 7 ‰ indicate significant deviation from nitrogen fixation indicative 0 ‰, and therefore substantial input of nitrogen from sources other than N_2, such as nitrate from the water column (*37*).

Some marine communities derive large percentages of their total nitrogen requirement from N_2 fixation, such as the surface waters of the subtropical North Pacific Gyre, where ~ 50% of the total nitrogen requirement can be derived from cyanobacterial

diazotrophy (*38*), as well as some shallow benthic environments, such as the Tikehau Lagoon in French Polynesia, where ~ 25% of nitrogen used for growth in microbial mats is derived from largely cyanobacterial nitrogen fixation (*20*). However, nitrogen fixation has been observed to contribute only 0.1% of nitrogen input in Narragansett Bay sediments, and 4% to the Rhode River Estuary in the Chesapeake Bay sediments (*26*, *and references therein*). These comparisons suggest that although 3% N_2-derived nitrogen for growth in methane seeps appears low, it is similar to that observed in other non-cyanobacterial, coastal benthic communities, and suggests that diazotrophy in deep-sea environments with enhanced productivity may play a similar ecological role as diazotrophy in shallow sediments. However, benthic nitrogen fixation in the Narragansett Bay was recently shown to demonstrate significant seasonal variation, resulting in a revised estimate of 20–60% of total nitrogen contributed by diazotrophy when averaged over the course of year (*19*). This 100X increased revised number indicates that our understanding of the significance of diazotrophy even in shallow sediments is still evolving.

Vertical distribution of N_2 fixation in methane seep sediment

In both A1 and A2, $^{15}N_2$ incorporation was limited to a particular depth horizon: 6–9 cm for A1, and 3–6 cm for A2, with little to no diazotrophy observed in the adjacent horizons (Figure 2 and Figure 3). This is likely due to diazotroph abundance/activity, and ultimately to variations in pore water geochemistry. Although changes in bioavailable N concentrations (NH_4^+, NO_3^{2-}, NO_2^{2-}) is an obvious potential explanation, the N profiles in the 12 cores investigated from the area showed no sharp changes in bioavailable N mid-

core that could explain such peaks in nitrogen fixation by localized nitrogen limitation (Figure 1). Additionally, the ammonium concentrations detected within the incubations at 275 days demonstrate low levels of ammonium throughout the methane-amended incubations from core 1, and only relatively small differences between those from A2 (see SI Discussion D).

However, sulfate and methane concentrations are known to demonstrate steep gradients in the top 10 cm of methane seep sediment (*12, 39–41*), and could be the cause of this spatially restricted enhanced diazotrophy. In marine sediment, the depth of the sulfate methane transition zone (SMTZ)—where both methane seeping up from below, and sulfate diffusing down from above, are simultaneously accessible—is known to dictate the location of the peak in abundance and activity of the ANME-SRB (*10, 42–44*). Although this zone is typically more poorly defined in methane seep sediment, which is driven by advection and often disturbed by bioturbation, than diffusion-driven benthos, ANME-SRB aggregates still peak within regions of optimal chemical availability generally within the top 10 cm of seep sediment (*12, 39, 40*).

ANME-SRB aggregates were therefore enumerated via microscopy with depth in core A1. ANME-SRB aggregates were found in all depths from 0-15 cm, but they were most abundant (reaching 1 x 10^6 aggs/ml sediment slurry) in the same depth horizon as the peak of nitrogen fixation (Figure 3). Similarly, the ANME-2-SRB aggregates in two depths within core A2 were enumerated and found to be most abundant (reaching 1.2 x 10^6 aggs/ml sediment slurry) at the depth with greater nitrogen fixation. This suggests that the horizon of maximum nitrogen fixation is due to enhanced activity by the diazotrophic ANME-SRB aggregates, likely due to optimal chemical conditions *in situ,*

and potentially within a SMTZ. Furthermore, the virtual lack of nitrogen fixation detected outside of this zone demonstrates that other diazotrophs in seep sediment are absent or not as active.

Interestingly, the distribution of ANME-SRB aggregates with depth is broader than the narrow peak of N_2 fixation. This demonstrates that although aggregates are present in high concentrations in the incubations flanking the depth with the spike in diazotrophy, they are not fixing nitrogen. One possible explanation for variability in metabolic behavior of the ANME-SRB between incubations is that the available nutrients within the sediment, other than sulfate and methane (which were added equally to all incubations), may be different, and result in different levels of growth. To test if the peak of nitrogen fixation was due to increased growth potential, we compared the rates of nitrogen fixation to the rates of potential growth (via $^{15}NH_4^+$ incorporation) in core A2. Although the shallow (3–6 cm) depth horizon of core A2 shows > 10X the nitrogen fixation than the deeper sediment (9–12 cm), it only demonstrates ~ 1.5X the potential total growth than the deeper sediment (Table 1). Greater total growth may therefore contribute to the greater nitrogen fixation observed, but it is an insufficient explanation for the entire difference in diazotrophy.

The size of ANME-SRB aggregates could also play a role in variable diazotrophy. Aggregate dimensions have been implicated in ANME-SRB activity before (*33, 45*) and may be particularly important to the rate of nitrogen fixation. In fact, the existence of chemical microniches within the aggregates may explain why diazotrophy can occur in sediments with relatively high levels of ammonium in the pore waters. The size and shape of the ANME-SRB aggregates in core A1 were therefore characterized with depth

(see SI Discussion D). No trend in the circularity (a measure of the aggregate's deviation from perfectly circular when viewed in two dimensions, and potentially indicative of different ANME-2 subgroups due to morphological variations between the subgroups observed by (*35*)) coincided with the mid-core peak in diazotrophy (SI Table 2). However, the median aggregate size reached a minimum at 6–9 cm, with aggregate diameters of 3.5 μM (SI Table 2, SI Figure 2). Although small size would not likely stimulate diazotrophy, the way large aggregates with nitrogen-deprived cells at the center might, reduced aggregate size may be a response to nutrient limitation, and it is therefore not unexpected to find coincident with nitrogen fixation. It is also possible that small aggregates sizes are indicative of more frequent aggregate budding to yield new aggregates (evidence for the budding theory of aggregate replication can be found in (*5, 28*)). In the following section, diazotrophy within individual ANME-2-SRB aggregates is measured to investigate if physical parameters (e.g., size) are indeed correlated with their rate of N_2 consumption.

NanoSIMS analysis of ANME-2-SRB aggregates

Fluorescence *in situ* Hybridization coupled to Nanoscale Secondary Ion Mass Spectrometry (FISH-NanoSIMS) directly confirmed that SRB-associated ANME-2 archaea are fixing nitrogen in the sediment incubation from core A1 6–9 cm (Figures 4 and 5). The level of ^{15}N enrichment, and therefore N_2 fixation, observed within ANME-2-SRB aggregates after 5 months was similar to that previously reported from Eel River Basin incubations after 6 months (*5*), with whole aggregate $^{15}N/^{14}N$ values reaching up to

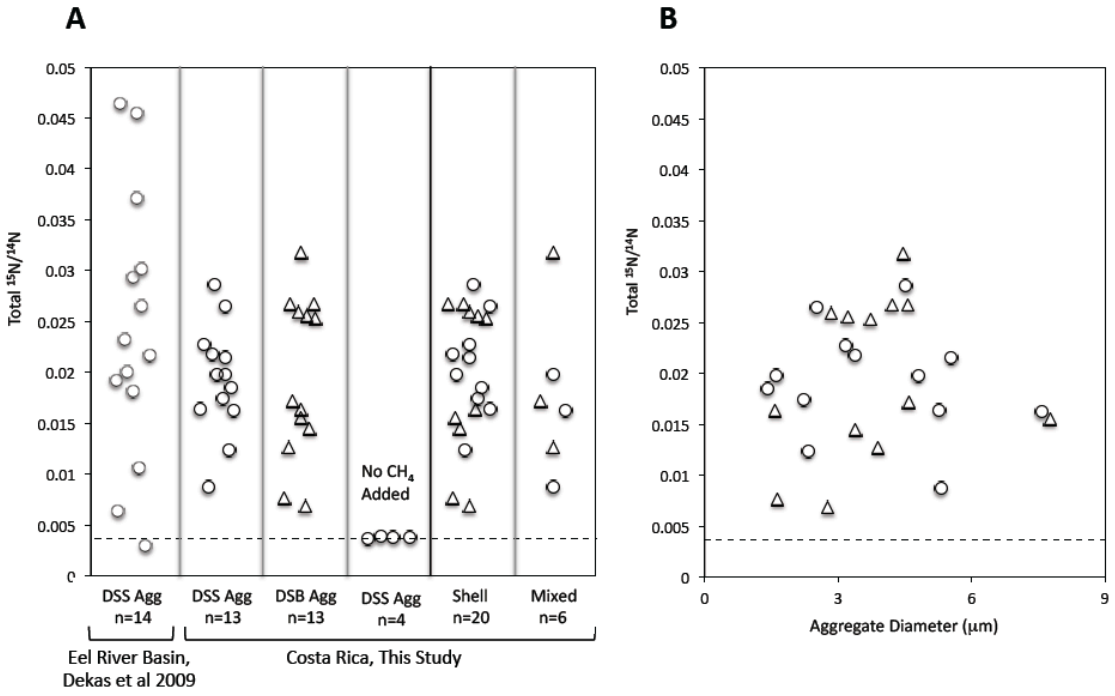

Figure 4. NanoSIMS analysis of ANME-2-SRB aggregates in $^{15}N_2$ incubations of methane seep sediment from the Eel River Basin (in gray, 6 months of incubation, Dekas et al. 2009) and Costa Rica Mound 12, core A1 6–9 cm (in black, 5 months of incubation, this study). Except where noted, aggregates were incubated under a headspace of methane. All data points represent the $^{15}N/^{14}N$ of the total CN^- ions collected from a single ANME-2-SRB aggregate. Aggregates of ANME-2 associated with *Desulfosarcina/Desulfococcus* (DSS, identified via hybridization with probe DSS 568) are depicted as circles, aggregates of ANME-2 associated with members of the *Desulfobulbaceae* (DSB, identified via hybridization with probe DSB 652) are depicted as triangles. A. Variation in $^{15}N/^{14}N$ values between ANME-2-SRB aggregates from different sites, with different SRB partners, and with different ANME-2-SRB association morphology. The markers are distributed along the x-axis within a category randomly to aid in viewing. B. Variation in $^{15}N/^{14}N$ values of ANME-2-SRB aggregates with the diameter of the aggregate. Natural abundance $^{15}N/^{14}N$ is indicated by the dotted line in each plot.

0.032 in the Mound 12 incubations (natural abundance $^{15}N/^{14}N$ is 0.0036) (Figure 4A). The replication of this observation in a geographically distinct methane seep, at approximately 1,000 m water depth, suggests that the diazotrophic potential of ANME-2 archaea is a common phenomenon in methane seeps.

To investigate ANME-2 diazotrophy further, nanoscale isotopic maps were generated with depth through a total of 30 aggregates incubated with $^{15}N_2$ (26 incubated

with methane, 4 incubated without methane) to determine what physical parameters might affect their rate of N_2 fixation, such as aggregate size, morphology (pattern of association with the sulfate-reducing partner), or identity of the sulfate-reducing partner. We found that ^{15}N uptake from $^{15}N_2$ was often spatially correlated with low $^{13}C/^{12}C$ ratios (Figure 5), and no ^{15}N incorporation from $^{15}N_2$ was observed in the absence of methane (n=4) (Figure 4A). Both of these observations are consistent with a NanoSIMS analysis of the ANME-SRB from the Eel River Basin, and demonstrative of the methane dependent nature of ANME (and possibly also associated SRB) diazotrophy (*5*). Although aggregates of diameters ranging from 1.4 μm to 7.8 μm were analyzed from the Costa Rican sediment, no trend in the $^{15}N/^{14}N$ was observed with aggregate size (Figure 4B). Additionally, no difference in $^{15}N_2$ incorporation was observed whether the ANME-2-SRB association consisted of a "shell" (n=20) or "mixed" (n=6) morphology (Figure 4A). It has been hypothesized that different sub-clades of the ANME-2 associate with SRB in physically different ways, resulting in shell versus mixed morphology (*35*). If this is the case, our results suggest that these sub-clades fix nitrogen at approximately the same rate. Our comparison is limited by a low number of mixed aggregates analyzed, however, due to a low occurrence of mixed aggregates in the sample.

Although ANME-2 diazotrophy has been previously demonstrated when in association with *Desulfosarcina/Desulfococcus* (DSS) (*5*), whether or not this ability would be enhanced or inhibited by association with alternative SRB partners was unknown. FISH-NanoSIMS was therefore employed to investigate $^{15}N_2$ incorporation in aggregates of ANME-2 associated with members of the *Desulfobulbaceae* (DSB), and ANME-2 diazotrophy was again detected (Figure 5 A, B). Additionally, no difference in

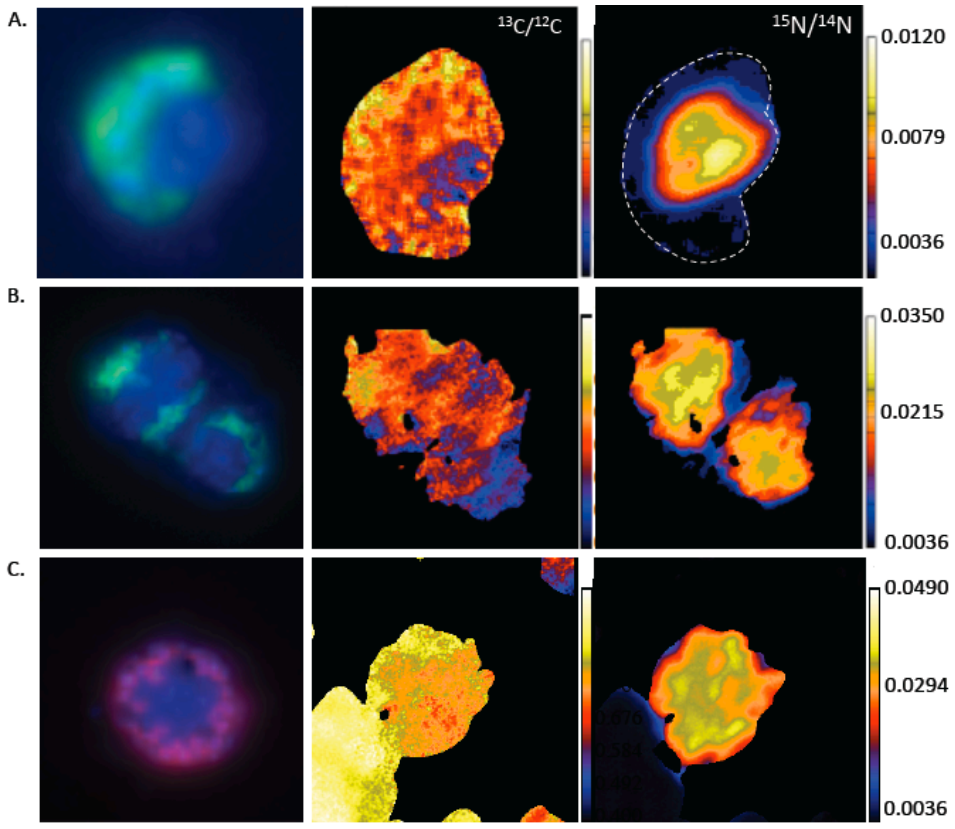

Figure 5. Isotopic composition of ANME-2-SRB aggregates incubated with $^{15}N_2$ and un-labeled methane determined via FISH-NanoSIMS. CARD-FISH images in the left panels, *Desulfobulbaceae* (probe DSB 658) in green, *Desulfosarcina/Desulfococcus* (probe DSS 658) in red, ANME-2 (DAPI-stained) in blue. Carbon isotope ratios in the center panels with color bar scale directly to right of image, with the following scales: A, max = 0.01222, min = 0.00952; B, max = 0.01126, min = 0.00360; C, max = 0.01045, min = 0.00400. Nitrogen isotope ratios in the right panels with color bar scale directly to the right of image. Natural abundance $^{15}N/^{14}N$, 0.00367, has been indicated by an arrow. Scales were selected for each aggregates to best demonstrate the patterns of isotopic distribution. Aggregate A: rastor size = 7 mm. Aggregate B: Rastor size = 12 mm. Aggregate C: Rastor size = 15 mm.

$^{15}N/^{14}N$ of the whole aggregate was observed whether the ANME were associated with DSS (n=13) or DSB (n=13) (Figure 4A).

Interestingly, although minor ^{15}N enrichment was also always observed in the DSS of ANME-2-DSS aggregates (Figure 5C and (*5*)), in two of the ANME-2-DSB aggregates incubated with $^{15}N_2$, the DSB do not appear enriched in ^{15}N (e.g., Figure 5A). Previously the ^{15}N enrichment of the associated DSS was interpreted as a sharing of

reduced nitrogen between the diazotrophic ANME and the DSS, however the possibility of independent diazotrophy of the DSS was not eliminated (*5*). The lack of ^{15}N enrichment in the associated DSB of some aggregates may be indicative of differences between the ANME-DSS and -DSB association, suggesting a lower degree of nutrient exchange between the ANME and DSB, and/or a less stable association. The ANME-DSB association was only discovered recently (*40, 46*), and although initially described as a partnership for the ANME-3, ANME-2 have subsequently been reported to associate with another lineage within the *Desulfobulbaceae* (*32*). Characterization of the differences between the ANME-DSS and ANME-DSB association are in progress (e.g., Green-Saxena et al., in prep (*47*)), and these differences may help discriminate between essential versus accessory components of the ANME-SRB relationship. Regardless of the differences, however, the observation of ^{15}N enrichment in the ANME-2 without ^{15}N in their bacterial partner highlights the primary ability of the ANME-2 to fix nitrogen.

nifH diversity in diazotrophic sediments

Despite the evidence that the ANME-2-SRB consortia represent the primary diazotrophs in seep sediment, diverse *nifH* sequences were detected in un-incubated sediment paired to the diazotrophic sediment incubations from core A1 and A2. Diverse *nifH* sequences have been recovered from several deep-sea sites previously, including sites of methane seepage (*2–5*). The diversity observed here spans three of the four groups of *nifH* sequences described in Raymond et al., 2004 (*48*) (Groups II, III, and IV; Figure 6B and C), with sequences clustering with those from methanogens, sulfate-

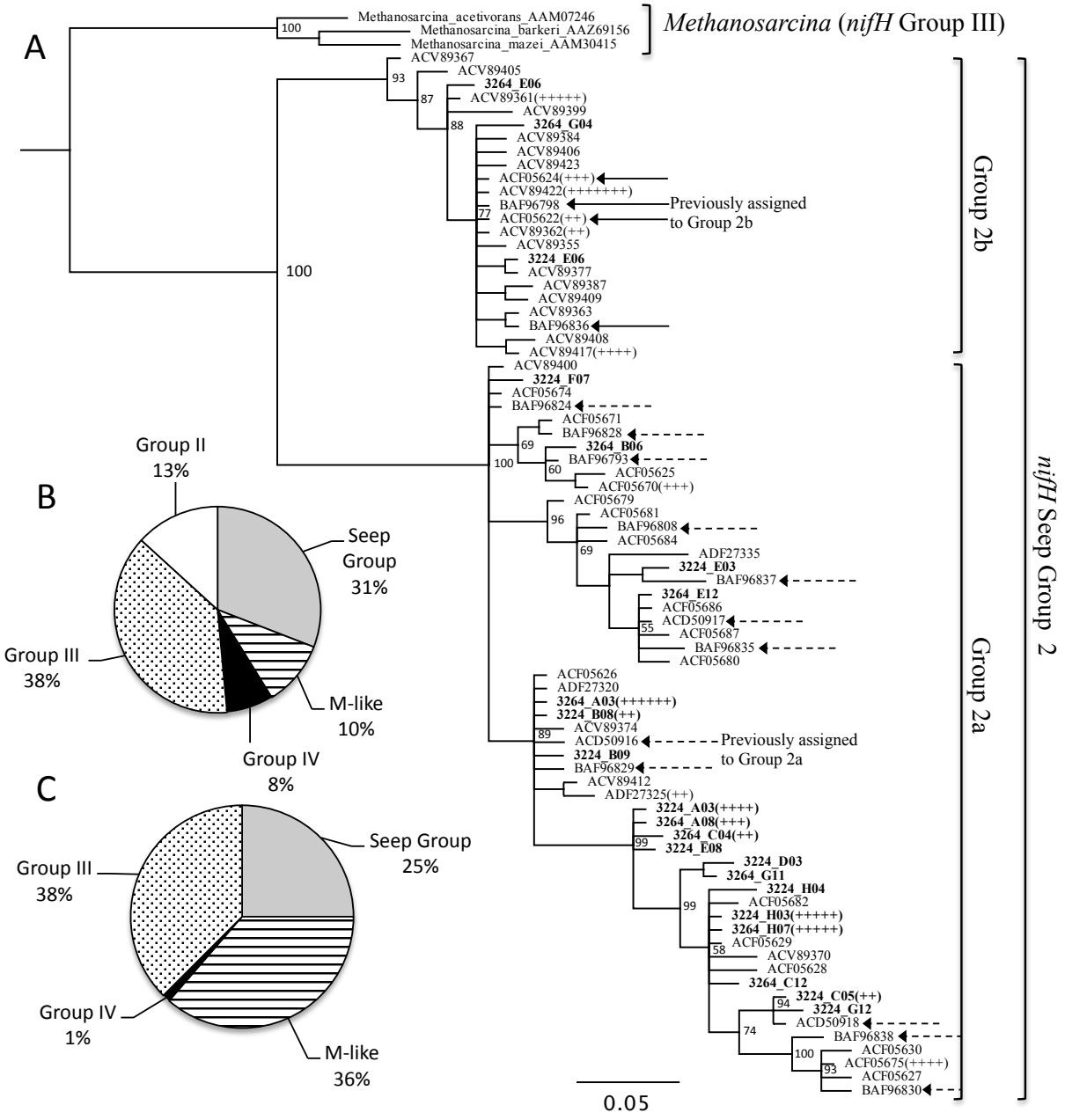

Figure 6. Phylogenetic identity of *nifH* sequences recovered from Costa Rica Mound 12 sediment. (A) Phylogenetic tree of the sub-set of *nifH* sequences detected that cluster within Seep Group 2, as named by Miyazaki et al 2009. The tree was constructed by Mr. Bayes (Basian Analysis) using deduced amino acid sequences. Frequency of taxon bipartition is shown as a percentage at major nodes. Sequences recovered from core A1 6-9 cm are numbered as 3224_ and from A2 3-6 cm as 3264_ , both in bold. The number of (+) indicates the number of identical sequences. Arrows indicate sequences that were grouped into 2a (dashed) or 2b (solid) by Miyazaki et al 2009. Major references are: ADF- and ACV- Eel River Basin incubated seep sediment (Dekas et al. 2009); ACF- Okhotsk Sea methane seep sediment (Dang et al 2009); BAF- Nankai Trough methane seep sediment (Miyazaki et al 2009); ACD- ANME-2-targeted cell-capture from Eel River Basin methane seep sediment (Pernthaler et al 2008). (B) and (C) Phylogenetic identity of the *nifH* sequences recovered from A1 6-9 cm (B), and A2 3-6 cm (C) as determined by a neighbor-joining tree of all sequences. Established *nif* groups are indicated. The "M-like" group refers to a previously undescribed clade discussed in the text.

reducing bacteria, and clostridia, as well as a previously identified putatively methane-seep specific clade (Figure 6A).

The methane-seep clade was originally named "Cluster III-x" by Dang et al., 2009 (*3*), when they noted that it contained exclusively sequences from methane seep sedimentary environments. Miyazaki et al. 2009 added to this group with *nifH* sequences from methane-rich sediments in the Nankai Trough, and re-named the group "Methane-Seep Group 2" (*4*). Furthermore, Miyazaki and colleagues proposed, on the basis of co-occurring archaeal 16s rRNA and *mcrA* genes belonging to the ANME, the high similarity to *nifH* sequences of *Methanosarcina*, and the inclusion of *nifH* sequences recovered from highly enriched samples of ANME-2c aggregates from the Eel River Basin (*49*), that the Methane-Seep Group 2 sequences could be hosted by ANME-2c (*4*). Although this may be the case, the observations (with the possible exception of the similarity to *Methanosarcina* sequences) are also consistent with an origin of the Methane-Seep Group 2 sequences within the ANME-associated SRB, whose abundance tracks that of the ANME-2 in the environment.

Unlike in the Nankai Trough sediments, where Methane-Seep Group 2 comprised 74% of all clones, only 25% and 31% of the two Costa Rican methane seep samples investigated here clustered within that group (Figure 6A and B). Still, a great diversity within Seep Group 2 was detected, spanning the previously proposed subgroups 2a and 2b, and demonstrating that perhaps subgroup 2a consists of several distinct further sub-groups. Significant fractions of the *nifH* sequences detected also fell within *nifH* Group III, which includes diverse anaerobic diazotrophs (38% of both libraries), as well as a previously un-named group that we call "*Methanosarcina*-like," or "M-like", in Figure

6A and B (36% and 10% of the two libraries). This group clusters with one clone detected by Dang and colleagues within Okhotsk Sea methane seep sediments (clone 40H-0N-1, ACF05660) and *Methanosarcina* sequences in "Cluster IIIb" of *nifH* Group III as named by Dang and colleagues. Future investigations of *nifH* sequences in these environments will be necessary to definitively link 16S rRNA identity to the newly described *nifH* groups, as well as assess which of these groups actually contribute to nitrogen fixation on the seafloor.

CONCLUSIONS

Methane seep diazotrophy appears to be dictated by chemical gradients affecting the activity of the ANME-2-SRB aggregates, resulting in narrow (< 3 cm) peaks of nitrogen fixation mediated by these aggregates between 3–9 cm beneath the seafloor. Although diverse *nifH* sequences suggest a diversity of diazotrophs in these sediments, as in other previously studied deep-sea sites, the methane dependent nature of the diazotrophy observed, and the exclusive peak of nitrogen fixation corresponding to the peak in abundance of ANME-2-SRB, strongly suggest that the majority—if not all—of nitrogen fixed in methane seep sediment is due to the ANME-2-SRB aggregates. By combining the bulk nitrogen fixation measured with the ANME-2-SRB-specific measurements of nitrogen fixation within a given sample, we can theoretically calculate the contribution of the ANME-2-SRB to the total, as in Ploug et al. 2010 (*50*). However, there are currently too many unknown parameters of the ANME and SRB cells (e.g., N content) to perform such a calculation without margins of error below two orders of magnitude (see SI Discussion F). A direct calculation of the contribution of ANME

diazotrophy to total seep diazotrophy must therefore await their further biochemical characterization.

The direct observation of nitrogen fixation by the ANME-2 in Mound 12 Costa Rica sediment via FISH-NanoSIMS is the first observation of diazotrophy in ANME archaea outside of the Eel River Basin methane seep system, and suggests the ability is ubiquitous in the globally distributed population of ANME-2. Although a relatively small percentage of the potential nitrogen required for community growth is obtained by diazotrophy (3%), the overall rate of nitrogen fixation in seep sediment appears to be higher than that in background sediments, and is about 1.5 orders of magnitude greater than previously published rates of deep-sea abyssal plain nitrogen fixation (*6*). Enhanced diazotrophy at Mound 12 indicates that hotspots of activity on the seafloor may mediate more nitrogen fixation than previously recognized. Further explorations of deep-sea diazotrophy, including at other areas of enhanced localized productivity, as well as undisturbed sediments, will continue to shape our understanding of the importance of deep-sea benthic nitrogen fixation in nitrogen and carbon cycling.

EXPERIMENTAL PROCEDURES

Site Description. Mound 12 is a mud volcano on the convergent continental margin southwest of Costa Rica. It extends about 30 m into the water column with a diameter of 1–1.6 km, and is part of a system of gas and fluid venting features that in total mediate the upward flow of an estimated 20 x 10^6 moles CH_4 $year^{-1}$ (*51, 52*). At 1,000 m water depth, this Costa Rican seep system (CR) represents a different physiochemical setting than the Eel River Basin methane seep system (ERB) (where diazotrophic ANME-2 were

collected previously (*5*)), with greater pressure (~ 50 atm, ERB; ~ 100 atm, CR) as well as higher O_2 levels (< 0.5 ml/L ERB; ~ 1 ml/L, CR), and dense communities of diverse macrofauna (*51–53*).

Sample collection. Seafloor sediment push-cores were collected using the submersible *Alvin* in February 2009 (AT 15-44) and January 2010 (AT 15-59) at Mound 12 and other nearby sites of methane seepage at depths ranging from 950 meters to 1,010 meters (SI Table 1). Sediment cores were extruded from push-core liners in 1, 3, or 5 cm increments on-board, immediately after collection. Sub-samples of each depth horizon were preserved for later analysis or processed immediately (see below). All cores used for the quantification of nitrogen species were collected on AT 15-44; all cores used for ^{15}N-labeling incubations were collected on AT 15-59 (SI Table 1).

^{15}N-labeling bottle incubations. ^{15}N uptake was chosen to observe nitrogen fixation because it provides access both to total rates, measured by Elemental Analysis coupled to Isotope Ratio Mass Spectrometry (EA-IRMS), and single cell observations of diazotrophy, measured by Nanoscale Secondary Ion Mass Spectrometry (NanoSIMS). Additionally, it can be preferable over the Acetylene Reduction Assay (*54*) to measure diazotrophy in marine sediment because of the inhibitory effect acetylene can have on a diverse set of benthic microbes, including methanogens, methanotrophs, nitrifiers, denitrifiers, and sulfate-reducing bacteria (*24*, *and references therein*). Indeed, acetylene was shown to inhibit the ANME-SRB consortia in Eel River Basin sediment (*5*).

Six cores were selected for ^{15}N-labeling experiments to represent a range of methane flux regimes. A transect of three cores were collected on a single Alvin dive (AD4587) at one mat-covered location: A2 (gray mat coverage), A3 (white mat coverage), and O1 (just outside of visible mat coverage). On the same dive, an additional core, O2, was collected further from the mat site, where there were no signs of active methane seepage, but carbonate pavements suggested previous methane seepage. Three ml of sediment from each of two depth horizons, 3–6 cm and 9–12 cm, from each of the four cores were separately mixed with 6 ml of argon-sparged filtered seawater collected at the sampling site, achieving a 1:2 ratio of sediment to seawater, in 35 ml serum bottles. Bottles were set up in quadruplicate for each depth of each core. The bottles were sealed with butyl stoppers and metal clamps. The headspace of each bottle was replaced with either methane or argon, and either $^{15}NH_4$ (1 mM final concentration) or $^{15}N_2$ (1 ml) was added. Each of the four bottles from each depth therefore had a unique combination of amendments. Another core, A1, was collected within a white mat on Alvin Dive 4586 and serum bottle incubations amended with methane and $^{15}N_2$ (1 ml) were set-up from each sediment depth horizon (0–3 cm, 3–6 cm, 6–9 cm, 9–12 cm, and 12–15 cm). Sediment from the 3–6 cm horizon of core A1 was also used to set-up incubations with a headspace of argon instead of methane and $^{15}NH_4$ (2 mM) instead of $^{15}N_2$. The final core selected for incubations was collected with a multi-coring device on the opposite site of Mound 12 from the majority of the methane seepage (SI Figure 1, (*51*)), and sediment slurries were made from the 0–10 cm depth and the 10–25 cm depth horizons. These were all incubated in the presence of methane with either $^{15}N_2$ (1 ml) or $^{15}NH_4$ (1 mM). All bottle incubations were assembled the same night the cores were collected. Each

bottle contained an approximately 1:2 slurry: headspace ratio, with the headspace over-pressured to 2 atm, and stored at 4-8 degrees C (slightly above the *in situ* temperature). Sub-samples were collected via needle and syringe at 4, 63, 139, and 275 days, and preserved according to the procedures described below.

Long incubations times were employed both due to the slow rate of growth of dominant seep organisms, with doubling times of methanotrophic archaea reported to be 3–7 months (*27, 33, 34, 55*), and to allow sufficient time for diazotrophy to be observed. Because the fraction of total N bound in living matter in a sediment sample is typically small, long incubations with $^{15}N_2$ can be necessary to see an increase in the bulk $^{15}N/^{14}N$ ratio, even when diazotrophs are extremely active (*24*).

Bulk $\delta^{15}N$ and $\delta^{13}C$ isotopic analysis. Sediment sub-samples for bulk isotopic analysis were centrifuged briefly, the supernatant removed, and the sediment pellet stored at -20ºC until analysis. Sediments incubated with $^{15}NH_4^+$ were washed to remove unincorporated $^{15}NH_4^+$: PBS was added to sediment pellets, vortexed, centrifuged at 15,000 g for 15 minutes, PBS removed, 2 M KCL added as recommended by (*33*), vortexed, incubated at RT for 1 hour, centrifuged, KCL removed, PBS added, vortexed, centrifuged, and PBS removed. Testing determined that the KCL incubation did remove more $^{15}NH_4^+$ than a third wash with PBS (reduced the carry-over signal by ~ 10%). Despite washing, un-incorporated $^{15}NH_4^+$ was not completely removed from the sediments, which was evident in killed sediments briefly incubated with $^{15}NH_4^+$ and then processed normally. This is likely due to ammonium adsorbsion to the sediments, and has been reported previously in $^{15}NH_4^+$ sediment labeling experiments (*33*). The baseline $\delta^{15}N$ for $^{15}NH_4^+$- incubated

sediments was determined to be approximately 100–150 ‰, but does not affect the calculation of $^{15}NH_4$ uptake with time.

The pelleted samples were baked at 60ºC for 36 hours and the dried sediment cakes homogenized manually with a metal spatula. Dried sediment was weighed (30-70 mg) in silver cups, subjected to acid fumigation for 5 hours (to remove carbonate material (*56*)), and dried at 60 ºC overnight. The sediment-containing silver cups were then put inside tin cups for structural support, crimped, and sent to the UC Davis Stable Isotope Facility. There the $^{15}N/^{14}N$ was measured using an Elementar Vario EL Cube elemental analyzer interfaced to a PDZ Europa 20-20 isotope ratio mass spectrometer.

UC Davis reports a long-term standard deviation of 0.3 ‰ for ^{15}N measurements. We found the average difference between duplicate samples analyzed (n=12 pairs) to be 1.4 ‰, with a standard deviation of 0.75, for sediments incubated with $^{15}N_2$. In this study we therefore have only considered changes in $\delta^{15}N > 1.4$ ‰ over the course of the experiment a definite indication of nitrogen fixation. This is likely a conservative cut-off, because if the instrumental variation was indeed this great, we should observe as many negative changes as we do positive changes below 1.4 ‰, and instead, we see 12 samples with increases in $\delta^{15}N < 1.4$ ‰ over time, and only one decrease. This suggests that the lower precision in the environmental sample analysis may be due to incomplete homogenization of the dried sediment cake or the sample slurry itself before the paired sub-samples were removed, and that the higher $\delta^{15}N$ detected in some replicates was indeed due to nitrogen fixation, not instrumental error. The effect of over-estimating the error of the EA-IRMS analysis would be an underestimation of nitrogen fixation in the sediment incubations with low levels of nitrogen fixation (resulting in changes of $\delta^{15}N <$

1.4 ‰). The average difference between duplicate samples incubated with $^{15}NH_4$ (n=3) was 35.6 ‰, with a standard deviation of 35.7. The larger error here is likely due to increased variability introduced in the washing process, but compared to the differences between samples of this type (up to ~ 1000 ‰), this variability is small.

Fluorescence in situ Hybridization coupled to Nanoscale Secondary Ion Mass Spectrometry (FISH-NanoSIMS). Sediment sub-samples for FISH-NanoSIMS analysis were fixed with 2% paraformaldehyde, incubated at 4 ºC overnight, and washed with PBS, then PBS:EtOH (1:1), and brought up in 1 ml 95% EtOH. Washed fixed samples were stored at -20 ºC. FISH-NanoSIMS was performed as described previously (*5, 57*). Briefly, a Percoll gradient (Sigma-Aldrich #P4937) followed by filtration on either a 0.22 um Durapore or 3.0 um Isopore filter (Millipore) to concentrate the cells and remove sediment prior to FISH and DAPI staining. Cells were deposited onto custom cut indium tin oxide (ITO) coated glass. CARD-FISH was conducted on the ITO-attached cells using DSS 658 (60% formamide) (*12*) and DSB 652 (25% formamide) (*47*) and Alexa green and red fluorophores using previously described protocols for CARD-FISH (*58, 59*). In order to compare the $^{15}N/^{14}N$ ratio of DSB and DSS aggregates in the same NanoSIMS session (and therefore the most similar tuning conditions), samples for NanoSIMS analysis were hybridized with both probes sequentially. Without a Cy5 (or equivalent) filter set, we were unable to additionally hybridize the ANME-2 cells in the same NanoSIMS sample. However, dual hybridizations of EelMS932 (*12*) and either DSS 658 or DSB 652 were carried out separately on seep sediment from Mound 12 and demonstrated that the vast majority of the presumed ANME-2 cells associated with the

hybridized sulfate-reducing bacteria indeed hybridized with the EelMS932 probe. Cells of interest were located and imaged using a Delta Vision RT microscope and Applied Precision software.

The samples were then analyzed using a CAMECA NanoSIMS 50L housed at Caltech, with a mass resolving power of approximately 5,000. A Cs+ primary ion beam (2–8 pA) with a nominal spot size of 100–200 nm was used to raster over cells of interest. Seven masses were routinely collected: $^{12}C^-$, $^{13}C^-$, $^{12}C^{14}N^-$, $^{13}C^{14}N^-$, $^{28}Si^-$, $^{31}P^-$, and $^{32}S^-$ using electron multipliers. Square images of 3 to 25 um on a side were collected at 256 x 256 or 512 x 512 pixels resolution, for periods lasting one to twenty hours, until the target biomass was completely analyzed or decreased in size by at least one half. Images were processed using commercially available L'Image software (developed by L. Nittler, Carnegie Institution of Washington, Washington D.C.).

Microscopic enumeration of ANME-SRB aggregates. Paraformaldehyde fixed sediment was diluted in PBS, sonicated, and collected on 0.2 μm Isopore filters. Three to five filters were prepared for each sample, DAPI stained, and examined using an epifluorescence microscope. Filters for core A1 were coded so that they were counted blind. 100 frames were examined per filter, equivalent to 10 to 100 aggregates per filter total. Images were collected of each frame containing an ANME-SRB aggregate, identified by their distinct morphology and the characteristic different intensities of DAPI staining in the bacteria and archaea (as seen in *12*).

Determining ANME-SRB aggregate size and shape with depth in core A1. The cross-sectional area of aggregates was determined by manually outlining images of DAPI-stained aggregates and calculating the area using publically available ImageJ software. The focal plane was adjusted before imaging to capture the largest cross-sectional area of the aggregate. Fifty aggregates were measured for each depth horizon, except for 0–3 cm, when only thirty aggregates total were observed on the filters from that horizon. Aggregate areas were measured rather than diameters, due to the presence of non-spherical aggregates, including ellipsoidal and non-symmetrical aggregates, sometimes containing several spherical lobes (e.g., Figure 5B). The circularity (a measure of a shape's deviation from perfectly circular; $circularity = 4\pi(area/perimeter^2)$) of each aggregate was also measured. Approximate diameters were calculated from the measured area by assuming a perfect circle.

DNA extractions. DNA was extracted from non-incubated sediment frozen on-board at -80 ºC in order to assess the diversity of potential diazotrophs within natural communities. Sediments were selected for DNA extraction based on the observation of diazotrophy in the paired sediment incubations from the same depth horizon (A1 depth 6–9 cm and A2 depth 3–6 cm). DNA was extracted using the MoBio RNA Powersoil Total RNA Isolation Kit (cat # 12866-25) with the RNA Powersoil DNA Elution Accessory Kit (cat # 12867-25), with the following modifications: after the addition of SR2, the mixture was divided into four 2 ml screw top tubes and bead beated for 45 seconds at speed 5.5 three times. The mixture was centrifuged at 2500 xg for 10 min, then the aqueous layers removed and recombined in a 15 ml tube. The rest of the protocol

was followed by the manufacturer's instructions, with the incubation with SR4 at room temperature. DNA pellets were re-suspended in 100 μl SR7 and stored at -80 ºC immediately.

nifH Clone Libraries. nifH clone libraries were constructed from DNA extracted from sediment within A1 6–9 cm and A2 3–6 cm using the *nifH* primers designed for deep-sea samples in (*2*). 25 μl PCR reactions containing 1 μl 10 mM R primer (*nifH* 132aa R), 1 μl 10 mM F primer (*nifH* 10aa F) (*2*), 1 μl template, 2.5 μl 10X ExTaq PCR buffer (Takara), 0.25 μl ExTaq (Takara), 0.5 μl 10 mM dNTPs (New England Biolabs), 0.5 μl 10 mg/ml BSA, and 18.25 μl water were performed. The following PCR program was used: 94ºC 2 min, [94ºC 1 min, 50ºC 1 min, 72ºC 1 min] x 45, 72ºC 5 min. The products of this reaction were plate purified (Millipore Multiscreen Filter Plates), brought up in 30 μl 10mM Tris, and ligated using the TOPO TA Cloning Kit (Invitrogen). The ligations were transformed using One Shot TOP10 chemically competent E. coli cells (Invitrogen). 95 colonies from each library were picked, grown overnight in LB broth and amplified using M13 primers for 30 cycles. The M13 products were plate purified and sent for unidirectional sequencing using T3 primers at Laragen Sequencing using an ABI Prism 3730 DNA sequencer (n=68, core A1, and n=88, core A2).

nifH phylogenetic analysis. Sequences were translated into deduced amino acid sequences and a neighbor-joining tree of all sequences generated (1,000 boot strap replicates) using Geneious Pro software. The alignment was made using default gap penalties in ClustalW. Sequences within Methane Seep 2 clade (*4*) were used to generate

a Bayesian Inference phylogeny in Mr. Bayes. The Mr. Bayes analysis consisted of 12,300,000 generations, ending with an average standard deviation of split frequencies of 0.008288. A burn in percent of 25 was applied, leaving 36,902 trees that were used to construct the consensus tree in Figure 6. The frequency of the taxon bipartitions were calculated as percentages.

Analytical Procedures. Sulfide concentrations were measured in both squeezed sediment core pore water and incubated sediment slurry via the Cline Assay after precipitation as zinc sulfide (*60*). Nitrate and nitrite concentrations from cruise AT 15-49 were analyzed by converting NO_x^- to NO and analyzing with an Antek chemiluminescence detector. Nitrate was determined by difference with nitrite measurements, which were also made by an Antek chemiluminescence detector. Ammonium in squeezed push core pore water from cruise AT 15-49 was analyzed via the indol-phenol method in filtered sample water (500 μl) preserved with 200 μl phenol-EtOH solution (5.5 ml phenol, 49 ml EtOH, 2 ml H_2O) and stored at 4°C until analysis. All N species measurements from AT 15-49 were made at the University of Georgia, Athens. Ammonium concentrations from incubations were measured on a Dionex DX-500 Ion Chromatograph at the Caltech Environmental Analysis Center. Methane was measured via Gas Chromotography by Bill Ussler at the Monterey Bay Aquarium Research Institute.

ACKNOWLEGEMENTS

We would like to thank Lisa Levin, Burt Thomas, David Fike, Jake Bailey, Rachel Poretsky, Shana Goffredi, and the crew and science party of AT 15-44 and AT 15-59 for

assistance in sample collection. We thank Yunbin Guan and John Eiler for assistance with NanoSIMS operations. We thank Abigail Green-Saxena helpful discussions and for assistance with CARD-FISH in the laboratory. We thank Abigail Green-Saxena (again) and Roland Hatzenpichler for detailed reviews of this manuscript. We thank Bill Ussler at the Monterey Bay Aquarium Research Institute and Nathan Dalleska at the Caltech Environmental Analysis Center for assistance with methane and ammonium measurements, respectively. We thank Steve Skinner for assistance with the maps in SI Figure 1. Funding was provided by the DOE (Early Career Award DE-SC0003940 to V.J.O) and the NSF (MCB-0348492 to V.J.O and a Graduate Research Fellowship to A.E.D). The Caltech Center for Microanalysis, housing the NanoSIMS 50L, is partially funded by the Gordon and Betty Moore Foundation.

WORKS CITED

1. M. P. Mehta, J. A. Baross, Nitrogen fixation at 92˚C by a hydrothermal vent archaeon. *Science* **314**, 1783 (2006).
2. M. P. Mehta, D. A. Butterfield, J. A. Baross, Phylogenetic diversity of nitrogenase (*nifH*) genes in deep-sea and hydrothermal vent environments of the Juan de Fuca Ridge. *Applied and Environmental Microbiology* **69**, 960 (2003).
3. H. Dang, X. Luan, J. Zhao, J. Li, Diverse and novel *nifH* and *nifH*-like gene sequences in the deep-sea methane seep sediments of the Okhotsk Sea. *Applied and Environmental Microbiology* **75**, 2238 (2009).
4. J. Miyazaki *et al.*, Molecular characterization of potential nitrogen fixation by anaerobic methane-oxidizing archaea in the methane seep sediments at the number 8 Kumano Knoll in the Kumano Basin, offshore of Japan. *Applied and Environmental Microbiology* **75**, 7153 (2009).
5. A. E. Dekas, R. S. Poretsky, V. J. Orphan, Deep-sea archaea fix and share nitrogen in methane-consuming microbial consortia. *Science* **326**, 422 (2009).
6. E. O. Hartwig, S. O. Stanley, Nitrogen Fixation in Atlantic deep-sea and Coastal sediments. *Deep-Sea Research* **25**, 411 (1978).
7. L. A. Codispoti, An oceanic fixed nitrogen sink exceeding 400 Tg N a^{-1} vs the concept of homeostasis in the fixed-nitrogen inventory. *Biogeosciences* **4**, 233 (2007).
8. C. Mahaffey, A. F. Michaels, D. G. Capone, The conundrum of marine N_2 fixation. *American Journal of Science* **305**, 546 (2005).

9. T. DeVries, C. Deutsch, F. Primeau, B. Chang, A. Devol, Global rates of water-column denitrification derived from nitrogen gas measurements. *Nature Geoscience* **5**, 547 (2012).
10. W. S. Reeburgh, Oceanic methane biogeochemistry. *Chem Rev* **107**, 486 (Feb, 2007).
11. V. J. Orphan, C. H. House, K. U. Hinrichs, K. D. McKeegan, E. F. DeLong, Methane-consuming archaea revealed by directly coupled isotopic and phylogenetic analysis. *Science* **293**, 484 (2001).
12. A. Boetius *et al.*, A marine microbial consortium apparently mediating anaerobic oxidation of methane. *Nature* **407**, 623 (2000).
13. A. Teske, D. Nelson, in *The Prokaryotes,* M. Dworkin, S. Falkow, E. Rosenberg, K.-H. Schleifer, E. Stackebrandt, Eds. (Springer New York, 2006), p. 784.
14. L. A. Levin, Ecology of cold seep sediments: Interactions of fauna with flow, chemistry and microbes. *Oceanography and Marine Biology: An Annual Review* **43**, 1 (2005).
15. J. A. Sohm, E. A. Webb, D. G. Capone, Emerging patterns of marine nitrogen fixation. *Nature Reviews Microbiology* **9**, 499 (2011).
16. P. G. Falkowski, Evolution of the nitrogen cycle and its influence on the biological sequestration of CO_2 in the ocean. *Nature* **387**, 272 (1997).
17. R. W. Howarth, Nutrient Limitation of Net Primary Production in Marine Ecosystems. *Annu Rev Ecol Syst* **19**, 89 (1988).
18. M. A. Saito *et al.*, Iron conservation by reduction of metalloenzyme inventories in the marine diazotroph Crocosphaera watsonii. *PNAS* **108**, 2184 (2011).
19. R. W. Fulweiler, S. W. Nixon, B. A. Buckley, S. L. Granger, Reversal of the net dinitrogen gas flux in coastal marine sediments. *Nature* **448**, 180 (2007).
20. C. Charpy-Roubaud, L. Charpy, A. W. D. Larkum, Atmospheric dinitrogen fixation by benthic communities of Tikehau Lagoon (Tuamotu Archipelago, French Polynesia) and its contribution to benthic primary production. *Marine Biology* **139**, 991 (2001).
21. V. J. Bertics *et al.*, Occurrence of benthic microbial nitrogen fixation coupled to sulfate reduction in the seasonally hypoxic Eckernforde Bay, Baltic Sea. *Biogeosciences Discussions* **9**, 6489 (2012).
22. R. W. Fulweiler, S. W. Nixon, B. A. Buckley, S. L. Granger, Net Sediment N_2 Fluxes in a Coastal Marine System-Experimental Manipulations and a Conceptual Model. *Ecosystems* **11**, 1168 (2008).
23. D. White, *The Physiology and Biochemistry of Prokaryotes*. Oxford University Press, New York, ed. Third, 2007.
24. D. G. Capone, in *Nitrogen Cycling in Coastal Marine Environments,* T. H. Blackburn, J. Sorensen, Eds. (John Wiley & Sons, New York, 1988), p. 85.
25. J. P. Montoya, M. Voss, P. Kahler, D. G. Capone, A Simple, High-Precision, High-Sensitivity Tracer Assay for N_2 Fixation. *Applied and Environmental Microbiology* **62**, 986 (1996).
26. R. W. Howarth, R. Marino, J. Lane, Nitrogen fixation in freshwater, estuarine, and marine ecosystems. 1. Rates and importance. *Limnology and Oceanography* **33**, 669 (1988).

27. K. Nauhaus, M. Albrecht, M. Elvert, A. Boetius, F. Widdel, In vitro cell growth of marine archaeal-bacterial consortia during anaerobic oxidation of methane with sulfate. *Environmental Microbiology* **9**, 187 (2007).
28. K. Nauhaus, A. Boetius, M. Kruger, F. Widdel, In vitro demonstration of anaerobic oxidation of methane coupled to sulphate reduction in sediment from a marine gas hydrate area. *Environmental Microbiology* **4**, 296 (2002).
29. M. T. Madigan, J. M. Martinko, P. M. Dunlap, D. P. Clark, *Brock Biology of Microorganisms*. (Pearson Education, Inc., San Francisco, ed. 12, 2009).
30. V. J. Bertics *et al.*, Burrowing deeper into benthic nitrogen cycling: the impact of bioturbation on nitrogen fixation coupled to sulfate reduction. *Mar Ecol–Prog Ser* **409**, 1 (2010).
31. T. F. Steppe, H. W. Paerl, Potential N_2 fixation by sulfate-reducing bacteria in a marine intertidal microbial mat. *Aquatic Microbial Ecology* **28**, 1 (2002).
32. A. Pernthaler *et al.*, Diverse syntrophic partnerships from deep-sea methane vents revealed by direct cell capture and metagenomics. *PNAS* **105**, 7052 (2008).
33. V. J. Orphan, K. A. Turk, A. M. Green, C. H. House, Patterns of ^{15}N assimilation and growth of methanotrophic ANME-2 archaea and sulfate-reducing bacteria within structured syntrophic consortia revealed by FISH-SIMS. *Environmental Microbiology*, (2009).
34. M. Krueger, H. Wolters, M. Gehre, S. B. Joye, H. H. Richnow, Tracing the slow growth of anaerobic methane-oxidizing communities by ^{15}N-labelling techniques. *FEMS Microbiology Ecology* **63**, 401 (Mar, 2008).
35. K. Knittel, T. Losekann, A. Boetius, R. Kort, R. Amann, Diversity and distribution of methanotrophic archaea at cold seeps. *Applied and Environmental Microbiology* **71**, 467 (2005).
36. P. R. Girguis, V. J. Orphan, S. J. Hallam, E. F. DeLong, Growth and methane oxidation rates of anaerobic methanotrophic archaea in a continuous-flow bioreactor. *Applied and Environmental Microbiology* **69**, 5472 (2003).
37. J. P. Montoya, in *Nitrogen in the Marine Environment,* D. Capone, D. A. Bronk, M. R. Mulholland, E. J. Carpenter, Eds. (Elsevier, Boston, 2008), p. 1277.
38. D. Karl *et al.*, The role of nitrogen fixation in biogeochemical cycling in the subtropical North Pacific Ocean. *Nature* **388**, 533 (Aug 7, 1997).
39. C. Hensen, K. Wallmann, M. Schmidt, C. R. Ranero, E. Suess, Fluid expulsion related to mud extrusion off Costa Rica—A window to the subducting slab. *Geology* **32**, 201 (2004).
40. H. Niemann *et al.*, Novel microbial communities of the Haakon Mosby mud volcano and their role as a methane sink. *Nature* **443**, 854 (2006).
41. V. J. Orphan *et al.*, Comparative analysis of methane-oxidizing archaea and sulfate-reducing bacteria in anoxic marine sediments. *Applied and Environmental Microbiology* **67**, 1922 (2001).
42. N. J. Knab, A. W. Dale, K. Lettmann, H. Fossing, B. B. Jorgensen, Thermodynamic and kinetic control on anaerobic oxidation of methane in marine sediments. *Geochim Cosmochim Ac* **72**, 3746 (2008).
43. T. Treude *et al.*, Anaerobic oxidation of methane and sulfate reduction along the Chilean continental margin. *Geochim Cosmochim Ac* **69**, 2767 (2005).

44. B. K. Harrison, H. Zhang, W. Berelson, V. J. Orphan, Variations in Archaeal and Bacterial Diversity Associated with the Sulfate-Methane Transition Zone in Continental Margin Sediments (Santa Barbara Basin, California). *Applied and Environmental Microbiology* **75**, 1487 (2009).
45. B. Orcutt, C. Meile, Constraints on mechanisms and rates of anaerobic oxidation of methane by microbial consortia: process-based modeling of ANME-2 archaea and sulfate reducing bacteria interactions. *Biogeosciences* **5**, 1587 (2008).
46. T. Lösekann *et al.*, Diversity and abundance of aerobic and anaerobic methane oxidizers at the Haakon Mosby mud volcano, Barents Sea. *Applied and Environmental Microbiology* **73**, 3348 (2007).
47. A. M. Green-Saxena, A. E. Dekas, V. J. Orphan, Distinct nitrate use by separate families of sulfate-reducing bacteria associated with ANME-II clade of anaerobic methane-oxidizing archaea, (in prep).
48. J. Raymond, J. L. Siefert, C. R. Staples, R. E. Blankenship, The natural history of nitrogen fixation. *Molecular Biology and Evolution* **21**, 541 (2004).
49. A. Pernthaler *et al.*, Diverse syntrophic partnerships from deep-sea methane vents revealed by direct cell capture and metagenomics. *PNAS* **105**, 7052 (2008).
50. H. Ploug *et al.*, Carbon and nitrogen fluxes associated with the cyanobacterium Aphanizomenon sp. in the Baltic Sea. *ISME Journal* (2010).
51. S. Mau *et al.*, Estimates of methane output from mud extrusions at the erosive convergent margin off Costa Rica. *Marine Geology* **225**, 129 (2006).
52. H. Sahling *et al.*, Fluid seepage at the continental margin offshore Costa Rica and southern Nicaragua. *Geochem Geophy Geosy* **9**, (2008).
53. G. Bohrmann *et al.*, Widespread fluid expulsion along the seafloor of the Costa Rica convergent margin. *Terra Nova* **14**, 69 (2002).
54. W. D. Stewart, G. P. Fitzgerald, R. H. Burris, In situ studies on N_2 fixation using the acetylene reduction technique. *PNAS* **58**, 2071 (1967).
55. P. R. Girguis, A. E. Cozen, E. F. DeLong, Growth and population dynamics of anaerobic methane-oxidizing archaea and sulfate-reducing bacteria in a continuous-flow bioreactor. *Applied and Environmental Microbiology* **71**, 3725 (2005).
56. D. Harris, W. R. Horwath, C. van Kessel, Acid fumigation of soils to remove carbonates prior to total organic carbon or carbon-13 isotopic analysis. *Soil Sci Soc Am J* **65**, 1853 (2001).
57. A. E. Dekas, V. J. Orphan, Identification of Diazotrophic Microorganisms in Marine Sediment Via Fluorescence *in situ* Hybridization Coupled to Nanoscale Secondary Ion Mass Spectrometry (Fish-Nanosims). *Methods in Enzymology* **486**, 281 (2011).
58. A. Pernthaler, J. Pernthaler, R. Amann, Fluorescence *in situ* hybridization and catalyzed reporter deposition for the identification of marine bacteria. *Applied and Environmental Microbiology* **68**, 3094 (2002).
59. A. Pernthaler, J. Pernthaler, Fluorescence *in situ* hybridization for the identification of environmental microbes. *Methods Mol Biol* **353**, 153 (2007).
60. J. Cline, Spectrophotometric determination of hydrogen sulfide in natural waters. *Limnology and Oceanography* **14**, 454 (1969).

SUPPLEMENTAL DISCUSSION

A: Ammonium, nitrate and nitrite concentrations in sediment pore water

Ammonium concentrations measured in 12 sediment push cores collected in and around the Costa Rica methane seeps on Atlantis cruise AT15-44 (see locations in SI Table 1, SI Figure 1) varied from not detectable (< 0.5 μM) to nearly 2.5 mM, with most values less than 250 μM (Figure 1, M and N). Ammonium was not depleted in areas of methane seepage (n=10) relative to background cores (n=2), suggesting that seep sediment is not preferentially depleted in ammonium, which is consistent with previous findings at Gulf of Mexico methane seeps (*1*). There was no consistent trend in ammonium concentrations with depth; in some cores ammonium increased with depth, while in others ammonium decreased. However, a spike in ammonium was often seen in the most surficial sample analyzed (Figure 1, A, B, D, E, F, G). This could be due to the breakdown of organic matter by heterotrophic bacteria, which can produce ammonium, and occurs less with depth in the sediment due to the depletion of suitable electron acceptors with depth.

Increased concentrations of nitrate were also observed in the top-most sediment layers, with concentrations up to around 40 μM, while remaining below 5 μM in deeper sediments (Figure 1). The core depicted in Figure 1-D is an exception, and nitrate levels reached up to 240 μM in the top half of the core. Elevated nitrate and ammonium in surficial seep sediments has been observed before (including at Mound 12, (*2*)), and is hypothesized to be due to sulfide oxidizing bacteria, such as *Beggiatoa*, *Thioploca* and *Thiomargarita*, living at the sediment water interface (*1, 3, 4*). These large bacteria concentrate and store nitrate at intracellular concentrations up to and beyond 200 mM,

and may be lysed while squeezing the sediments to extract porewater (*5–7*). Additionally, sulfide oxidizing bacteria can couple sulfide oxidation to dissimilatory nitrate reduction to ammonium (DNRA), producing a peak in ammonium in these horizons, and recycling N within the sediments rather than leaching it via denitrification (*6, 8*). DNRA may be particularly likely in the mat samples that show an elevation in both nitrate and ammonium at the surface (Figure 1B, D, E, G) Although this may be a significant source of ammonium in these sediments, the conversion of NO_3^{2-} to NH_4^+ does not represent new bioavailable nitrogen to the system, unlike the conversion of N_2 to NH_4^+.

The values of ammonium observed are in the range where methanogenic diazotrophs cease fixing nitrogen in pure cultures (25–100 μM, with complete inhibition after 100 μM (*9*)), however the concentrations required to inhibit diazotrophs in environment samples have been shown to be much higher. Nitrogen fixation has been shown to occur in shallow marine sediments with up to 1-2 mM ammonium, suggesting that in some sediments even high levels ammonium do not preclude the occurrence of nitrogen fixation (*10, 11*). Whether this is because nitrogen limitation still occurs within microniches within these seemingly ammonium-replete sediments, or because nitrogen fixation is pursued regardless of the availability of other nitrogen sources, perhaps because of other roles it may play in the ecosystem (e.g., hydrogen production), is unknown. The concentrations of ammonium observed here are similar to those observed in Gulf of Mexico methane seeps (0–770 μM NH_4^+; (*1, 3, 12*), where low values of $\delta^{15}N$ relative to nearby non-seep sediment suggested the possibility of nitrogen fixation (*1*). The level of bioavailable nitrogen observed at Costa Rica was therefore not expected to

inhibit nitrogen fixation, but the trends do suggest active uptake and recycling of nitrogen species typical of methane seep sediment.

B. Lateral Distribution of Nitrogen Fixation at Mound 12

Sediment cores A2, A3, and O1 were collected along a linear transect (~ 1 meter long) within and outside a sulfide oxidizing microbial mat (total area was several square meters) in order to investigate the lateral distribution of N_2 fixation on relatively small scales, within a single habitat (SI Figure 1). At Mound 12, methane seepage has been shown to be variable over lateral distances of less than 40 cm (*2, 13*), which is consistent with heterogeneity in flow observed at other methane seep locations (*14*). Given the demonstrated methane dependence of seep diazotrophs, steep drop-offs in diazotrophy could therefore be expected between sediments at close proximity. Accordingly, cores A2, A3, and O1 displayed evidence of quite different microbial activities, with no nitrogen fixation observed in core A3 or O1 between 3–6 cm, despite diazotrophy in core A2 in this interval. Additionally, the magnitude and trend of $^{15}NH_4^+$ uptake with time differed between cores A2 and A3 versus O1. Also, Core O1 demonstrated methane-independent $^{15}NH_4^+$ incorporation, while cores A2 and A3 did not.

These cores likely contain different microbial communities, dictated by their local chemistry, and resulting in metabolic differences between them. However, it is also possible that the whole-core communities are not significantly different, but rather distributed with depth differently. For instance, it is possible that core A3 hosts an equivalent amount of diazotrophic microbes as core A2, but that they occurs outside of the 3–6 cm horizon, and are not captured by this 2-depth experimental setup. For each of

these cores, as well as O2 and O3, only two depth horizons were incubated. Therefore, the apparent lateral differences may not be as extreme as they appear, and the differences observed between the cores may be a reflection of the variability in community position with depth in different cores (likely due to variations in vertical chemical gradients). Therefore the rates of ^{15}N uptake in the depth horizons from cores with only two depths incubated should not be interpreted necessarily as the maximum N_2 uptake occurring throughout the core.

Based on the comparison of the three cores taken within areas of active methane seepage and the three taken outside, nitrogen fixation appears to be enhanced in sediment with high methane flux. The diazotrophic enrichment within methane-rich sediments could be due to higher rates of overall growth, a local depletion of nutrients resulting from high productivity levels, or specifically related to the higher abundance of ANME-SRB consortia. Diazotrophs are present and active in background sediment however, and although fixing nitrogen at minor rates compared to seep diazotrophs, may prove geochemically significant due to the greater coverage of the Earth's oceans with background sediment (by definition) than methane seeps. However, if the diazotrophy observed in cores O1 and O2 is due to a relic methane seep community, and O3 is the core truly representative of undisturbed background oceanic sediment, deep-sea benthic nitrogen fixation outside of productivity hotspots, such as seeps and vents, may be inconsequential.

C. Ammonium uptake in outside cores and implications for their exposure to previous methane seepage

Interestingly, while growth with methane occurred immediately in the active cores, it occurred only after a ~ 20 week lag time in the outside cores (Figure 2). It is possible that their methane-dependent communities are a relic from previous exposure to methane seepage, which required a lag time before showing full activity in the presence of methane again. The temporal and spatial variability of methane seepage, as well as the proximity of O1 to a sulfide-oxidizing microbial mat, and the presence of authigenic carbonates where O2 was collected (indicative of at least former methane seepage), supports this hypothesis. The lag time in $^{15}NH_4^+$ uptake in the presence of methane in O1 and O2 was mirrored in the methane-dependent sulfide production curve (data not shown), which specifically suggests that the methane-dependent growth is due to AOM activity. Ultimately, active and outside cores showed similar levels of potential protein synthesis, with the exception of core O3, which showed only minor ^{15}N uptake over the course of the incubation (2.9×10^2 and 3.4×10^2 nmol NH_4 fixed per gram dry weight sediment during 275 days). This core, which was collected the furthest from active methane seepage, demonstrates similar levels of growth when incubated with methane as the other cores demonstrate without methane, suggesting that it does not contain a methanotrophic community indicative of previous methane exposure.

D. Ammonium concentrations in microcosm experiments measured at 275 days

Ammonium concentrations were measured at the end of the incubation experiments. Although the possibility of production of ammonium with time in the

incubation cannot be eliminated, it is unlikely due to the expectation that ammonium is consumed by growing chemolithoautotrophs faster than it might be produced by heterotrophic feeding, nitrogen fixation, and even dissimilatory nitrate reduction to ammonium (DNRA). Although DNRA has the potential to be a significant source of ammonium, is it likely to only be mediated in the uppermost sediment horizon (0–3 cm) due to the location of sulfide-oxidizing microbes potentially mediating DNRA. The levels of ammonium in the no-methane incubations are generally higher than the incubations with methane (Table 1). Since the incubations were set up with paired sets of sediment, and the same anoxic filtered sea water, we interpret this difference as evidence for greater NH_4^+ consumption in the with-methane incubations, due to greater activity and growth, over the course of the experiment. Both sets of incubations likely started with ammonium levels higher than that observed in the no-methane bottles at the end of the incubation. Although we cannot extrapolate what those values of ammonium may have been, we can suggest that nitrogen fixation in these sediments occurs at ammonium levels of at least 50 μm, as the values of ammonium in both A1 3–6 cm no-methane and O1 3–6 cm no-methane, which both showed diazotrophic activity, were above 50 μm at the end of the incubation (Table 1).

E. Aggregate Size and Shape with Depth

The ANME-SRB aggregates in core A1 were physically characterized with depth, to determine if the size or shape of the aggregates varied with respect to the peak in nitrogen fixation within the 6–9 cm horizon. The cross-sectional area of aggregates was determined by manually outlining DAPI-stained images of aggregates and calculating the

area using ImageJ software. Aggregate areas were measured rather than diameters, due to the presence of non-spherical aggregates, including ellipsoidal and non-symmetrical aggregates, sometimes containing several spherical lobes (e.g., Figure 5 B). The circularity (a measure of a shape's deviation from perfectly circular; *circularity* = $4\pi(area/perimeter^2)$) of each aggregate was also measured. Aggregates in this core had areas ranging from 2.5 to 1,117 μm^2 (corresponding to diameters of 1.8 to 37.7 μm if the aggregates are assumed to be perfect spheres) (SI Figure 2). The median aggregate area in the five depths investigated ranged from 9.68 +/- 1.55 μm^2 to 14.85 +/- 2.05 μm^2 (corresponding to diameters of spherical aggregates of 3.51 and 4.35 μm, respectively) (SI Table 2). These sizes are consistent with what has been reported previously at the Hydrate Ridge methane seep system (*15–17*). No trend in aggregate circularity mirrored the trend in nitrogen fixation (although there was a general decrease in circularity with depth), however the median aggregate size did reach a minimum at 6–9 cm (SI Table 2).

F. Challenges in calculating a percentage of the total nitrogen fixed by the ANME-2-SRB by comparing EA-IRMS and NanoSIMS data

Theoretically the contribution of ANME-2-SRB to total seep diazotrophy could be directly calculated by comparing the total nitrogen fixed in a given sediment sample and the total nitrogen fixed by the ANME-2-SRB population (a similar calculation as seen in (*18*)). The total nitrogen fixed by the ANME-2-SRB population could be calculated if the average nitrogen fixed by each ANME-2-SRB aggregate and the number of aggregates in the sample were known. Although the abundance of aggregates is known, and the average $^{15}N/^{14}N$ ratio of the incubated aggregates is known, the actual

amount of N_2 fixed per aggregate, and therefore of the population, cannot be calculated without knowing the average N content of an aggregate. Using the range of values reported for the N content of other marine cells, as well as the range of values reported for the size of the ANME and SRB (in order to calculate the number of cells per aggregate of a known size), the result—the percentage of total nitrogen fixed by the ANME-2-SRB—varies by over two orders of magnitude. Until more biochemical information about these microorganisms is known, and in particular, how much nitrogen they contain per cell and/or the average biovolumes of the cells, we are unable to perform this calculation without detrimental potential error. Further biochemical characterization of the ANME-2-SRB is therefore currently underway, and will hopefully close the range of parameters sufficiently to make meaningful comparisons between the bulk and single-cell isotopic measurements in the future.

WORKS CITED in Supplemental Discussion

1. S. Joye *et al.*, The anaerobic oxidation of methane and sulfate reduction in sediments from Gulf of Mexico cold seeps. *Chemical Geology* **205**, 219 (2004).
2. P. Linke, K. Wallmann, E. Suess, C. Hensen, G. Rehder, In situ benthic fluxes from an intermittently active mud volcano at the Costa Rica convergent margin. *Earth Planet Sc Lett* **235**, 79 (2005).
3. M. Bowles, S. Joye, High rates of denitrification and nitrate removal in cold seep sediments. *ISME J* **5**, 565 (2011).
4. J. V. Bailey *et al.*, Dimorphism in methane seep-dwelling ecotypes of the largest known bacteria. *ISME Journal* **5**, 1926 (2011).
5. A. Teske, D. Nelson, in *The Prokaryotes,* M. Dworkin, S. Falkow, E. Rosenberg, K.-H. Schleifer, E. Stackebrandt, Eds. (Springer New York, 2006), p. 784.
6. B. Thamdrup, D. E. Canfield, Pathways of carbon oxidation in continental margin sediments off central Chile. *Limnol Oceanogr* **41**, 1629 (1996).
7. S. C. McHatton, J. P. Barry, H. W. Jannasch, D. C. Nelson, High Nitrate Concentrations in Vacuolate, Autotrophic Marine Beggiatoa spp. *Applied and Environmental Microbiology* **62**, 954 (1996).

8. M. Sayama, N. Risgaard-Petersen, L. P. Nielsen, H. Fossing, P. B. Christensen, Impact of bacterial NO_3^- transport on sediment biogeochemistry. *Applied and Environmental Microbiology* **71**, 7575 (2005).
9. P. S. Kessler, C. Daniel, J. A. Leigh, Ammonia switch-off of nitrogen fixation in the methanogenic archaeon Methanococcus maripaludis: Mechanistic features and requirement for the novel GLnB homologues, $NifI_1$ and $NifI_2$. *Journal of Bacteriology* **183**, 882 (2001).
10. D. G. Capone, in *Nitrogen Cycling in Coastal Marine Environments,* T. H. Blackburn, J. Sorensen, Eds. (John Wiley & Sons, New York, 1988), p. 85.
11. V. J. Bertics *et al.*, Occurrence of benthic microbial nitrogen fixation coupled to sulfate reduction in the seasonally hypoxic Eckernforde Bay, Baltic Sea. *Biogeosciences Discussions* **9**, 6489 (2012).
12. M. W. Bowles, V. A. Samarkin, K. M. Bowles, S. B. Joye, Weak coupling between sulfate reduction and the anaerobic oxidation of methane in methane-rich seafloor sediments during ex situ incubation. *Geochim Cosmochim Ac* **75**, 500 (2011).
13. S. Mau, G. Rehder, I. G. Arroyo, J. Gossler, E. Suess, Indications of a link between seismotectonics and CH4 release from seeps off Costa Rica. *Geochem Geophy Geosy* **8**, (2007).
14. M. D. Tryon, K. M. Brown, Complex flow patterns through Hydrate Ridge and their impact on seep biota. *Geophys Res Lett* **28**, 2863 (2001).
15. A. Boetius *et al.*, A marine microbial consortium apparently mediating anaerobic oxidation of methane. *Nature* **407**, 623 (2000).
16. K. Nauhaus, M. Albrecht, M. Elvert, A. Boetius, F. Widdel, In vitro cell growth of marine archaeal-bacterial consortia during anaerobic oxidation of methane with sulfate. *Environmental microbiology* **9**, 187 (2007).
17. K. Knittel *et al.*, Activity, distribution, and diversity of sulfate reducers and other bacteria in sediments above gas hydrate (Cascadia Margin, Oregon). *Geomicrobiology Journal* **20**, 269 (2003).
18. H. Ploug *et al.*, Carbon and nitrogen fluxes associated with the cyanobacterium Aphanizomenon sp. in the Baltic Sea. *ISME J*, (2010).

SI Table 1. Description of sediment pushcores investigated in this study.

Location and Collection Information								Site Description					
Core Name	PC #	Alvin Dive	Atlantis Cruise	Date Collected	Site Name	Latitude (°N)	Longitude (°W)	Water Depth (m)	Surficial Cover	Distance from microbial mat	Methane Range (uM)	Sulfide Range (mM)	$d^{13}C$
A1	7	4586	AT 15-59	1/7/10	Mound 12	8 55.7909	84 18.6899	988	White microbial mat	Within	17 – 105	1.5 – 6	-21.1 – -20.2
A2	6	4587	AT 15-59	1/8/10	Mound 12	8 55.8370	84 18.7128	988	Gray microbial mat	Within	10 – 94	3.5 – 11	-21.3 – -20.5
A3	7	4587	AT 15-59	1/8/10	Mound 12	8 55.8370	84 18.7128	988	White microbial mat	Within	110 – 750	4.9 – 10	-21.3 – -20.4
O1	8	4587	AT 15-59	1/8/10	Mound 12	8 55.8370	84 18.7128	988	None visible	< 1 m	BDL[+] – 2.7	BDL	-23.6 – -22.0
O2	1	4587	AT 15-59	1/8/10	Mound 12	8 55.8609	84 18.7815	1001	Carbonate rocks	> 100 m	0.3– 8.5	BDL	-22.4 – -20.3
O3	2	MC*	AT 15-59	1/7/10	Northeast of Mound 12	8 55.9995	84 18.4437	988		> 100 m		BDL	-19.3 – -18.5
NA	3	4501	AT 15-44	2/22/09	Mound 12	8 55.8511	84 18.7188	990	White microbial mat	Within			
NB	3	4511	AT 15-44	3/5/09	Mound 12	8 55.7746	84 18.7711	997	White microbial mat	Within			
NC	6	4502	AT 15-44	2/23/09	Mound 12	8 55.78	84 18.77	997	White microbial mat	Within			
ND	6	4510	AT 15-44	3/4/09	Jaco Summit	9 10.2883	84 47.9184	745	White microbial mat	Within			
NE	6	4512	AT 15-44	3/6/09	Quepos Landslide	9 1.2271	84 30.0288	410	Orange microbial mat	Within			
NF	6	4501	AT 15-44	2/22/09	Mound 12	8 55.8511	84 18.7188	990	Gray microbial mat	Within			
NG	1	4510	AT 15-44	3/4/09	Jaco Summit	9 10.2883	84 47.9184	745	Gray microbial mat	Within			
NH	5	4502	AT 15-44	2/23/09	Mound 12	8 55.77	84 18.77	995	Gray microbial mat	Within			
NI	8	4502	AT 15-44	2/23/09	Mound 12	8 55.78	84 18.77	995	Gray microbial mat	Within			
NJ	2	4504	AT 15-44	2/25/09	Mound 11	8 55.3845	84 18.2248	1010	Gray microbial mat	Within			
NK	19	MC*	AT 15-44	3/5/09	West of Mound 12	8 55.894	84 19.007	1000	No Data	> 100 m			
NL	5	4501	AT 15-44	2/22/09	Mound 12	8 55.8511	84 18.7188	990	None visible	< 1 m			

* Collected via multicore, not on an Alvin dive.
[+] Below detection limit.

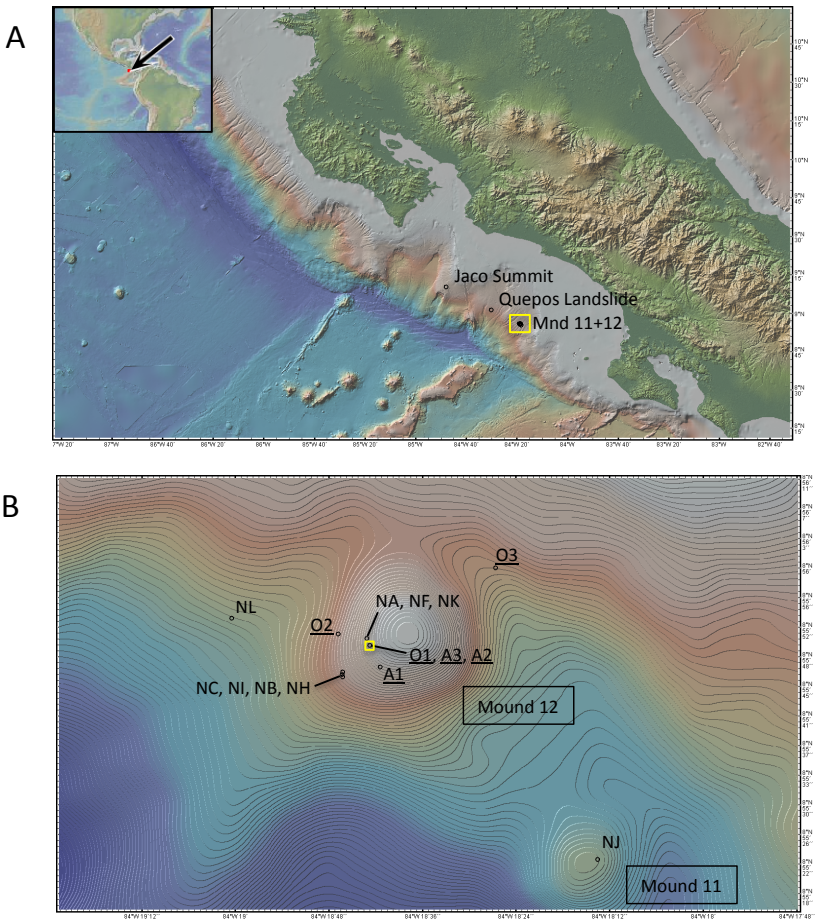

SI Figure 1. Location of pushcore sampling. **A:** Location of three sampling sites off the coast of Costa Rica. Yellow box indicates area of detail in image B. **B:** Location of core sampling on Mound 12 and 11. Yellow box indicates area of detail in image C. **C:** Photo taken by Alvin of the microbial mat sampling site for cores O1, A2 and A3. The two red laser points in the center right are 10 cm apart. Mat classifications were confirmed by visual examination of the filaments topping each core once back on-board. Cores analyzed for concentrations of N begin with "N"; cores used for ^{15}N-labelling experiments begin with "O" or "A". Maps were made with publically available GeoMapApp.

SI Table 2. Summary of physical parameters of ANME-SRB Aggregates in core A1. Diameters were calculated from the measured areas assuming a spherical cross-section, for comparison purposes.

	Area				Diameter (Calculated)		Circularity= $4\pi(\text{area}/\text{perimeter}^2)$			
			Standard Deviations						Standard Deviations	
Depth	Average	Median	Average	Median	Average	Median	Average	Median	Average	Median
0-3 cm	17.51	13.18	3.96	2.47	4.72	4.10	0.8697	0.8865	0.0125	0.0359
3-6 cm	15.09	10.76	2.32	2.41	4.38	3.70	0.8792	0.8960	0.0149	0.0098
6-9 cm	15.88	9.68	4.17	1.55	4.50	3.51	0.8726	0.8877	0.0140	0.0139
9-12 cm	14.83	11.54	2.42	1.70	4.35	3.83	0.8478	0.8673	0.0223	0.0090
12-15 cm	48.06	14.85	26.79	2.05	7.82	4.35	0.8146	0.8372	0.0095	0.0133

SI Figure 2. Histograms of ANME-SRB aggregate size (calculated diameter) for each of five depths in core A1. 50-60 aggregates on each of 3 different filters were measured for each depth. For depths with <50 aggregates detected in 100 frames per filter, the total number of aggregates detected were measured. (i.e. Depth 0-3 cm, 30 aggregates measured; Depth 12-15 cm, 70 aggregates measured.) Depth 12-15 had one additional aggregate with a diameter of 37.71 uM, which is not included below.

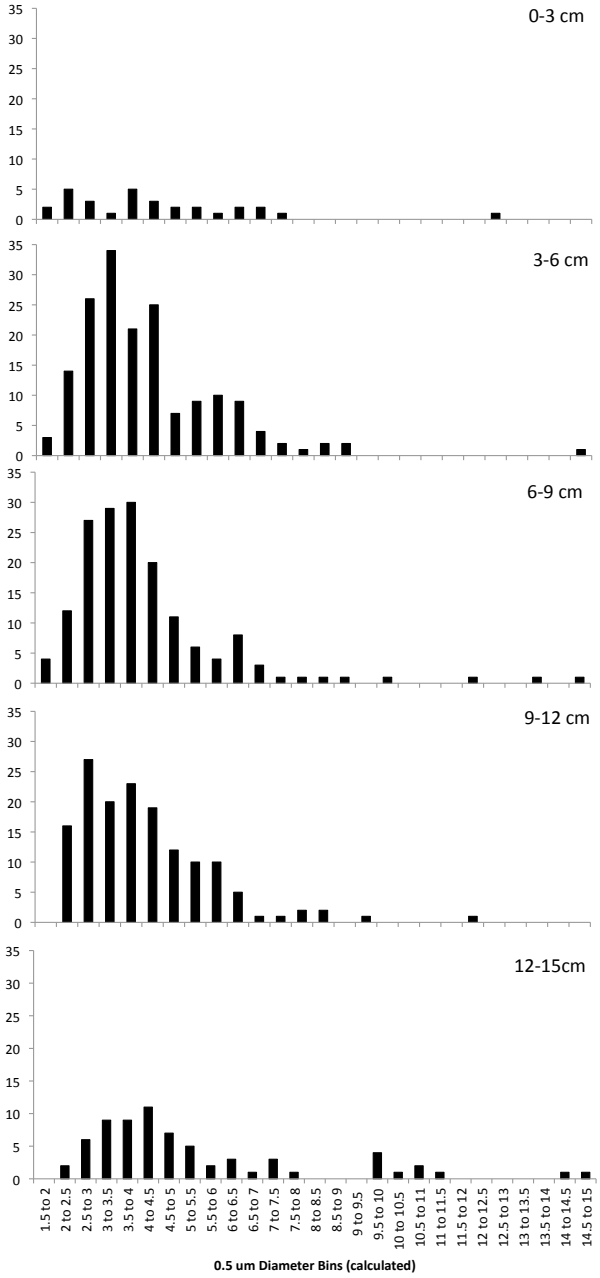

C h a p t e r 4

Investigating the Diversity and Activity of Diazotrophic Microorganisms in Methane Seep Sediment via mRNA Expression and FISH-NanoSIMS

Anne E. Dekas, Stephanie A. Connon, Grayson L. Chadwick,
Aditi Dasgupta, and Victoria J. Orphan

California Institute of Technology, Pasadena, CA 91106

SUMMARY

Methane seep microbial ecosystems are phylogenetically diverse and metabolically complex, containing clusters of methanotrophic archaea (ANME) and sulfate-reducing bacteria (SRB), as well as a diversity of "free-living" bacteria and archaea. Although the relationship between the ANME and two physically associated SRB (members of the *Desulfosarcina/Desulfococcus,* DSS and *Desulfobulbaceae,* DSB) has been identified, the nature of any chemical interplay between the ANME-DSS/DSB clusters and the surrounding community of microbes, free-living or attached, including free-living members of the DSS and DSB, is not clear. In the current study we investigate the relationship between these groups by probing the activity of microorganisms in seep sediment incubated either with methane (when ANME-DSS/DSB are active) and without methane (when ANME-DSS/DSB have been shown to be inactive). Our studies consists of three components: (1) a transcript analysis of bacterial 16S rRNA, *mcrA* (encoding methyl coenzyme M reductase A), *aprA* (encoding adenosine-5'-phosphosulfate reductase alpha subunit), and *nifH* (encoding dinitrogenase reductase) within the communities incubated with and without methane, (2) a targeted analysis of growth potential and diazotrophic activity within three single-cell seep populations (DSS, DSB, and ANME-1) using Fluorescence *in situ* Hybridization coupled to Nanoscale Secondary Ion Mass Spectrometry (FISH-NanoSIMS), and (3) a multi-faceted approach to investigating the efficiency and specificity of bromopropanesulfonate as an inhibitor of AOM.

We find that *Deltaproteobacteria* are relatively more active with methane than without, and that the detection of transcripts from *Desulfosarcina* Seep Group SRB1 are dependent on the presence of methane. This is consistent with their previously described role in the anaerobic oxidation of methane (AOM). We identify three groups of bacteria (*Gammaproteobacteria, Planctomycetes,* and *Chloroflexi*) whose relative transcript numbers are unaffected by the presence of methane, suggesting no direct relationship with the ANME or AOM, despite a previous study which found evidence for a potential physical association between a sub-set of these groups and the ANME (*1*). Although ANME-2c were responsible for nearly all (98%) of the ANME-related transcripts, a diversity of *nifH* transcripts were detected, suggesting organisms other than the ANME may mediate diazotrophy in seep sediments. We employed FISH-NanoSIMS to test this

hypothesis, and detect $^{15}N_2$ uptake by single-cell members of the DSB, however only in the presence of methane. Both DSS and DSB single cells are active (synthesize new proteins) in the absence of methane, showing a divergence from their ANME-associated relatives, and suggesting that methane-dependent $^{15}N_2$-incorporation observed in the DSB is due to sharing with the ANME rather than diazotrophic ability. However, we cannot eliminate the possibility of methane dependence and therefore methane-dependent diazotrophy in subgroups within the DSB at this time. This chapter delves into the complicated relationships between microorganisms at methane seeps and their role in carbon, sulfur and nitrogen cycling, with a focus on the often abundant yet generally under-studied free-living fraction of this community.

INTRODUCTION

Nowhere is the role of microbial life as a driver of both climate and ecosystem productivity more evident than at marine methane seeps. Methane, a potent greenhouse, is produced in marine sediments around the globe by both thermogenic and biogenic processes. It is estimated that 10^7 Tg of carbon is stored as methane clathrates in marine sediments, with approximately 300 Tg seeping upwards annually, the equivalent of 60% of the global annual methane emission (*2–4*). However, an efficient microbial filter prevents the passage of the majority of this methane to the overlying water column, and therefore the atmosphere, by oxidizing it before it reaches the seafloor. This process, known as the anaerobic oxidation of methane (AOM), not only reduces methane emissions from the oceans to just 2% of the global (*2*), but also fuels a diverse and large oasis of micro- and macrofauna at localized sites of methane seepage ("methane seeps") (*5*).

The organisms responsible for AOM were identified just over ten years ago, and research on the mechanism of the metabolism(s) is ongoing. Three phylogenetically distinct groups of marine archaea have been identified as methanotrophic: ANME-1 (*6*), ANME-2 (*7, 8*), and ANME-3 (*9, 10*). Methane oxidation is thought to occur within the

ANME groups via "reverse methanogenesis" coupled to sulfate reduction, which (at least in the case of ANME-2 and -3) occurs within closely associated sulfate-reducing bacteria (SRB) (*8, 11, 12*). It is unknown how or if the ANME-1, which are typically found without associated symbionts, couple the oxidation of methane to sulfate (*6, 13, 14*). It is additionally unknown how the two metabolisms, AOM and sulfate reduction, are coupled between the ANME-2/3 and the associated SRB (*2, 3*). The SRB associated with the ANME-2 and ANME-3 have been identified as members of the *Desulfosarcina/Desulfococcus* (DSS) *(8, 15)*, as well as the *Desulfobulbaceae* (DSB) *(9, 10, 16)*. Despite the close relation of the ANME-associated SRB to the free-living cultured representatives of these groups, they appear to be physiologically quite different, and/or undergo physiological changes when living in partnership with the ANME. In particular, associated SRB do not appear to reduce sulfate in the absence of methane, suggesting an obligate interaction with the ANME (*17, 18*).

The density of microorganisms in methane seep sediment can be substantially elevated from that of surrounding sediments (~ 2 orders of magnitude greater), and up to 9.6 $x10^{10}$ cells cm^{-3} (*19*). This increased biomass is supported by the additional organic carbon and electron donors harnessed by AOM (*20*). Interestingly, although ANME and associated DSS/DSB are enriched in seep samples, free-living single cells are enriched as well (*19*). The mechanism by which these free-living cells are supported by the introduction of methane, however, and whether it is a direct or indirect effect (i.e., dependence on methane vs. dependence on the products of AOM), is unknown. Sulfate-reducing bacteria comprise up to 20% of the free-living cells at methane seeps (*21*), and have received more research attention than any other group within the free-living

fraction. However, most studies to date have focused on the phylogenetic identity and quantification of the free-living SRB rather than their activity or chemical contribution to the ecosystem (*9, 19, 21, 22*). Examining the activity of the free-living population within methane sediment is challenging, because the contribution of the free-living versus ANME-aggregated cells cannot be differentiated in standard bulk experiments. There is therefore a great deal of uncertainty related to what fraction of this community is active, and how they interact with the ANME-SRB aggregates. It is likely that the ANME-SRB provide nutrients to this population (even if just in the form of increased organic matter), but it is also possible that the free-living microbes mediate ecosystem functions that benefit the ANME-SRB as well.

The lack of knowledge regarding the chemical interaction between the free-living seep community and the ANME may be a significant oversight. Particularly for the ANME-1, chemical interactions with non-associated microbes may play an important role in the mechanism of methane oxidation. With increasing evidence that nanowires and conductive “microcables” carry elections millimeter distances and couple spatially discrete reactions, direct physical association may be an over-emphasized component of symbiosis (*23–25*). However, regardless of potential extracellular electron transfer, metabolisms mediated by the free-living population may produce and/or consume molecules relevant to the AOM process, such as sulfide, hydrogen, and/or essential nutrients for growth. Without any direct contact with the ANME-SRB, this population may have an effect on their productivity, and vice versa.

It is also possible that the diversity of bacteria detected at methane seeps includes some that are physically associated with ANME, but have yet to be described as partners. One limitation of fluorescence *in situ* hybridization (FISH), the technique most often used to observe microbial associations in environmental samples, is that only phylogenetic groups targeted by FISH probes are observed. Therefore, observations of partnerships can be limited by our ability to hypothesize potential partners. Using a different and more broad approach, particularly ANME-2-targeted "magneto-FISH" and subsequent metagenomics of separated ANME-2-containing clusters, Pernthaler and colleagues uncovered a greater diversity of bacteria physically associated with the ANME-2 (*1*). However, whether or not these diverse and less-frequent associations are due to a chemical partnership with the ANME is still unknown.

One potentially significant but currently unknown metabolic capability within free-living methane seep bacteria is nitrogen fixation, the ability to convert N_2 to NH_3, and thereby alleviate nitrogen limitation. It has been proposed recently that methane seeps may be nitrogen limited, driven by elevated activity due to the input of methane, but not an additional source of nitrogen (*26*). Accordingly, uptake of $^{15}N_2$, indicative of nitrogen fixation, was observed in methane seep samples, and the ANME-2 identified as diazotrophs (i.e., mediators of nitrogen fixation) (*26*). The ANME-2 have been proposed as the primary diazotrophs in methane seep sediment, due to the observed nitrogen fixation's nearly 100% dependence on methane, as well as the spatial correlation of nitrogen fixation rates with ANME-SRB aggregates (Chapter 3). However, a wide diversity of *nifH* sequences, encoding dinitrogenase reductase, have been recovered from several deep-sea locations of methane seepage (*26–28*). This raises the possibility that

members of the methane seep community other than the ANME-2 may be able to fix nitrogen. The methane dependence of the diazotrophy observed suggests that the methanotrophic archaea (ANME) or their physically associated SRB are the primary diazotrophs, however the diversity of sequences suggests more potential diazotrophs than the ANME and the associated DSS and DSB. Additionally, in a highly interconnected ecosystem where even the free-living portion of the population may be indirectly dependent on methane, via the products of AOM, methane dependence of diazotrophy may not mean it is mediated specifically by the ANME-DSS/DSB.

In the current work we therefore investigate: (1) the activity of seep microbes, particularly that of free-living bacteria, in the presence and absence of methane and (2) the diversity of diazotrophs in the sediments, and the potential for the free-living community to provide a source of bioavailable nitrogen to the system. We probe the diversity (via DNA analysis) and activity (via RNA analysis and FISH-NanoSIMS analysis of $^{15}NH_4$- and $^{15}N_2$-uptake) of the methane seep community in the presence and absence of methane, and therefore when the ANME-SRB consortia are and are not active. Observing bacteria that show different activity patterns with and without methane will identify them as potentially metabolically influenced by the ANME-SRB, whether or not physically associated with them. We use a set of microcosm experiments for these analyses containing sediment from a submarine mud volcano off the west coast of Costa Rica. This sediment was previously shown to contain active diazotrophs (ANME-2), and to host an active population of sulfate-reducing bacteria (incubations from Core A2, 3–6 cm horizon, fully described in Chapter 3 of this dissertation). Finally, we attempt to identify a specific inhibitor of methanotrophy, to allow the differentiation between free-

living SRB that are directly dependent on methane, and those that are dependent on the products of the methane-dependent ANME. Together, these experiments will create a greater understanding of the potential relationships between the ANME and the diversity of microbes present at methane seeps.

EXPERIMENTAL PROCEDURES

Sample collection and summary. Seafloor sediment push-cores (PC) investigated in this study were collected using the submersible *Alvin* in October 2006 (AT15-11) within the Eel River Basin (ERB) methane seep system along the ERB Southern Ridge (approximately 40˚ 47.192'N, 124˚ 35.706'W; 520 m) and in January 2010 (AT15-59) at Mound 12, a methane-seeping mud volcano off the coast of Costa Rica (approximately 8˚ 55.8'N, 84˚ 18.7'W; 988 m). Sediment cores were extruded from push-core liners in 3 cm increments on-board immediately after collection, and either stored in mylar bags flushed with Ar at 4˚C (AD4254 PC14 and AD4587 PC5), or immediately combined with Ar-sparged filtered seawater and aliquoted into anaerobic serum bottles (AD4586 PC7 and AD4587 PC6). Push cores used in this study are as follows: AT15-11: AD4254 PC14, collected within a microbial mat (microcosm incubations investigating growth and diazotrophy followed by NanoSIMS investigation of ANME-1); AT15-59: AD4587 PC6, collected within a microbial mat (microcosm incubations investigating growth and diazotrophy followed by DNA and RNA analysis, and NanoSIMS analysis), AD4586 PC7, collected within a microbial mat (microcosm incubations investigating growth and diazotrophy, followed by NanoSIMS analysis), and AD4587 PC5, collected within the same microbial mat as AD4587 PC6 (microcosm incubations investigating the effect of

potential inhibitors to methanotrophy, followed by NanoSIMS and EA-IRMS analysis). Additional information about sample sampling locations and descriptions can be found in (*26*) and (*29*).

^{15}N-labeling bottle incubations. Sediments were homogenized with Ar-sparged filtered seawater collected near core sampling. Sediment slurries were aliquoted into serum bottles with butyl stoppers, crimped, and stored at 4˚C. Incubation setup details for sediments from cores [AD4254 PC14] and [AD4586 PC7 and AD4587 PC6] can be found in (*26*) and (*29*), respectively. The sediment slurry from AD4587 PC5 was divided into approximately 20 ml aliquots in 60 ml serum bottles and incubated at 4˚C for 6 months. Three structural analogues of methyl co-enzyme M and potential inhibitors of anaerobic methanotrophy were added: bromoethanesulfonate (BES), bromopropanesulfonate (BPS), and bromopropionate (BP). The potential inhibitors were added to final concentrations of 2 and 20 mM. In a test experiment, addition of these compounds at these concentrations did not significantly alter the pH of the seawater used for the experiments (although a pH effect was observed when added to nanopure water) (data not shown). Sub-samples of the microcosm experiments were taken with syringes throughout the incubation period, and preserved for sulfide analysis by precipitation with zinc acetate, elemental analysis by freezing at -20˚C, fluorescence *in situ* hybridization (FISH) by fixing with 2% paraformaldehyde overnight at 4˚C, washing and storing at -20˚C, and nucleic acid extraction by flash freezing in liquid nitrogen and storing at -80˚C.

DNA and RNA extractions and reverse transcription reactions. One ml sediment slurry samples for nucleic acid extraction were collected at each sampling time, flash frozen in liquid N_2 and stored at -80 ºC until processing. DNA and RNA were extracted from selected samples from the same 1 ml of sediment slurry using the MoBio RNA Powersoil Total RNA Isolation Kit (cat# 12866-25) and the RNA Powersoil DNA Elution Accessory Kit (cat# 12867-25), with the following modifications: after the addition of SR2, the mixture is divided into four 2 ml screw top tubes and bead beated by a Bio 101 FastPrep FP120 bead beater for 45 seconds at speed 5.5 three times. The mixtures were recombined before centrifugation at 2,500 xg for 10 min, and the removal of the aqueous layer. The rest of the protocol was followed by the manufacturer's instructions, with the incubation with SR4 at room temperature. RNA and DNA pellets were re-suspended in 100 ul SR7. DNA was stored at -80ºC immediately. The RNA extracts were treated with the Ambion TURBO DNA-free Kit (cat# AM1907) according to the manufacturer's instructions, and cleaned using the Qiagen RNeasy Kit (cat# 74104), according to the RNA Clean-up Protocol provided by the manufacturer. RNA was eluted with 2 additions of 30 μl RNase free water, and either converted to cDNA immediately or stored at -80 ºC until further processing. The Invitrogen Superscript III First Strand Synthesis Supermix (cat# 18080-400) was used for the reverse transcriptase reaction to generate cDNA from RNA.

DNA and cDNA Clone Libraries. All libraries were generated from RNA and DNA extracted simultaneously from incubations of AD4587 PC6 sediment of the 3-6 cm horizon at the 20 week time point. This sediment horizon was selected because

incubations with (CR15) and without (CR17) methane were available for comparison, and the $^{15}N_2$ incubation with methane incubation (CR15) was previously shown to fix nitrogen (*29*). *nifH* clone libraries were constructed from cDNA (CR15 and CR17) and DNA (CR15, CR17). Twenty-five μl PCR reactions containing 1 μl 10 μM R primer, 1 μl 10 μM F primer, 1 μl template, 2.5 μl 10X ExTaq PCR buffer (Takara), 0.3 μl ExTaq (Takara), 0.5 μl 10 mM dNTPs (New England Biolabs), 0.5 μl 10 μg/μl BSA, and 18.2 μl water were performed. Primers used were nifHf_10aa and nifHr_132aa (*30*). To reduce spurious bands, a touch-down PCR program was used to amplify *nifH* in the 139 day time point from incubation CR15, according to the program in SI Table 2. In all cases, DNA, cDNA, and RNA-only (no RT reaction) were the templates in the PCR reactions. No amplicon was visible in any of the RNA-only reactions when 4 μl were run on an electrophoresis gel, demonstrating the lack of DNA contamination in the RNA extract. For samples CR15 and 17, DNA and cDNA PCR products were re-conditioned before ligation, using the same PCR cocktail recipe except 5 μl of template and 14.2 μl of water. The re-conditioning reaction consisted of 5 cycles of 94ºC 20 s, 52ºC 30 s, and 72ºC 40 s. The products of this reaction were plate purified (Millipore Multiscreen filter plates, ref# MSNU03010), brought up in 30 ul 10 mM Tris, and ligated (1 μl of cDNA, 0.5 μl of DNA) with the Invitrogen TOPO TA Cloning Kit (cat# 45-0030). The ligations were transformed using Top Ten chemically competent E. coli cells. Ninety-six colonies from each library were picked, grown overnight in LB broth and amplified using M13 primers for 30 cycles. The M13 products were visualized to confirm the correct size insert, plate purified, and sent for unidirectional sequencing using T3 primers at Laragen Sequencing (Culver City, CA). NifH libraries were also attempted from cDNA generated from CR17,

the paired incubation with no methane added. Although a faint amplicon was observed, the visualized M13 products revealed that the inserts were of variable size, and although 16 representative M13 products were sequenced, none of them were *nifH* sequences.

mcrA libraries were also constructed from both cDNA (CR15 and CR17) and DNA (CR15). The PCR cocktail was the same as described above, except primers mcrA_F 5'-GGT GGT GTM GGA TTC ACA CAR-3' and mcrA_R 5'-TTC ATT GCR TAG TTW GGR TAG-3' were used, modified from (*31*). PCR conditions are listed in SI Table 2. No amplicon was observed for the RNA-only controls via gel electrophoresis. Several bands could be seen for the CR17 cDNA amplification, so the correct size band was cut out and extracted from the gel using the Wizard SV Gel and PCR Clean-up System. CR15 cDNA and DNA were reconditioned with 3 cycles of PCR and 1 μl template, and gel-purified CR17 cDNA was reconditioned with 5 cycles of PCR and 5 μl template (based on the quantity of DNA after the first PCR). Ligation, transformation, and sequencing were performed as described above, with the exception that only 17 colonies grew from CR17, all of which were picked.

aprA libraries were also constructed from both cDNA (CR15 and CR17) and DNA (CR15 and CR17). The PCR cocktail was the same as described above, except APS primers AprA-1-FW and AprA-5-RV were used (*32*). PCR conditions are listed in SI Table 2. No amplicon was observed for the RNA-only controls via gel electrophoresis. PCR products were reconditioned using 2 ul template and 5 cycles. Ligation, transformation and sequencing were performed as described above, with the exception that although hundreds of colonies grew, only 16 clones from the CR17 DNA library

were sequenced. Since these 16 clones were similar to those recovered in the full CR15 DNA library, further sequencing of the CR17 library was deemed unnecessary.

Bacterial 16S rRNA libraries were also constructed from both cDNA (CR15 and CR17) and DNA (CR15 and CR17). The PCR cocktail was the same as described above, except 16S bacterial rRNA was targeted with primers 27F 5'-AGA GTT TGA TYM TGG CTC-3' and 1492R 5'-GGYTAC CTT GTT ACG ACT T-3' modified from Lane 1991 (*33*). PCR conditions are listed in SI Table 2. No amplicon was observed for the RNA-only controls via gel electrophoresis. No re-conditioning was performed before ligating. Ligation and transformation were performed as described above.

Phylogenetic Analysis and Identification. Bacterial 16S rRNA: Sequences were trimmed and examined for quality using Sequencher software. Sequences were aligned in Arb and added to an internal lab database of bacterial 16S rRNA sequences via Parsimony. Phylogenetic associations were determined based on the placement of the clones within the tree, and the sequence similarity to the nearest neighbors.

mcrA and nifH: Sequences were trimmed and examined for quality using Sequencher software and then loaded into Geneious Pro (*34*). Sequences were translated *in silico* and then aligned using ClustalW. Phylogenetic trees were generated by Maximum Likelihood (PhyML) using aLRT (*mcrA*) or Neighbor Joining with 1,000 bootstrap replicates (*nifH*).

aprA: Sequences were trimmed and examined for quality using Sequencher software. Phylogenetic trees were not generated. Phylogenetic identities at the phylum level (family level within the Proteobacteria) were determined by grouping the nucleotide

sequences into 90% similarity bins and BLASTing randomly selected sequences from each bin against the NCBI public database. Phylogenetic classifications were determined by the published phylogenies for the nearest neighbor recovered by the BLAST search.

Fluorescence In Situ Hybridization coupled to Nanoscale Secondary Ion Mass Spectrometry (FISH-NanoSIMS). FISH-NanoSIMS was performed as described previously (*26, 35*). Briefly, sediment centrifugation in a 1:1 PBS:Percoll gradient (Sigma-Aldrich #P4937), followed by filtration on a 0.2 μm Durapore filter. Cells were deposited onto custom cut indium tin oxide (ITO) coated glass, or un-coated glass that was gold sputtered after sample deposition and mapping. CARD-FISH was conducted on the ITO-attached cells using the DSS 658 (60% formamide), DSB 652 (25% formamide), and ANME-1c 350 (30% formamide, hybridization performed in microwave) probes and Alexa green and red fluorophores (*36, 37*), followed by DAPI staining. Cell of interest were located and imaged using a Delta Vision RT microscope and Applied Precision software.

A CAMECA NanoSIMS 50L housed at Caltech, with a mass resolving power of approximately 5,000, was used to analyzed specific single cells identified with FISH. A Cs^+ primary on beam (2–8 pA) with a nominal spot size of 100-200 nm was used to rastor over cells of interest. Seven masses were routinely collected: ^{12}C, ^{13}C, $^{14}N^{12}C$, $^{14}N^{13}C$, ^{28}Si, ^{31}P, and ^{32}S using electron multipliers. Square images of 3 to 10 μm on a side were collected at 256 x 256 or 512 x 512 pixels resolution, for 0.5 to 5 hours. The length of analysis, and therefore the number of counts collected, was often limited by the

dislocation of the cell on the sample surface due to charging issues. Images were processed using the L'Image software.

$\delta^{15}N$ isotopic analysis via EA-IRMS. A subset of samples from the inhibitor microcosm experiments were selected for nitrogen isotopic analysis. Sediments were washed as described previously (*29*), dried, and packed in tin cups. Isotope measurements were made on a Costech Elemental Analyzer coupled to a Delta V Isotope Ratio Mass Spectrometer at Washington University in St. Louis.

Determination of sulfide concentrations. Sulfide concentrations in the inhibitor microcosm experiments were measured by combining liquid removed via a syringe from the experiments with 1M zinc acetate at a ratio of 1:1. Samples were stored at room temperature until analyzed via the Cline Assay in a 96-well format spectrophotometer.

RESULTS and DISCUSSION

DNA and RNA analysis of Diazotrophic Sediments

Molecular investigations of DNA, and in particular those targeting 16S rRNA, *mcrA* (encoding methyl coenzyme M reductase A) and *dsrAB (encoding dissimilatory sulfite reductase)*, have been pursued extensively in methane seep sediment (e.g., *9, 19, 38–46*). However, it is widely accepted that investigations of DNA indicate the genetic potential that exists, or once existed (in the case of intact extracellular DNA, and DNA within no longer functional cells), rather than microbial activity (see Discussion in *47*). Due to the short lifetime of transcripts, investigating RNA, and particularly mRNA, can

provide a more accurate impression of microbial activity (although there are still limitations to this proxy for actual protein activity). However, many fewer studies have approached the diversity of methane seep sediment at the transcript level (e.g., *13, 27, 47*). This disparity may be due to the challenges of extracting intact mRNA from slow-growing sediment samples, where transcript levels may be low and native RNases are ubiquitous.

In the current work we tested several protocols and commercially available products for RNA and DNA co-extraction, purification (including the removal of all contaminating DNA from the RNA) and reverse transcription, in order to optimize the quantity and quality of cDNA generated from small quantities (subsamples of ongoing incubations) of seep sediment. We then investigated the transcripts of four genes in each of two sediment incubation bottles, one amended with a methane headspace (CR15), and the other with an argon headspace (CR17), both containing an aliquot of homogenized sediment from within a methane seep-associated microbial mat (Core A2, 3–6 cm, Chapter 3). By comparing the transcripts in the with-methane versus the no-methane bottles, we can observe which portion of the community is dependent on methane and/or AOM byproducts. The four genes selected for analysis were 16S bacterial rRNA, to target the bacterial community, methyl coenzyme M reductase A (*mcrA*), to target methanotrophs and methanogens, adenosine-5'-phosphosulfate reductase alpha subunit (*aprA*), to target sulfate-reducing and sulfide-oxidizing microbes, and dinitrogenase reductase (*nifH*), to target organisms capable of nitrogen fixation. To our knowledge this is the first methane seep report of *aprA* transcripts, and only the second of *nifH* transcripts (*27*).

16S bacterial rRNA RNA and DNA analysis

The DNA 16S rRNA libraries generated from each incubation after 4 months showed nearly identical communities, indicating that significant divergence of the populations did not occur during the experiment (Figure 1). This is expected despite the different conditions within the bottles because the growth rates of deep-sea marine microorganisms (growing at 4˚C) tend to be extremely slow (doubling times of 3–7 months, (*48–51*)). A great diversity of sequences was observed within these libraries, with the three most abundant phyla being: *Gammaproteobacteria* (CR15: 18%, CR17:11%), *Chloroflexi* (CR15: 11%, CR17: 18%), and *Deltaproteobacteria* (CR15: 22%, CR17: 21%), which is generally consistent with what has been observed previously at methane seeps.

The *Deltaproteobacteria* comprised the highest number of bacterial transcripts under both the with-CH_4 and no-CH_4 conditions, although relatively more deltaproteobacterial transcripts were detected with methane. This is consistent with a high fraction of ANME-associated *Deltaproteobacteria* in this sample, including known ANME-partners *Desulfosarcina* and *Desulfobulbus*, both of which were relatively more active (i.e., more transcripts were detected) with methane than without. The activity of the *Deltaproteobacteria* without methane, and particular that of *Desulfocapsa*, indicates a methane-independent, presumably free-living community of *Deltaproteobacteria*. Interestingly, no sulfide production was detected without methane (Chapter 3, Table 1), suggesting that the *Deltaproteobacteria* active without methane are either not conventional sulfate reducers, reduce sulfate at levels below our detection limit, or reduce

Figure 1. Relative abundances of DNA and cDNA sequence-groups recovered from Costa Rican methane seep incubations with and without methane (CR15 and CR17, respectively). Percentage of library is shown if ≥ 5%. The deltaproteobacteria in the 16S bacterial library are sub-divided and in the second row and the number of clones (not percentages) indicated if ≥ 2 clones.

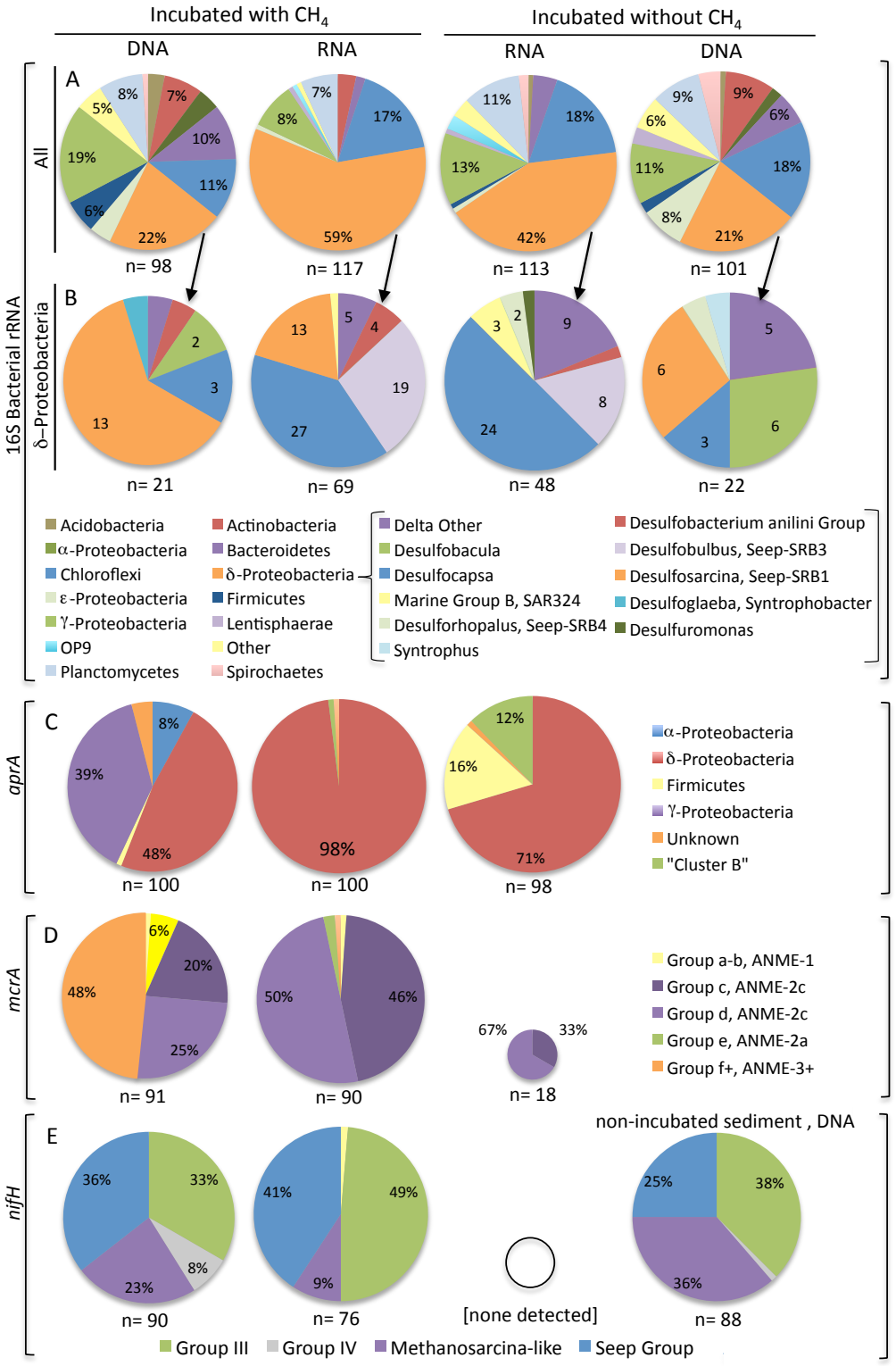

sulfate producing sulfide which is then rapidly converted back to sulfate by sulfide-oxidizing bacteria. The phylum with the greatest percentage difference between relative transcript abundance in the with-methane (CR15) and the no-methane (CR17) conditions were the *Actinobacteria* (100% change, from 3% to 0%). A future library targeting this group specifically might determine if this difference is due to a dependence on methane and/or AOM by-products.

Interestingly, the *Gammaproteobacteria*, *Planctomycetes,* and *Chloroflexi* did not demonstrate a preference for either the with-methane or no-methane incubation (as assessed by relative transcript abundance), suggesting that they operate primarily independently of methane metabolism on this timescale. Members of the *Gammaproteobacteria* and *Planctomycetes* have previously been implicated as attached to the ANME-2, as they were co-extracted from a sediment seep sample with a physical capture targeting the ANME-2, however an association with the ANME was not confirmed visually (*1*). It remains a possibility that these groups are dependent on the increased biomass at methane seeps, and therefore increased organic material for heterotrophic metabolism, which is ultimately due to AOM. Longer-term incubations would be necessary to investigate the long-term effects of methane on the diversity of bacteria.

Although *Alpha-* and *Betaproteobacteria* were also previously implicated as involved in AOM due to their physical co-extraction with ANME from the sediments during ANME-2-targeted “bead capture” (comprising 9% and 32% of the total bacterial diversity in the captured sample, respectively), and their subsequent visualization of physical association with ANME-2 via FISH, we were not able to assess their

dependence on methane/AOM in this study because neither family was represented in either the with-methane or no-methane incubation (*1*). However, the absence of detected transcripts suggests that they are not significant partners to the ANME-2 in this Costa Rican seep sample.

aprA gene RNA and DNA analysis

Both of the *aprA* cDNA libraries demonstrated a significance difference from the DNA library in that the 39% of the DNA library from *Gammaproteobacteria* sequences were not found in the cDNA libraries (Figure 1). It is possible that the *Gammaproteobacteria* sequences belong to sulfide-oxidizing bacteria, which without an electron acceptor in these sulfidic incubations were not active. Indeed, the nearest neighbor in the public NCBI database to many of the *Gammaproteobacteria* sequences recovered in the DNA library were known to be sulfide-oxidizing bacteria (data not shown).

Another noticeable difference in the *aprA* libraries is the relative increase in activity of *Firmicutes* and sequences from "Cluster B" described by (*21*). The *Firmicutes* sequences were most closely related to *Desulfotomaculum*, a genus of sulfate-reducing bacteria not known to associate with the ANME. It is therefore not surprising that it may be relatively more active in an incubation without methane. However, the lack of sulfide production in this incubation given the transcripts of putative sulfate-reducing bacteria remains puzzling (Chapter 3). The recent isolation of two syntrophic propionate-oxidizing bacteria belonging to the *Desulfotomaculum* demonstrates that there is metabolic diversity within this group, and is evidence for non-sulfate-reducing members

of the *Desulfotomaculum* (*52*). Cluster B currently consists exclusively of deeply branching *aprA* DNA sequences from methane seeps in the Gulf of Mexico. Although the function of Cluster B is not known, its detection to date only at methane seeps suggests that these organisms are related to methane cycling. It is possible that they are equally active in both the with-methane and no-methane incubations, but the high activity of the *Deltaproteobacteria* in the with-methane sample swamps out the signal of Cluster B in that incubation. The relatively increased activity of the *Deltaproteobacteria* in this incubation mirrors the activity observed in the 16S rRNA library. Further analysis of the *aprA* Deltaproteobacterial sequences will allow the identification of which *Deltaproteobacteria* were responsible for the increased activity with methane.

mcrA gene RNA and DNA analysis

The mcrA groups a–e have been relatively well paired with the 16S rRNA identities of the ANME, with mcrA groups a and b belonging to ANME-1, c and d to ANME-2c, e to ANME-2a, and f to ANME-3 (*9, 43*). However, we discovered a great diversity of ANME-3-like sequences in the DNA clone library, extending beyond the previously described cluster. Although some sequences are closely related to the sequences used to describe *mcrA* group f (*9*), approximately one third of the sequences occupy a phylogenic space between the described *mcrA* group f and the *mcrA* sequences of known methanogenic archaea (Figure 2). It is therefore unknown if these sequences belong to methanotrophs or methanogens. Interestingly, although ANME-3 and ANME-3-like sequences are abundant in the DNA library (48% total), neither are detected as transcripts. Although this is intuitive if the ANME-3-like sequences are indeed from

Figure 2. Phylogenetic analysis of *mcrA* sequences. Deduced amino acid sequences were aligned using ClustalW and the tree was generated by Maximum Likelihood in PhyML. Sequences from this study begin with CR15-, and the cDNA sequences from this study are in bold. Representative sequences from this study are shown; parenthesis indicate number of sequences ≥ 99.3% similar to the clone shown. SH-like aLRT (approximate Likelihood Ratio Test) branch supports for major branches are shown.

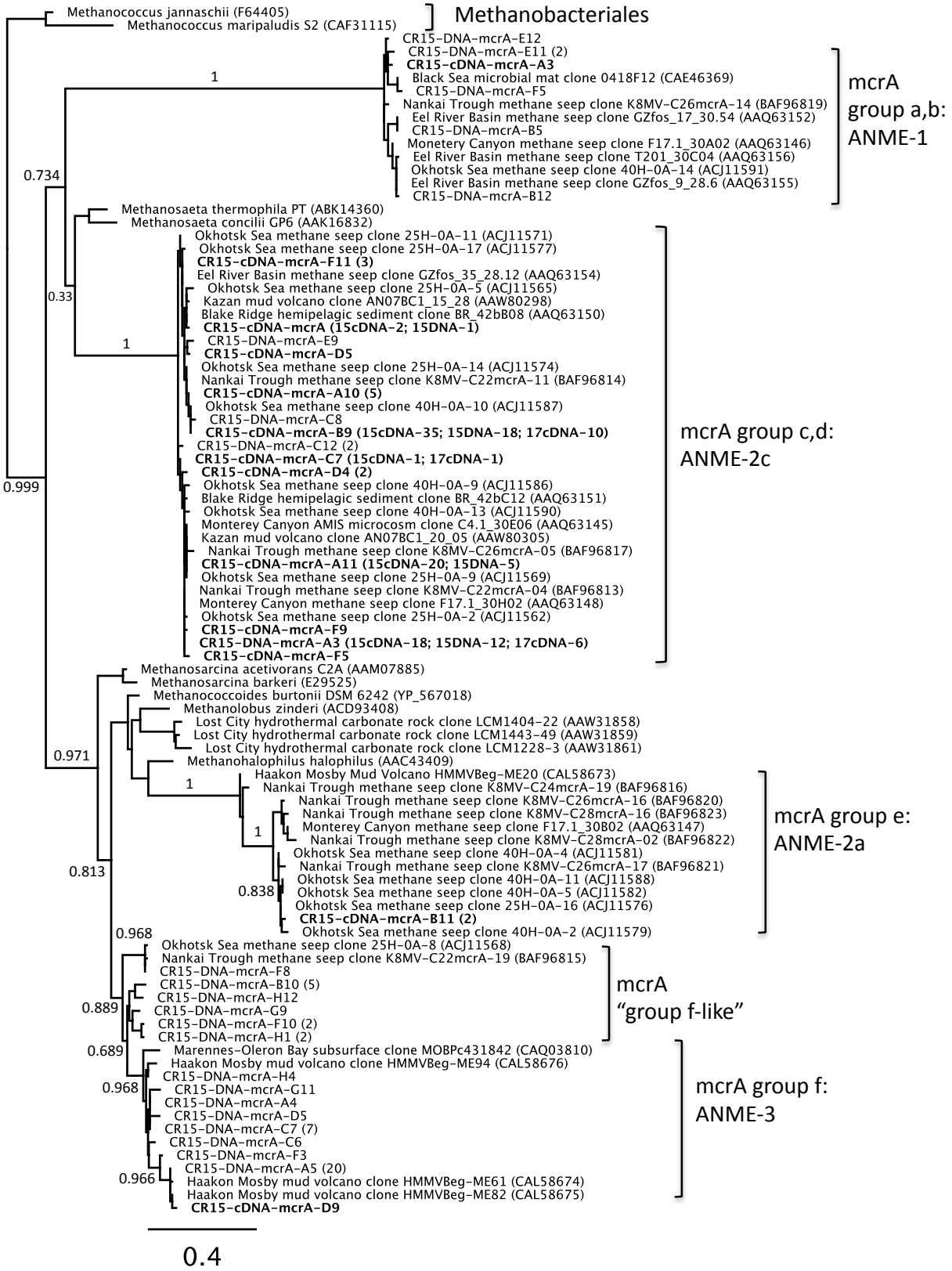

methanogens, it is surprising that the ANME-3 methanotrophs were not active in these incubations. It is clear that the ANME-2c were the most active ANME group, suggesting that the majority of the AOM occurring in these sediments can be attributed to them. Although ANME-1 sequences were recovered from the DNA (6%) of the library, only one ANME-1 clone was recovered from the cDNA (1%) of the library.

Due to the weak amplification of *mcrA* from the no-methane bottle, only 18 sequences were obtained, and all of these belonged to ANME-2c. Why these methanotroph transcripts were present in the absence of methane is unknown, but there a several possibilities. There may be low levels of methane in the incubation after 4.5 months, produced by methanogens, which support the methanotrophic ANME-2. However, transcripts from methanogens were not detected in this incubation. Another possibility is methanogenic activity in the ANME-2c. It has been proposed that the ANME can produce methane when it is thermodynamically favorable, and isotopic measurements of the ANME-1 and ANME-2 have supported this possibility (*53, 54*). A third possibility is that mRNA turnover is not as rapid in these sediments as other environments due to low temperature, and/or a different strategy related to low energy yields and a desire to "re-use" transcripts. If this is the case, and mRNA is more stable in these samples, transcript analyses must be considered carefully, because the transcripts present may not reflect the current conditions.

nifH gene RNA and DNA analysis

The *nifH* transcripts were identified as *nifH* groups I–IV, described by (*55*) and others. These groups do not correspond to known 16S rRNA phylogenies, so although

identity may be inferred by the relationship with *nifH* sequences of known diazotrophs, most assignments other than those from full genomes of cultured representatives or environmental fosmids are only putative. Linking diazotrophic activity to phylogenetic identity is currently an active effort in nitrogen fixation research.

A diversity of *nifH* sequences were detected in the DNA extract, consistent with the diversity observed in hotspots of productivity in the deep-sea previously, including at methane seeps, mud volcanoes, and hydrothermal vents (*26–28, 30*). A *nifH* DNA clone library was previously generated from the original sediment collected in parallel to the incubated sediment investigated here (Chapter 3, re-shown in this Chapter, Figure 1). The *nifH* diversity and proportions recovered in these two libraries are extremely similar, and suggest that the incubations contain communities representative of the *in situ* population (also seen in Figure 3).

The *nifH* cDNA was diverse, and mirrored the *nifH* sequences recovered in the DNA library fairly closely (Figure 1 and 2). One important difference between these libraries is the detection of *nifH* group IV sequences in the DNA but not the cDNA. Group IV contains *nifH* homologues that have not been proven to be functional. Their absence from the cDNA library therefore confirms the purity of the RNA converted to cDNA. Transcripts from *nifH* Group III were the most abundant, comprising 49% of the library, while the methane seep *nifH* clade was the second-most abundant, at 41%. The methane seep clade ("Methane Seep Group 2" in (*27*)) has previously been putatively assigned to the ANME-2 archaea (*26, 27*), while Group III hosts a range of anaerobic microbes, including methanogens and sulfate-reducing bacteria.

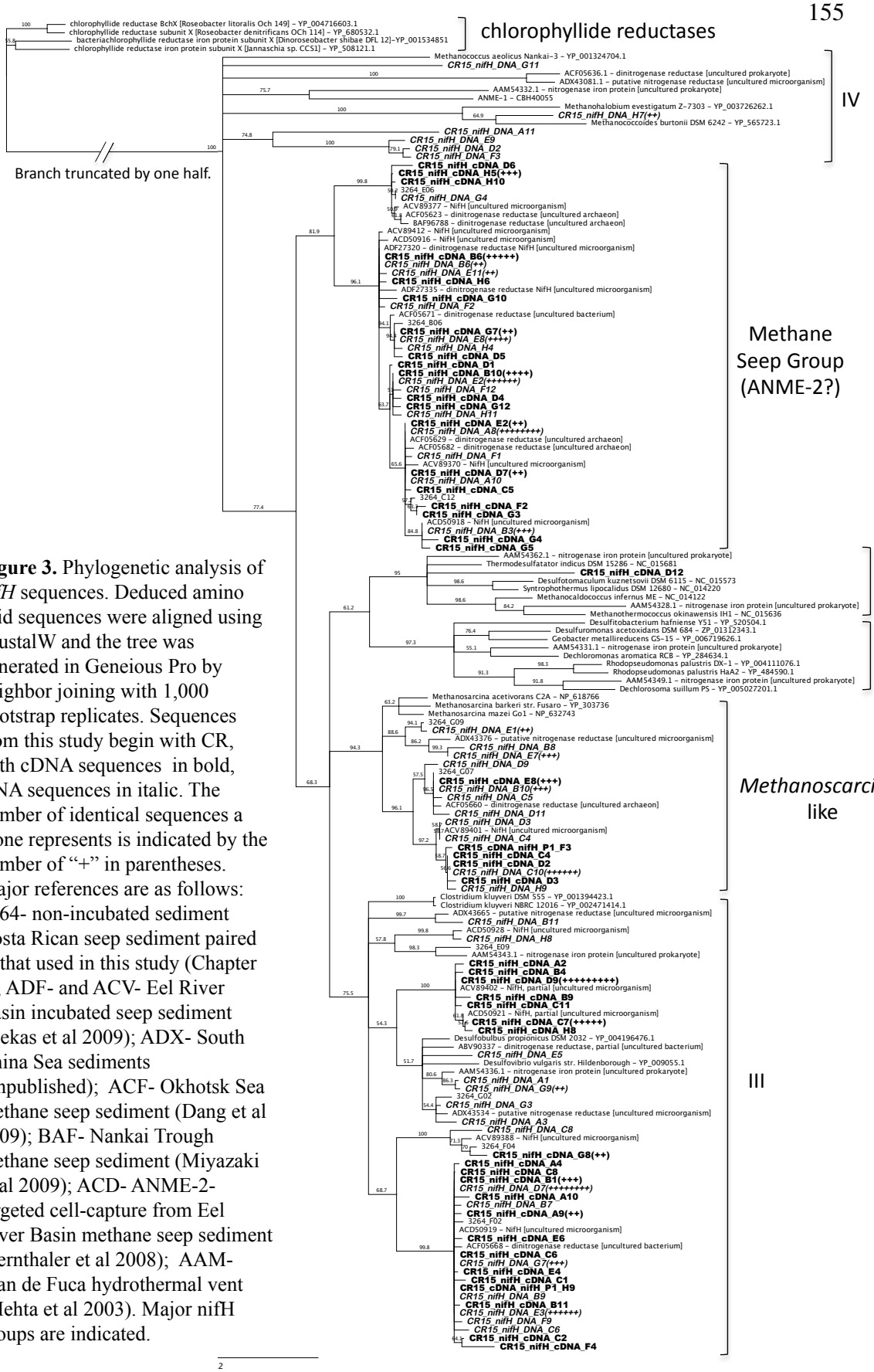

Figure 3. Phylogenetic analysis of *nifH* sequences. Deduced amino acid sequences were aligned using ClustalW and the tree was generated in Geneious Pro by neighbor joining with 1,000 bootstrap replicates. Sequences from this study begin with CR, with cDNA sequences in bold, DNA sequences in italic. The number of identical sequences a clone represents is indicated by the number of "+" in parentheses. Major references are as follows: 3264- non-incubated sediment Costa Rican seep sediment paired to that used in this study (Chapter 3); ADF- and ACV- Eel River Basin incubated seep sediment (Dekas et al 2009); ADX- South China Sea sediments (unpublished); ACF- Okhotsk Sea methane seep sediment (Dang et al 2009); BAF- Nankai Trough methane seep sediment (Miyazaki et al 2009); ACD- ANME-2-targeted cell-capture from Eel River Basin methane seep sediment (Pernthaler et al 2008); AAM- Juan de Fuca hydrothermal vent (Mehta et al 2003). Major nifH groups are indicated.

Interestingly, a third, yet classified group contained 9% of the *nifH* transcripts (Figure 3). Although some of the sequences within this group have previously been included in Group III in other published *nifH* phylogenies (*27, 28*), we resist this classification on the basis of the group failing to cluster within Group III in either a Neighboring Joining tree (Figure 3) or a Bayesian analysis performed with Mr. Bayes (not shown). We therefore tentatively call this group "*Methanosarcina*-like" for its proximity to the *Methanosarcina* sequences. Although these sequences may be from methanogens, their expression during high methane concentrations suggests otherwise. Although they are possibility associated with methanotrophs, the *mcrA* sequences suggest that only one group of ANME are dominant, the ANME-2, which are allegedly represented in the *nifH* methane seep clade. However, as discussed in Chapter 3, the evidence linking Seep Group 2 to the ANME-2 is tenuous, and the hosting of these sequences within the SRB associated with the ANME-2 is also a possibility. Additional considerations are the possibility that the ANME (or SRB) contain multiple *nif* operons, as well as horizontal gene transfer events resulting in closely related *nifH* sequences within only distantly related microorganisms. Furthermore, it is possible that although the ANME-2 dominate the *mcrA* sequences, there are other active populations of ANME present at lower levels, and these contribute disproportionately to the *nifH* transcripts (e.g., 1–2% of the mcrA transcripts and 9% of the *nifH* transcripts). We therefore do not propose a link between the *Methanosarcina*-like sequences and any 16S rRNA phylogenetic group at this time.

In a previous study of *nifH* transcripts from methane seep sediment, Miyazaki et al. (2009) found that 96% of the sequences clustered within the methane seep clade (*27*).

In comparison, our library with only 49% methane seep clade clones is much more diverse. This diversity may suggest that several diazotrophs are important contributors to bioavailable nitrogen in this system. However, the nitrogen fixation previously measured by elemental analysis isotope ratio mass spectrometry (EA-IRMS) in this incubation (Chapter 3) was demonstrated to be nearly completely dependent on methane. This suggests that the diversity of diazotrophs observed via the RNA analysis are either dependent on methane (i.e., methanotrophs), dependent on the products of AOM (i.e., ANME-associated or free-living SRB), or simply not functional/not used in nitrogen fixation, despite their transcription. Although it cannot be discounted, the possibility that these transcripts are not used in nitrogen fixation seems low, because of their phylogenetic association with functional *nifH* sequences. Therefore, there is likely a diversity of diazotrophs directly or indirectly dependent on methane in these samples. Investigating the ability of single cells in the sediment to take up $^{15}N_2$ (fix nitrogen) and $^{15}NH_4$ (as a proxy for protein synthesis) is therefore the next step in understanding both the diversity of diazotrophs in the sample and the relationship of these microbes with methane and the ANME.

NanoSIMS analysis of single cells, including *Desulfosarcina/Desulfococcus* and *Desulfobulbaceae*

The close relation of transcribed *nifH* sequences in CR15 to that of known diazotrophic sulfate-reducing bacteria suggest that diazotrophic sulfate-reducing bacteria may be responsible for (at least some of) the diversity in *nifH* transcripts observed

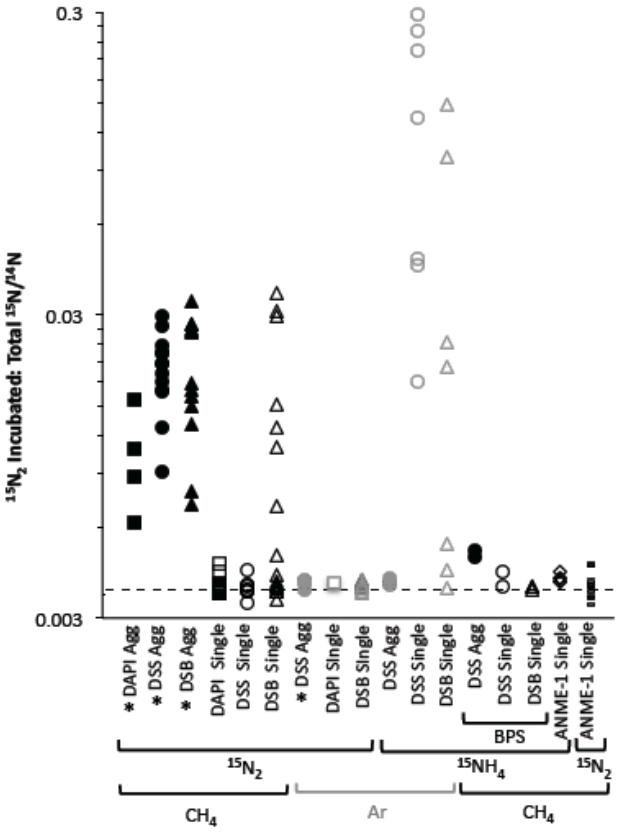

Figure 4. ^{15}N-uptake from $^{15}N_2$ or $^{15}NH_4^+$ (as indicated) in ANME-SRB aggregates ("agg") and single cells ("single"), 160 targets total. Aggregates in solid symbols, single cells in open symbols, with-methane in black, no-methane in gray, natural abundance $^{15}N/^{14}N$ as the dashed line. Data in categories with * are from Chapter 3 and are included for comparison here.

(Figure 3). Free-living *Desulfosarcina/Desulfococcus* (DSS) and *Desulfobulbaceae* (DSB) cells were therefore targeted with FISH-NanoSIMS to determine whether or not they fix nitrogen. Single DSS cells did not take up ^{15}N from $^{15}N_2$ (n=7), however single DSB cells were enriched in ^{15}N in the same incubations (n=22, 8/22 enriched), including several that appear to be dividing (Figure 4 and 5). Interestingly, however, when FISH-NanoSIMS was performed on single DSB in paired $^{15}N_2$ incubations without methane, no ^{15}N enrichment was observed (n=25) (Figure 4). Nitrogen fixation dependent on methane is unexpected for free-living sulfate-reducing bacteria, which are not thought to be dependent on methane for growth. The DSB were demonstrated, in fact, to grow independently of methane by analyzing DSB single cells in paired incubations with

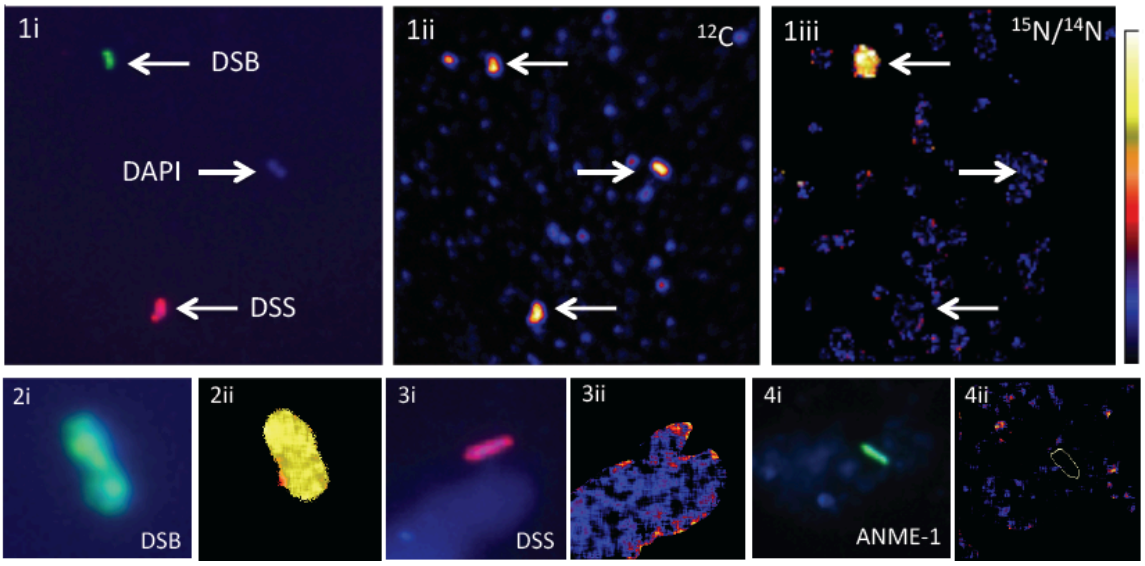

Figure 5. Preferential uptake of $^{15}N_2$ in *Desulfobulbaceae* single cells from Costa Rica methane seep sediment incubation CR8. Cells were incubated with $^{15}N_2$ and a headspace of methane for 4.5 months. Left panels: FISH image of *Desulfobulbaceae* (green, DSB 652), *Desulfosarcina/Desulfococcus* (red, DSS 658), and an unidentified single cell (blue, DAPI stained). Center and right panels: corresponding ^{12}C and $^{15}N/^{14}N$ ion images collected on the CAMECA NanoSIMS 50 L ($^{15}N/^{14}N$ ratio is collected as $^{12}C^{15}N^-/^{12}C^{14}N^-$). Scale bar at right shows increasing ion counts in warmer colors. The bottom of both scale bars is natural abundance (0.0036) and the top is 0.013 in the top image, 0.045 in the bottom image. The DSB pictured on the bottom is not the same as the DSB cell above.

$^{15}NH_4^+$ and a headspace of argon, rather than methane. Growth evidenced by $^{15}NH_4$ uptake occurred in both DSB (n=7, 4/7 enriched) and DSS (n=7, 7/7 enriched) cells analyzed under these conditions, showing that although there is heterogeneity in growth rates within an environmental population (as seen previously by (*26, 51*)), neither require methane to grow (Figure 4).

There are several possible explanations for the pattern of ^{15}N observed in the DSB single cells. First, the cells hybridized with the DSB probe (DSB 652) are actually a diverse group of organisms within the *Desulfobulbaceae*. Some of these subgroups may be directly or indirectly (e.g., if surviving off of organic matter or other metabolites/growth factors produced by the ANME) methane dependent, and also able to

fix nitrogen. The low fraction of DSB cells relative to DSS cells demonstrating ^{15}N enrichment from $^{15}NH_4$ without methane (57% versus 100%) leaves the possibility of free-living, methane-dependent, diazotrophic DSB subgroups feasible. Further FISH-NanoSIMS would need to be performed using subfamily-specific FISH probes to determine whether or not this is the case. There is evidence for diazotrophy within the *Desulfobulbaceae*, with *nif* genes found in the *Desulfobulbus propionicus* genome (*56*).

Another explanation is that the ANME fix N_2 only in the presence of methane (Figure 4), pass fixed ^{15}N-products to the closely associated, non-diazotrophic DSB cells, which then dissociate from the ANME, and result in ^{15}N-labeled single DSB cells only in the presence of methane. The dissociation could either be part of the natural life cycle of the ANME-DSB association, or it could be an indication of a fragile association disrupted during processing for FISH-NanoSIMS. Regardless, this type of association is different from that observed for the DSS, which although always ^{15}N-enriched when associated with ^{15}N-enriched ANME, were never observed as ^{15}N-enriched as single cells in diazotrophic conditions. The ANME-DSS association may therefore either be more permanent, or physically stronger.

The ^{15}N-enrichment observed in the DSB cells is unlikely due to non-specific recycling of fixed ^{15}N-products in the incubation, because neither the DSS single cells, nor unidentified DAPI-stained single cells (n=27) showed ^{15}N-enrichment. The methane-dependent ^{15}N-enrichment in the DSB cells from $^{15}N_2$ therefore must either indicate DSB diazotrophy or a specific sharing of ^{15}N with a closely associated diazotrophic partner, such as the ANME, followed by dissociation.

NanoSIMS analysis of ANME-1 single cells

In addition to sulfate-reducing bacteria, it is possible that ANME groups other than the ANME-2 mediate nitrogen fixation. Because the active methanotroph community in CR15 was nearly 100% ANME-2, we targeted sediment incubated with $^{15}N_2$ from the Eel River Basin (ERB) previously shown to host diazotrophic ANME-2 (*26*). Although no molecular information is available on the archaeal diversity or activity in this sediment, it was hypothesized that there would be a greater diversity of ANME in this sample than in CR15, because the ERB experiment was conducted with sediment homogenized from all depths within a core, while the CR15 incubation only included sediment from 3–6 cm (the hypothesized methane-sulfate transition zone). As there is evidence that the ANME stratify with depth (*41, 42*), the ERB incubation was therefore determined to be preferable for this investigation.

We targeted ANME-1 single cells with FISH-NanoSIMS, and although ANME-1 were detected in the ERB sediment via CARD-FISH, we found that ANME-1 single cells did not take up ^{15}N in 6 months (n=10, Figure 4, Figure 5.4). Although the ANME-1 metagenome revealed *nif*-like genes (*14*), it has been hypothesized that the ANME-1 *nifH* homologues are non-functional, due to their phylogenetic placement in *nifH* Group IV. Our results are consistent with this hypothesis. However, when ANME-1 were investigated in parallel incubations with $^{15}NH_4$, no ^{15}N-uptake was observed from $^{15}NH_4$ either (Figure 4). This is in contrast to the activity of the ANME-2 cells from the same sediment, which showed high levels of ^{15}N-uptake under the same conditions. This indicated that the ANME-1 were not actively growing in these incubations, or were growing extremely slowly, despite the success of the ANME-2. Lower rates of activity in

the ANME-1 relative to the ANME-2 has been demonstrated previously (20X lower, (*17*)), however this disparity may also suggest that ANME-1 and ANME-2 have different ideal growth conditions, and that the conditions employed here favored the ANME-2. Regardless, we cannot eliminate the possibility of diazotrophy by the ANME-1 based on these data, which were collected while the ANME-1 were not active.

Investigating Structural Inhibitors of Methyl Co-Enzyme M Reductase

A difference in activity (specifically, a difference in ^{15}N-uptake from $^{15}N_2$) under methane versus argon headspaces was observed in members of the *Desulfobulbaceae* (DSB) (see above discussion). Whether or not this difference was due to a physiological dependence on methane (directly via methane usage, or indirectly via usage of ANME-produced compounds), or a direct N-transfer from the methane-dependent ANME, is unknown. Although $^{15}NH_4$ uptake by the DSB in the absence of methane suggested the latter was more likely the case, the less than 100% population activity without methane left open the possibility of methane-dependency in some DSB subgroups. In order to investigate the activity of the DSB and other free-living cells in the presence of methane when the ANME archaea were inactivated, to differentiate between these possibilities and investigate the relationship of the ANME more generally with the free-living population, we sought to utilize a specific inhibitor of anaerobic methanotrophy.

Chemical inhibitors have been an integral part in the investigation of the anaerobic oxidation of methane (AOM) since the early research on the topic in the 1980s (*57, 58*). One study used bromoethanesulfonate, a structural analogue of methyl coenzyme M, the substrate for methyl coenzyme M reductase, a key enzyme in

methanogenesis (*59, 60*), to demonstrate that AOM likely operates via the enzymatic reversal of methanogenesis, including the usage of methyl coenzyme M reductase (*11*). This hypothesis was later supported by metagenomic analysis of the ANME (*12, 14*), as well as in vitro studies of methyl coenzyme M reductase (*61*) and despite some evidence to the contrary, is the current most widely supported model for the mechanism of AOM (*2, 62*). Another frequently used inhibitor in the study of AOM is sodium molybdate, a structural analogue of sulfate, and therefore an inhibitor of sulfate reduction (*59*), to demonstrate the coupling of AOM to sulfate reduction (*17, 63*).

Although valuable to these early contributions in the field, "specific inhibitors" (i.e., intended to inhibit a specific subset of the population) are inevitably complicated in diverse environmental samples. Two general problems can arise, resulting from a series of unintended effects, and need to be considered when evaluating results of inhibition studies: (1) less than 100% inhibition of the targeted subgroup, (2) inadvertent inhibition of other members of the community (*59*). Bromoethanesulfonate, the most widely used inhibitor of AOM in sediments, is becoming notorious for incomplete inhibition of AOM in some AOM communities (*11, 57, 63*), while nearly 100% effective in others (*17*). The poor inhibition in some communities could be due to a combination of insufficient additions, variation in AOM mechanisms, and an imperfect match with the methyl-coenzyme M reductase active site. It is possible that other compounds may be a better inhibitor of the enzyme, and many have been investigated and identified in vitro (*64*). Beyond the fit in the active site, however, the relationship of the inhibitor with the rest of the community is paramount. If community members are able to degrade the compound, its efficacy in inhibiting a purified enzyme in vitro is moot. Alternatively, if the

compound inflicts adverse effects on the greater community, specificity is lost and the experiment is undermined. Before using a specific inhibitor of AOM on these samples, we therefore launched an investigation of three potential structural analogues of methyl coenzyme M, bromoethanesulfonate (BES), bromopropionate (BP), and bromopropanesulfonate (BPS), and sought to evaluate them on both aforementioned criteria: inhibition of the target group and specificity.

Bromopropanesulfonate inhibited 97% of methane-dependent sulfide production (a proxy for AOM, (*18*)) at 2 mM over 6 weeks, significantly more than inhibited by either bromoethanesulfonate (23%) or bromopropionate (28%) at the same concentration during the same time period (Figure 6B). Inhibition was observed at each time point during the analysis, as well (Figure 6A). A great variation in the inhibition efficiency of 2 mM BES and BP was observed in the two replicate experiments of two different seep sediment samples (4 bottles for each inhibitor) with the effect of BES ranging from -22% (an increase in activity) to 76% inhibition, and that of BP from 11–65%. Little variation was seen in the four bottles amended with 2 mM BPS, with inhibition ranging from 94–100%. At 20 mM, the difference between the inhibitors was not as great, with 59% average inhibition from BES, 100% from BP, and 96% from BPS. The effect of BPS was therefore similar to that of $NaMO_4$ (Figure 6 B).

The same trend in inhibition efficiency was seen in methane-dependent $^{15}NH_4$-uptake (a proxy for growth of methanotrophs), measured by Elemental Analysis coupled to Isotope Ratio Mass Spectrometry (EA-IRMS) in these samples. At 2 mM, BES inhibited 18.4% of methane-dependent growth, BP did not inhibit growth, and BPS inhibited 85% (Figure 6C and D). Additionally, after 6 months, BPS inhibited 91% of

Figure 6. Effect of inhibitors on respiration and growth in microcosm experiments of Costa Rican methane seep sediment. A: Sulfide production over time. Experiments with inhibitors are dashed as indicated in the legend. Gray indicates a concentration of 2 mM, black of 20 mM. Points represent the average of the measurement in four bottles. B: Percent inhibition of methane-dependent sulfide production (sulfide production in bottles with methane less sulfide production in bottles without methane) with the addition of each inhibitor after 6 weeks. Concentrations as shown. Bars represent the average of the measurement in four bottles. Error bars represent one standard deviation. C: ^{15}N-uptake from $^{15}NH_4$, as a proxy for growth, over time. Lines and colors are as indicated for (A). D: Percent inhibition of methane-dependent ^{15}N-uptake with the addition of each inhibitor at 2 mM. Time incubated as shown.

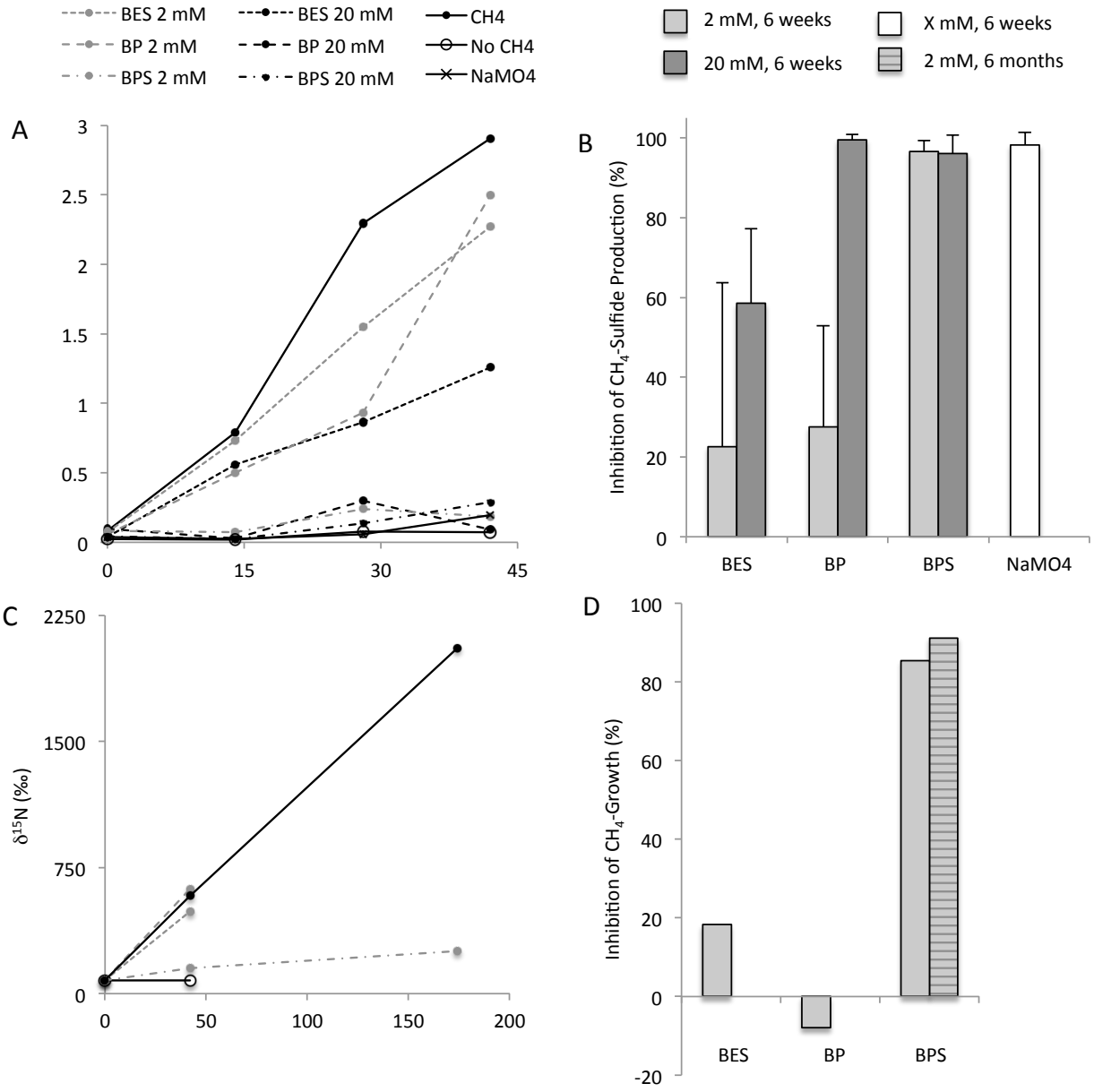

methane-dependent growth, indicating its resistivity to degradation and therefore utility in even long-term incubations (Figure 6C and D).

Due to its superior inhibition of methane-dependent sulfide production particularly at low concentrations (low concentrations are preferable in order to reduce potential indirect effects on the community by addition of increasing amounts of the inhibitor) and the long-life of its effect, we determined BPS was the most effective inhibitor of AOM, and proceeded to test its specificity. During an admittedly brief NanoSIMS analysis, we observed that BPS did inhibit $^{15}NH_4$-uptake in ANME-DSS aggregates during 6 weeks of incubation with methane, resulting in only a slight ^{15}N-enrichment (n=2, total $^{15}N/^{14}N$ was 0.00487 and 0.00461, compared to 0.0036 natural abundance) that could be due to $^{15}NH_4$-binding abiotically to the complex EPS (*51*), and/or clay matrix surrounding the ANME aggregates (see Appendix A for description of the clay matrix). Interestingly, however, free-living *Desulfosarcina/Desulfococcus* (DSS) cells (identified via positive hybridization with DSS 658, n=3) as well as members of the *Desulfobulbaceae* (identified via positive hybridization with DSB 652, n=3), also appeared to be inhibited by BPS, with even lower levels of ^{15}N-enrichment than observed in the ANME-DSS aggregates (Figure 4).

The reason for the inhibitory effect BPS apparently confers on the growth of some free-living sulfate-reducing bacteria is unknown. The possibility that the DSS and DSB (or subgroups thereof) contain methyl coenzyme M reductase, and rely on it for growth, seems remote, especially since 100% of the DSS cells investigated grew in the absence of methane (see above). Additionally, immunological localization of coenzyme M reductase in ANME-DSS aggregates indicated the protein was only present in the

archaeal cells (*65*). However, free-living DSS were not investigated, and may be physiologically different from their ANME-associated relatives in this respect.

Alternatively, we could be observing a yet uncharacterized interaction between BPS and components of the canonical SRB metabolism or physiology, as has been observed with BES. Like BPS, BES is a chemically reactive electrophile, which has been shown to impart increasing inhibition of activity and growth in sulfate-reducing bacteria above 10 mM (*17*). Concentrations of BPS were purposely kept low here (2 mM), but it is possible that lower concentrations are required to increase the specificity of the inhibition. This, however, may decrease the efficiency of the inhibition on AOM. Further testing, starting with additional NanoSIMS analysis of SRB in this experiment, will be necessary to substantiate this observation and make further conclusions about the effect of BPS on free-living sulfate-reducing bacteria. Regardless, its utility as a specific inhibitor of AOM, allowing the investigation of the free-living sulfate-reducing bacteria in the presence of methane while AOM is inhibited, is not likely high. We therefore did not perform experiments to this end. This analysis does, however, demonstrate the value of targeted-single-cell NanoSIMS analysis in determining the specificity of inhibitors. We predict that as more inhibitors are subject to this stringent test of specificity, more will be recognized as inferring inadvertent effects on the diversity of community members.

CONCLUSIONS

Especially given the insufficient nature of several “specific” inhibitors, examining the metabolic capabilities and activity of particular species and groups within

environmental samples is challenging. In the current work we benefited from the ability to investigate the role of the ANME-SRB in the activity of the greater community by adding and removing methane, thereby selectively inhibiting the ANME-SRB clusters. However, we are then unable to differentiate between direct methane dependence and dependence on the products of AOM. Even more difficult is observing chemical interactions in the other direction, i.e., the effect of the free-living population on the ANME-SRB. Separating the ANME-SRB from the rest of the population and observing activity could be one approach, however achieving such a separation while maintaining viability would be difficult. Most single cells and ANME-SRB aggregates are embedded in a matrix of EPS (extracellular polymeric substance) and sediment, making even anoxic size-selective filtration insufficient to separate these groups. Although a "sediment-free" nearly pure co-culture of the ANME-SRB now exists (*50, 66*), it took years of transfer enrichments to establish, and thus may have selected for a subset of the ANME-SRB that are not dependent on the neighboring diversity, and potentially not representative of the *in situ* ANME-SRB behavior. Indeed, the fact that only one nearly pure ANME-SRB system has been established, and all other attempts to isolate these consortia have failed, suggests that the ANME-SRB and their diverse free-living neighbors are more interdependent than currently appreciated. It is therefore important, despite the challenges and experimental limitations, to pursue the metabolic capabilities and the chemical relationships between the members of the seep community.

In the present study we have investigated the activity of the methane seep microbial community in the presence and absence of methane via transcript analysis, and hypothesized, based on the transcripts recovered, that a diversity of diazotrophs may be

active in methane seep sediment. We tested this hypothesis by specifically targeting the diazotrophic capability of three groups of single-cells within the sediment (two sulfate-reducing bacterial groups and the ANME-1) with FISH-NanoSIMS. Although we were not able to definitively identify any of these as diazotrophs, we uncovered several interesting side-plots, including (1) the first direct evidence that free-living DSS and DSB (at least subgroups thereof) are active in seep sediment (with or without methane) (2) the interesting, and seemingly unrelated options that either (a) subgroups of the DSB are diazotrophic (this possibility requires that these subgroups also be dependent on methane) or (b) DSB maintain a relationship with the ANME-2 that is less stable than that of the DSS, (3) ANME-1 are not active, or at least do not grow at detectable rates, in the same sediment incubations as active ANME-2, suggesting different ideal growth conditions, and (4) none of BES, BPS, or BP is an ideal choice as a specific inhibitor of AOM. These findings, in addition the diversity of activity revealed via the transcripts, suggest a complex and interconnected seep ecosystem that despite considerable research efforts, still remains to be completely understood.

ACKNOWLEGEMENTS

We would like to thank the crew and science party of AT15-11 and AT15-59 for making sample collection possible and assisting in processing samples, especially Lisa Levin, Jake Bailey, and Shana Goffredi. We thank the entire Orphan Lab group for their help in the laboratory and in the field.

WORKS CITED

1. A. Pernthaler *et al.*, Diverse syntrophic partnerships from deep-sea methane vents revealed by direct cell capture and metagenomics. *Proceedings of the National Academy of Sciences* **105**, 7052 (2008).
2. W. S. Reeburgh, Oceanic methane biogeochemistry. *Chem Rev* **107**, 486 (2007).
3. K. Knittel, A. Boetius, Anaerobic oxidation of methane: progress with an unknown process. *Annu Rev Microbiol* **63**, 311 (2009).
4. K. U. Hinrichs, A. Boetius, in *Ocean Margin Systems,* G. Wefer *et al.*, Eds. (Springer-Verlag, Berlin, 2002), p. 457.
5. L. A. Levin, Ecology of cold seep sediments: Interactions of fauna with flow, chemistry and microbes. *Oceanogr Mar Biol* **43**, 1 (2005).
6. V. J. Orphan, C. H. House, K. U. Hinrichs, K. D. McKeegan, E. F. DeLong, Multiple archaeal groups mediate methane oxidation in anoxic cold seep sediments. *Proceedings of the National Academy of Sciences of the United States of America* **99**, 7663 (2002).
7. V. J. Orphan, C. H. House, K. U. Hinrichs, K. D. McKeegan, E. F. DeLong, Methane-consuming archaea revealed by directly coupled isotopic and phylogenetic analysis. *Science (New York, NY,* **293**, 484 (2001).
8. A. Boetius *et al.*, A marine microbial consortium apparently mediating anaerobic oxidation of methane. *Nature* **407**, 623 (2000).
9. T. Lösekann *et al.*, Diversity and abundance of aerobic and anaerobic methane oxidizers at the Haakon Mosby mud volcano, Barents Sea. *Applied and Environmental Microbiology* **73**, 3348 (2007).
10. H. Niemann *et al.*, Novel microbial communities of the Haakon Mosby mud volcano and their role as a methane sink. *Nature* **443**, 854 (2006).
11. T. Hoehler, M. Alperin, D. Albert, C. Martens, Field and laboratory studies of methane oxidation in an anoxic marine sediment: Evidence for a methanogen-sulfate reducer consortium. *Global Biogeochemical Cycles* **8**, 451 (1994).
12. S. J. Hallam *et al.*, Reverse methanogenesis: testing the hypothesis with environmental genomics. *Science (New York, NY,* **305**, 1457 (2004).
13. K. G. Lloyd, M. J. Alperin, A. Teske, Environmental evidence for net methane production and oxidation in putative ANaerobic MEthanotrophic (ANME) archaea. *Environmental Microbiology* **13**, 2548 (2011).
14. A. Meyerdierks *et al.*, Metagenome and mRNA expression analyses of anaerobic methanotrophic archaea of the ANME-1 group. *Environmental Microbiology* **12**, 422 (2010).
15. V. J. Orphan *et al.*, Comparative analysis of methane-oxidizing archaea and sulfate-reducing bacteria in anoxic marine sediments. *Applied and Environmental Microbiology* **67**, 1922 (2001).
16. A. Pernthaler *et al.*, Diverse syntrophic partnerships from deep-sea methane vents revealed by direct cell capture and metagenomics. *Proceedings of the National Academy of Sciences of the United States of America* **105**, 7052 (2008).
17. K. Nauhaus, T. Treude, A. Boetius, M. Kruger, Environmental regulation of the anaerobic oxidation of methane: a comparison of ANME-I and ANME-II communities. *Environmental Microbiology* **7**, 98 (2005).

18. K. Nauhaus, A. Boetius, M. Kruger, F. Widdel, In vitro demonstration of anaerobic oxidation of methane coupled to sulphate reduction in sediment from a marine gas hydrate area. *Environmental Microbiology* **4**, 296 (2002).
19. K. Knittel *et al.*, Activity, distribution, and diversity of sulfate reducers and other bacteria in sediments above gas hydrate (Cascadia margin, Oregon). *Geomicrobiology Journal* **20**, 269 (2003).
20. D. L. Valentine, Biogeochemistry and microbial ecology of methane oxidation in anoxic environments: a review. *Antonie van Leeuwenhoek* **81**, 271 (2002).
21. S. Kleindienst, A. Ramette, R. Amann, K. Knittel, Distribution and in situ abundance of sulfate-reducing bacteria in diverse marine hydrocarbon seep sediments. *Environmental Microbiology*, (2012).
22. L. Schreiber, T. Holler, K. Knittel, A. Meyerdierks, R. Amann, Identification of the dominant sulfate-reducing bacterial partner of anaerobic methanotrophs of the ANME-2 clade. *Environmental Microbiology* **12**, 2327 (2010).
23. L. P. Nielsen, N. Risgaard-Petersen, H. Fossing, P. B. Christensen, M. Sayama, Electric currents couple spatially separated biogeochemical processes in marine sediment. *Nature* **463**, 1071 (2010).
24. M. Y. El-Naggar *et al.*, Electrical transport along bacterial nanowires from Shewanella oneidensis MR-1. *Proceedings of the National Academy of Sciences of the United States of America* **107**, 18127 (2010).
25. L. P. Nielsen *et al.*, paper presented at the 14th International Symposium on Microbial Ecology, Copenhagen, Denmark, 2012.
26. A. E. Dekas, R. S. Poretsky, V. J. Orphan, Deep-sea archaea fix and share nitrogen in methane-consuming microbial consortia. *Science (New York, NY,* **326**, 422 (2009).
27. J. Miyazaki *et al.*, Molecular characterization of potential nitrogen fixation by anaerobic methane-oxidizing archaea in the methane seep sediments at the number 8 Kumano Knoll in the Kumano Basin, offshore of Japan. *Applied and Environmental Microbiology* **75**, 7153 (2009).
28. H. Dang, X. Luan, J. Zhao, J. Li, Diverse and novel nifH and nifH-like gene sequences in the deep-sea methane seep sediments of the Okhotsk Sea. *Applied and environmental microbiology* **75**, 2238 (2009).
29. A. E. Dekas *et al.*, Investigating Methane Seep Nitrogen Fixation at Mound 12, Costa Rica: Spatial Distribution of Diazotrophy and Significance of the ANME Archaea. (Chapter 3 of this dissertation).
30. M. P. Mehta, D. A. Butterfield, J. A. Baross, Phylogenetic diversity of nitrogenase (nifH) genes in deep-sea and hydrothermal vent environments of the Juan de Fuca Ridge. *Applied and Environmental Microbiology* **69**, 960 (2003).
31. P. E. Luton, J. M. Wayne, R. J. Sharp, P. W. Riley, The mcrA gene as an alternative to 16S rRNA in the phylogenetic analysis of methanogen populations in landfill. *Microbiology* **148**, 3521 (2002).
32. B. Meyer, J. Kuever, Molecular analysis of the diversity of sulfate-reducing and sulfur-oxidizing prokaryotes in the environment, using aprA as functional marker gene. *Applied and Environmental Microbiology* **73**, 7664 (2007).
33. D. J. Lane, in *Nucleic Acid Techniques in Bacterial Systematics,* E. Stackebrandt, M. Goodfellow, Eds. (John Wiley & Sons, New York, 1991), p. 115.

34. A. Drummond *et al.* Geneious Pro Software (2011).
35. A. E. Dekas, V. J. Orphan, Identification of Diazotrophic Microorganisms in Marine Sediment Via Fluorescence in Situ Hybridization Coupled to Nanoscale Secondary Ion Mass Spectrometry (FISH-NanoSIMS). *Method Enzymol* **486**, 281 (2011).
36. A. Pernthaler, J. Pernthaler, Fluorescence in situ hybridization for the identification of environmental microbes. *Methods Mol Biol* **353**, 153 (2007).
37. A. Pernthaler, J. Pernthaler, R. Amann, Fluorescence in situ hybridization and catalyzed reporter deposition for the identification of marine bacteria. *Applied and Environmental Microbiology* **68**, 3094 (2002).
38. V. J. Orphan *et al.*, Comparative analysis of methane-oxidizing archaea and sulfate-reducing bacteria in anoxic marine sediments. *Applied and Environmental Microbiology* **67**, 1922 (2001).
39. M. G. Pachiadaki, V. Lykousis, E. G. Stefanou, K. A. Kormas, Prokaryotic community structure and diversity in the sediments of an active submarine mud volcano (Kazan mud volcano, East Mediterranean Sea). *FEMS Microbiol Ecol* **72**, 429 (2010).
40. B. K. Harrison, H. Zhang, W. Berelson, V. J. Orphan, Variations in Archaeal and Bacterial Diversity Associated with the Sulfate-Methane Transition Zone in Continental Margin Sediments (Santa Barbara Basin, California). *Applied and Environmental Microbiology* **75**, 1487 (2009).
41. I. Roalkvam *et al.*, Fine-Scale Community Structure Analysis of ANME in Nyegga Sediments with High and Low Methane Flux. *Frontiers in Microbiology* **3**, 216 (2012).
42. I. Roalkvam *et al.*, New insight into stratification of anaerobic methanotrophs in cold seep sediments. *FEMS Microbiol Ecol* **78**, 233 (2011).
43. S. J. Hallam, P. R. Girguis, C. M. Preston, P. M. Richardson, E. F. DeLong, Identification of methyl coenzyme M reductase A (mcrA) genes associated with methane-oxidizing archaea. *Applied and environmental microbiology* **69**, 5483 (2003).
44. H. J. Mills, C. Hodges, K. Wilson, I. R. Macdonald, P. A. Sobecky, Microbial diversity in sediments associated with surface-breaching gas hydrate mounds in the Gulf of Mexico. *FEMS Microbiol Ecol* **46**, 39 (2003).
45. F. Inagaki *et al.*, Characterization of C1-metabolizing prokaryotic communities in methane seep habitats at the Kuroshima Knoll, southern Ryukyu Arc, by analyzing pmoA, mmoX, mxaF, mcrA, and 16S rRNA genes. *Applied and Environmental Microbiology* **70**, 7445 (2004).
46. G. C. Jagersma *et al.*, Microbial diversity and community structure of a highly active anaerobic methane-oxidizing sulfate-reducing enrichment. *Environmental Microbiology* **11**, 3223 (2009).
47. K. G. Lloyd *et al.*, Spatial structure and activity of sedimentary microbial communities underlying a Beggiatoa spp. mat in a Gulf of Mexico hydrocarbon seep. *PloS One* **5**, e8738 (2010).
48. P. R. Girguis, A. E. Cozen, E. F. DeLong, Growth and population dynamics of anaerobic methane-oxidizing archaea and sulfate-reducing bacteria in a

continuous-flow bioreactor. *Applied and Environmental Microbiology* **71**, 3725 (2005).

49. M. Krueger, H. Wolters, M. Gehre, S. B. Joye, H. H. Richnow, Tracing the slow growth of anaerobic methane-oxidizing communities by N-15-labelling techniques. *Fems Microbiology Ecology* **63**, 401 (2008).
50. K. Nauhaus, M. Albrecht, M. Elvert, A. Boetius, F. Widdel, In vitro cell growth of marine archaeal-bacterial consortia during anaerobic oxidation of methane with sulfate. *Environmental Microbiology* **9**, 187 (2007).
51. V. J. Orphan, K. A. Turk, A. M. Green, C. H. House, Patterns of ^{15}N assimilation and growth of methanotrophic ANME-2 archaea and sulfate-reducing bacteria within structured syntrophic consortia revealed by FISH-SIMS. *Environmental Microbiology*, (2009).
52. H. Imachi *et al.*, Non-sulfate-reducing, syntrophic bacteria affiliated with desulfotomaculum cluster I are widely distributed in methanogenic environments. *Applied and Environmental Microbiology* **72**, 2080 (2006).
53. M. Alperin, T. Hoehler, Anaerobic methane oxidation by archaea/sulfate-reducing bacteria aggregates: 1. Thermodynamic and physical constraints. *American Journal of Science* **309**, 869 (2009).
54. C. H. House *et al.*, Extensive carbon isotopic heterogeneity among methane seep microbiota. *Environmental Microbiology* **11**, 2207 (2009).
55. J. Raymond, J. L. Siefert, C. R. Staples, R. E. Blankenship, The natural history of nitrogen fixation. *Molecular Biology and Evolution* **21**, 541 (2004).
56. I. Pagani *et al.*, Complete genome sequence of Desulfobulbus propionicus type strain (1pr3). *Standards in Genomic Sciences* **4**, 100 (2011).
57. D. Alperin, W. S. Reeburgh, Inhibition experiments on anaerobic methane oxidation. *Applied and Environmental Microbiology*, 940 (1985).
58. A. J. B. Zehnder, T. D. Brock, Methane Formation and Methane Oxidation by Methanogenic Bacteria. *Journal of Bacteriology* **137**, 420 (1979).
59. R. S. Oremland, D. G. Capone, Use of Specific Inhibitors in Biogeochemistry and Microbial Ecology. *Advances in Microbial Ecology* **10**, 285 (1988).
60. R. K. Thauer, Biochemistry of methanogenesis: a tribute to Marjory Stephenson. *Microbiol—UK* **144**, 2377 (1998).
61. S. Scheller, M. Goenrich, R. Boecher, R. K. Thauer, B. Jaun, The key nickel enzyme of methanogenesis catalyses the anaerobic oxidation of methane. *Nature* **465**, 606 (2010).
62. M. Strous, in *Handbook of Hydrocarbon and Lipid Microbiology,* K. N. Timmis, Ed. (Springer-Verlag, Berlin, 2010), p. 3078.
63. B. Orcutt, V. Samarkin, A. Boetius, S. Joye, On the relationship between methane production and oxidation by anaerobic methanotrophic communities from cold seeps of the Gulf of Mexico. *Environmental Microbiology* **10**, 1108 (2008).
64. M. Goenrich *et al.*, Probing the reactivity of Ni in the active site of methyl-coenzyme M reductase with substrate analogues. *J Biol Inorg Chem* **9**, 691 (2004).
65. C. Heller, M. Hoppert, J. Reitner, Immunological localization of coenzyme M reductase in anaerobic methane-oxidizing archaea of ANME 1 and ANME 2 type. *Geomicrobiology Journal* **25**, 149 (2008).

66. T. Holler *et al.*, Carbon and sulfur back flux during anaerobic microbial oxidation of methane and coupled sulfate reduction. *Proceedings of the National Academy of Sciences of the United States of America* **108**, E1484 (2011).

SI Table 1. PCR conditions used in this study.

Target Gene	Primers	Sample	Step 1	Step 2	Step 3	Step 4	Step 5	Cycles of Steps 2-4
nifH	10aa and 13aa (ref)	CR15, CR17	94, 2 min	94, 20 s	62, 30 s	72, 40 s		1
				94, 20 s	61, 30 s	72, 40 s		1
				94, 20 s	60, 30 s	72, 40 s		2
				94, 20 s	59, 30 s	72, 40 s		2
				94, 20 s	58, 30 s	72, 40 s		2
				94, 20 s	57, 30 s	72, 40 s		2
				94, 20 s	56, 30 s	72, 40 s		2
				94, 20 s	55, 30 s	72, 40 s		2
				94, 20 s	54, 30 s	72, 40 s		2
				94, 20 s	53, 30 s	72, 40 s		2
				94, 20 s	52, 30 s	72, 40 s	72, 5 min	35
mcrA		CR15, CR17	94, 2 min	94, 1 min	50, 1 min	72, I min	72, 5 min	35
aprA		CR15, CR17	94, 3 min	94, 30 s	55, 55 s	72, 45 s	72, 6 min	35 (DNA), 40 (cDNA)
16S rRNA	8F and 1492 R	CR15, CR17	94, 2 min	94, 30 s	54 1 min	72, 1:30 min	72 5 min	26

C h a p t e r 5

Investigating the Biogeochemical Controls on Deep-Sea Diazotrophy and Its Significance to Local and Global Ecosystems

Anne E. Dekas[1], Grayson Chadwick[1], Stephanie A. Connon[1], David Fike[2], Dwight McCay[2], Abigail Green-Saxena[1], Nathan Dalleska,[1] and Victoria J. Orphan[1]

[1]*California Institute of Technology, Pasadena, CA 91106*
[2]*Washington University at St. Louis, St. Louis, MO 63130*

ABSTRACT

Nitrogen fixation, or diazotrophy, the conversion of N_2 to NH_3, is critical to both alleviating nitrogen limitation in terrestrial and pelagic ecosystems and closing the loop of the nitrogen cycle. However, little is known about N_2 fixation in the deep-sea, a habitat covering the majority of the planet and hosting several climactically relevant microbial metabolisms. To explore the magnitude, distribution, and biogeochemical controls on N_2 fixation in deep sediments, we conducted over four hundred microcosm experiments amended with either $^{15}N_2$ or $^{15}NH_4^+$, using 50 diverse sediment samples, including methane seep, whale-fall, and undisturbed (background) sediments from down to 2893 m water depth. We observed nitrogen fixation within each sample investigated, and at rates higher than those previously reported for the deep-sea (up to 3.24 $x10^{-2}$ nmol N_2 g_{dwt}^{-1} hr^{-1} averaged over 13 months). N_2 fixation contributed on average 6% and up to 39% of the community nitrogen growth requirement, demonstrating that it is a significant nitrogen source to some benthic communities. N_2 fixation was heterogeneously distributed and dependent on the addition of CH_4 in seep sediments, consistent with previous work showing that diazotrophy is mediated primarily by methanotrophs and/or physically associated symbionts in spatially constricted sediment depth horizons (Chapter 3). Diazotrophy was only minimally enhanced by the addition of CH_4 in whale-fall and background cores. The decreased CH_4 dependency combined with evidence for sulfate-reduction and methanogenesis in these experiments suggests that diverse microbes may be responsible for diazotrophy in the whale-fall and background samples. To determine the geochemical controls on diazotrophy, an ammonia inhibition experiment was carried out, and demonstrated an inhibition of nitrogen fixation by high levels of ammonium (> 288 μM) in methane seep sediment. Combined, our data suggest that benthic diazotrophy is carried out by a diverse and well-distributed group of bacteria and archaea, and its distribution and magnitude is greater than previously realized.

INTRODUCTION

Deep-sea sediments represent an enormous habitat for microbial life, hosting up to 10,000 more microbial cells per unit volume than surface marine waters, and covering approximately 2/3 of the entire planet (*1*). Within these sediments heterotrophic bacteria act as the final goalie preventing organic carbon burial, and localized communities of diverse autotrophs cycle carbon, nitrogen and sulfur at potentially globally relevant rates. Despite the suite of chemical conversions catalyzed in this habitat, the deep-sea is among the most under-studied habitats on Earth, due to sampling and experimental difficulties (*2*). Nitrogen cycling in these locales, and particularly whether or not the sediments act as a net source or a net sink of bioavailable nitrogen (e.g., ammonium), is unknown. The marine nitrogen cycle, and particularly the sources of sinks of ammonium, are currently the subject of much debate, as underappreciated sources are realized, methodologies are re-evaluated, and flux estimates are dramatically revised (*3–7*). Understanding the role of marine sediments, and particularly the abundant deep marine sediments (here defined as > 100 m), in marine nitrogen cycling is therefore a timely pursuit, contributing to a much larger discussion on whether or not the marine nitrogen cycle is balanced (*8–11*).

In the current work, we investigate nitrogen fixation, the biological conversion of relatively inert N_2 to bioavailable NH_3, in a subset of this expansive habitat. In addition to a potential contribution to the marine nitrogen cycle, deep-sea diazotrophy may alleviate nitrogen limitation in areas of enhanced productivity in the benthos, thereby affecting the rate of localized microbial metabolisms. Although growth in marine sediments is typically assumed to be limited by the slow deposition of organic matter (*1*), a handful of reports in the last ten years have described findings consistent with localized nitrogen

limitation in the deep-sea: a diazotrophic methanogen was isolated from a hydrothermal vent (*12*), methanotrophic archaea abundant at cold methane seeps were shown to fix nitrogen (*13*), and a long list of *nifH* sequences, those involved in nitrogen fixation, were detected at vents, seeps and mud volcanoes (*14–16*). Nitrogen fixation is considered a response to nitrogen limitation because it is typically only mediated if other sources of nitrogen are not present. Requiring approximately 16 ATP per mol of N_2 fixed, nitrogen fixation is typically an expensive last resort to obtain nitrogen for growth (*17*). If deep-sea nitrogen fixation is extensive, our understanding of what limits the rate of benthic metabolisms, as well as the calculated sources of ammonium to the marine nitrogen cycle, may change. Alternatively, if the deep-sea is replete with nitrogen sources, and diazotrophy is scarce, why such a diversity of *nifH* genes are maintained, at least some of which are functional, becomes an equally intriguing question.

Although the recent molecular evidence suggests substantial deep-sea nitrogen fixation, at least at localized areas of enhanced productivity, few direct measurements of nitrogen fixation rates have been made in deep-sea sediments, making it difficult to assess the impact of this metabolism locally or globally. In 1978 Hartwig and Stanley reported negligible rates of nitrogen fixation in abyssal sediment measured by the acetylene reduction assay (*18*), which is known to inhibit many microorganisms abundant in benthic environments (*19, 20*). More recently, Dekas and colleagues measured nitrogen fixation in methane seep sediment via $^{15}N_2$-uptake at rates over an order of magnitude greater than those observed by Hartwig and Stanley, and similar to those measured in coastal benthic environments (Chapter 3). Dekas and colleagues found diazotrophy to be extremely heterogeneously distributed within seep sediment, with

intriguing peaks of nitrogen fixation with depth in the sediment, and much greater rates of nitrogen fixation within the seep sediment than within background sediments. However, only a small number of samples at a single methane seep were investigated, and further investigation was deemed necessary to explore the distribution of diazotrophy within methane seep cores, as well as establish whether or not methane seeps were truly hotspots of nitrogen fixation in the deep-sea.

The work presented here follows up on and expands upon the observations presented in Chapter 3 by examining a much larger and more diverse sample set, with a focus on the biogeochemical controls regulating the heterogeneous distribution of nitrogen fixation. A total of six deep-sea environments were investigated, including three methane seeps (Hydrate Ridge North, Hydrate Ridge South, and Monterey Canyon), and three sites of sunk whale carcasses (hereafter referred to as whale-falls), at depths of 600 to nearly 3,000 m. The whale-fall sites were included in the study because as discussed in Chapter 3, methane seeps may represent preferentially N-limited environments, due to the input of carbon unaccompanied by nitrogen, similar to that experienced in other communities dominated by autotrophs. Whale biomass is a source of both carbon and nitrogen to the seafloor, allowing us to test whether methane seeps host enhanced nitrogen fixation because they relieve carbon and electron donor limitation, or because their balance of carbon and nitrogen is tipped to the point of nitrogen limitation by the addition of carbon without nitrogen. Interestingly, previous studies in coastal environments have shown that the addition of complex organic matter favors net denitrification over nitrogen fixation (*6*), suggesting that nitrogen fixation rates beneath whale-falls may be lower than those in background sediments. At each site, samples were

also collected 1 to 13,000 m away from the sites of carbon loading to compare the rates of diazotrophy at methane seeps and whale-falls to that of background sediment, and assess the significance of nitrogen fixation in undisturbed seafloor.

A series of experiments were employed to assess potential nitrogen limitation in deep-sea sediments, as well as metabolic activity in varying geochemical conditions. Concentrations of ammonium and nitrate were measured at each site at varying distances from the centers of carbon loading, to directly measure the availability of nitrogen in benthic ecosystems. Microcosm experiments using labeled $^{15}N_2$ and $^{15}NH_4^+$ were employed to measure rates of nitrogen fixation and total protein synthesis (a proxy for total potential growth), as well as sulfate reduction, methanogenesis, and the anaerobic oxidation of methane. The microcosm experiments were carried out using sediment from a total of ten 15-cm-long push-cores, at 3-cm-depth resolution, totaling 50 discrete sediment samples, to acquire a 3-D perspective of microbial activity. Finally, rates of nitrogen fixation are compared to incubation and *in situ* biogeochemical parameters, allowing an assessment of which microbial communities might dominate diazotrophy at the different sites. This study addresses the magnitude and distribution of diazotrophy in geochemically diverse habitats, and builds upon our knowledge of more well-studied carbon and sulfur metabolisms in these productive deep-sea environments.

EXPERIMENTAL PROCEDURES

Site Descriptions. Hydrate Ridge (HR) is one of a series of accretionary ridges along the Cascadia convergent margin. The ridge is about 25 km long and 15 km wide and extends approximately 600 m above the seafloor. The northern peak reaches 600 m water depth,

and is characterized by carbonate pavement, while the southern peak reaches a slightly lower 800 m water depth, with a primarily sedimentary surficial cover. Fluid and methane flow upward from deeper sediments through faults, supplying the surficial ecosystems with methane, and either destabilizing shallow hydrates and causing additional methane advection or forming secondary hydrates (*21–23*). Both HR north and south host benthic communities typical of methane seeps, including sulfide-oxidizing microbial mats (*Beggiatoa sp.*) and clam fields (*Calyptogena sp.*) (*21, 24*).

Monterey Canyon extends west out of Monterey, CA, and contains a diverse array of benthic environments, including methane seeps (*25, 26*), whale-falls (*27*), and undisturbed background sediments. Whale-fall 2983 (cores from which are referred to here as W1), a 10 m Gray whale, was discovered in February of 2002 and is estimated to have naturally fallen approximately 1 year prior (*28*). This discovery spurred interest in the study of the transient ecosystems associated with sunken marine mammals, and subsequently five beached whales were additionally towed out to sea and sunk for the purpose of scientific research. Whale-fall 633 (cores from which are referred to here as W2), also a 10 m Gray whale, was sunk in April 2007. Whale-fall 1018 is a headless (head was removed prior to deposition) 17 m long blue whale, implanted in October of 2004. Whale-falls 633 and 1018 are located in the Monterey Canyon oxygen minimum zone, defined by oxygen values below 0.5 ml/L. The whale-falls host diverse and dynamic microbial and macrofaunal populations, described in (*27–31*). The methane seeps in Monterey Canyon are described as hosting a range of seep-associated macrofauna, including sulfide-oxidizing microbial mats (*Beggiatoa sp.*), clam fields (*Calyptogena sp.*), and vestimeniferan worms (*Lamellibrachia sp.*). The site chosen for

sampling in the current study was characterized primarily by the presence of *Calyptogena*.

Sample Collection. Twenty-one push cores from Hydrate Ridge were collected on R/V Atlantis cruise AT 15-68 in July–August of 2010 using DSV *Alvin,* owned by the US Navy and operated by the Woods Hole Oceanographic Institute (WHOI). Thirteen push cores from Monterey Canyon were collected using ROV *Doc Ricketts,* owned and operated by the Monterey Bay Aquarium Research Institute (MBARI) in October 2010. Each core was visually identified as one of three types of sediment: methane-rich (indicated by microbial mats of sulfide-oxidizing bacteria or the presence of clams), whale-fall (under or immediately adjacent to whale bones), or background (no surficial features). These classifications were confirmed by subsequent geochemical analysis of the sediment pore water where possible. Exact sampling sites and descriptions are listed in SI Table 1, and maps can be found in SI Figure 1. Cores were sub-sampled in 1, 3, or 5 cm increments with depth, and stored within whirlpaks in mylar bags flushed with argon for 2–5 days after collection.

Determination of bioavailable nitrogen concentrations. To investigate the extent of potential nitrogen limitation on the deep-sea floor, a survey of 30 sediment push cores was conducted, including 13 from Monterey Canyon and 17 from Hydrate Ridge (see SI Table 1 and SI Figure 1 for sampling locations). Push core pore water squeezed from sediments immediately after collection was filtered via a 0.2 μm filter and frozen until analysis. Parallel ion chromatography systems operated simultaneously (Dionex DX-500,

Environmental Analysis Center, Caltech) were used to measure ammonium, nitrate, nitrite and sulfate in the pore water samples. A single autosampler loaded both systems' sample loops serially. The 10 microliter sample loop on the anion IC system was loaded first, followed by a 5 microliter sample loop on the cation IC system. Temperatures of the columns and detectors were not controlled.

Nitrite, nitrate and sulfate were resolved from other anionic components in the sample using a Dionex AS-19 separator (4 x 250mm) column protected by an AG-19 guard (*4 x 50 mm). A hydroxide gradient was produced using a potassium hydroxide eluent generator cartridge and pumped at 1 mL per minute. The gradient began with a 10 mM hold for 5 minutes, increased linearly to 48.5 mM at 27 minutes and finally to 50 mM at 41 minutes. 10 minutes were allowed between analyses to return the column to initial conditions. Nitrite and nitrate were determined for UV absorption at 214 nm using a Dionex AD25 Absorbance detector downstream from the conductivity detection system. Suppressed conductivity detection using a Dionex ASRS-300 4mm suppressor operated in eluent recycle mode with an applied current of 100 mA was applied to detect all other anions, including redundant measurement of nitrite and nitrate. A carbonate removal device (Dionex CRD 200 4mm) was installed between the suppressor eluent out and the conductivity detector eluent in ports.

Ammonium was resolved from other cationic components using a Dionex CS-16 separator column (5 x 250 mm) protected by a CG-16 guard column (5x50). A methylsulfonate gradient was produced using a methylsulfonic acid based eluent generated cartridge and pumped at 1 mL per minute. The gradient began with a 10 mM methylsulfonate hold for 5 minutes, then increased to 20 mM at 20 minutes following a

nonlinear curve (Chromeleon curve 7, concave up), increased further to 40 mM at 41 minutes following a nonlinear curve (Chromeleon curve 1, concave down). 10 minutes were allowed between analyses to return the column to initial conditions. Suppressed conductivity detection using a Dionex CSRS-300 4mm suppressor operated in eluent recycle mode with an applied current of 100 mA.

Standard curves were generated for each species. For nitrate, nitrite, and sulfate, standard measurements were fitted to a linear curve; for ammonium, standard measurements were fitted to a quadratic curve. Standard ranges were 10 uM to 2 mM (nitrate, nitrite, ammonium) and 500 uM to 32 mM (sulfate). Standard deviation of repeated injections of a standard (250 uM ammonium, nitrate and nitrite, 8000 uM sulfate) throughout the analysis were 5.0 uM (ammonium), 4.2 uM (nitrate), 5.8 uM (nitrate) and 113 uM (sulfate).

Bioavailable nitrogen concentrations were also quantified in the microcosm experiments (see below) at the beginning and end of the incubation. For each set of incubations aliquoted from a single homogenized sediment slurry, only one t=0 measurement was collected. Sub-sampled slurry was centrifuged briefly (~ 15 s) to pellet the sediments and the supernatant removed, filtered, stored and processed via IC as described above.

^{15}N-Labeling microcosm experiment setup and sub-sampling. Five push-cores from each of Hydrate Ridge (from 3 microbial mat, HR-M1, HR-M2, and HR-M3, 1 clam bed, HR-C, and 1 background site, HR-B) and Monterey Canyon (from 2 whale-fall, MC-W1 and MC-W2, 1 clam bed, MC-C, and 2 off-whale sites, MC-B1 and MC-B2) were selected

for microcosm incubations (core descriptions in SI Table 1, incubation descriptions in Tables 1 and 2). Cores were divided into five 3-cm-thick depth horizons, and each section was mixed 1:1 with argon-sparged filtered bottom water collected near the sediment sampling site. 20–25 ml of slurry from each core depth horizon was aliquoted into each of ten 60 ml serum bottles either within an anaerobic chamber (MC incubations) or at the bottom of an argon-filled bucket (HR incubations). Bottles were sealed with butyl stoppers and aluminum crimp caps. The headspaces were flushed and replaced with Ar or CH_4. The MC incubations were pressurized to 30 psi by adding additional Ar or CH_4 immediately after setup. The HR incubations were pressurized with additional gas only after 27 days, due to restrictions on traveling with over-pressured methane. Immediately after setup, 5 ml N_2 was added to each incubation; for the $^{15}N_2$-labeling experiments, 50% of the added N_2 was ^{15}N-labeled. For $^{15}NH_4^+$ incubations, $^{15}NH_4Cl$ was added to a final concentration of 1 mM. The 10 incubations from each core depth were therefore amended with either Ar or CH_4 headspaces, plus either $^{15}N_2$ or $^{15}NH_4Cl$, resulting in $^{15}N_2$ plus CH_4 or Ar incubations in triplicate, and $^{15}NH_4^+$ plus CH_4 or Ar incubations in duplicate. A total of 228 (MC) and 192 (HR) incubations were prepared.

Bottles were incubated at 4˚C, and sub-samples were taken at t=0, 34 days (1.1 months), 111 days (3.6 months), 258 days (8.3 months) and 401 days (12.9 months) for the Hydrate Ridge incubations, and at t=0, 66 days (2.1 months), 200 days (6.5 months) and 411 days (13.3 months) for the Monterey Canyon incubations. A total of approximately 2.5 ml of slurry was removed via syringe at each time point, after shaking the bottle to homogenize the slurry, with fractions fixed with 2% paraformaldehyde (500 µl slurry plus 1 ml PFA, 4˚C overnight, two washes with PBS, PBS+EtOH, and final re-

suspension in EtOH), frozen at -80˚C (1 ml), or centrifuged briefly before freezing both liquid supernatant (500–1000 μl) and pelleted sediment (200–500 μl) separately at -20˚C.

For the ammonium inhibition experiment, sediment from core HR-AI, 0-12 cm, was homogenized with Ar-sparged filtered bottom water in an anaerobic chamber. Approximately 29 ml of slurry was aliquoted into each of fourteen 60 ml bottles. The bottles were amended with $^{15}NH_4^+$ at different levels, and a headspace of CH_4 or Ar at 30 psi. Bottles were sub-sampled at t=0, and incubated for 236 days (7.6 months) at 4˚C.

Bulk $\delta^{15}N$ isotopic analysis and TN. Sediment slurry sub-samples of each microcosm experiment were centrifuged briefly after removal via syringe, the supernatant removed (to remove additional salts) and frozen at -20˚C. At the end of the experiment, frozen sediment pellets from unique incubation conditions were re-suspended in nanopure water, pipetted into tin cups, and dried overnight. For samples incubated with $^{15}NH_4^+$, sediment was washed before drying as described in (*32*). Cups were weighed, crimped and analyzed on a Costech Elemental Analyzer coupled to a Delta V Isotope Ratio Mass Spectrometer (EA-IRMS) at Washington University in St. Louis. Instrumental precision on the standards was < 0.2‰ (standard deviation). The average difference between replicate samples of $^{15}N_2$-incubated sediment was 8.6‰ (4.47% of the $\delta^{15}N$ value, n=6 pairs) and of $^{15}NH_4^+$-incubated sediment was 143.0‰ (7.15% of the $\delta^{15}N$ value, n=11 pairs). Larger variations were observed between replicates of higher $\delta^{15}N$, likely due to spatial heterogeneity in sample activity and incomplete homogenization before sampling. Comparison of replicate bottle incubations of the same incubation conditions showed 3.2% variability in $^{15}N_2$ incubations (n=1 pair) and 16.9% variability in $^{15}NH_4^+$

incubations (n=2 pairs). More measurements of replicate bottles need to be carried out to constrain the variability between bottles. No increase in $\delta^{15}N$ was observed in control experiments of MC sediment with no ^{15}N-source added, in either live (n=2) or dead (autoclaved) (n=2) sediments, however killed samples (autoclaved or amended with 0.05% $HgCl_2$) incubated with either $^{15}N_2$ or $^{15}NH_4^+$ displayed approximately 5–15% of the ^{15}N-enrichment observed in paired live samples. This is likely due to incomplete inactivation of the microbial communities.

Nitrogen Fixation and Total Potential Growth. Atom% ^{15}N enrichment values obtained by EA-IRMS analysis (see above) at t=0 and t=258 days (8.3 months, HR) or t=411 days (13.3 months, MC) were converted to rates of nitrogen fixation and total potential growth based on the equations in (*33*). ^{15}N-uptake from $^{15}NH_4^+$ has been used previously as a proxy for total protein synthesis, and therefore total potential growth, in environments with slow-growing, uncultured organisms (*34, 35*). There was assumed to be no N_2 or NH_4^+ present at the start of the incubation other than what was added; an assumption likely leading to underestimates in both rate calculations. The initial concentration of N_2 was likely low, because the filtered seawater added to the incubations was sparged with Ar. The only N_2 present therefore would have been that dissolved in the pore water, but when homogenized with the filtered seawater this would have been severely diluted. Pore water NH_4^+ would have been similarly diluted. Assuming a porosity of 50%, a 200 μM initial concentration would be diluted to approximately 66 μM in the incubation slurry, which would in turn dilute the ^{15}N-label of the $^{15}NH_4^+$ by 6–7%.

nifH clone library and phylogenetic analysis of sequences. DNA was extracted from a sub-sample of the homogenized sediment slurry of HR-AI (a microbial mat core used for the ammonium inhibition experiment) before aliquots were taken for individual incubations using the Ultraclean Soil DNA Isolation Kit (MoBio Laboratories, CA) as in (*13*). *nifH* gene sequences were amplified with primers modified from (*14*) to include inosine in place of triplicate and quadruplicate degeneracies (nifHfa10aa_5i:GGIAARGGIGGIATIGGIAARTC, nifHra132aa_4i:GGCATIGCRAAICCICCRCAIAC, ordered from Integrated DNA Technologies, Inc.). Three parallel PCRs were performed with HotMaster Taq DNA Polymerase (5 PRIME, Inc., MD) with the following program: 2 min 94°C; 25 cycle of 30 s 94°C, 30 s 55°C, 1 min 72°C; 10 min 72°C. All three PCRs were pooled and cleaned with a Multiscreen Filter Plate for PCR cleanup (Millipore, MA), and cloned into the TOPO TA Cloning Kit for Sequencing (Invitrogen, CA). 37 clones were sequenced by Laragen, Inc., (Culver City, CA) using the T7 vector primer.

The *nifH* subgroup assignments were determined by a multiple sequence alignment of the amino acid sequences and subgroup reference sequences followed by phylogenetic tree construction in the Geneious software package (publically available at http://www.geneious.com/) (*36*). Alignment was performed by the Geneious alignment method with the Blosum62 cost matrix and default gap penalties. Tree construction employed the Jukes-Cantor genetic distance model and the Neighbor-Joining tree building method with 1000 bootstrap replicates. All the sequences from HR-AI clustered within previously described *nifH* groups [Fig. S2, (*13*)].

Determination of Sulfate Concentrations and Total Bacterial Sulfate Reduction. To measure the extent of bacterial sulfate reduction (SR) occurring in the incubated sediment, sulfate concentrations were measured at the beginning and end of the incubation experiment. Sulfate was measured via IC in the same samples collected for bioavailable nitrogen, as described above. Total bacterial sulfate reduction was determined by difference between the final concentration of sulfate and the initial. Although the anaerobic oxidation of sulfide back to sulfate via nitrate is possible, nitrate concentrations in both the HR and MC incubations were low (below the detection limit, data not shown), eliminating this possibility here.

Determination of AOM . Comparison of sulfate reduction between paired incubations with and without methane added revealed the amount of sulfate reduction dependent on methane. The approximate rate of the anaerobic oxidation of methane (AOM) was therefore determined assuming a 1:1 coupling of methane oxidation and methane-dependent sulfate reduction (*37*). Because of the possibility of methanogenesis in the incubations without methane added, the calculation of methane-dependent sulfate reduction is likely an underestimate, resulting in an underestimate of AOM, as well.

Determination of Sulfide Concentrations. Pore water squeezed from sediments immediately after extrusion from the push core liner was mixed 1:1 with zinc acetate and stored at RT until analysis for sulfide via the Cline Assay (*38*). A spectrophotometer in 96-well plate reader format was used to quantify the chlorometric reaction. The average

of three reads for each reaction was compared to a standard curve prepared from fresh $Na_2S{\cdot}9H_2O$ salts in filtered seawater with the same concentration of zinc acetate.

RESULTS

Total Nitrogen (TN) and $\delta^{15}N$ of Sediments

Sediment sampled directly from Hydrate Ridge (HR) and Monterey Canyon (MC) push cores (before incubation) contained total nitrogen (TN) concentrations of 0.12–0.42% and 0.09–0.35% respectively, and $\delta^{15}N$ values of 4.7–9.1‰ and 5.1–11‰, respectively, (Tables 1 and 2). At HR microbial mat sites (n=3), TN was universally lower than in a background core collected almost 13 km from known methane seepage. In the mat cores, TN was often greatest in the most surficial depth horizon, with a minimum mid-core, and a subsequent increase in the lower depths. The highest TN at HR was observed at the clam field, at 0.42% in sediment from 0–3 cm and decreasing to 0.21% in sediment from 12–15 cm. The surficial elevation above background at the clam site could be due to the macrofaunal biomass. The background core contained 0.27% nitrogen and did not vary with depth.

In Monterey Canyon, surficial sediments beneath Whale-fall 2983 were elevated in TN despite the 9 year time lapse since whale deposition, at 0.35% N (0–3 cm, MC-W1) compared to approximately 0.20% TN in a core collected 28 m from the whale (0–15 cm, MC-B1). And although the N content of the background core remained relatively constant with depth the N content beneath Whale-fall 2983 decreased to 0.10% at 9–12 cm before increasing again to 0.18% at 12–15 cm. Although more recently deposited (3 years before sampling), surficial sediment under Whale-fall 633 was only minimally

Table 1. Metabolic Activity in Mesocosm Experiments of Hydrate Ridge Sediment. Homogenized sediment slurry was divided into incubations bottles amended with methane or argon and $^{15}N_2$ or $^{15}NH_4^+$. bdl = below detection limit; adl = above detection limit (for $[NH_4^+]$ the upper detection limit is 2 mM)

						$^{15}N_2$-Ammended Incubations									$^{15}NH_4$-Ammended Incubations			
						SO_4^{2-} and CH_4 Metabolism			$[NH_4^+]$				N_2 Fixation			Estimates of Potential Total Growth			
Incubation Set-up			*in situ* Sed Geochem																
Core	Depth (cmbsf)	Headspace	$[NH_4^+]$ (mM)	TN (wt%)	$\delta^{15}N$ (‰)	SO_4^{2-} Reduction (mM)	SO_4^{2-} Reduction Dependent on CH_4 (%)	Estimated CH_4 Consumed via AOM (mM)	$[NH_4^+]_{t=0}$ (mM)	$[NH_4^+]_{final}$ (mM)	$[NH_4^+]_{avg}$ (mM)	Change in $[NH_4^+]$ (mM)	Rate of N_2 Fixation (nmol N_2 g dry wt sed^{-1} hr^{-1})	Quantity of N_2 Fixed (nmol N_2 g dry wt sed^{-1})	N_2 fixation Dependent on CH_4 (%)	Rate of NH_4^+ Assimilation (nmol NH_4^+ g dry wt sed^{-1} hr^{-1})	Quantity of NH_4^+ Assimilated (nmol NH_4^+ g dry wt sed^{-1})	NH_4^+ Assimilation Dependent on CH_4 (%)	N Assimilated from N_2 versus NH_4^+ (%)
HR-M1	0-3	CH_4	306.7	0.22%	7.8	28.0	78.0	21.8	496.1	1102.8	799.5	606.7	1.58E-05	0.2	100.0	1.35E-01	1328.1	50.8	0.0
HR-M1	0-3	Ar				6.1			496.1	1163.0	829.5	666.9	bdl	bdl		6.62E-02	653.2		0.0
HR-M1	3-6	CH_4	251.9	0.16%	7.5	25.4	84.8	21.6	155.7	bdl	77.9	-155.7	1.66E-02	163.9	99.9	2.14E-01	2115.6	86.2	15.5
HR-M1	3-6	Ar				3.9			155.7	152.3	154.0	-3.4	1.43E-05	0.1		2.96E-02	291.6		0.1
HR-M1	6-9	CH_4	197.8	0.15%	7.5	3.6	27.0	1.0	142.2	31.1	86.6	-111.1	8.38E-05	0.8	100.0	2.97E-02	292.9	26.7	0.6
HR-M1	6-9	Ar				2.6			142.2	39.2	90.7	-103.0	bdl	bdl		2.18E-02	214.7		0.0
HR-M1	9-10	CH_4	141.4	0.18%	8.9				14.5				3.53E-04	3.5	100.0				
HR-M1	9-10	Ar							14.5				bdl	bdl					
HR-C	0-3	CH_4	23.5	0.42%	9.1				33.3				6.75E-05	0.7	100.0	3.55E-01	3500.2	72.5	0.0
HR-C	0-3	Ar							33.3				bdl	bdl		9.76E-02	962.7		0.0
HR-C	3-6	CH_4	32.5	0.39%	8.9	28.0	79.3	22.2	40.1	367.0	203.6	326.9	1.08E-05	0.1	100.0	2.16E-01	2131.7	57.4	0.0
HR-C	3-6	Ar				5.8			40.1				bdl	bdl		9.21E-02	908.1		0.0
HR-C	6-9	CH_4	35.0	0.33%	8.5	28.0	81.3	22.8	37.0	57.3	47.1	20.4	1.86E-02	183.4	99.9	2.22E-01	2185.4	76.5	16.8
HR-C	6-9	Ar				5.2			37.0	145.1	91.0	108.1	2.42E-05	0.2		5.20E-02	513.2		0.1
HR-C	9-12	CH_4	49.2	0.26%	8.6	27.9	83.1	23.2	88.4	10.0	49.2	-78.4	1.33E-02	131.6	99.5	1.99E-01	1962.9	84.5	13.4
HR-C	9-12	Ar				4.7			88.4	98.6	93.5	10.2	6.46E-05	0.6		3.09E-02	304.6		0.4
HR-C	12-15	CH_4	61.2	0.21%	8.4	27.8	83.8	23.3	80.8	bdl	40.4	-80.8	2.35E-02	231.5	100.0	1.85E-01	1825.7	48.7	25.4
HR-C	12-15	Ar				4.5			80.8	86.0	83.4	5.2	bdl	bdl		9.49E-02	936.4		0.0
HR-M2	0-3	CH_4	75.3	0.14%	6.1	27.6			357.1	1329.0	843.0	971.9	1.25E-04	1.2	52.2				
HR-M2	0-3	Ar							357.1				5.98E-05	0.6					
HR-M2	3-6	CH_4		0.12%	6.1	27.8			23.9	107.3	65.6	83.5	1.05E-04	1.0	0.0				
HR-M2	3-6	Ar							23.9				1.37E-04	1.4					
HR-M2	6-9	CH_4				19.3			11.0	96.3	53.7	85.3	*2.44E-04*	*2.4*	50.3				
HR-M2	6-9	Ar							11.0				*1.21E-04*	*1.2*					
HR-M2	9-12	CH_4		0.12%	5.9	4.0			12.4	114.0	63.2	101.6	2.37E-04	2.3	11.8				
HR-M2	9-12	Ar							22.0				2.09E-04	2.1					
HR-M2	12-15	CH_4		0.13%	4.7	3.6			6.5	94.9	50.7	88.4	3.01E-04	3.0	70.4				
HR-M2	12-15	Ar							6.5				8.90E-05	0.9					
HR-B	0-5	CH_4	5.2	0.27%	8.6	4.4	32.7	1.5	20.7	95.2	57.9	74.4	1.67E-02	164.4	88.6	8.62E-02	850.2	1.9	38.7
HR-B	0-5	Ar				3.0			20.7	81.0	50.9	60.3	1.90E-03	18.7		8.46E-02	834.2		4.5
HR-B	5-10	CH_4	27.6	0.27%	8.6	2.9	38.9	1.1	23.1	44.8	34.0	21.7	4.33E-03	42.7	98.8	4.83E-02	476.5	11.2	17.9
HR-B	5-10	Ar				1.8			23.1	57.1	40.1	34.0	5.13E-05	0.5		4.29E-02	423.1		0.2
HR-B	10-15	CH_4	29.1	0.27%	8.5	0.6	0.0	-0.1	22.8	46.3	34.5	23.5	3.20E-04	3.2	0.0	3.61E-02	356.4	4.5	1.8
HR-B	10-15	Ar				0.7			22.8	38.0	30.4	15.2	9.95E-05	1.0		3.45E-02	340.2		0.6
HR-B	15-20	CH_4	29.4	0.26%	8.5	0.9	0.0	-0.1	25.5	36.8	31.1	11.3	1.29E-04	1.3	0.0	3.98E-02	392.6	18.1	0.7
HR-B	15-20	Ar				1.0			25.5	40.5	33.0	15.1	1.31E-05	0.1		3.26E-02	321.6		0.1
HR-M3	0-3	CH_4	265.7	0.17%	5.1	22.5	70.0	15.8	691.8	adl		+	1.85E-04	1.8	24.4				
HR-M3	0-3	Ar				6.8			691.8	adl		+	1.40E-04	1.4					
HR-M3	3-6	CH_4	298.9	0.12%	6.7	21.6	87.7	18.9	116.0	0.0	58.0	-116.0	3.02E-03	29.8	88.8				
HR-M3	3-6	Ar				2.7			116.0	127.8	121.9	11.8	3.38E-04	3.3					
HR-M3	6-9	CH_4	47.5	0.13%	7.0	17.6	80.8	14.2	131.9	bdl	66.0	-131.9	4.00E-03	39.5	86.8				
HR-M3	6-9	Ar				3.4			131.9	123.2	127.5	-8.7	5.26E-04	5.2					
HR-M3	9-12	CH_4	69.3	0.13%	6.9	16.1	82.0	13.2	135.3	bdl	67.6	-135.3	1.90E-04	1.9	0.0				
HR-M3	9-12	Ar				2.9			135.3	105.8	120.6	-29.5	6.10E-04	6.0					
HR-M3	12-15	CH_4	67.6	0.16%	7.5				282.9				1.39E-04	1.4	42.3				
HR-M3	12-15	Ar							282.9				8.01E-05	0.8					

Table 2. Metabolic Activity in Mesocosm Experiments of Monterey Canyon Sediment. Homogenized sediment slurry was divided into incubations bottles amended with methane or argon and $^{15}N_2$ or $^{15}NH_4^+$.

							$^{15}N_2$-Ammended Incubations									$^{15}NH_4$-Ammended Incubations			
							SO_4^{2-} and CH_4 Metabolism			$[NH_4^+]$				N_2 Fixation			Estimates of Potential Total Growth			
Incubation Set-up				*in situ* Sed Geochem																
Core		Depth (cmbsf)	Headspace	$[NH_4^+]$ (mM)	TN (wt%)	$\delta^{15}N$ (‰)	SO_4^{2-} Reduction (mM)	SO_4^{2-} Reduction Dependent on CH_4 (%)	Estimated CH_4 Consumed via AOM (mM)	$[NH_4^+]_{t=0}$ (mM)	$[NH_4^+]_{final}$ (mM)	$[NH_4^+]_{avg}$ (mM)	Change in $[NH_4^+]$ (mM)	Rate of N_2 Fixation (nmol N_2 g dry wt sed^{-1} hr^{-1})	Quantity of N_2 Fixed (nmol N_2 g dry wt sed^{-1})	N_2 fixation Dependent on CH_4 (%)	Rate of NH_4^+ Assimilation (nmol NH_4^+ g dry wt sed^{-1} hr^{-1})	Quantity of NH_4^+ Assimilated (nmol NH_4^+ g dry wt sed^{-1})	NH_4^+ Assimilation Dependent on CH_4 (%)	N Assimilated from N_2 versus NH_4^+ (%)
MC-W1	1	0-3	CH_4	58.0	0.35%	9.8	2.1	3.5	0.1	4.3	249.8	127.0	245.4	1.94E-02	120.3	0.0	1.94E-01	1914.5	3.1	12.6
MC-W1	4	0-3	Ar				2.0			4.3	234.7	119.5	230.4	1.35E-02	132.7		1.88E-01	1855.6		14.3
MC-W1	11	3-6	CH_4	116.0	0.28%	11.0	3.7	0.0	0.0	214.3	749.9	482.1	535.6	1.03E-03	6.4	23.2	8.96E-02	883.6	0.0	1.4
MC-W1	14	3-6	Ar				4.7			214.3	640.0	427.2	425.7	4.96E-04	4.9		1.10E-01	1085.8		0.9
MC-W1	21	6-9	CH_4	379.9	0.19%	8.1	4.0	22.8	0.9	254.3	350.4	302.3	96.1	1.62E-03	10.0	9.0	6.07E-02	598.9	3.0	3.3
MC-W1	24	6-9	Ar				3.1			254.3	387.7	321.0	133.4	9.24E-04	9.1		5.89E-02	581.2		3.1
MC-W1	31	9-12	CH_4	586.6	0.10%	7.0	16.8	86.5	14.5	267.2	77.7	172.5	-189.5	1.11E-03	6.9	25.9	8.57E-02	845.1	68.7	1.6
MC-W1	34	9-12	Ar				2.3			267.2	271.5	269.4	4.3	5.17E-04	5.1		2.68E-02	264.8		3.9
MC-W1	41	12-15	CH_4	618.6	0.18%	7.2	6.6	78.1	5.1	264.4	203.8	234.1	-60.5	1.06E-03	6.5	16.1	7.78E-02	767.8	63.5	1.7
MC-W1	44	12-15	Ar				1.4			264.4	312.0	288.2	47.6	5.57E-04	5.5		2.84E-02	280.3		3.9
MC-B1	51	0-3	CH_4	15.2	0.19%	7.4	8.1	21.4	1.7	58.0	184.6	121.3	126.6	3.24E-02	200.6	12.7	1.86E-01	1837.0	0.0	21.8
MC-B1	54	0-3	Ar				6.4			58.0	131.3	94.7	73.4	1.78E-02	175.1		2.13E-01	2105.7		16.6
MC-B1	61	3-6	CH_4	22.0	0.19%	7.5	6.4	3.2	0.2	187.0	283.9	235.5	96.9	6.24E-04	3.9	0.0	8.34E-02	822.7	0.0	0.9
MC-B1	64	3-6	Ar				6.2			187.0	315.2	251.1	128.2	4.22E-04	4.2		1.09E-01	1071.4		0.8
MC-B1	71	6-9	CH_4	29.8	0.19%	7.3	3.6	0.0	0.0	25.3	45.5	35.4	20.2	9.56E-04	5.9	0.0	6.26E-02	617.9	6.4	1.9
MC-B1	74	6-9	Ar				5.2			25.3	40.4	32.9	15.2	4.75E-03	46.8		5.86E-02	578.3		16.2
MC-B1	81	9-12	CH_4	38.1	0.20%	7.4	6.6	6.0	0.4	22.8	30.5	26.6	7.8	1.51E-02	93.8	9.6	1.04E-01	1024.3	0.0	18.3
MC-B1	84	9-12	Ar				6.2			22.8	23.4	23.1	0.7	8.59E-03	84.8		1.17E-01	1157.2		14.7
MC-B1	91	12-15	CH_4	39.8	0.22%	7.3	3.9	0.0	0.0	24.3	50.3	37.3	26.0	1.09E-03	6.7	0.0	6.88E-02	678.6	5.4	2.0
MC-B1	94	12-15	Ar				5.5			24.3	23.4	23.8	-0.9	2.72E-03	26.8		6.51E-02	642.2		8.4
MC-W2	101	0-3	CH_4	23.3	0.23%	7.9								6.74E-04	4.2	2.8	2.45E-01	2421.5	34.7	0.3
MC-W2	104	0-3	Ar											4.11E-04	4.1		1.60E-01	1581.5		0.5
MC-W2	111	3-6	CH_4	5.8	0.21%	7.7	17.2	60.1	10.3	61.3	471.2	266.2	409.9	8.61E-04	5.3	0.0	1.53E-01	1512.2	33.7	0.7
MC-W2	114	3-6	Ar				6.9			61.3	638.0	349.6	576.7	5.43E-04	5.4		1.02E-01	1002.5		1.1
MC-W2	121	6-9	CH_4	59.9	0.16%	7.1	15.0	65.8	9.9	29.4	148.6	89.0	119.2	1.02E-03	6.3	0.0	1.17E-01	1153.8	39.9	1.1
MC-W2	124	6-9	Ar				5.1			29.4	276.6	153.0	247.2	6.88E-04	6.8		7.04E-02	693.9		2.0
MC-W2	131	9-12	CH_4	71.2	0.14%	6.8	15.5	59.0	9.1	28.8	bdl	14.4	-28.8	7.59E-03	47.0	0.0	1.44E-01	1418.0	45.8	6.6
MC-W2	134	9-12	Ar				6.3			28.8	bdl	14.4	-28.8	6.75E-03	66.5		7.79E-02	768.3		17.3
MC-W2	141	12-15	CH_4	86.5	0.14%	6.7	16.5	0.0	0.0	36.7	bdl	18.4	-36.7	2.17E-02	134.2	82.3	1.78E-01	1756.4	70.0	15.3
MC-W2	144	12-15	Ar				18.8			36.7	46.5	41.6	9.7	2.41E-03	23.8		5.33E-02	526.2		9.1
MC-C	151	0-3	CH_4	25.0	0.11%	5.1								7.44E-04	4.6	0.0	6.87E-02	677.7	7.5	1.4
MC-C	154	0-3	Ar											6.50E-04	6.4		6.36E-02	627.1		2.0
MC-C	161	3-6	CH_4	52.7	0.11%	5.9								1.28E-03	7.9	0.0	9.08E-02	895.4	20.0	1.8
MC-C	164	3-6	Ar											1.07E-02	105.3		7.27E-02	716.7		29.4
MC-C	171	6-9	CH_4	18.6	0.09%	6.1								9.28E-04	5.7	0.0	5.21E-02	514.3	9.5	2.2
MC-C	174	6-9	Ar											8.04E-04	7.9		4.72E-02	465.5		3.4
MC-C	184	9-12	CH_4	136.2	0.13%	6.1								1.21E-03	7.5	0.0	7.81E-02	769.9	0.0	2.0
MC-C	181	9-12	Ar											1.06E-03	10.5		7.94E-02	783.2		2.7
MC-C	191	12-15	CH_4	171.9	0.10%	6.2								6.25E-04	3.9	0.0	6.62E-02	653.5	19.7	1.2
MC-C	192	12-15	Ar											6.66E-04	6.6		5.32E-02	524.8		2.5
MC-B2	201	3-6	CH_4	112.2	0.21%	7.1	14.7	57.7	8.5	36.0	195.5	115.7	159.5	8.83E-04	5.5	0.0	1.83E-01	1801.5	25.1	0.6
MC-B2	204	3-6	Ar				6.2			36.0	491.1	263.6	455.1	5.69E-04	5.6		1.37E-01	1348.4		0.8
MC-B2	211	9-12	CH_4	106.3	0.18%	7.0	15.6	77.5	12.1	28.4	1.1	14.7	-27.3	3.07E-03	19.0	0.0	1.73E-01	1709.3	47.9	2.2
MC-B2	214	9-12	Ar				3.5			28.4	138.8	83.6	110.4	6.50E-03	64.1		9.03E-02	891.1		14.4

elevated in TN compared to a core collected 38 m away (0.23% versus 0.21%). The TN beneath Whale-fall 633 did decrease with depth to 0.14%, while the background core was consistent between the 3–6 and 9–12 cm horizons, potentially suggesting greater N-usage and depletion at the whale-fall than in reference sediment.

Bioavailable nitrogen concentrations in deep-sea sediments

Bioavailable nitrogen (ammonium, nitrate and nitrite) concentrations were determined in pore water squeezed from 3-cm-deep sediment intervals (Figures 1 and 2) from each core analyzed (17 cores from HR, 13 cores from MC; nitrite was not measured in MC cores). Concentrations of nitrite at Hydrate Ridge were the lowest of the three nitrogen species, ranging from not detectable to 13.6 μM in methane-rich cores, and not detectable to 8.4 μM in background cores. Levels of nitrate were slightly higher. The highest concentration of nitrate within a core was most often in the most surficial depth horizon, as has been observed previously at methane seep sites (Chapter 3, and reference therein). Nitrate concentrations ranged from not detected to 1228 μM in methane-rich cores, not detectable to 18 μM in whale-fall cores, and not detectable to 19.5 μM in background cores. Ammonium is the most abundant of the three nitrogen species investigated, and ranges from 3.7 to 575 μM in methane-rich cores, 3.8 to 618 μM in whale-fall cores, and not detected to 112 μM in background cores. Although ammonium concentrations often decreased with depth, as the nitrate concentrations did, there was more heterogeneity in the ammonium trends with depth, and in some cases increased. Generally, the background cores contained lower concentrations of bioavailable nitrogen than cores taken either at methane seeps or whale-fall sites.

Figure 1. Concentrations of ammonium (solid line with circles, top axis, in μM), nitrate (dashed line with squares, bottom axis, in μM) and nitrite (dashed line with triangles, bottom axis, in μM) with depth (cm below seafloor) in sediment cores from Hydrate Ridge. Additional information about each core is listed in SI Table 1. Cores with asterisks were collected immediately adjacent to cores used for mesocosm experiments.

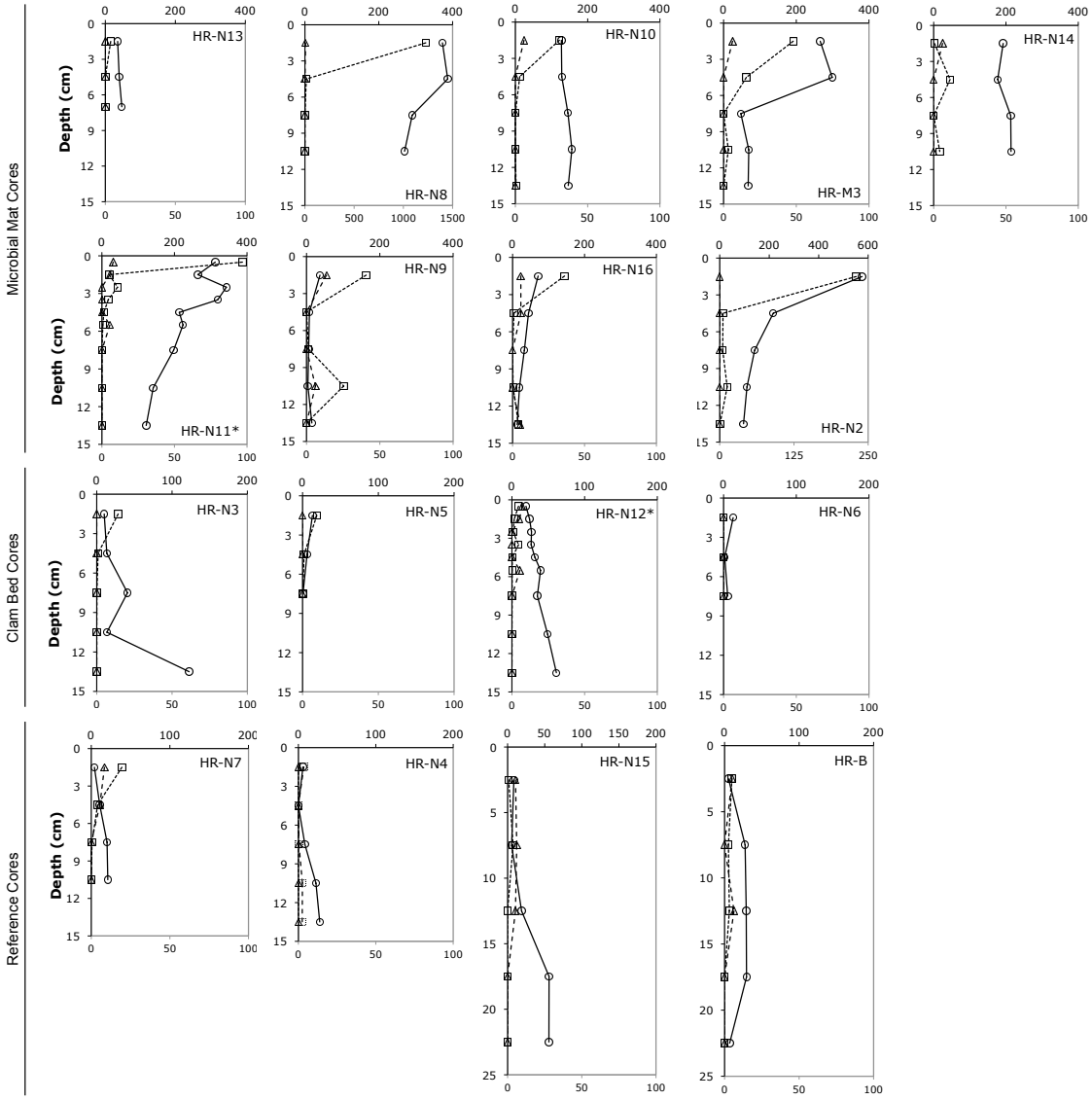

Figure 2. Concentrations of ammonium (solid line with circles, top axis, in μM) and nitrate (dashed line with squares, bottom axis, in μM) with depth (cm below seafloor) in sediment cores from Monterey Canyon. Axis scales are consistent within each site, but vary between sites. Distance from area of carbon-loading (whale or methane seep) is indicated. Additional information about each core is listed in SI Table 1.

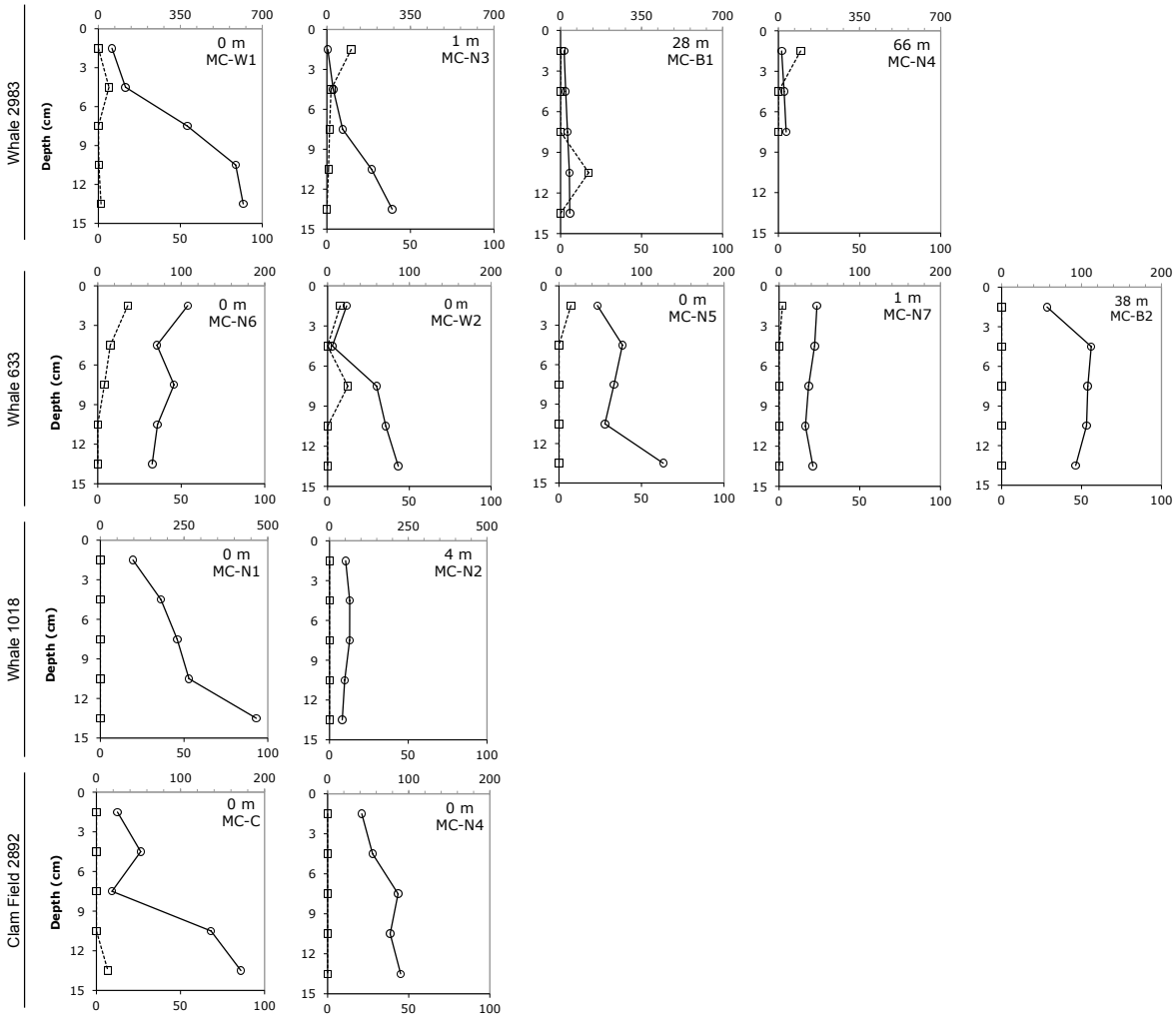

Sulfate Reduction and the Anaerobic Oxidation of Methane in microcosm experiments

In HR methane-rich sediments (both mat and clam sites), sulfate reduction (SR) in the presence of methane is extensive, with a nearly complete depletion of sulfate in some sediment horizons over the course of the experiment. The activity was largely methane dependent, with about 80% of SR in these sediments only occurring in the presence of methane (Table 1). This suggests high levels of methane oxidation coupled to sulfate reduction (AOM), which has been observed extensively at methane seep sites previously [(*39*), and references therein]. Incubations of sediment from the background core collected at HR showed lower levels of sulfate reduction (approximately 7X less), as well as a reduced methane dependency of the sulfate consumption (Table 1).

Total sulfate reduction in whale-fall cores from Monterey Canyon (MC) was generally less than observed in the methane seep cores from HR, despite the longer incubation time of the MC samples (13 versus 8 months). Similar values of sulfate reduction were observed at whale-falls and in background sediments. The sulfate reduction observed in the whale-fall cores was less dependent on methane than the methane-rich cores at HR, as expected. However, the sulfate reduction in some sediments, particularly the deep horizons beneath Whale-fall 2893 and throughout the sediment beneath Whale-fall 633, also exhibited high methane dependence (86.5% and up to 65.8%, respectively).

Changes in the concentration of bioavailable N during the microcosm experiments

Although several incubations from both HR and MC exhibited a depletion of NH_4^+ over the course of the experiment, as would be expected as microbial growth occurred, the majority of the incubations showed an increase in NH_4^+ over time (Table 1). The extent of the production varied from barely detectable to greater than 500 μM. The NH_4^+ production was often the greatest in the most surficial sediments from a given core, and did not vary systematically based on whether or not methane was present.

Nitrogen fixation measured via ^{15}N-uptake from $^{15}N_2$

Nitrogen fixation in the microcosm experiments was measured by the quantification of ^{15}N enrichment in sediment incubated with $^{15}N_2$ (50% labeled, 6% of the headspace) and either methane or argon. Nitrogen fixation was observed in all cores investigated, with a maximum rate at Hydrate Ridge of 2.35 $x10^{-2}$ nmol N_2 fixed g_{dw}^{-1} hr^{-1} occurring beneath a clam field (12–15 cm depth, core HR-C), and the maximum rate at Monterey Canyon of 3.24 $x10^{-2}$ nmol N_2 fixed g_{dw}^{-1} hr^{-1} occurring in a background core collected 28 m from Whale-fall 2983 (0–3 cm, core MC-B1) (Tables 1 and 2).

Within Hydrate Ridge sediments (n=5 cores), the amount of diazotrophy varied greatly between and within cores, and depending on the presence or absence of methane (Table 1, Figure 3). Consistent with what has been observed previously in methane seep sediment (Chapter 3), nitrogen fixation was nearly 100% dependent on methane (Table 1, Figure 3 K–N), and peaked within narrow depth intervals within the core (Figure 3 F, H, I). Diazotrophy was observed beneath both microbial mats and clam fields at HR, at similar rates, however at deeper sediment depths beneath the clam field (core HR-C).

Figure 3. Nitrogen fixation and ammonium uptake with depth in Hydrate Ridge mesocosm experiments during an 8.3 month incubation. Experiments amended with methane in are shown in black, with argon in gray. The ammonium profiles in the pushcores used for sediment incubations, or immediately adjacent cores, are shown to the left. Depth intervals are shown in cm below the seafloor. "nm" indicates no sediment incubated from those depths.

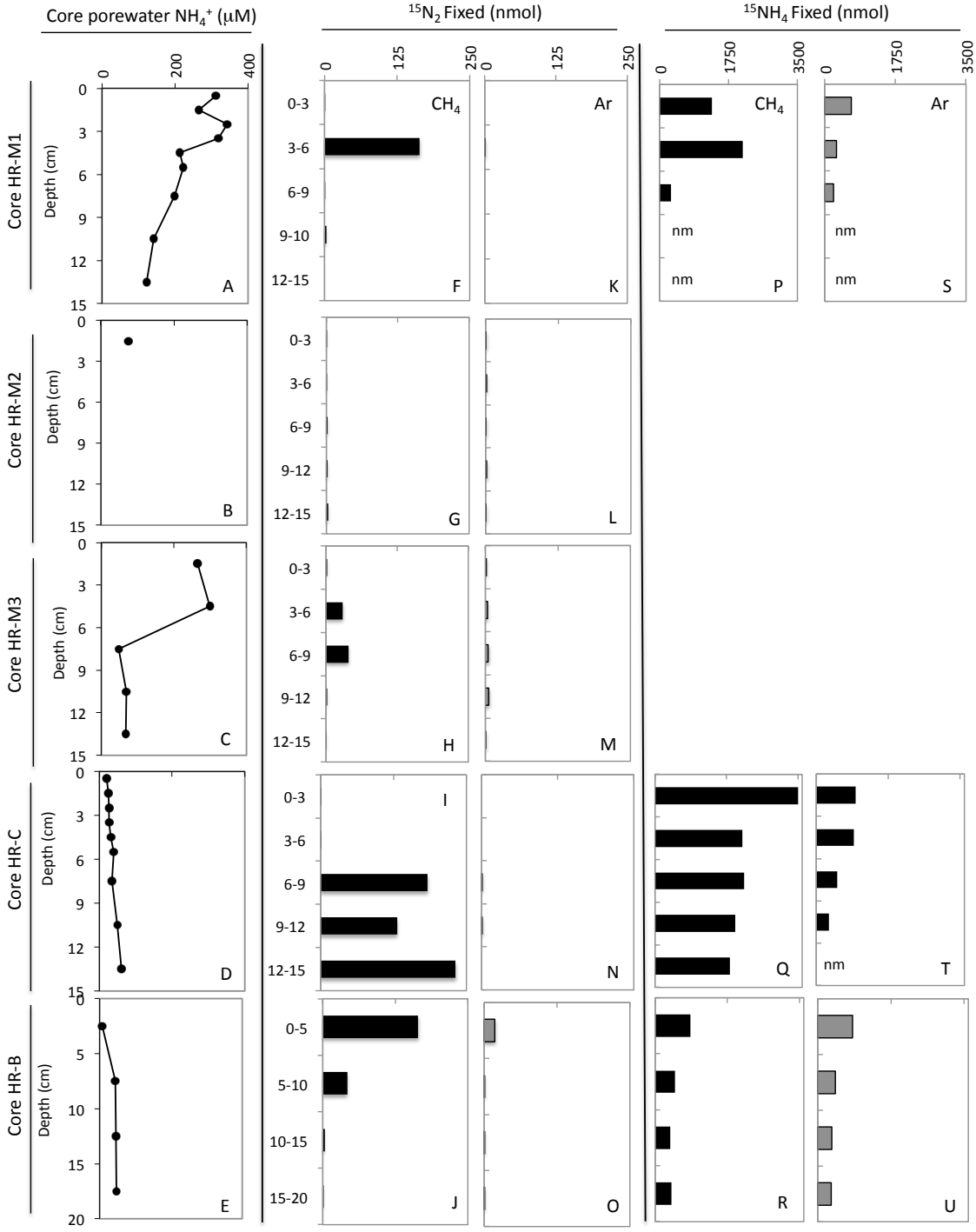

Figure 4. Nitrogen fixation and ammonium uptake with depth in Monterey Canyon mesocosm experiments during an 13.3 month incubation. Experiments amended with methane in are shown in black, with argon in gray. The ammonium profiles in the pushcores used for sediment incubations, or immediately adjacent cores, are shown to the left. Depth intervals are shown in cm below the seafloor. "nm" indicates no sediment incubated from those depths.

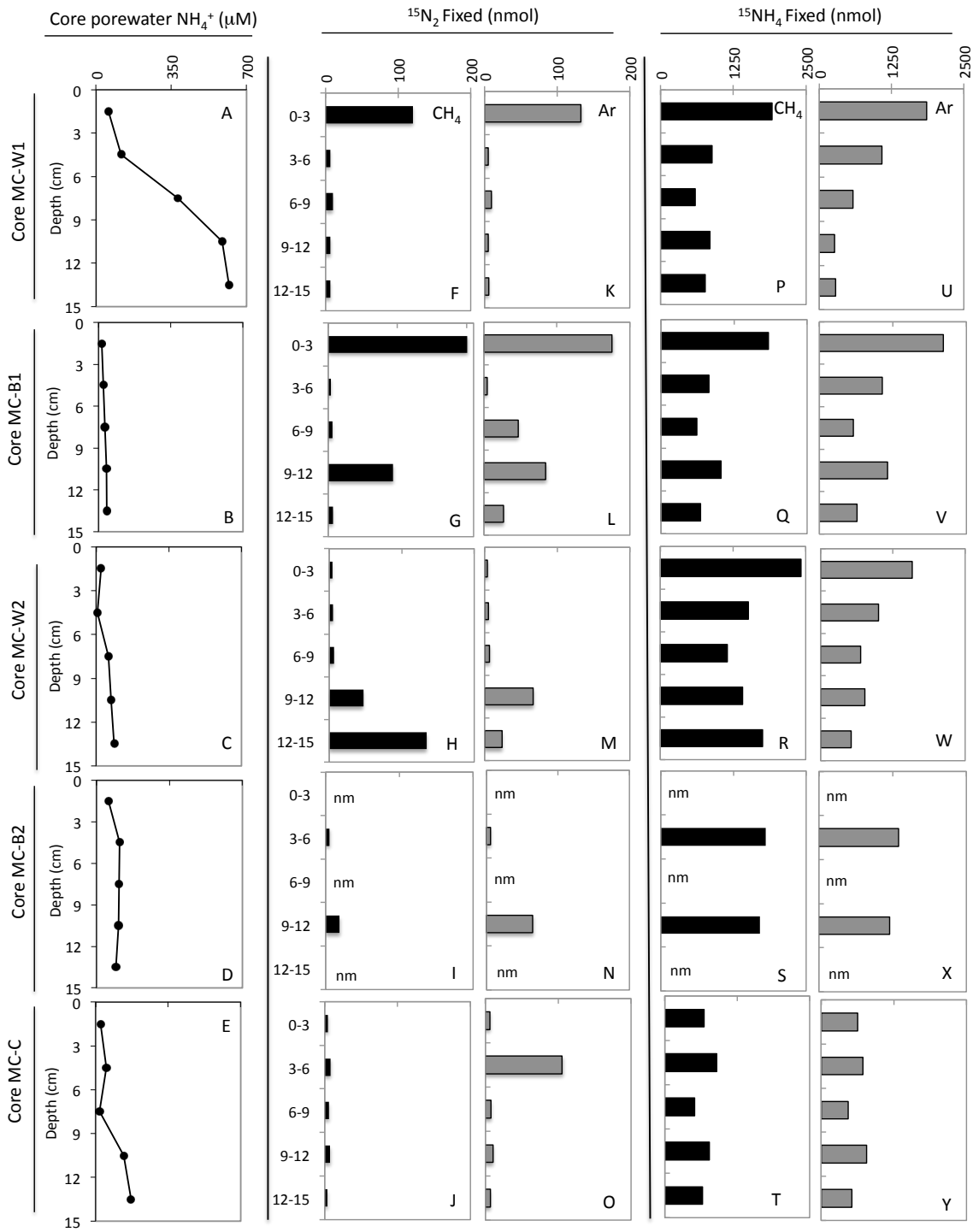

Nitrogen fixation was also observed within the background core at Hydrate Ridge, however rather than peaking in the middle of the core, or towards the bottom, the peak occurred at the top, and was less dependent on methane than in methane seep sediments (89% methane dependent versus ~ 100% in seep sediment).

Nitrogen fixation was also variable within Monterey Canyon sediments, both between and within cores (n=5 cores) (Table 2, Figure 4). In the two cores investigated that were collected beneath whale-falls (MC-W1 and MC-W2), nitrogen fixation was not distributed equally with depth in the core, and like the trend observed in methane seep sediment, was limited to particular depth horizons (Figure 4 K, M). However, the majority of this diazotrophy was not methane dependent (0–26% in MC-W1 and 0–82% in MC-W2). Rates of nitrogen fixation in both MC-W1 and MC-W2 were on the same order of magnitude as those within methane seep sediment (Table 2).

Sediment from the two cores collected away from the whale-falls in Monterey Canyon, MC-B1 (collected approximately 28 m from W1), and MC-B2 (collected approximately 38 m from W2) also demonstrated high rates of nitrogen fixation (Table 1, Figure 3 L, N). The diazotrophy was also limited to particular depth horizons, although in MC-B1 there appears to be two distinct peaks, likely mediated by two different microbial communities. Additionally, the nitrogen fixation was generally not methane dependent (0–10%). The sediment from a core collected within a methane seep near W1, MC-C, demonstrated unexpected patterns of nitrogen fixation. Although a typical peak in N_2 fixation was observed mid-core, it was only observed in the incubation without methane.

Total growth potential measured via ^{15}N-uptake from $^{15}N_2$

^{15}N-uptake from $^{15}NH_4^+$ was observed in all depths of all cores incubated, both with and without methane, indicating new protein synthesis (a proxy for total potential growth, TPG) in all of the microcosm experiments (Tables 1 and 2, Figures 3 (Q–U) and 4 (P–Y)). Although some depths demonstrated more growth than others, and these often corresponded to depths containing enhanced nitrogen fixation, rates of ^{15}N uptake from $^{15}NH_4^+$ were more equally distributed throughout the sediments than ^{15}N uptake from $^{15}N_2$. Although TPG in HR methane seep cores was largely dependent on methane (25–86%, average 56%), as observed previously (Chapter 3), TPG at whale-falls at MC was less methane-dependent (0–70%, average 36%), and that in cores taken away from seeping areas and whale-falls was variable but in general even less so (2–18%, average 9%, and 0–48%, average 12%, respectively).

Ammonium inhibition experiment

To directly test the effect of NH_4^+ on diazotrophy in methane seep sediment, incubations of a single homogenized sediment slurry were amended with varying concentrations of NH_4^+ (0–5 mM). A negative effect was observed, with decreasing nitrogen fixation at higher concentrations of ammonium (Figure 6A). In one replicate set of incubations, nitrogen fixation occurred at up to 288 μM NH_4^+, but in another set, nitrogen fixation was observed at greater than 1089 μM NH_4^+.

Figure 6. (A) Effect of NH_4^+ addition on nitrogen fixation in methane seep sediment. The bars reflect the $\delta^{15}N$ values of bulk sediment after 236 days (7.6 months) with different amounts of ammonium added (results from duplicate bottles at each concentration are shown). The dotted line shows the average $\delta^{15}N$ of the bottles at t=0; values above this line indicate nitrogen fixation occurred over the course of the experiment. The amount of NH_4^+ added at the beginning of the incubation is shown on the X-axis, and the measured concentration of NH_4^+ in one of the duplicate bottles at the end of the experiment is shown in parenthesis. Bars darken with greater ammonium added. (B) Classification of *nifH* genes recovered from the sediment before NH_4^+ was added based on a neighbor-joining tree. *nifH* groups indicated are described in Raymond 2004 and Miyazaki 2009. (C) Sulfide production in the bottles during incubation with varying concentrations of ammonium added (circles). Lines darken with greater ammonium added, and the shades correspond to the concentrations in A. The no methane-added incubation is also plotted (x's) and an autoclaved control (triangles). Each sulfide measurement represents the average of that measured in each of the two duplicate bottles at each ammonium concentration.

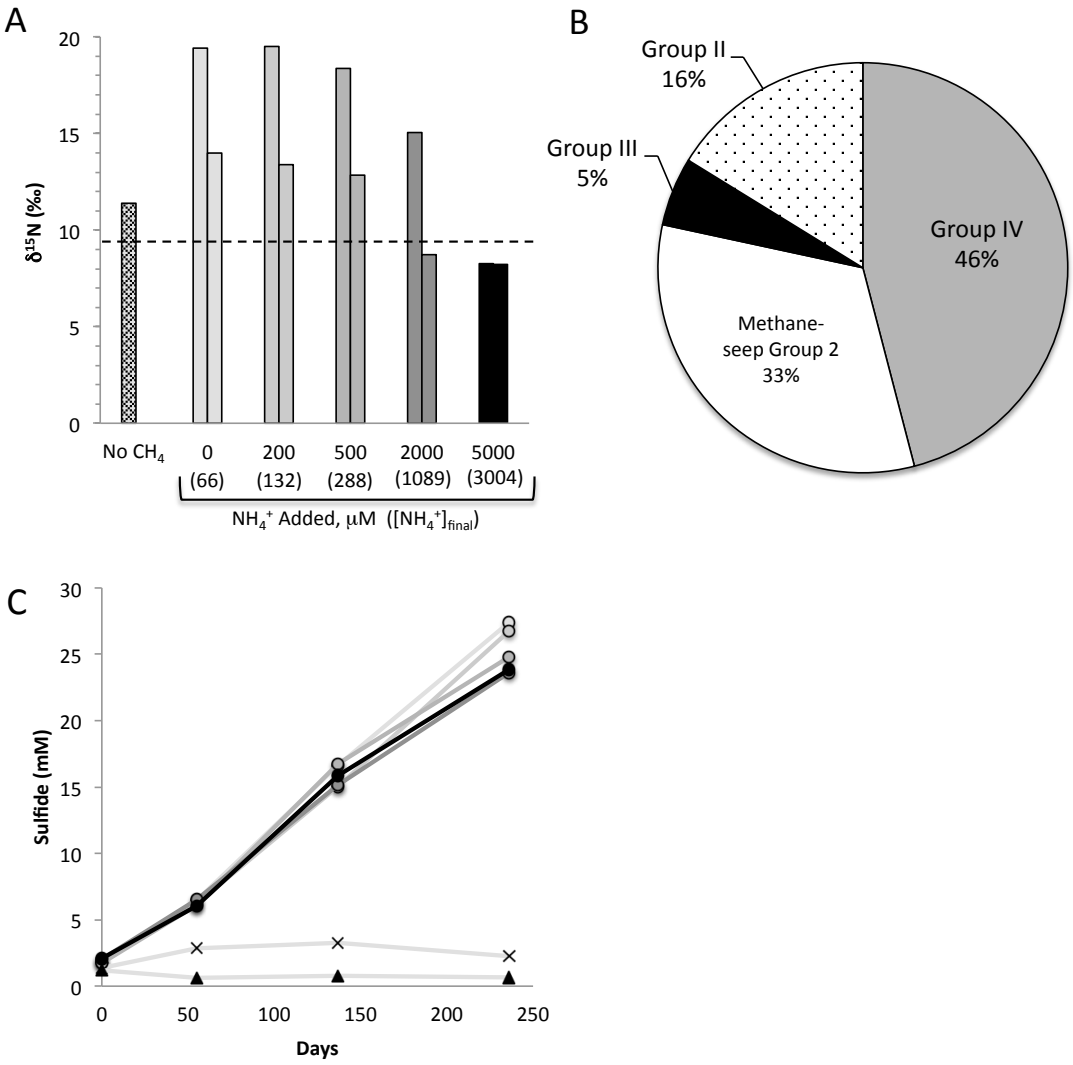

Sulfide concentrations

Sulfide concentrations were generally high in cores collected at Hydrate Ridge within areas of presumed methane seepage (SI Table 1). Cores classified as background sediment based on the lack of indicative chemosynthetic communities contained undetectable sulfide, confirming the classifications (SI Table 1). Sulfide was also measured in the ammonium inhibition microcosm experiments to determine the effect of additional ammonium on sulfate reduction, as a proxy for overall ecosystem functioning. No significant effect on sulfate reduction due to additional ammonium added was observed (Figure 6C). The increase in sulfide was accompanied by a decrease in sulfate, confirming sulfate reduction as the source of the sulfide (data not shown).

nifH libraries from ammonium inhibition experiment

In order to investigate which diazotrophs were present in the NH_4^+ addition experiment, a *nifH* library (n=37 clones) was generated from the sediment slurry preserved at the beginning of the experiment, before aliquots were sub-divided. A diversity of *nifH* sequences were detected, falling within four clades of the *nifH* phylogeny (clades as described in (*40*) and (*16*): Group II, consisting of obligate anaerobes, and particularly methanogenic archaea and sulfate-reducing bacteria (16% of library, n=6 clones), Group III, typically containing alternative, or Mo-independent nitrogenases, usually in organisms also containing the genetic potential for the traditional MoFe nitrogenase as well (5% of library, n=2), Group IV, containing *nifH* homologues not shown to be involved in nitrogen fixation, including ANME-1 *nifH* homologues (46%

of library, n=17 clones), and Methane-seep Group 2, containing putative ANME-2 *nifH* sequences (33% of library, n=12 clones) (Figure 6, B).

DISCUSSION

Magnitude and Distribution of Diazotrophy

Comparison of nitrogen fixation rates to previous observations

To our knowledge, the maximum rates of nitrogen fixation observed at both Hydrate Ridge and Monterey Canyon are the highest ever reported for deep-sea sediments, exceeding those detected by Hartwig and Stanley in the abyssal plain of the Atlantic Ocean by > 50X (2,800 m water depth) (*18*), and those detected in Chapter 3 at a mud volcano off the coast of Costa Rica by 2.4X (1,000 m water depth). Additionally, because the rates reported here are calculated over the entire length of the experiment (8 or 13 months), as if nitrogen fixation during this time was linear, it is likely that these rates are lower than the maximum rate of nitrogen fixation that occurred during a shorter period within the incubation. Dekas et al. found that rates of nitrogen fixation decreased after the first five months of incubation in microcosm experiments such as these (Chapter 3). Therefore, analyzing the $\delta^{15}N$ of intermediate time points in these experiments will likely lead to upward revisions in the maximum rates.

Significance to the local ecosystems

Interestingly, not only was the magnitude of nitrogen fixation generally high in the sediments, it represented a large fraction of the total nitrogen required for growth by these communities. By comparing the amount of nitrogen obtained from N_2 to that

obtained from NH_4^+, we calculate the percentage of nitrogen obtained from diazotrophy (Tables 1 and 2). This is essentially a measure of how significant of a nitrogen source diazotrophy is to the local community, however may be an underestimate, because the addition of ammonium may stimulate growth. At Hydrate Ridge, communities within methane-rich cores obtained up to 25.4% of the total nitrogen requirement from diazotrophy, and the percentage was even higher in the background core, (~ 38.7%). In Monterey Canyon, at whale-fall sites, up to 17% of N was obtained from diazotrophy, at the clam field up to 20.0%, and in background cores up to 47.9%. The average contribution of nitrogen fixation to the total nitrogen requirement across all samples was 6%. This dependence on nitrogen fixation is much greater than that observed in other benthic systems (e.g., Chapter 3 and references within (*2*)), and suggests diazotrophy is an essential component of growth in the deep-sea habitat. However, values of $\delta^{15}N$ in the sediments were generally high (Table 1), which is unusual for communities deriving a significant portion of nitrogen from air ($\delta^{15}N_{air}$=0‰) (*41*). This may be explained if the living cells, which do obtain a large fraction of N from diazotrophy and do have low values of $\delta^{15}N$, are only a small fraction of a larger pool of sedimentary nitrogen, which may have originated in ecosystems not dependent on nitrogen fixation.

Distribution of nitrogen fixation

Notable in the current findings is not only the magnitude of diazotrophy observed and its significance to the local ecosystems, but also the ubiquity of this capability in diverse samples. We hypothesized that nitrogen fixation would be enhanced in methane seeps relative to background sediments, due to potential nitrogen limitation at methane

seeps, discussed in Chapters 2 and 3, and that it would be inhibited at whale-fall sites, due to the availability of complex organic material including nitrogen. However, the maximum rates of nitrogen fixation observed within background sediments, at methane seeps, and at whale-falls were comparable. Nitrogen fixation beneath whale-falls, where up to 160 tons of organic matter is deposited at a rate 2,000X that of natural organic matter deposition to the seafloor (*42*), is surprising. Benthic productivity may be limited by organic matter, and stimulating growth may stimulate nitrogen fixation (*1, 18*). However, nitrogen fixation is highly regulated in the presence of ammonium, and the degradation of whale biomass is likely to produce substantial PON, which in turn would be mineralized to ammonium. These and other potential controls on diazotrophy are discussed in more detail in the next section.

The peak in nitrogen fixation mid-core in diazotrophic methane-rich cores confirms the trend observed in Chapter 3, and is likely due to steep chemical gradients within the sediments. In the case of cores from beneath microbial mats and clam fields, this peak in diazotrophy is likely dictated by the methane and sulfate concentrations, which can dictate both the abundance and activity of microbes with depth, and particularly that of methanotrophic archaea, ANME (as discussed in Chapter 3, and below). The deepening of the horizon of nitrogen fixation in the clam bed core from Hydrate Ridge (HR-C) is likely due to a deepening of the traditional chemical gradients beneath the clam field. This is common underneath clam fields, and is driven by bioturbation (e.g., (*43*)). The chemical gradients dictating the hot-spot distribution of diazotrophy in the background and whale-fall cores are likely different than in the

methane-rich cores, and may be complex. Similar to the profiles within methane-rich cores, they do not correspond directly to depleted levels of ammonium.

Significance to marine nitrogen cycling

Although areas of enhanced productivity on the seafloor (e.g., methane seeps and whale-falls) are globally distributed and host high levels of nitrogen fixation, it is difficult to estimate the contribution of these sites to the marine system while the total area they comprise is still a subject of great uncertainty (*39*). Likely, the diazotrophy observed in the three cores collected away from the sites of carbon input have the most relevance for deep-sea nitrogen fixation, because the area they represent is so great. Additionally, in two of the three background cores, the maximum rate of nitrogen fixation rivaled that of the carbon-loaded sediments. In fact, the core collected 28 m from Whale-fall 2983 demonstrated the highest rate of nitrogen fixation in the entire study. Not only is this therefore the highest rate yet observed in the deep-sea, it is also from the deepest sediments yet to demonstrate nitrogen fixation. Although Hartwig and Stanley investigated sediments at 4,800 m, no acetylene reduction was detected there (*18*). If diazotrophy at these levels is representative of background sediments, nitrogen fixation in deep-sea sediments could be paramount.

Whale-falls have been shown to affect the chemistry and microbial metabolisms occurring up to 10 m away from whale deposition, referred to as a "bull's eye" of organic matter loading, a dispersal likely due to bioturbation (*29, 31, 44*). It is therefore possible that even at distances as great as 28 and 38 m, where the background samples for this study were collected (see SI Figure 1 for map), there could be an impact on the

surrounding sediments. However, the total nitrogen measured at both off-whale-fall sampling sites was consistently about 0.2% with depth, unlike the cores collected at whale-falls which showed great variation in the total nitrogen with depth, with an enrichment at the top. This decreases the likelihood that the background cores were affected by the whale biomass, but it remains a possibility. The background core at Hydrate Ridge was collected nearly 13 km from known sites of methane seepage, suggesting that is representative of background seafloor.

The extent to which rates of nitrogen fixation in bottle experiments reflect the *in situ* activity is not known, with factors in incubation experiments such as these resulting in potential underestimates (e.g., non-ideal growth conditions including the build-up of metabolic end-products and lower than *in situ* pressure may slow growth, in addition to a lower concentration of N_2 than is assumed to be present in pore waters), and overestimates (e.g., the dilution of ambient nitrogen sources with the addition of filtered seawater) of *in situ* rates of nitrogen fixation. However, as is discussed in the sections below, we consider the former effects more likely to effect the rate of diazotrophy than the later, since only very high levels of ammonium are likely to inhibit diazotrophy. Investigating the ^{15}N-uptake at higher temporal resolution in the preserved samples will allow us to determine if nitrogen fixation occurred immediately or after a lag time, which will suggest whether or not it was occurring *in situ*.

Despite the magnitude and distribution of diazotrophy observed here, the extent to which benthic cycling interacts with the overlying water column is still not known. It is possible that although substantial new nitrogen is produced in marine sediments, it does not flux up and contribute to marine biogeochemical processes. An attempt was made to

measure the net flux of N_2 at the sediment water interface at Hydrate Ridge, using the N_2/Ar technique previously used to measure N_2 flux in and out of Narragansett Bay sediments (*6*). However, the continual formation of gas bubbles in the whole-core experiments due to supersaturated gases coming out of solution at the decreased pressure of sea-level prevented accurate measurements of the N_2/Ar ratio in the water and undermined the experiment (data not shown). The method therefore needs to be modified for the examination of deep, pressurized samples, and may require *in situ* measurements. Alternatively, nitrogen profiles at higher resolution may also aid in indicating if there is a flux of ammonium out of the sediments.

Biological controls on deep-sea benthic nitrogen fixation: connections to rates of sulfate reduction, anaerobic oxidation of methane, and methanogenesis

Nitrogen fixation is mediated exclusively by bacteria and archaea, and only a sub-set of these kingdoms. Although diazotrophy has been studied for over 100 years, we are still learning about the diversity and physiological limits of the microorganisms capable of fixing N_2. For example, the recognition that nitrogen fixation was mediated by archaea as well as bacteria occurred only in 1984, with the simultaneous reports of two diazotrophic methanogens (*45, 46*), the upper temperature limit of nitrogen fixation was just extended by 28˚C to 92˚C in 2006 (*12*), the lowest metabolic energy yield required to support diazotrophy was extended in 2009 with the discovery that the methanotrophic ANME could fix nitrogen (yielding just 25–50 kJ mol_{CH4}^{-1}) (*13*), and the recognition of the significant role of diazotrophs other than filamentous cyanobacteria in the water column, such as unicellular cyanobacteria and heterotrophic diazotrophs, has continued to

develop in the last five years (*5, 47*). With each one of these discoveries, our perception of the range of potential diazotrophs, as well as the range of habitats where one might find diazotrophs, expands. It is therefore an exciting time to study diazotrophs in the deep benthos: although there is little precedent for deep-sea diazotrophs, there is precedent for surprises in the exploration of diazotrophs nearly everywhere.

Currently only two diazotrophs have been identified in the deep-sea: *Methanocaldococcus jannaschii*, isolated from a hydrothermal vent and demonstrated to fix nitrogen in pure culture (*12*), and the anaerobic methanotrophic ANME-2 archaea, demonstrated to fix nitrogen by fluorescence *in situ* hybridization (FISH) coupled to single-cell Nanoscale Secondary Ion Mass Spectrometry (NanoSIMS) analysis of $^{15}N_2$ incubated methane seep sediment (*13*). However, relatives of several diazotrophic sulfate-reducing bacteria (e.g., members of the *Desulfovibrio* and *Desulfotomaculum (48)*) and methanogenic archaea (e.g., members of the *Methanosarcina* and *Methanococcus (48)*), are abundant in marine sediments, and may fix nitrogen as well. In particular, sulfate-reducing bacteria have been shown to be important in nitrogen fixation in coastal marine sediments (*49, 50*). Furthermore, the diverse *nifH* sequences recovered from deep-sea sediments suggests that many anaerobic microorganisms in the sediments may be able to fix nitrogen (*14–16*).

The sediments investigated in this study show geochemical evidence for communities mediating sulfate reduction (SR, detected by depletion of sulfate), anaerobic methanotrophy (AOM, detected by rates of methane-dependent sulfate reduction), methanogenesis (implicated when total potential growth (TPG) is inhibited by the addition of methane) and other, unknown groups of microbes (likely when sulfate

reduction rates are low, but TPG is high and unaffected by the presence or absence of methane).

Hydrate Ridge: Diazotrophy linked with AOM in methane seep sediment

The geochemical evidence, both high rates of methane-dependent sulfate reduction and high rates of methane-dependent TPG, suggests that the methane-rich cores are dominated by anaerobic methanotrophs (likely the ANME and sulfate-reducing partners (SRB) such as *Desulfosarcina*). This is consistent with previous work that showed up to 94% of total microbial cells in Hydrate Ridge methane seep sediment can be ANME-SRB consortia (*51*). Nitrogen fixation in methane-rich cores was nearly 100% dependent on methane, further suggesting that the ANME, possibly in addition to the sulfate-reducing partners, are the primary diazotrophs at these sites. This is supported by a molecular investigation of *nifH* sequences in a microbial mat core from HR, where nearly 100% of the putatively functional *nifH* genes recovered clustered with either putative ANME-2 *nifH* sequences or those clades containing sulfate-reducing bacteria and/or methanogens (discussed below). Figure 5B demonstrates the positive correlation between nitrogen fixation and sulfate reduction in the presence of methane within methane-rich cores. These results are consistent with what was discovered at Costa Rican sites of methane seepage, where diazotrophy was not only methane dependent, but the peak in nitrogen fixation with depth (similar to the vertical profiles observed in this study) was spatially correlated with the maximum number of ANME-SRB aggregates (Chapter 3). Interestingly, and also consistent with the results found in Costa Rica, high levels of methane-dependent sulfate reduction in methane-seep cores does not always

Figure 5. Relationship between the amount of nitrogen fixed during the incubation and the average $[NH_4^+]$ in the incubation bottle (A,D,G), the amount of SO_4^{2-} consumed (i.e. sulfate reduction) in the incubation bottle (B,E,H), and the amount of $^{15}NH_4^+$ assimilated (indicating potential total growth) in a parallel incubation bottle (C,F,I). Incubation bottles with a methane headspace are depicted as circles; incubation bottles with an argon headspace are depicted as x's. To demonstrate trends within different communities, the data is divided into three categories based on the type of sediment incubated: CH_4-rich (A-C), including sediment from both HR and MC, Whale (D-E), including sediment from MC, and Background (G-I), including sediment from both HR and MC.

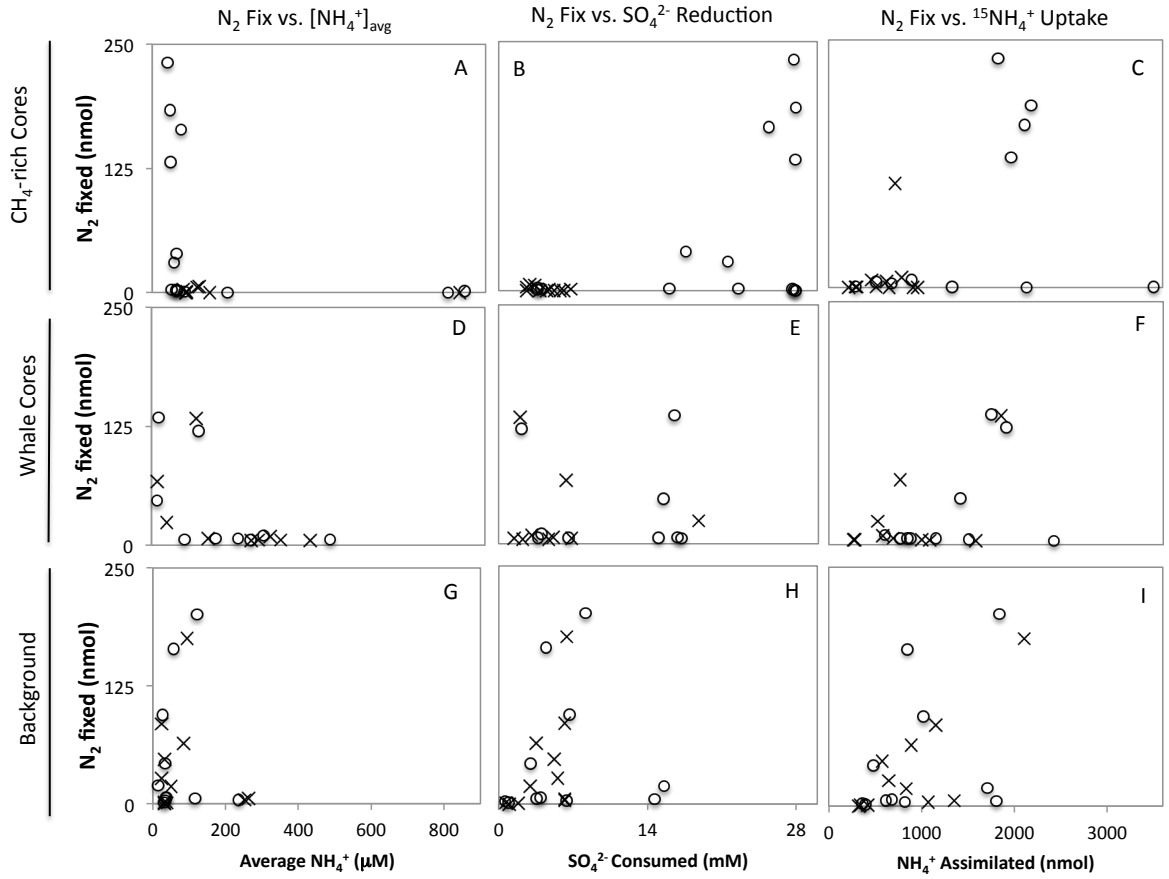

correspond to nitrogen fixation activity (Figure 5B and Table 1), demonstrating that geochemical parameters in addition to microbial distribution likely dictate when a particular group of organisms initiates diazotrophy.

Monterey Canyon Whale-fall and Clam-bed sediments: Geochemical evidence for metabolically diverse diazotrophs

Sediments beneath whale-falls, and specifically at Whale-fall 2983, have been described previously to include a more diverse community of microorganisms that in methane seep habitats, including primarily sulfate-reducing bacteria and methanogenic archaea (*29, 31*). Interestingly, Goffredi and Orphan found that beneath Whale-fall 2983, methanogens are active despite the co-occurrence of sulfate-reducing bacteria, which usually out-compete methanogens for substrates such as hydrogen and acetate. Sulfate reduction was detected in whale-fall sediments in this study, as well as evidence of methanogenesis. Sulfate reduction rates were generally lower in the whale-fall than methane seep sediments, and were often less dependent on methane, suggesting free-living sulfate-reducing bacteria rather than those in symbiosis with the ANME (0-87%, average 38% in MC-W1 and 0–66%, average 46% in MC-W2) (Table 2, Figure 5 F). Interestingly, unlike in a previous study of sulfate reduction at a whale-fall at 1675 m, where sulfate reduction was enhanced beneath a 7-year-old whale-fall (*44*), in this study detected rates of sulfate reduction were nearly equivalent at each whale-fall and its paired core collected 20–50 m away (with the exception a peak in sulfate reduction at 9–12 cm beneath Whale-fall 2983).

Sulfate reduction within some sediment horizons beneath both Whale-fall 2893 and Whale-fall 633 were methane dependent, suggesting that AOM may also be an important metabolic process within discrete horizons beneath the whale-falls. This is consistent with the results of Goffredi and colleagues, who showed elevated levels of methane, presumably generated by the extensive community of methanogens also observed, and detected 16S rRNA sequences belonging to ANME-3 and high $\delta^{13}C$ of pore water methane, indicative of AOM. (*29*). Elevated concentrations of methane beneath another whale-fall at 1675 m water depth also implicated an active community of methanogens, and methanotrophy was hypothesized there, although no AOM activity was detected (*44*).

Despite the evidence for AOM in these whale-falls cores, the diazotrophy does not appear to be dominated by the ANME. Interestingly, although the majority of sulfate reduction is methane dependent under Whale-fall 633, as well as in the deeper depths beneath Whale-fall 2983, and a large portion of the total potential growth is methane-dependent in each, nitrogen fixation is nearly independent of methane under Whale-fall 633 (except for the deepest horizon) and less than 25% of nitrogen fixation under Whale-fall 2983 is methane dependent. This suggests that although AOM may occur in these sediments, nitrogen fixation appears to be dominated by other diazotrophs. In fact, diazotrophy often decreased with the addition of methane. The reason for this decrease is not understood, however one possibility is CH_4 inhibition of methanogens. Cultured relatives of some of the methanogen phylotypes detected under Whale-fall 2983 previously, such as members of the *Methanosarcina*, are capable of nitrogen fixation (*29,*

48). This suggests that diazotrophic methanogens may be active under whale-falls, and potentially the most productive generators of new nitrogen.

An unusual trend in diazotrophy was observed in a core collected at a methane seep-associated *Calyptogena* bed at Monterey Canyon (MC-C), and may also be linked to methanogenetic activity. In this core, the peak in diazotrophy at 3–6 cm appeared to be inhibited by methane, which is inconsistent with the observations of diazotrophy in methane seep sediment at Hydrate Ridge. Due to the dense cover of large clams (~ 10–15 cm) at this site, the core was collected directly next to the clam bed, rather than within it (See SI Figure 1). Steep chemical gradients have been demonstrated around the edges of chemosynthetic communities at methane seep previously, suggesting that perhaps this core was not actually rich in methane (*52*). Indeed, preliminary methane measurements of the pore water revealed undetectable methane (data not shown). This is supported by low fractions of TPG dependent on methane (0–20%). This core should therefore be considered as a transitional habitat between methane seepage and background sediments, and may indeed be dominated by methanogens.

In the most surficial horizon under Whale-fall 2983, where one of the highest rates of nitrogen fixation was observed, both TPG and high levels of nitrogen fixation were unaffected by the presence or absence of methane (1914.5 and 1855.5 nmol NH4 g_{dw}^{-1}, respectively; 120.3 and 132.7 nmol N_2 g_{dw}^{-1}, respectively), and virtually no sulfate reduction was detected in the sediments (2.1 and 2.0 mM SO_4^{2-} reduced, respectively). This suggests that a different community of diazotrophs is present here, excluding sulfate-reducing bacteria, methanogens, and anaerobic methanotrophs. Sulfide-oxidizing bacteria, which have been shown to fix nitrogen in pure culture, may be prevalent in the

surficial layers, however their activity in anaerobic, nitrate-depleted incubations would likely be electron-acceptor limited. A great diversity of bacterial diversity has been previously described at Whale-fall 2983, and relatives of some of the detected phylotypes are known to fix nitrogen (e.g., within the Firmicutes) (*31*). It is unknown at this time what diazotrophs are active within this sample, but this activity suggests that a truly wide variety of microorganisms in the deep-sea may be capable of diazotrophy.

Background sediments and globally significant diazotrophs

The background cores show evidence of primarily free-living (not methane-dependent, ANME-associated) sulfate-reducing bacterial communities. The rate of nitrogen fixation shows a positive trend with sulfate reduction in these cores, independent of methane (Figure 5H). Nitrogen fixation is frequently driven by sulfate-reducing bacteria in shallow marine sediments (*2, 49, 50*), and sulfate-reducing bacteria may ultimately be the largest contributors of new nitrogen to deep marine sediments. Although methanotrophs and methanogens may be significant at localized sites of organic loading, the SRB in the large area of seafloor that is unaffected by such inputs may ultimately contribute more new nitrogen. AOM does occur in diffusion-driven (not seeping) marine sediments throughout continental margins (*39*), and the ANME-SRB may dominate nitrogen fixation there, however the fraction of the seafloor that continental margins comprise is small. Alternatively, if deep-sea nitrogen fixation is regulated by the availability of organic matter, it is possible that although representing a smaller area of the ocean, continental margins could account for more diazotrophic activity than abyssal plain sediments, due to the more productive surface waters along the

coasts. More research will be necessary to determine which microbial guild is the most significant to deep-sea diazotrophy, however the present work has expanded the understanding of which organisms may contribute, by linking geochemical evidence for sulfate-reducing bacteria and methanogenesis to diazotrophy for the first time in the deep-sea.

Geochemical controls on deep-sea benthic nitrogen fixation: under what geochemical circumstances do the diazotrophs fix nitrogen?

Presence of the enzymatic machinery necessary for nitrogen fixation (i.e., nitrogenase) is a prerequisite for diazotrophic activity. However, the distribution of organisms capable of producing nitrogenase, and even of their activity, is a poor predictor of the distribution of diazotrophic activity. This is evident in Figure 5 B, E, and F, and discussed briefly above: although enhanced sulfate reduction (SR) or anaerobic oxidation of methane (AOM) often corresponds to increasing nitrogen fixation in these samples, a secondary trend is also observed, where increased SR or AOM is completely unaccompanied by increased rates of nitrogen fixation. Thus, general activity of diazotrophs is a necessary but insufficient requirement for nitrogen fixation, and we must consider the geochemical parameters in the sediments to understand the variability in diazotrophy.

Investigating the biogeochemical controls on diazotrophy in terrestrial and pelagic environments has already been a long and complex research pursuit, and has revealed factors involved such as concentrations of ammonium, organic carbon, trace metals such as iron and molybdenum, light, oxygen, pH, salinity and temperature [reviewed in (*2, 19,*

20, 47, 53)]. The controls on anaerobic diazotrophy within deep-sea sediments may be different from those in terrestrial and pelagic systems, as metal concentrations, temperature, light and pressure in the deep-sea are fundamentally different. Already, a deviation from the behavior of aerobic diazotrophs has been observed in anaerobic coastal sediments, where nitrogen fixation has been reported in the presence of extremely high levels of ammonium (over 1000 μM) (*50*). The environmental parameters dictating when the potential to fix nitrogen is realized will be the focus of this section, with a particular focus on carbon-loading and nitrogen availability.

Impact of methane and organic matter on diazotrophy

The sampling sites (methane seep, whale-fall, and background) were selected to represent a range of biogeochemical parameters, but particularly investigate the effect of carbon loading on deep-sea diazotrophy. As already discussed, concentrations of organic matter are often implicated as regulating deep-sea productivity, as both an electron donor and a carbon source. At both methane seeps and whale-fall sites, carbon limitation is alleviated by the input of either methane or whale biomass. We observed similar rates of nitrogen fixation in the methane seep and background controls when methane was added to both sets of incubations, demonstrating a nearly equivalent potential to fix nitrogen. However, comparing the methane seep cores incubated with methane to the background cores incubated without methane reveals that the maximum nitrogen fixation in methane seep cores exceed those in the background cores by over an order of magnitude (231.5 nmol g_{dw}^{-1} and 18.7 nmol d_{gw}^{-1}). This latter comparison is likely more accurate, since each type of sediment is evaluated in its *in situ* geochemistry. These results suggest that

carbon loading in the form of methane does enhance nitrogen fixation in the deep-sea, and that adding methane to background sediments may stimulate diazotrophic activity.

At the whale-fall sites, there is no difference in nitrogen fixation rates between sediments at whale-falls or sediments collected 28–38 m away from the whale-fall, whether or not methane is added. As already discussed, it is possible that the whale deposition affected the off-site sediments, even at these depths, however based on the total nitrogen values detected, whale influence seems minimal at these sites. Alternatively, it is possible that the whale-falls, with whales deposited nine and three years ago (Whale-fall 2983 and Whale-fall 633, respectively), no longer represent carbon-rich sites. Remnants of the deposition at each site is confirmed by an elevated total nitrogen (TN) content in the surficial sediments beneath Whale-fall 2983, and visible, whole vertebrae of Whale-fall 633. Despite these indications that the original carbon loading of the sediments is still present to some degree, the lack of direct measurements of TN makes it difficult to assure that these sediments are still carbon-loaded. However, as recently as 2007 direct measurements of TN beneath Whale-fall 2983 (6 years after deposition) did reveal elevated values (3.2%) (*29*).

Previous studies of whale-falls have indicated that although the same general progression of macrofaunal ecosystems occurs, reflecting the changing nutrient composition of the decaying whale, the time scale on which this occurs varies, due to oxygen content, temperature, and rate of sedimentation at the whale-fall site (*27, 42*). Whale-fall 2983 and Whale-fall 633 are likely in the "sulphophilic" phase of whale-fall ecosystems, which can last from about one year after deposition to several decades (*42*). This phase is characterized by the slow degradation of recalcitrant carbon—mostly lipids

in the whale bones—by sulfate-reducing bacteria, producing elevated levels of sulfide which can support chemoautotrophic communities, much like those observed at methane seeps and hydrothermal vents (*42, 44*). Therefore, even if the TN of the sediments is not enriched, the sulfide generated may provide an electron donor, if not carbon source, at these sites. The presence of oxidized metals in the sediments, however, may scavenge the sulfide and keep pore water concentrations low, as described under Whale-fall 2983 previously (*29*). Additionally, the rates of sulfate reduction were not generally enhanced beneath either Whale-fall 2983 or Whale-fall 633, inconsistent with what has been observed under other whale-falls (*44*). These systems are clearly complex, and more direct measurements are needed to assess the differences in the conditions between the whale-fall and background cores. If either carbon or electron donors are more abundant at the whale-falls than away from the site, it does not appear to have an effect on the rates of diazotrophy.

Impact of ammonium on diazotrophy

Traditionally, concentrations of ammonium are the most direct regulator of diazotrophy in active cells. Genetic regulatory systems are present in both bacterial and archaeal diazotrophs to prevent nitrogen fixation in the face of high ammonium concentrations at both transcriptional and port-translational levels (*54, 55*). This prevents a draining of ATP during unnecessary nitrogen fixation, and intuitively would be particularly important in energy-limited diazotrophs. The regulatory *nifI*$_1$ and *nifI*$_2$ genes, required for post-translational "ammonium switch-off" regulation in *Methanococcus maripaludis* (the regulatory system for which has been studied more extensively than any

other methanogen) (*56*), have been detected in deep-sea sediments, and particularly within partial *nif* operons putatively belonging to the ANME archaea (*13*). However, the extent to which the *nifI* genes, or other regulatory mechanisms, regulate nitrogen fixation in the deep-sea is unknown. The apparent diversity of diazotrophs, observed previously via *nifH* sequences and here via varying metabolic activity in concert with diazotrophy, make it likely that several regulatory systems and/or responses to ammonium occur in these sediments.

In the microcosm experiments, diazotrophy was negatively correlated with average concentrations of ammonium over the course of the experiment (Figure 5A, D, G). Although there was no detectable effect under average concentrations (average of t=0 and t=final concentrations) of about 100 μM in methane-rich cores, and 200 μM in whale-fall and background cores, no nitrogen fixation was observed above average concentrations of 200 μM. It should be noted that this comparison is based on average ammonium concentrations over the course of the entire experiment, which means that if the concentration was lower during part of it, nitrogen fixation may have been favored then. This trend should therefore be interpreted as a general response to increasing ammonium rather than a tolerance to particular concentrations. Additional samples taken throughout the time course need to be evaluated for both $\delta^{15}N$ and ammonium to determine under exactly what concentrations of ammonium the diazotrophy occurred.

Nonetheless, these results are similar to previous results in shallow benthic environments, which although occasionally show low levels of diazotrophy in the presence of extremely high levels of ammonium, often show no indication of inhibition below 200–400 μM (*19, 50*). Whether 200–400 μM ammonium is actually a threshold of

inhibition in benthic diazotrophs, or whether community differences between high- and low-level ammonium samples explain the trend, has not been addressed previously. Additionally, the number of samples investigated at high ammonium concentrations has been relatively few (*19*). The physiological implications of either an ammonium inhibition or a lack thereof in deep-sea diazotrophs is great: the former implies the existence of a complex regulatory genetic system, and the latter implies fundamental differences between these other known diazotrophs.

Ammonium inhibition experiment

Therefore, to directly test the effect of ammonium on diazotrophy in methane seep sediment, an ammonium inhibition experiment was carried out. The sediment from a single core was homogenized, slurried with filtered seawater, and aliquoted into separate bottles amended with varying concentrations of ammonium (0–5 mM). Sulfate reduction was measured via sulfide production over the course of the experiment to ensure that the addition of ammonium did not fundamentally perturb the dominant microbial processes. Consistent with the negative correlation observed between diazotrophy in the incubations and the concentration of ammonium, a negative correlation was observed in the controlled experiments, suggesting that like better-studied mesophilic diazotrophs, including methanogens (*56, 57*), deep-sea diazotrophs undergo regulation as ammonium concentrations rise, as well.

However, the ammonium inhibition response occurred at concentrations of NH_4^+ much higher than those typically observed to inhibit diazotrophy in pure cultures: diazotrophic activity in *Methanococcus maripaludis* begins to be inhibited at 25 μM

NH_4^+, and ceases completely at 100 μM (*56*). In this experiment, we observe methane-dependent nitrogen fixation in duplicate incubation bottles at 288 μM NH_4^+ or greater. NH_4^+ was measured at the beginning and end of the experiment, and the lower of the two measurements (which in all cases in this experiment was the final concentration) is considered the minimum NH_4^+ present during the fixation observed. This means that at least some nitrogen fixation occurred at higher concentrations of ammonium, and as it was drawn down. Additionally, nitrogen fixation was observed in one of two duplicate bottles amended with 2000 μM NH_4^+, and with a final concentration of 1089 μM. Nitrogen fixation at concentrations of 1089 μM or greater is therefore also a possibility, and will be explored further. The reason for nitrogen fixation at levels of ammonium high enough to support the growth of traditional diazotrophs is not currently known. However, it is possible that chemical microniches develop within the sediment pore spaces, and that the bulk ammonium concentration measured is not what is experienced by an individual diazotrophic cell.

Molecular analysis of the sediment used in the ammonium inhibition experiment revealed that 33% of the *nifH* genes present grouped with putative ANME-2 *nifH* sequences in a putatively methane seep-specific *nifH* clade. Sequences related to those of the *nifH* homologues of ANME-1 were also abundant (46% of the library), but ANME-1 *nif* homologues have not yet been shown to be functional or expressed (*58*), and their phylogenetic placement within *nifH* Group IV, an uncharacterized group containing *nifH* sequences from several organisms not able to fix nitrogen (*40*), suggests that they are not used in nitrogen fixation. It is therefore likely that the main diazotrophs in the sediment used for the ammonium inhibition experiment were ANME-2, which is additionally

supported by the extensive methane-dependent sulfate reduction observed during the diazotrophy, and the methane-dependent nature of the $^{15}N_2$-uptake. (Figure 6C). This implies that ANME-2 diazotrophy is sensitive to ammonium, but only at concentrations higher than those typical of methane seep sediment (Figure 1 and (*32*).

Production of ammonium in the microcosm experiments

While observing the relationship between ammonium concentrations and diazotrophy, we noticed an unexpected trend in the ammonium concentrations within the microcosms over time, in both methane- and argon-amended experiments: a production of ammonium. This observation, occurring in both sediment incubations from Hydrate Ridge and Monterey Canyon, is intriguing, and may be explained by nitrogen fixation, dissimilatory nitrate reduction to ammonium (DNRA) or the breakdown of organic matter by heterotrophic microorganisms. It is unlikely due to nitrogen fixation, because NH_4^+ production is not proportional, or even positively correlated, with $^{15}N_2$ uptake. DNRA is unlikely as well, because nitrate concentrations were below the detection limit in the HR and MC incubations at the beginning and end of the experiment. Furthermore, nitrite was not detected, eliminating the possibility of tightly coupled nitrate production and consumption. The breakdown of organic matter by heterotrophic microbes is a possible explanation for increased NH_4^+. The lack of oxygen, nitrate and nitrite in the incubation suggests that sulfate or oxidized metals (e.g., iron or manganese oxides) may act as the electron acceptor for heterotrophic metabolism in these sediments. However, the large amounts of NH_4^+ produced (in some cases ~ 1,000 μM), and therefore the high concentrations of organic matter required, make even this explanation potentially

incomplete. Further work will be necessary to explore the possible mechanisms behind the NH_4^+ production. Regardless, the observation of increasing NH_4^+ in these incubations suggests a significant component of the nitrogen cycle at methane seeps has not yet been fully elucidated.

FUTURE WORK

This chapter is a draft of a manuscript that will be submitted for publication after several additional analyses are conducted. In particular, the following work is planned: (1) Acquisition of additional $\delta^{15}N$ values via EA-IRMS for a subset of incubations including (a) replicate microcosm experiments to determine the variability between bottles, as well as (b) intermediate time points (specifically at 1.1 months and 3.6 months for HR incubations, and 2.1 months and 6.5 months for the Monterey Canyon incubations) to obtain shorter-term rate data as well as investigate when nitrogen fixation occurred during the incubation; (2) Acquisition of total carbon measurements via EA-IRMS to determine if the whale-fall sites are indeed still carbon-rich, (3) Determination of methane concentrations in (a) samples preserved immediately after collection to determine the *in situ* methane concentrations, as well as (b) final incubation bottles incubated with a headspace of Ar, to determine the extent of methanogenesis; (4) Determination of ammonium concentrations via IC during these intermediate time points, to compare the concentration of ammonium present during shorter periods of nitrogen fixing activity, (5) Apply statistical methods to the trends observed between nitrogen fixation and various metabolic activities (SR, AOM, TPG) as well as incubation conditions ($[NH_4^+]$) and *in situ* geochemistry (CH_4, HS^-, NH_4^+), and (6) Confirm the

presence of microorganisms associated with the incubations using fluorescence *in situ* hybridization (FISH), particularly the presence of ANME at the whale-fall sites. Although these analyses will bolster the story described above, additional research on deep-sea diazotrophy, including the investigation of more sediments in deeper, abyssal plain sediments, will be necessary to continue to explore the themes discussed here.

CONCLUSIONS

A survey of nitrogen bioavailability and diazotrophy was conducted in samples collected at methane seep, whale-fall, and unperturbed sediments representative of background seafloor. Although ammonium concentrations suggested the sediments were not depleted in nitrogen, extensive nitrogen fixation was observed, at rates far exceeding those measured in deep-sea sediments previously, in both carbon-loaded and background sediments. The high rates of diazotrophy in background sediments, even without the addition of additional carbon, particularly suggest that nitrogen fixation could be a nearly ubiquitous metabolism on the seafloor. Additionally, geochemical evidence linked diazotrophy to sulfate reduction, the anaerobic oxidation of methane, potentially methanogenesis, and other, as yet unidentified benthic metabolisms, greatly expanding the range of potentially diazotrophs in the deep-sea. Together, the widespread observation of diazotrophy, including in background cores, the lack of inhibition by environmentally relevant concentrations of ammonium, and the potentially diverse organisms capable of nitrogen fixation, underscore the importance of future work quantifying the impact of this metabolism on overlying water column processes.

ACKNOWLEDGEMENTS

We thank the crew and science parties of Atlantis cruise AT-15-68, particularly Lisa Levin, Ally Pasulka, Josh Steele, Jeffrey Marlow, Jennifer Glass, and Elizabeth Trembath-Reichert, and of MBARI Western Flyer DR204-208, particularly Shana Goffredi, Bob Vrijenhoek, Julio Harvey, and Lonny Lundsten, for assistance in sample collection and acquisition of contextual data. We thank the members of the Orphan Lab Group for their help in the laboratory and many fruitful discussions.

WORKS CITED

1. B. B. Jorgensen, A. Boetius, Feast and famine—microbial life in the deep-sea bed. *Nat Rev Microbiol* **5**, 770 (2007).
2. E. J. Carpenter, D. G. Capone, in *Nitrogen in the Marine Environment,* D. G. Capone, D. Bronk, M. Mulholland, E. J. Carpenter, Eds. (Elsevier, Academic Press, San Diego, 2008), p. 141.
3. J. A. Brandes, A. H. Devol, C. Deutsch, New developments in the marine nitrogen cycle. *Chem Rev* **107**, 577 (2007).
4. C. Deutsch, J. L. Sarmiento, D. M. Sigman, N. Gruber, J. P. Dunne, Spatial coupling of nitrogen inputs and losses in the ocean. *Nature* **445**, 163 (2007).
5. J. P. Zehr, Nitrogen fixation by marine cyanobacteria. *Trends Microbiol* **19**, 162 (2011).
6. R. W. Fulweiler, S. W. Nixon, B. A. Buckley, S. L. Granger, Reversal of the net dinitrogen gas flux in coastal marine sediments. *Nature* **448**, 180 (2007).
7. T. Grosskopf *et al.*, Doubling of marine dinitrogen-fixation rates based on direct measurements. *Nature* **488**, 361 (2012).
8. L. A. Codispoti, An oceanic fixed nitrogen sink exceeding 400 Tg N a^{-1} vs the concept of homeostasis in the fixed-nitrogen inventory. *Biogeosciences* **4**, 233 (2007).
9. T. DeVries, C. Deutsch, F. Primeau, B. Chang, A. Devol, Global rates of water-column denitrification derived from nitrogen gas measurements. *Nature Geoscience* **5**, 547 (2012).
10. C. Mahaffey, A. F. Michaels, D. G. Capone, The conundrum of marine N_2 fixation. *Am J Sci* **305**, 546 (2005).
11. M. A. Altabet, Constraints on oceanic N balance/imbalance from sedimentary N-15 records. *Biogeosciences* **4**, 75 (2007).
12. M. P. Mehta, J. A. Baross, Nitrogen fixation at 92˚C by a hydrothermal vent archaeon. *Science* **314**, 1783 (2006).
13. A. E. Dekas, R. S. Poretsky, V. J. Orphan, Deep-sea archaea fix and share nitrogen in methane-consuming microbial consortia. *Science* **326**, 422 (2009).

14. M. P. Mehta, D. A. Butterfield, J. A. Baross, Phylogenetic diversity of nitrogenase (*nifH*) genes in deep-sea and hydrothermal vent environments of the Juan de Fuca Ridge. *Applied and Environmental Microbiology* **69**, 960 (2003).
15. H. Dang, X. Luan, J. Zhao, J. Li, Diverse and novel nifH and nifH-like gene sequences in the deep-sea methane seep sediments of the Okhotsk Sea. *Applied and Environmental Microbiology* **75**, 2238 (2009).
16. J. Miyazaki *et al.*, Molecular characterization of potential nitrogen fixation by anaerobic methane-oxidizing archaea in the methane seep sediments at the number 8 Kumano Knoll in the Kumano Basin, offshore of Japan. *Applied and Environmental Microbiology* **75**, 7153 (2009).
17. D. White, *The Physiology and Biochemistry of Prokaryotes*. (Oxford University Press, New York, ed. Third, 2007).
18. E. O. Hartwig, S. O. Stanley, Nitrogen Fixation in Atlantic deep-sea and Coastal sediments. *Deep-Sea Research* **25**, 411 (1978).
19. D. G. Capone, in *Nitrogen Cycling in Coastal Marine Environments,* T. H. Blackburn, J. Sorensen, Eds. (John Wiley & Sons, New York, 1988), p. 85.
20. Karl *et al.*, Dinitrogen Fixation in the world's oceans. *Biogeochemistry* **57/58**, 47 (2002).
21. M. E. Torres *et al.*, Fluid and chemical fluxes in and out of sediments hosting methane hydrate deposits on Hydrate Ridge, OR, I: Hydrological provinces. *Earth Planet Sc Lett* **201**, 525 (2002).
22. E. Suess *et al.*, Gas hydrate destabilization: enhanced dewatering, benthic material turnover and large methane plumes at the Cascadia convergent margin. *Earth Planet Sc Lett* **170**, 1 (1999).
23. E. Suess *et al.*, in *Natural gas hydrates: occurrence, distribution and detection, Geophysical Monograph Series,* C. Paull, W. P. Dillon, Eds. (American Geophysical Union, Washington DC, 2001), vol. 124, p. 87.
24. T. Treude, A. Boetius, K. Knittel, K. Wallmann, B. B. Jorgensen, Anaerobic oxidation of methane above gas hydrates at Hydrate Ridge, NE Pacific Ocean. *Mar Ecol—Prog Ser* **264**, 1 (2003).
25. J. P. Barry *et al.*, Biologic and geologic characteristics of cold seeps in Monterey bay, California. *Deep-Sea Res Pt I* **43**, 1739 (1996).
26. P. R. Girguis, V. J. Orphan, S. J. Hallam, E. F. DeLong, Growth and methane oxidation rates of anaerobic methanotrophic archaea in a continuous-flow bioreactor. *Applied and Environmental Microbiology* **69**, 5472 (2003).
27. L. Lundsten *et al.*, Time-series analysis of six whale-fall communities in Monterey Canyon, California, USA. *Deep-Sea Res Pt I* **57**, 1573 (2010).
28. S. K. Goffredi, C. K. Paull, K. Fulton-Bennett, L. A. Hurtado, R. C. Vrijenhoek, Unusual benthic fauna associated with a whale fall in Monterey Canyon, California. *Deep-Sea Research Pt I* **51**, 1295 (2004).
29. S. K. Goffredi, R. Wilpiszeski, R. Lee, V. J. Orphan, Temporal evolution of methane cycling and phylogenetic diversity of archaea in sediments from a deep-sea whale-fall in Monterey Canyon, California. *ISME J* **2**, 204 (2008).
30. C. E. Braby, G. W. Rouse, S. B. Johnson, W. J. Jones, R. C. Vrijenhoek, Bathymetric and temporal variation among Osedax boneworms and associated

megafauna on whale-falls in Monterey Bay, California. *Deep-Sea Research Pt I* **54**, 1773 (2007).
31. S. K. Goffredi, V. J. Orphan, Bacterial community shifts in taxa and diversity in response to localized organic loading in the deep sea. *Environmental Microbiology* **12**, 344 (2009).
32. A. E. Dekas *et al.*, Investigating Methane Seep Nitrogen Fixation at Mound 12, Costa Rica: Spatial Distribution of Diazotrophy and Significance of the ANME Archaea. (in prep) Chapter 3 of this dissertation.
33. J. P. Montoya, M. Voss, P. Kahler, D. G. Capone, A Simple, High-Precision, High-Sensitivity Tracer Assay for N_2 Fixation. *Applied and environmental microbiology* **62**, 986 (1996).
34. V. J. Orphan, K. A. Turk, A. M. Green, C. H. House, Patterns of ^{15}N assimilation and growth of methanotrophic ANME-2 archaea and sulfate-reducing bacteria within structured syntrophic consortia revealed by FISH-SIMS. *Environmental Microbiology*, (2009).
35. M. Krueger, H. Wolters, M. Gehre, S. B. Joye, H. H. Richnow, Tracing the slow growth of anaerobic methane-oxidizing communities by N-15-labelling techniques. *FEMS Microbiology Ecology* **63**, 401 (2008).
36. A. Drummond *et al.* Geneious Pro Software v.5.4 (2011).
37. K. Nauhaus, A. Boetius, M. Kruger, F. Widdel, In vitro demonstration of anaerobic oxidation of methane coupled to sulphate reduction in sediment from a marine gas hydrate area. *Environmental Microbiology* **4**, 296 (2002).
38. J. Cline, Spectrophotometric determination of hydrogen sulfide in natural waters. *Limnology and Oceanography* **14**, 454 (1969).
39. W. S. Reeburgh, Oceanic methane biogeochemistry. *Chem Rev* **107**, 486 (2007).
40. J. Raymond, J. L. Siefert, C. R. Staples, R. E. Blankenship, The natural history of nitrogen fixation. *Molecular Biology and Evolution* **21**, 541 (2004).
41. J. P. Montoya, in *Nitrogen in the Marine Environment,* D. Capone, D. A. Bronk, M. R. Mulholland, E. J. Carpenter, Eds. (Elsevier, Boston, 2008), pp. 1277-1302.
42. C. R. Smith, Ecology of Whale Falls at the Deep-Sea Floor. *Oceanography and Marine Biology: an Annual Review* **41**, 311 (2003).
43. V. J. Orphan *et al.*, Geological, geochemical, and microbiological heterogeneity of seafloor methane vents in the Eel River Basin, offshore California. *Chemical Geology*, 265 (2004).
44. T. Treude *et al.*, Biogeochemistry of a deep-sea whale fall: sulfate reduction, sulfide efflux and methanogenesis. *Marine Ecology Progress Series* **382**, 1 (2009).
45. P. A. Murray, S. H. Zinder, Nitrogen-Fixation by a Methanogenic Archaebacterium. *Nature* **312**, 284 (1984).
46. N. Belay, R. Sparling, L. Daniels, Dinitrogen Fixation by a Thermophilic Methanogenic Bacterium. *Nature* **312**, 286 (1984).
47. J. A. Sohm, E. A. Webb, D. G. Capone, Emerging patterns of marine nitrogen fixation. *Nat Rev Microbiol* **9**, 499 (2011).
48. M. T. Madigan, J. M. Martinko, P. M. Dunlap, D. P. Clark, *Brock Biology of Microorganisms*. (Pearson Education, Inc. , San Francisco, ed. 12, 2009).

49. V. J. Bertics *et al.*, Burrowing deeper into benthic nitrogen cycling: the impact of bioturbation on nitrogen fixation coupled to sulfate reduction. *Mar Ecol—Prog Ser* **409**, 1 (2010).
50. V. J. Bertics *et al.*, Occurrence of benthic microbial nitrogen fixation coupled to sulfate reduction in the seasonally hypoxic Eckernforde Bay, Baltic Sea. *Biogeosciences Discussions* **9**, 6489 (2012).
51. A. Boetius *et al.*, A marine microbial consortium apparently mediating anaerobic oxidation of methane. *Nature* **407**, 623 (2000).
52. K. G. Lloyd *et al.*, Spatial structure and activity of sedimentary microbial communities underlying a Beggiatoa spp. mat in a Gulf of Mexico hydrocarbon seep. *PloS One* **5**, e8738 (2010).
53. R. W. Howarth, R. Marino, J. J. Cole, Nitrogen-Fixation in Fresh-Water, Estuarine, and Marine Ecosystems .2. Biogeochemical Controls. *Limnology and Oceanography* **33**, 688 (1988).
54. K. Dixon, Genetic Regulation of Biological Nitrogen Fixation. *Nature Reviews* **2**, 621 (2004).
55. J. A. Leigh, Nitrogen Fixation in Methanogens: The Archaeal Perspective. *Curr Issues Mol Biol* **2**, 125 (2000).
56. P. S. Kessler, C. Daniel, J. A. Leigh, Ammonia switch-off of nitrogen fixation in the methanogenic archaeon Methanococcus maripaludis: Mechanistic features and requirement for the novel GLnB homologues, $NifI_1$ and $NifI_2$. *Journal of Bacteriology* **183**, 882 (2001).
57. J. L. Ramos, F. Madueno, M. G. Guerrero, Regulation of Nitrogenase Levels in Anabaena Sp Atcc-33047 and Other Filamentous Cyanobacteria. *Archives of Microbiology* **141**, 105 (1985).
58. A. Meyerdierks *et al.*, Metagenome and mRNA expression analyses of anaerobic methanotrophic archaea of the ANME-1 group. *Environmental Microbiology* **12**, 422 (2010).

SI Table 1. Description of sediment pushcores investigated in this study. All Hydrate Ridge Elevators (denoted "E") and the "basket" samples were collected on J2-593. Pushcores in bold were used for ^{15}N-incubations. *bdl = below detection limit, for HR sulfde the detection limit was 0.12 mM. "+" Cores were collected with a multicorer rather than a submersible. Distance from C-input from these sites were calculated from HR-N8. All distances were determined in GoogleEarth.

	Collection Information					Location			Site Description					
	Core Name	Dive or Elevator #	PC #	Cruise #	Date Collected	Site Name	Latitude (°N)	Longitude (°W)	Water Depth (m)	Temp (°C)	Oxygen (ml/L)	Surficial Cover	Distance from Carbon input (m)	Sulfide Range (mM)
Monterey Canyon	MC-N1	DR209	53		**10/29/2010**	Whale 1018	36.771329	122.083005	1020.0	3.74	0.37	Whale Vertebrae	0 (Within)	
	MC-N2	DR209	57		**10/29/2010**	Whale 1018 Area	36.771353	122.082978	1020.2	3.77	0.36	Undisturbed sediment	4	
	MC-W1	**DR204**	**56**		**10/25/2010**	**Whale 2893**	36.613683	122.435142	2893.0	1.68	2.11	**Remains of whale skull**	**0**	
	MC-N3	DR204	80		10/25/2010	Whale 2893 Area	36.613699	122.435143	2893.5	1.69	2.11	Undisturbed sediment	1	
	MC-B1	**DR204**	**65**		**10/25/2010**	**Whale 2893 Area**	36.613617	122.435442	2893.2	1.68	2.10	Undisturbed sediment	**28**	
	MC-N4	DR208	80		10/28/2010	Whale 2893 Area	36.613111	122.435327	2893.7	1.69	1.77	Undisturbed sediment	66	
	MC-C	**DR208**	**60**		**10/28/2010**	**Whale 2893 Area**	36.608863	122.434825	2883.1	1.69	1.72	**Clam bed**	**0**	
	MC-N4	DR208	79		10/28/2010	Whale 2893 Area	36.60938	122.434375	2887.7	1.69	1.74	Clam bed	0	
	MC-W2	**DR207**	**43**		**10/27/2010**	**Whale 633**	36.802124	121.993932	632.5	4.72	0.33	**Whale Vertebrae**	**0**	
	MC-N5	DR207	65		10/27/2010	Whale 633	36.802121	121.993954	632.7	4.82	0.32	Whale Vertebrae	0	
	MC-N6	DR205	53		10/26/2010	Whale 633	36.802122	121.99393	633	4.71	0.31	Whale skull	0	
	MC-N7	DR207	64		10/27/2010	Whale 633 Area	36.802093	121.994013	632.77	4.69	0.32	Undisturbed sediment	1	
	MC-B2	**DR205**	**52**		**10/26/2010**	**Whale 633 Area**	36.802464	121.993865	633	4.75	0.31	Undisturbed sediment	**38**	
Hydrate Ridge	HR-N2	AD4629	12	AT 15-68	8/1/2010	HR South	44 34.2295	125 8.8251	774			Microbial Mat	0	4.5 - 13.2
	HR-N3	AD4629	18	AT 15-68	8/1/2010	HR South	44 34.2224	125 8.8100	774			Clam bed	0	0.9 - 10.9
	HR-N4	AD4629	24	AT 15-68	8/1/2010	HR South	44 34.2284	125 8.8040	774			Undisturbed sediment	14	bdl*
	HR-N5	AD4631	9	AT 15-68	8/3/2010	HR North	44 40.1305	125 6.5169	615			Clam bed	0	2.5 - 6.1
	HR-N6	AD4631	2	AT 15-68	8/3/2010	HR North	44 40.1305	125 6.5169	615			Clam bed	0	3.4 - 10.8
	HR-M2	**AD4632**	**14**	**AT 15-68**	**8/4/2010**	**HR North**	**44 40.0269**	**125 5.9997**	**602**			**Microbial Mat**	**0**	**6.7 - 10.1**
	HR-N7	AD4632	17	AT 15-68	8/4/2010	HR North	44 40.0398	125 6.0284	602			Undisturbed sediment	41	bdl
	HR-N8	AD4633	2	AT 15-68	8/5/2010	HR Southeast Knoll	44 39.1419	125 1.7034	625			Microbial Mat	0	5.2 - 9.0
	HR-N9	AD4634	6	AT 15-68	8/6/2010	HR North	44 40.0285	125 6.0027	602			Microbial Mat	0	3.2 - 8.4
	HR-N16	AD4634	11	AT 15-68	8/6/2010	HR North	44 40.0290	125 6.0012	602			Microbial Mat	0	7.6 - 18.7
	HR-M1	**AD4635**	**17**	**AT 15-68**	**8/7/2010**	**HR South**	**44 34.2133**	**125 8.8176**	**774**			**Microbial Mat**	**0**	**nm**
	HR-C	**AD4635**	**15**	**AT 15-68**	**8/7/2010**	**HR South**	**44 34.1965**	**125 8.8538**	**775**			**Clam bed**	**0**	**1.6 - 18.3**
	HR-N10	AD4635	6	AT 15-68	8/7/2010	HR South	44 34.1965	125 8.8583	775			Microbial Mat	0	3.4 - 15.9
	HR-N11	AD4635	18	AT 15-68	8/7/2010	HR South	44 34.2133	125 8.8176	774			Microbial Mat	0	2.6 - 11.3
	HR-N12	AD4635	14	AT 15-68	8/7/2010	HR South	44 34.1965	125 8.8538	775			Clam bed	0	nd - 11.2
	HR-M3	**AD4636**	**10**	**AT 15-68**	**8/8/2010**	**HR South**	**44 34.1166**	**125 9.0282**	**794**			**Microbial Mat**	**0**	**3.5 - 16.0**
	HR-N13	AD4636	7	AT 15-68	8/8/2010	HR South	44 34.0664	125 9.1966	800			Microbial Mat	0	12.2 - 14.6
	HR-N14	AD4636	19	AT 15-68	8/8/2010	HR South	44 34.1830	125 8.8078	772			Microbial Mat	0	3.7 - 12.1
	HR-B	**MC3$^+$**		**AT 15-68**	**8/2/2010**	**Off-Site**	**44 35.2739**	**124 53.4987**	**600**			**Undisturbed sediment**	**12980**	**bdl**
	HR-N15	MC4$^+$		AT 15-68	8/5/2010	Off-Site	44 35.2767	124 53.56006	589			Undisturbed sediment	12910	bdl
	HR-AI	**AD4634**	**12**	**AT 15-68**	**8/6/2010**	**HR North**	**44 40.0285**	**125 6.0027**	**602**			**Microbial Mat w/ Bubbling**	**0**	**nm**

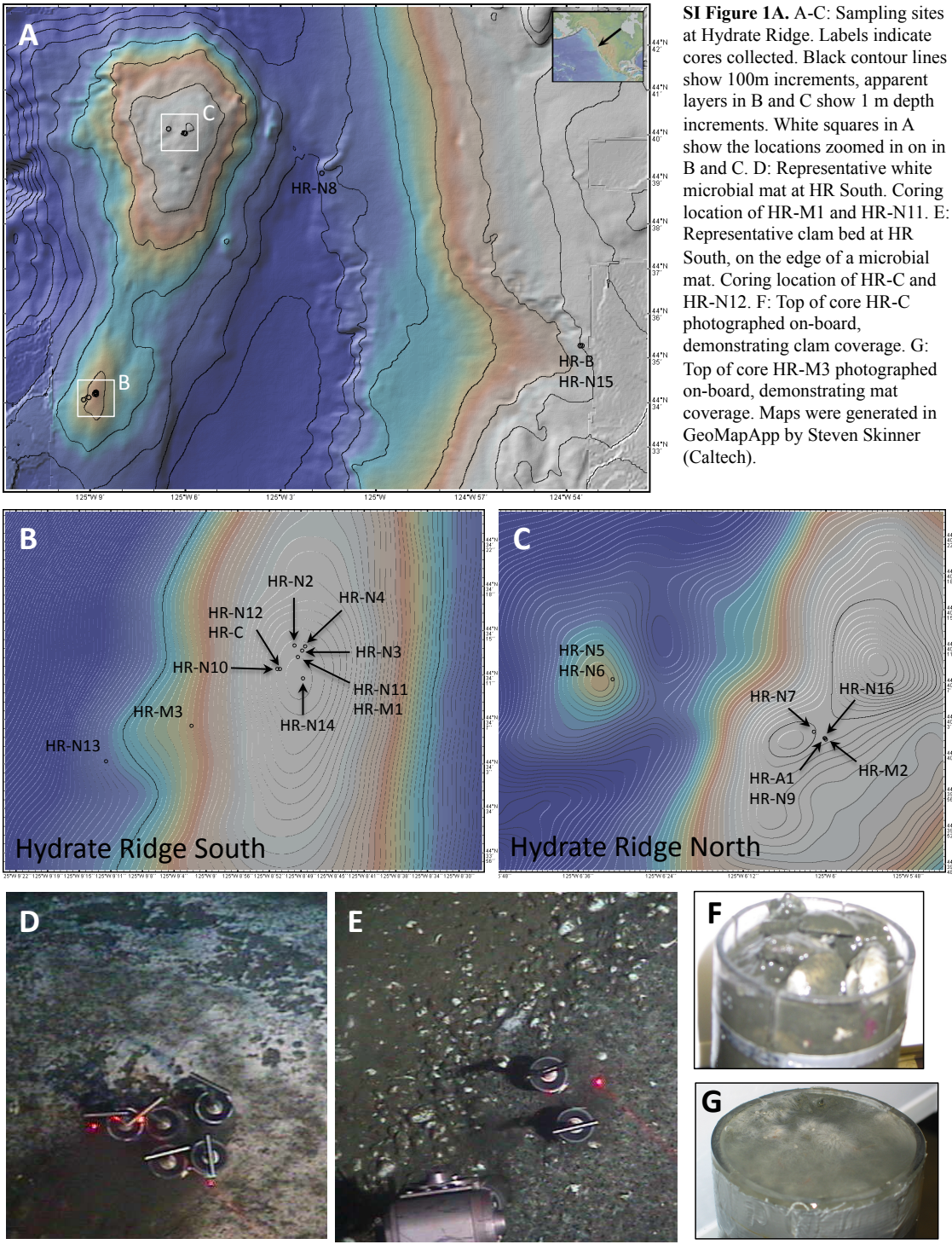

SI Figure 1A. A-C: Sampling sites at Hydrate Ridge. Labels indicate cores collected. Black contour lines show 100m increments, apparent layers in B and C show 1 m depth increments. White squares in A show the locations zoomed in on in B and C. D: Representative white microbial mat at HR South. Coring location of HR-M1 and HR-N11. E: Representative clam bed at HR South, on the edge of a microbial mat. Coring location of HR-C and HR-N12. F: Top of core HR-C photographed on-board, demonstrating clam coverage. G: Top of core HR-M3 photographed on-board, demonstrating mat coverage. Maps were generated in GeoMapApp by Steven Skinner (Caltech).

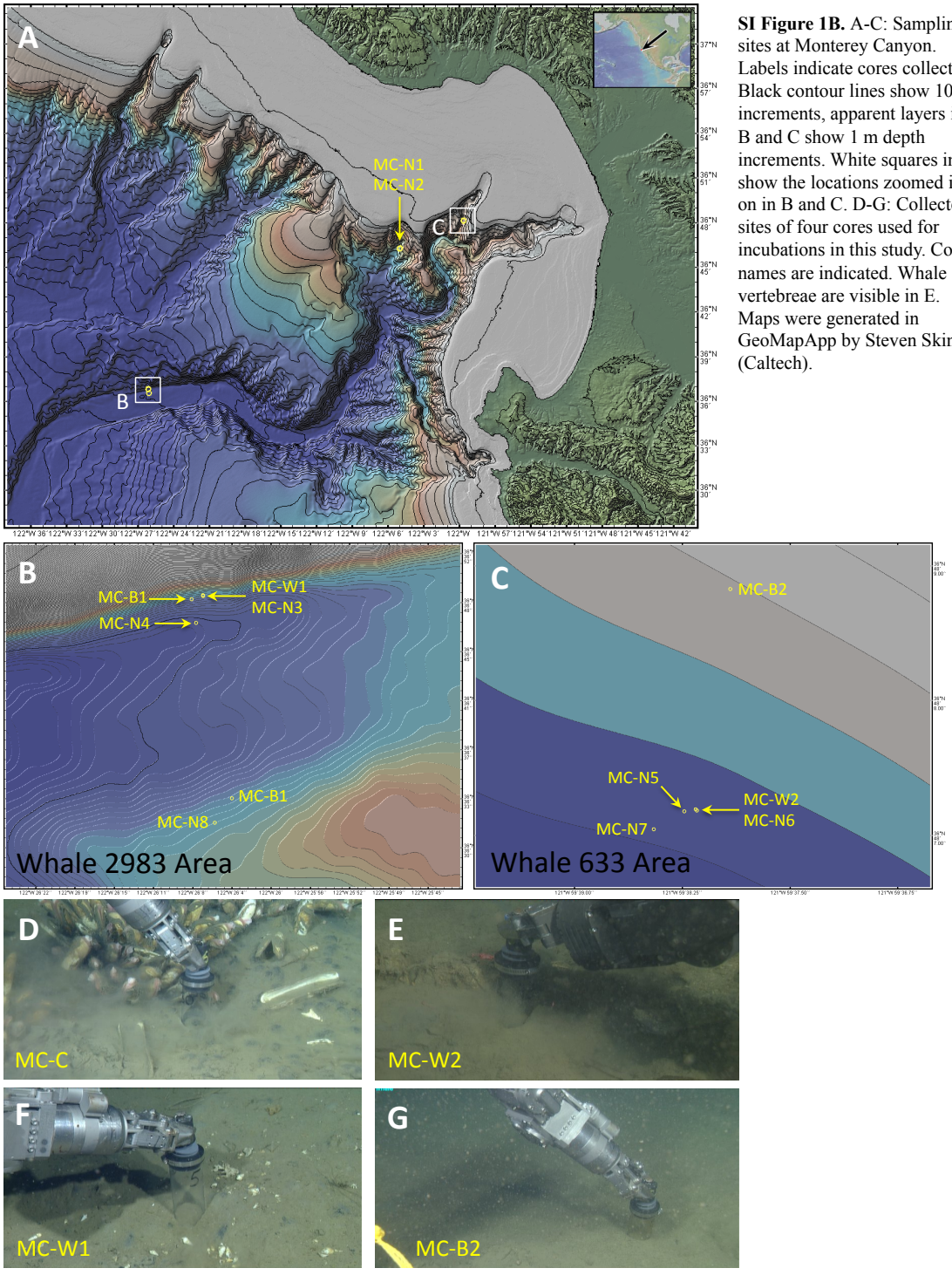

SI Figure 1B. A-C: Sampling sites at Monterey Canyon. Labels indicate cores collected. Black contour lines show 100m increments, apparent layers in B and C show 1 m depth increments. White squares in A show the locations zoomed in on in B and C. D-G: Collected sites of four cores used for incubations in this study. Core names are indicated. Whale vertebreae are visible in E. Maps were generated in GeoMapApp by Steven Skinner (Caltech).

A p p e n d i x A

Clay Shell Encrusts Microorganisms Mediating the Anaerobic Oxidation of Methane in Marine Sediments

Anne Dekas[1], Jake V. Bailey[1,2], Thomas F. Bristow[1,3], Sameer S. Walavalkar[1], Victoria J. Orphan[1]

[1]California Institute of Technology
[2]Present Affiliation: University of Minnesota
[3]Present Affiliation: NASA Ames Research Center

Explanation for Appendix: While investigating the diazotrophic capabilities of the ANME, I stumbled upon an interesting observation: a mineral shell encrusting the ANME-SRB aggregates. Although this crust had been rumored within the lab group, and some previous work had explored potential ways to remove it, it had not been described or recorded. Realizing it could be an important complicating factor for some of our other analyses (FISH and NanoSIMS, specifically), not to mention potentially an important contributor/inhibitor of the cells' metabolic processes, I decided to take a closer look. The following describes the preliminary results I collected over a few months during which I explored this tangent, with a cursory discussion of the potential significance. This is an important and still unexplained observation that I think deserves further investigation and eventual publication.

ABSTRACT

The biological anaerobic oxidation of methane (AOM) is credited for consuming greater than 80% of the methane naturally released in marine sediment, however many details regarding the mechanism of this metabolism remain unknown. Recently, the observation that the organisms mediating AOM, anaerobic methanotrophic archaea (ANME) and sulfate-reducing bacterial symbionts (SRB), attach to particular mineral fractions within the sediment suggested the potential importance of mineral interactions to AOM (*1*). In the present study, Scanning Electron Microscopy (SEM) of ANME-SRB aggregates enriched from Eel River Basin methane seep sediment in anaerobic incubations revealed a mineral crust encasing individual aggregates. Energy-dispersive X-ray Spectroscopy (EDS) revealed a composition of C, O, Si, Al, Mg, Na, and Fe, elements suggestive of organic material in combination with aluminosilicate clay. To investigate the ubiquity of this crust on the AOM aggregates, samples preserved directly after collection from Costa Rica margin methane seep sediments were also examined. A similar crust was observed surrounding these aggregates, demonstrating that the crust is not limited to aggregates from the Eel River Basin and not an artifact of incubation conditions. Species-specific FISH probes in combination with SEM-EDS revealed the presence of the crust on ANME-2 aggregates containing either the *Desulfosarcina/Desulfococcus* or *Desulfobulbaceae* sulfate-reducing partner, as well as

clusters of ANME-2 archaea alone. However, the crust was not observed on individual ANME-1 cells. To investigate the three-dimensional distribution of the clays within the aggregates, Focused Ion Beam (FIB) sectioning of an encrusted ANME-2/DSS aggregate followed by EDS and NanoSIMS analysis demonstrated that the mineral layer is a shell around the aggregate of cells, not distributed throughout the cluster. This is first description of a mineral crust around the ANME-SRB aggregates, and raises questions about the impact of this crust on AOM metabolism and growth.

INTRODUCTION

Over a decade of research has focused on the biological anaerobic oxidation of methane (AOM) and its role in reducing the flux of naturally released methane from the seafloor to the atmosphere. During this time, the archaeal groups ANME-1, -2, and -3, typically in association with one of several sulfate-reducing bacterial symbionts (SRB, including members of the *Desulfosarcina/Desulfococcus, DSS* and *Desulfobulbaceae, DSB*) have been identified as mediating the anaerobic oxidation of methane coupled to sulfate reduction. However, these microorganisms have not been obtained in culture, making their investigation difficult and leaving many questions regarding their symbiosis and the mechanism of their metabolisms unanswered. In particular, the intermediate compound passed between the ANME and SRB, and/or the physical mechanism of electron transfer, in order to couple the oxidation of methane to sulfate reduction between these two organisms, is unknown.

Several studies have recently suggested that the mineral matrix within which the ANME-SRB reside may be important to their methane metabolism. Beal and colleagues detected AOM coupled to iron and manganese reduction in sulfate-free incubations of methane seep sediment amended with ferrihydrite and birnessite (respectively) suggesting that the ANME and/or associated symbionts are capable of electron exchange with these minerals (*2*). Additionally, Harrison and colleagues observed co-extraction of

particular ANME-subgroups with different mineral fractions separated by density and magnetic susceptibility, suggesting preferential attachment or association with different minerals (*1*). In particular, ANME-1 were preferentially co-extracted with mineral partitions containing quartz, feldspar, and metal-free phyllosilicates, ANME-2ab with metal-bearing illites, and ANME-2c with pyrite. Mineral attachment of cells in sediments in subsurface samples is nearly ubiquitous, for varied purposes from predation defense to the acquisition of trace nutrients or electron donors/acceptors (see (*1*) and references therein). Additionally, the repeated suggestion and recent evidence for an extracellular shuttle of electrons through sediments via conductive nanowires or minerals (*3*–*5*) further underscores the importance of microbe-mineral interactions in sediment communities. Despite the evidence for mineral association with the ANME, and the precedence for metabolically critical interactions between cells and solid substrates, the role of mineral attachment in the ANME archaea in sulfate-rich methane sediments remains unknown.

Characterizing the physical association between cells and specific minerals is the first step in understanding what role minerals may play in metabolism and/or the cell life cycle. In the current study, we combine fluorescence *in situ* hybridization (FISH) with Scanning Electron Microscopy (SEM) and Energy-Dispersive X-ray Spectroscopy (EDS) to directly observe mineral associations of the ANME-SRB. The ANME-SRB aggregates investigated were collected at two different sites of methane seepage, one within the Eel River Basin and one along the Costa Rica Margin, in order to compare and contrast mineral associations within different sediments. We additionally utilize a Focused Ion Beam (FIB) to cut through the ANME-SRB aggregates and analyze the exposed cross-section with SEM-EDS as well as Nanoscale Secondary Ion Mass

Spectrometry (NanoSIMS) to investigate the 3-dimensional distribution of minerals throughout the ANME-SRB aggregates. This work characterizes the association of ANME-2/SRB with a never-before described mineral crust, and discusses both potential formation mechanisms as well as effects on ANME-SRB metabolism and growth.

ABBREVIATED METHODS

FISH, SEM, and EDS

Fluorescence *in situ* Hybridization (FISH) was performed on methane seep sediment from the Eel River Basin and the Costa Rica Pacific Margin as previously described (sampling and FISH details in Chapters 1–3). FISH probes ANME 932 (targeting ANME-2), DSS 658 (targeting *Desulfosarcina*/*Desulfococcus*), and DSB 652 (targeting *Desulfobulbaceae*) were employed, and cells were identified and mapped using an epifluorescence microscope (Applied Precision Delta Vision, Orphan Laboratory, Caltech). FISH-identified ANME-SRB aggregates were re-found and visualized via Scanning Electron Microscopy (SEM) (Zeiss 1550VP, Kavli Nanoscience Institute, Caltech), and point targets analyzed with Energy-Dispersive X-ray Spectrometry (EDS) (Oxford INCA 300, GPS Division Analytical Facility). All imaged aggregates were fixed with 4% formaldehyde or 2% paraformaldehyde, sonicated, filtered onto 0.2 um filters, and DAPI stained, before analysis. Some additionally underwent a Percoll gradient density separation (details in Chapter 2) and FISH.

Quantification of crust-containing aggregates

The fraction of ANME-SRB aggregates containing the aggregate crust was determined by examination of 100 aggregates in an minimally processed sample (samples were fixed with paraformaldehyde, stored in ethanol, sonicated and filtered into 0.2 um filters, however no density gradient was employed nor FISH). Aggregates were identified via DAPI staining and visualized via epifluorescence microscopy. Crusts were identified by a characteristic bending of light when changing the focal plane of the microscope. Although inferior to identification with SEM, the time-intensive mapping process required for identifying the aggregates via microscopy and re-locating them with the SEM made analyzing a large sample size with SEM unpractical. Out of the 100 samples analyzed via microscopy, 9 were re-found with SEM to confirm the classification of crust or no crust. SEM analysis confirmed the crust in 100% of the aggregates identified as crust-containing via microscopy (n=6), and 2 out of 3 aggregates identified as not-crust-containing in fact contained a crust. The microscope method of identification was therefore considered a conservative estimate for the number of crust-containing aggregates.

Thin sectioning with FIB and NanoSIMS

ANME-SRB aggregates identified via FISH and microscopy were re-found and analyzed on the CAMECA NanoSIMS 50L, housed at Caltech. Image collection parameters were as described in Chapter 3 of this dissertation, except the Si^- ion was simultaneously collected. Targets were analyzed for several hours to whole days in order to sputter away surficial layers and observe Si on the interior of the aggregate. Chemical

analysis of the aggregate interior was also achieved by Focus Ion Bean (FIB) (FEI Nova-600, Kavli Nanoscience Institute, Caltech) sectioning using a Ga^+ beam perpendicular to the sample surface, followed by EDS analysis. FIB has been employed previously to section single cells and allow chemical analysis of the cell interior (*6*).

ABBREVIATED RESULTS and DISCUSSION

Description and chemical composition

A flakey, mineral crust was observed on cell clusters of ANME-2 archaea and sulfate-reducing bacteria (SRB) during SEM analysis (Figure 1, 2). EDS revealed that target areas covered by crust were enriched in O, Si, Al, Mg, Na, and Fe, consistent with an aluminosilicate clay (Figure 1B), and weight percent oxides compositions for four aggregates were calculated (Table 1). The crust, with an approximately consistent composition, although sometimes including K, Fe and/or Ca, was found on aggregates from both the Eel River Basin and the Costa Rica margin (Figure 2), regardless of the phylogenetic identify of the sulfate-reducing bacterial partner (DSS or DSB) (Figure 2) or even the presence of a bacterial partner (Figure 1), and regardless of the type of association between the ANME and the SRB (shell, mixed, mixed clumpy, spanning the morphologies described by Knittel and colleagues (*7*)) (Figure 2). It has been proposed that different ANME-subgroups (2a, 2c, 3, etc.) associate with the bacterial partner in different ways (*7*). If true, the observations suggest that the crust is associated with several aggregate-containing ANME-subgroups. However, no crust was observed via SEM analysis on ANME-1 single cells (n=2), data not shown.

Frequency of occurrence and distribution on/within aggregate

The crust was detected on 86 out of 103 aggregates investigated in Costa Rican methane seep sediment (Figure 3), although this is believed to be a conservative estimate (see Methods). This suggests that the crust is a nearly ubiquitous feature of the aggregates within this sample. Previously published SEM images of the ANME-SRB aggregates from Black Sea microbial mats did not show a mineral crust (*7*), indicating that aggregates outside of direct contact with sediments may not maintain this association. This observation, plus the lack of crust on the ANME-1 cells, suggests that although the function of the crust is unknown, if a function indeed exists, it is not required in all aggregates. Cross-sectioning of the aggregates with perpendicular ion ablation (NanoSIMS and FIB) and subsequent analysis of the interior of the aggregate revealed that the clays are primarily on the exterior of the aggregates, allowing the classification of this association as a shell (Figure 4, 5).

Additional mineral associations

Additionally associations with solid substrates were observed in the aggregates during SEM-EDS analysis of methane seep sediment from the Costa Rican Margin, including diatom frustules embedded in the crust (Figure 6A) and Fe- and S-bearing minerals on top of and within the nest-like clay crust (Figure 6B). The Fe- and S-containing particles were observed in almost all aggregates investigated, and were typically spherical structures varying in size but small compared to the size of the ANME-SRB clusters (which are 5-15 um in diameter). The Fe_xS_x microcrystals were consistently composed of an approximately 1:1 ratio of Fe:S, suggesting that they were

not pyrite FeS_2, which has been found in methane seep sediment from the Eel River Basin and previously found to be in putative association with the ANME-2c (*1*). Rather, these features are more likely greigite, pyrrhotite, and/or mackinawite, with Fe:S ratios closer to 1:1. These reduced sulfur minerals may be a result of active sulfate reduction within the aggregates. The potential role of iron sulfides as both a product and mediator of microbial metabolism is great and has been described previously (*8, and references therein*).

Possible mechanisms of formation

Although the exact mechanism of the anaerobic oxidation of methane (AOM) is unknown, all currently favored potential mechanisms of AOM produce bicarbonate (HCO_3^-). This increases the alkalinity of the local environment, and causes the precipitation of calcium carbonate ($CaCO_3$), which forms macroscopic nodules, and even large edifices in regions where AOM is a dominant metabolism (e.g., methane seeps) (*9*). It was therefore initially assumed, after routine observations with epifluorescence light microscopy suggested a mineral shell around the ANME-SRB aggregates, that a shell, if indeed present, consisted of authigenic carbonate. However, SEM-EDS analysis quickly proved this hypothesis wrong, and revealed a composition consistent with an aluminosilicate clay. Inexplicable by a precipitation event, we are forced to explore other potential formation mechanisms for this association.

Several possibilities may explain the formation of this crust. Negatively charged clay particles in the sediments may be attracted to a positively charged cell surface, and therefore adhere to the aggregates. A positive surface charge has not previously been

documented in the ANME-SRB, but it has been demonstrated in other carbonate precipitation-catalyzing microbes as a defense against carbonate entombment (*10*), and is therefore an intriguing possibility here. Another possibility is that authigenic clay nucleation is occurring in the extracellular polymeric substance (EPS) that commonly surrounds AOM aggregates. EPS has been identified as a template for layer-silicate synthesis in other deep-sea microbial systems (*11*). Bio-formation of clays appears to be an evolving field, demonstrated and discussed in (*12*).

Comparison of the composition of the clays in the bulk sample versus the attached crust may indicate the specificity of the association and therefore give clues to its origin. Although the clay composition of the bulk sediment at the Eel River Basin was determined here (Table 2), attempts to do the same for the individual crusts via Raman Spectroscopy were inconclusive. We therefore cannot comment on the difference or similarity between the surrounding clays and the attached clays. The greater the difference between the compositions of the attached clay and the surrounding clay, the greater the likelihood that the mechanism of formation/attachment is specific to the ANME metabolism. After all, it is also possible that the ANME aggregates are simply sticky, and are collecting a random assortment of surrounding detritus. However, the inability to detach this mineral assemblage even with sonication, and the finding of some aggregates with no crust, as well as the ANME-1 single cells, does suggest that it may be a targeted attachment process. Regardless of its mechanism of formation, the close and persistent contact between these cells and the clay layer raise the question of chemical interaction between them.

Potential Impact on AOM Metabolism

Some prokaryotes—sulfate-reducing bacteria included—are able to reduce ferric iron in clay minerals in dissimilatory metabolism (*13, 14*). The observed presence of the clay crust on these aggregates is certainly not evidence for this interaction, however AOM coupled to iron reduction has been shown previously (*2*). Although sulfate is typically abundant in marine systems, making other electron acceptors unnecessary, it is possible that slightly below the methane-sulfate transition zone, where sulfate is depleted but methane is abundant, the ability to couple methane oxidation to iron reduction may confer an ecological advantage and the ability to fill a unique niche space even within marine sediments.

Another possible role for ANME-mineral interaction related to dissimilatory metabolism is electron transfer. Conductive minerals, and particularly iron sulfide minerals, have been hypothesized to play a role in extracellular electron transfer (EET) previously (*8*). EET is an increasingly popular explanation for the long distance coupling of reactions, with increasing evidence to suggest that it may be prevalent and significant in soils and sediments (*3–5*). To investigate this possibility in the ANME aggregates, we attempted to measure conductivity in the aggregates via Atomic Force Microscopy (Veeci Innova AFM, housed in the NanoBio Group at the University of Southern California). We failed to detect continuous conductivity through the aggregate (tracing an electrode across the top of the aggregate to see if a closed circuit could be established through the aggregate to the conductive surface below, data not shown). However, there may still be shorter-length paths of EET within the aggregate that we were unable to detect.

An adverse potential effect of the crust is limiting nutrient exchange at the cell surface. Even partial coverage of the aggregate surface with mineral solids may decrease the rate of diffusion into and out of particular cells. Diffusion in this system has been modeled previously (*15, 16*), but without consideration for potential physical barriers on the cell surface, effectively decreasing the diffusible surface area of the consortia. Reduced diffusion due to the crust may therefore facilitate the formation of chemical microniches not currently expected within the aggregates. These microniches may decrease the expected rate of some metabolic functions (e.g., AOM, if either methane or sulfate become diffusion-limited) and increase the need for others (e.g., nitrogen fixation, if the same were true for bioavailable N). Additionally, clay minerals may interact with chemicals as they pass into and out of the sediments, as well. The function, beneficial or not, of the crust to act as a chemical filter, for instance, binding with free ammonium or scavenging trace metals, is another possibility to be explored.

Finally, the effect of a clay shell on the aggregate can be considered in terms of the physical growth and replication of the aggregates. The crust appears to be extremely fragmented, and therefore likely expands as the cells grow and double within the aggregate. This model would also explain why the crust appears to be nearly exclusively on the outside of the aggregate; if the shell shape and size were fixed, one would expect lobes of cells individually covered in clay within an aggregate, reflecting individual growth spurts and subsequent entombment following by additional rounds of growth. The crust does suggest, however, that the ANME and SRB remain and duplicate within the aggregate, rather than collecting and discarding bacterial partners continually.

Although the ANME-DSS association is believed to be extremely stable, recent evidence (Chapter 4) suggested that perhaps the AMNE-DSB association was more transitory. Although the existence of the crust on the ANME-DSB aggregates does not eliminate the possibility of transient associations, it does seem to limit the availability of direct contact with the ANME to cells on the outside.

In summary, we have revealed the presence of an abundant and well-distributed aluminosilicate clay crust encapsulating the majority of ANME-2/SRB aggregates within methane seep sediments. Although we have not yet identified a mechanism of formation or any chemical interaction between the cells and the crust, possibilities abound, and additional analyses will be pursued.

WORKS CITED

1. B. Harrison, V. Orphan, Method for Assessing Mineral Composition-Dependent Patterns in Microbial Diversity Using Magnetic and Density Separation. *Geomicrobiology Journal* **29**, 435 (2012).
2. E. J. Beal, C. H. House, V. J. Orphan, Manganese- and iron-dependent marine methane oxidation. *Science* **325**, 184 (2009).
3. L. P. Nielsen, N. Risgaard-Petersen, H. Fossing, P. B. Christensen, M. Sayama, Electric currents couple spatially separated biogeochemical processes in marine sediment. *Nature* **463**, 1071 (2010).
4. L. P. Nielsen *et al.*, paper presented at the 14th International Symposium on Microbial Ecology, Copenhagen, Denmark, 2012.
5. M. Y. El-Naggar *et al.*, Electrical transport along bacterial nanowires from Shewanella oneidensis MR-1. *Proceedings of the National Academy of Sciences of the United States of America* **107**, 18127 (2010).
6. P. K. Weber *et al.*, NanoSIMS imaging of Bacillus spores sectioned by focused ion beam. *Journal of Microscopy* **238**, 189 (2009).
7. K. Knittel, T. Losekann, A. Boetius, R. Kort, R. Amann, Diversity and distribution of methanotrophic archaea at cold seeps. *Applied and Environmental Microbiology* **71**, 467 (2005).
8. R. Nakamura *et al.*, Biological iron-monosulfide production for efficient electricity harvesting from a deep-sea metal-reducing bacterium. *Chembiochem: A European Journal of Chemical Biology* **11**, 643 (2010).
9. W. S. Reeburgh, Oceanic methane biogeochemistry. *Chem Rev* **107**, 486 (2007).

10. R. Martinez, E. Gardes, O. Pokrovsky, J. Schott, E. Oelkers, Do photosynthetic bacteria have a protective mechanism against carbonate precipitation at their surfaces? *Geochim Cosmochim Ac* **74**, 1329 (2010).
11. M. Ueshima, Z. Tazaki, Possible Role of Microbial Polysaccharides in Nontronite Formation. *Clays and Clay Minerals* **49**, 292 (2001).
12. Z. Tazakai, Microbial Formation of a Halloysite-Like Mineral. *Clay and Clay Minerals* **53**, 224 (2005).
13. H. Dong, D. Jaisi, J. Kim, G. Zhang, Microbe-clay mineral interactions. *American Mineralogist* **94**, 1505 (2009).
14. Y.-L. Li *et al.*, Iron reduction and alteration of nontronite NAu-2 by a sulfate-reducing bacterium. *Geochim Cosmochim Ac* **68**, 3251 (2004).
15. B. Orcutt, C. Meile, Constraints on mechanisms and rates of anaerobic oxidation of methane by microbial consortia: process-based modeling of ANME-2 archaea and sulfate reducing bacteria interactions. *Biogeosciences* **5**, 1587 (2008).
16. K. B. Sorensen, K. Finster, N. B. Ramsing, Thermodynamic and kinetic requirements in anaerobic methane oxidizing consortia exclude hydrogen, acetate, and methanol as possible electron shuttles. *Microbial Ecology* **42**, 1 (2001).

Figure 1: Initial observations of a clay crust surrounding the microbial consortia mediating the anaerobic oxidation of methane. A: SEM and corresponding FISH images of three representative consortia. ANME-2 are hybridized with probe Eel 932 (pink) and *Desulfosarcina/Desulfococcus* hybridized with DSS 658 (green). In the center panel no archaeal probe was employed. Blue indicates a DAPI stain. B. EDS analysis of the two points indicated in A. Many EDS point analysis were collected on each aggregate, but only two representative analyses are shown. Point 1 targets the clay matrix and 2 targets a lobe of archaeal cells with apparently no or little crust-covering.

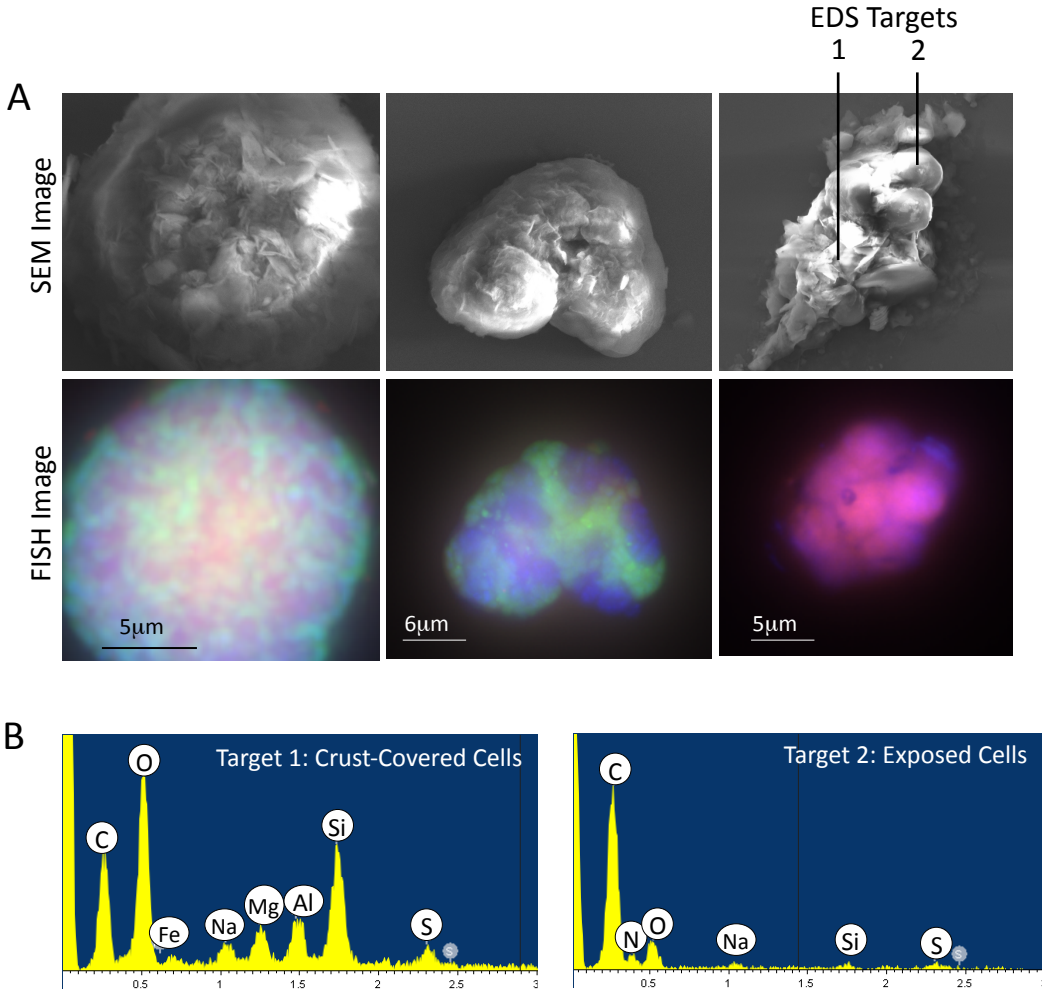

Figure 2: Additional coupled SEM and FISH analyses of the ANME-SRB aggregates demonstrating the presence of the crust regardless of the morphology of association between the ANME and SRB, with either Desulfobulbaceae (DSB 652, green) or *Desulfosarcina/Desulfococcus* (DSS 658, green) and from both the Eel River Basin and Costa Rica Margin methane seeps. Archaea are hybridized with Eel 932. No archaeal probe was employed in aggregate 1.

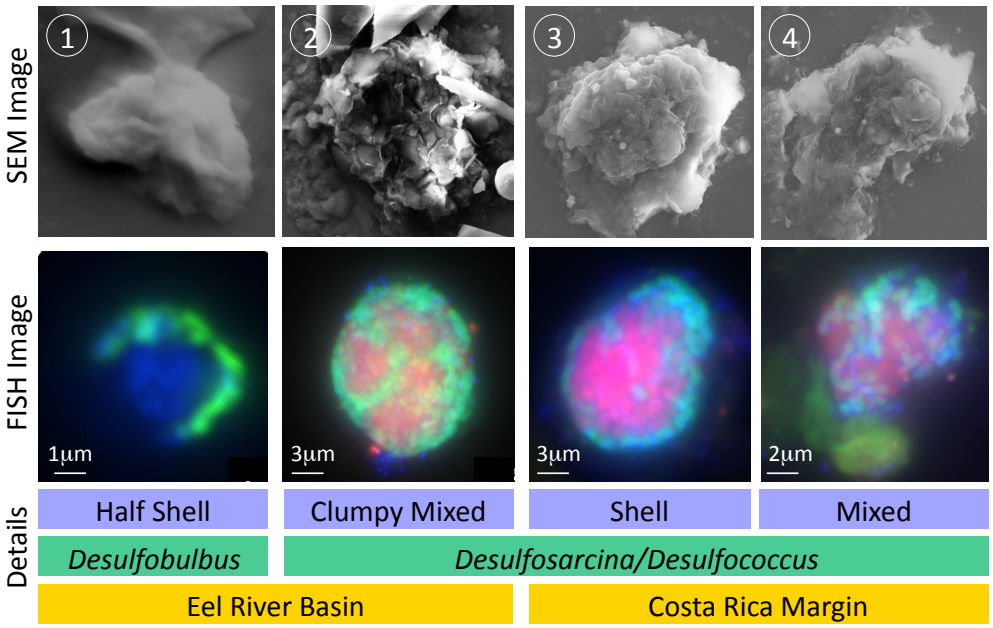

Table 1: Composition of crust calculated as weight percent oxides (wt % oxide). Representative EDS measurements of targets within the aggregates of Figure 2 (1–4) were used for the wt% oxide calculation.

Oxide	①	②	③	④
SiO_2	51.9	60.4	66.9	61.0
Al_2O_3	23.8	14.2	18.9	21.3
MgO	3.2	7.3	6.7	2.0
FeO		8.9		5.9
K_2O			3.5	
Na_2O	5.3	4.5		3.4
CaO		2.2	4.0	
SO_3	15.8	2.5		6.5

Figure 3: Quantitative analysis of the ubiquity of the crust revealed that over 85% (at least 86 out of 103, see Methods for why this is likely a conservative estimate) of the ANME-SRB aggregates in Costa Rica methane seep sediment were covered in a solid crust. Below, this comparison is shown, along with an example of an aggregate found without a crust. Again, pink indicates probe Eel 932, green indicates probe DSS 658.

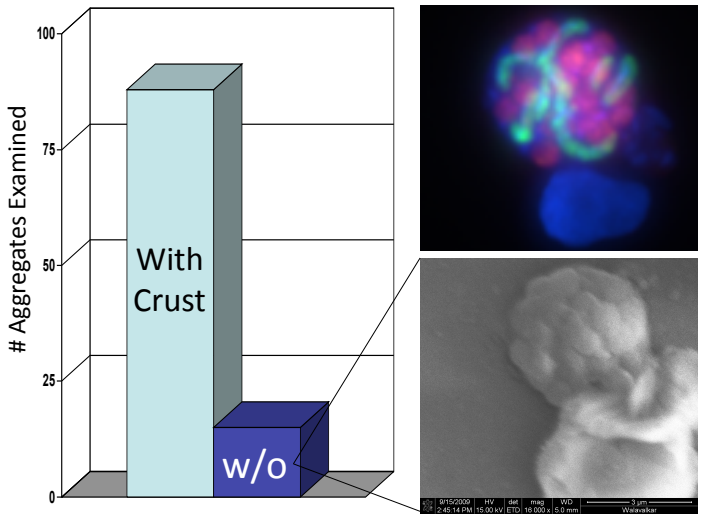

Figure 4: A Ga^+ Focused Ion Beam (FIB) was used to ablate the surface layer of an ANME-SRB aggregate and expose the interior layers (schematically depicted in A, images of the aggregate before and after FIB in B). A transect of EDS measurements were then made across the interior of the aggregate to determine the internal distribution of minerals (B). Clay-typical (Si, Al, Fe) and biomass-typical (C, N, S) elements are plotted separately, and show different trends in abundance. Clay-typical elements are enriched on the edges, while biomass-typical elements (expectedly) are abundant in the interior. The lack of interior distribution of the clay-typical elements suggests that the clay association can be classified as a shell, since it is not distributed throughout the cells. Indium concentrations are shown in both plots to show the contribution of surface-contamination, since the aggregate was measured on glass coated with indium tin oxide.

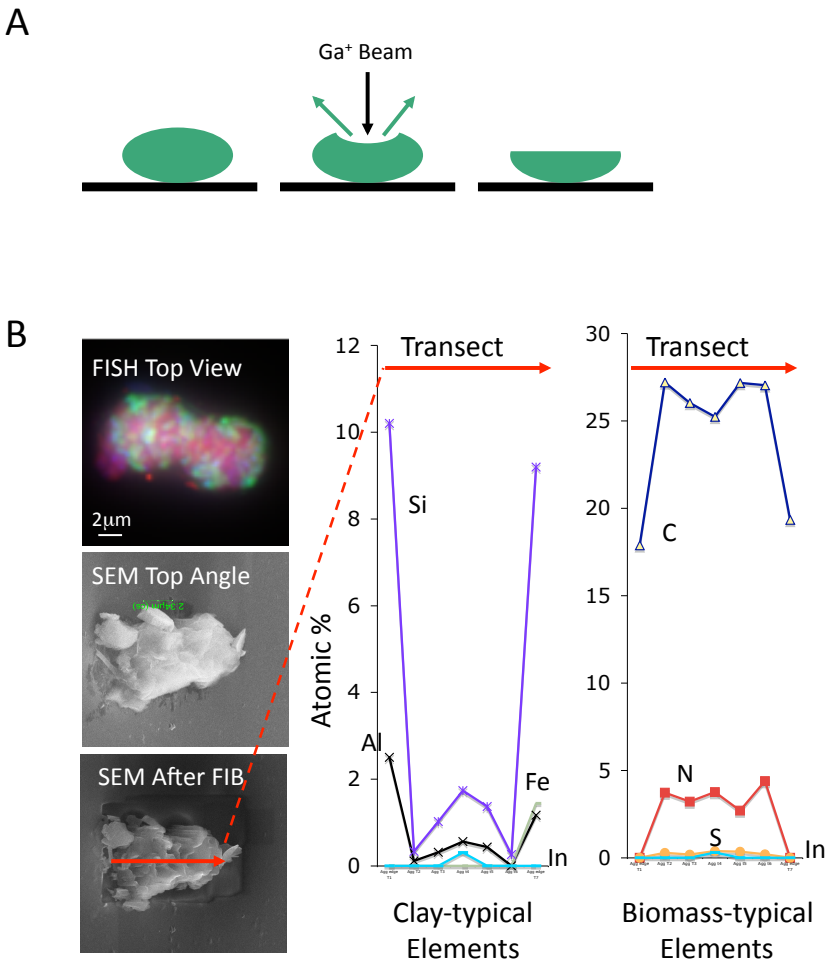

Figure 5: NanoSIMS analysis was also employed to measure the composition of the aggregate interior and confirm the FIB-EDS observation that the clay was nearly exclusively on the aggregate exterior. (A) Si was not observed on/in control clostridia spores, showing the lack of contamination from the ITO (indium tin oxide)-coated glass surface. (B) NanoSIMS Si analysis of the aggregate in Figure 3, showing the same pattern of clay distribution as the FIB-EDS analysis: lack of Si on the aggregate interior. (C) NanoSIMS Si analysis of two representative aggregates. FISH images show hybridization with Eel 932 (pink) and DSS 658 (green), DAPI in blue. No archaeal probe was employed in the top image. Initially, Si was detected primarily on the edges but also towards the center of the aggregate. After approximately ten hours of Cs^+ beam ablation, Si was primarily limited to the edges, however some internal lines of Si suggest the possibility of individually shelled lobes of cells within the aggregate. The NanoSIMS results must be considered carefully because low ion yields from the center of aggregates may be due to reduced conductivity and therefore charging complications in these locations. However, the detection patterns of other ions collected simultaneously (e.g., C-, CN-) suggested that this was not a problem (not shown).

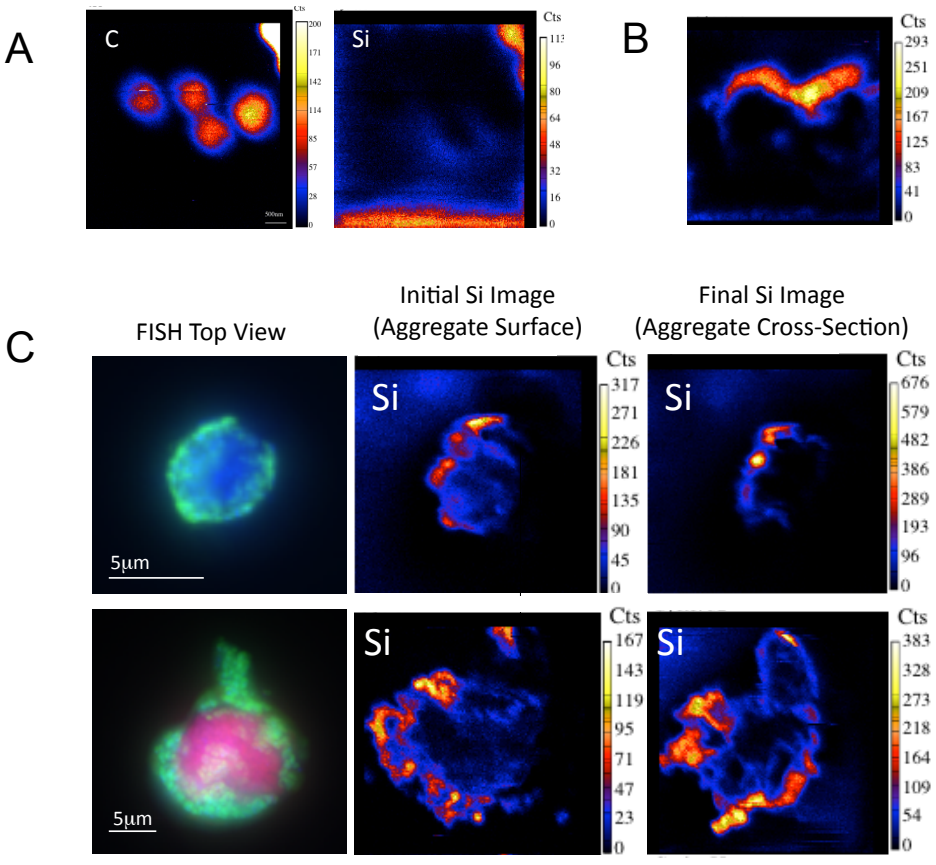

Figure 6: Additional mineral associations of the ANME-SRB. While investigating the most obvious mineral association of the ANME-SRB, the clay crust, other solid substrates were observed in association in with the ANME, as well. (A) An example of a diatom frustule embedded into the clay matrix (arrow, SEM image). This suggests that the shells, although primarily aluminosilicate clay, may also contain, and possibly trap, other detrital material. Many aggregates were observed in association with particles believed to be diatom frustules of a variety of morphologies, including both the honeycomb-type pictured here as well as long, thin, ladder-type frustules. (B) Iron sulfide minerals were regularly detected within the clay matrix (arrows), and appeared as relatively spherical nodules. (C) EDS analysis confirmed their iron and sulfur composition, at a ratio of approximately 1:1. Although the FISH images for these aggregates are not shown, they were identified via FISH prior to SEM analysis.

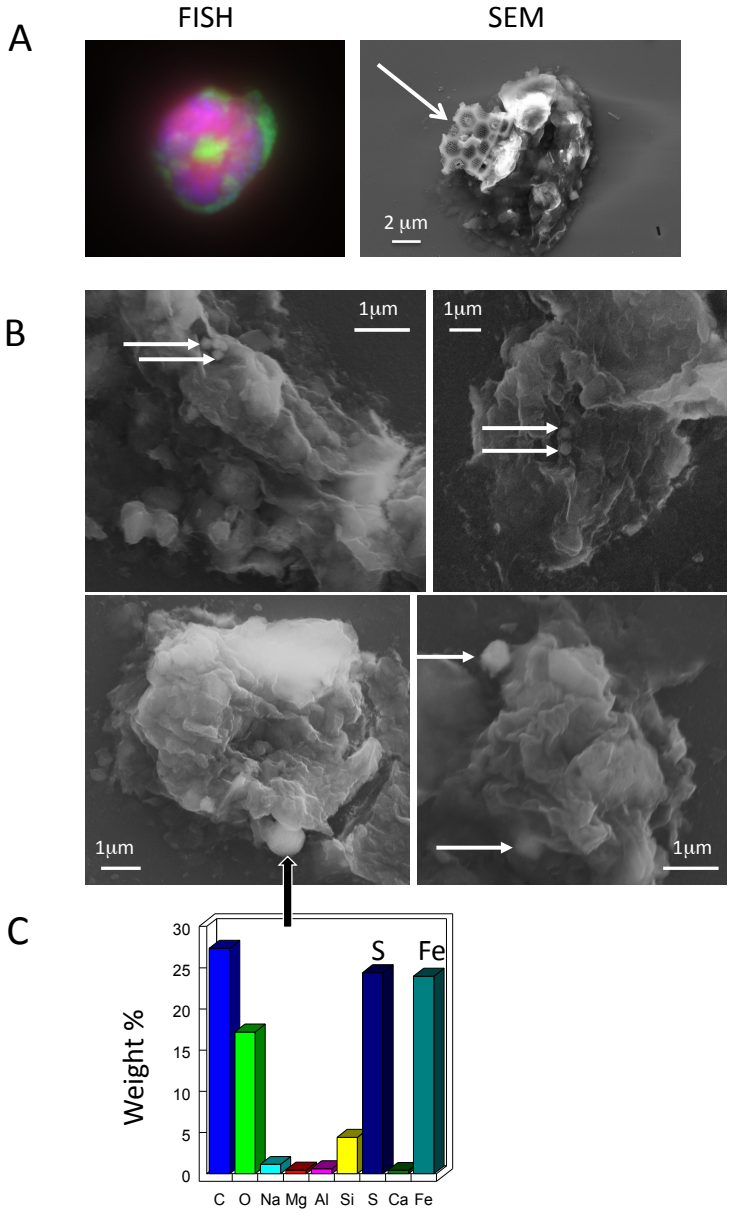

Table 2: XRD (X-ray Diffraction, UC Riverside) analysis of the bulk sediment containing the encrusted ANME-SRB aggregates indicated the presence of several different types of clay. Whether these are the same types of clay and/or in the same relative abundances in the crust is yet to be determined. Raman spectroscopy of the aggregates was attempted to determine the bonding structure of the mineral phase on individual aggregates and therefore the type of clay, however the analysis was not successful.

Mineral	**Wt %**
Chlorite	15
Feldspar	31
Halite	6
Illite	21
Quartz	26
Total	99